Production and hosting by Elsevier

OCEANOLOGIA

QUARTERLY JOURNAL
OF BASIC RESEARCH
IN MARINE SCIENCES
WITH EMPHASIS ON
EUROPEAN SEAS

66(1)
2024

PL ISSN 0078-3234

ScienceDirect

Oceanologia

Official Journal of the Polish Academy of Sciences

This journal is supported by the Ministry of Science and Higher Education, Warsaw, Poland

Indexed in: ISI Journal Master List, Science Citation Index Expanded, Scopus, Current Contents, Zoological Record, Thomson Scientific SSCI, Aquatic Sciences and Fisheries Abstracts, DOAJ

IMPACT FACTOR ANNOUNCED FOR 2022 IN THE 'JOURNAL CITATION REPORTS' IS 2.9; 5-year IF is 2.8. CITESCORE ANNOUNCED FOR 2022 IS 4.3

Publisher
Elsevier B.V.
Radarweg 29
1043 NX Amsterdam
The Netherlands

Senior Publisher
Tobias Wesselius
+31 6 5370 3539

ISSN 0078-3234

Oceanologia 66 (2024) v—vi

Available online at www.sciencedirect.com

ScienceDirect

journal homepage: www.journals.elsevier.com/oceanologia

EDITORIAL FOREWORD

Baltic Earth: Assessing the Baltic Earth System

Baltic Earth is an international and interdisciplinary network of scientists and institutions who share their time and expertise in an altruistic and non-hierarchical effort to improve the Earth system knowledge and capacity building in the Baltic Sea region. In this effort, Baltic Earth fosters research and its assessment, organizes workshops as well as summer and winter schools for master students and early career researchers, and forms a community of scientists that comes together at the large Baltic Earth conferences every second year, at a different location under a different scope.

This selection of papers is part of the more than 100 oral and poster contributions presented at the 4th Baltic Earth Conference, from 30 May to 3 June 2020 in Jastarnia, Poland. The conference was held under the short motto "Assessing the Baltic Earth System", which really means "assessing the state of scientific Earth system research in the Baltic Sea region", and refers to the so-called "BEAR" reports (Baltic Earth Assessment Reports), which represents a state-of-the-art overview over different aspects of the Baltic Sea Earth system.

The ten papers presented here in this Oceanologia Special Volume demonstrate a wide spectrum of current Baltic Earth research. They are based on presentations given at the conference and are very briefly described here, in a first-author alphabetical order.

One of the largely unknown aspects of the water cycle in the Baltic Sea, and coastal regions in general, is the distribution of groundwater and its dissolved ingredients along a land-ocean aquatic continuum, i.e. submarine groundwater discharge. **Von Ahn et al.** have investigated the effects of different sediment types on the quality of the discharged groundwater. They found a substantial difference in sandy vs. muddy surface sediments, with the latter modifying the composition of the discharge to a larger extent due to diagenetic effects.

Increasing droughts and heat waves are believed to be a consequence of the ongoing climate change, and when they coincide in time and space, the consequences can be even more harmful. **Klimavičius and Rimkus** investigated the number of drought and heatwave days between 1950 and 2022 in the eastern Baltic Sea region and concluded that while the number of heatwave days had increased, the number of drought days had decreased.

Human infrastructure significantly alters coastal environments, and **Liblik et al.** have investigated the impacts of a road dam, separating two bays from a previously interconnected water system. They could show an alteration in almost all aspects of the water quality, as temperature, seasonal cycles, water chemistry, biochemistry, hazardous substances distribution and ecology.

Merchel et al. demonstrate the versatile usability of Argo floats which are increasingly used in coastal and shelf seas. The alternative use as "virtual moorings", i.e., by forcing the float to remain at a fixed position for a specific period, allows additional information on the temporal and spatial variability of the measured oceanographic properties.

Using a combination of observations and modelling, **Najafzadeh et al.** have investigated the wave properties in the Gulf of Riga vs. the open Baltic Sea. They found the wave climate to be milder than in the open Baltic Sea, and interannual variations were below 10% of the average wave height; a long-term trend or seasonal variations were not detected.

Anders **Omstedt** and Hans **von Storch** had been active in BALTEX and its successor, Baltic Earth, for many years, also as chairpersons. In the article, they provide a brief overview of the developments and achievements of this international and interdisciplinary scientific network.

Solar irradiance in the Baltic Sea region has increased over the past half-century and this is connected to cloudiness. **Post and Aun** have investigated the atmospheric circulation variations leading to this increase. They showed that a shift in seasonality is partly explained by changes in atmospheric circulation.

Oxygen is an important biogeochemical indicator of ecosystem condition, and **Stoicescu et al.** have analyzed a long data series of oxygen measurements in the eastern Gulf of Finland. They found a substantial long-term declining trend in oxygen concentrations, about —27% since 1900, with an accelerated decrease during the recent decades. They attribute this to human activities like excess nutrient loads and surface warming.

https://doi.org/10.1016/S0078-3234(24)00033-2

Väli et al. present a high-resolution modelling study on analyzing surface mesoscale and submesoscale current structures as well as the distribution of kinetic energy in the Baltic Sea. These fields are inhomogeneously distributed, with a large seasonal variability. A time lag between wind energy and the Rossby number of about 2 months in spring was attributed to the decay of larger eddies into new, smaller and weaker eddies.

Finally, the study by **Zalewska et al.** documents the temperature changes in the water column of the southern Baltic Sea between 1959 and 2019. It shows the clear warming of all parts of the water column during all seasons and locations, with the strongest warming in spring and in the upper water layers.

We are happy to present this spectrum of Baltic Earth research, ranging from oceanography, meteorology, hydrology and regional climate science to operational and historical aspects of the scientific work in the Baltic Sea region. We sincerely hope that this Special Issue contributes to one of the Baltic Earth goals: to foster research and to make scientific results available to the greater community.

Guest Editors

Marcus Reckermann
E-mail address: marcus.reckermann@hereon.de

H.E. Markus Meier
E-mail address: markus.meier@io-warnemuende.de

Karol Kuliński
E-mail address: kroll@iopan.pl

Joanna Dudzińska-Nowak
E-mail address: joanna.dudzinska-nowak@usz.edu.pl

Oceanologia 66 (2024) 1—8

Available online at www.sciencedirect.com

ScienceDirect

journal homepage: www.journals.elsevier.com/oceanologia

ORIGINAL RESEARCH ARTICLE

The BALTEX/Baltic Earth program: Excursions and returns

Anders Omstedt[a,*], **Hans von Storch**[b]

[a] *Department of Marine Sciences, University of Gothenburg, Sweden*
[b] *Institute of Coastal Systems, Helmholtz-Zentrum Hereon, Geesthacht, Germany*

Received 16 December 2022; accepted 7 June 2023
Available online 20 June 2023

KEYWORDS
BALTEX;
Baltic Earth;
Water and energy cycles;
Biogeochemistry;
Carbon cycle;
Climate and environmental research;
Atmosphere-ocean-land surface modeling

Abstract The Baltic Sea Experiment (BALTEX) started in 1993 as part of the Global Energy and Water Cycle Experiment (GEWEX). It was later organized into three programs: BALTEX I, BALTEX II, and Baltic Earth. Here, we examine in a brief overview the overall BALTEX achievements, including program goals, risks encountered during the research journey, and knowledge development when finalizing the programs.

During three decades of climate and environmental studies of the Baltic Basin within the BALTEX/Baltic Earth programs, significant steps have been taken towards improved scientifically constructed knowledge and efforts to disseminate this knowledge to neighboring sciences and the public. These programs have illustrated the need to actively navigate the European research arena while remaining an independent science network. The well-organized International Baltic Earth Secretariat and many dedicated scientists made the research excursions safe and successful. The learning process relates to improved knowledge of the dynamics of the atmosphere—ocean—land climate system in the Baltic Sea region, the cycling of carbon and other substances, the region's anthropogenic climate and environmental changes, and how global warming and regional human activities can be detected outside natural variability.

* Corresponding author at: Department of Marine Sciences, University of Gothenburg, Sweden.
E-mail address: anders.omstedt@marine.gu.se (A. Omstedt).

Peer review under the responsibility of the Institute of Oceanology of the Polish Academy of Sciences.

Production and hosting by Elsevier

https://doi.org/10.1016/j.oceano.2023.06.001

1. Introduction

The water and energy cycles represent the heart of climate dynamics. They involve many complex processes, such as cloud formation, precipitation, evaporation, river runoff, and interaction with the biosphere and humans. In the late 1980s, the Global Energy and Water Cycle Experiment (GEWEX) was developed within the framework of the World Climate Research Programme (WCRP) (e.g., Chahine, 1992; Stephens et al., 2022). The water and energy cycles needed to be better observed and modeled for improved understanding and modeling of the global climate system. The spatial resolution of global models was coarse, and the GEWEX idea was to use the drainage basin concept to balance the scale problem caused by the inconsistency of point source data and global model resolution. Six continental-scale experiments were initiated in different climate zones, one of which was the Baltic Sea with its drainage basin, i.e., the Baltic Basin (Figure 1). Closing the water and energy cycles using the Baltic Basin allowed a consistent way to investigate how appropriate models could describe these cycles. This idea started the Baltic Sea Experiment (BALTEX) program (Raschke et al., 2001), which was later developed into the Baltic Earth program.

> "*The night passed, and the dawn came, and they sailed constantly*."

This famous quotation from Homer's *Odyssey* relates to Odysseus' voyage home for ten long years, encountering many dangers and obstacles. This story has been interpreted and retold in many ways; it is a symbol and a starting point for a large part of western culture, manifested in literature, art, and philosophy. In western culture, the influence of the *Odyssey* is mainly evident in the pervasive structure of excursion and return. The first step is belonging to the familiar, in which we recognize ourselves and which is the basis on which we encounter new, different, and exciting things. The second step is the excursion, leaving home and the familiar and opening oneself to new experiences. This

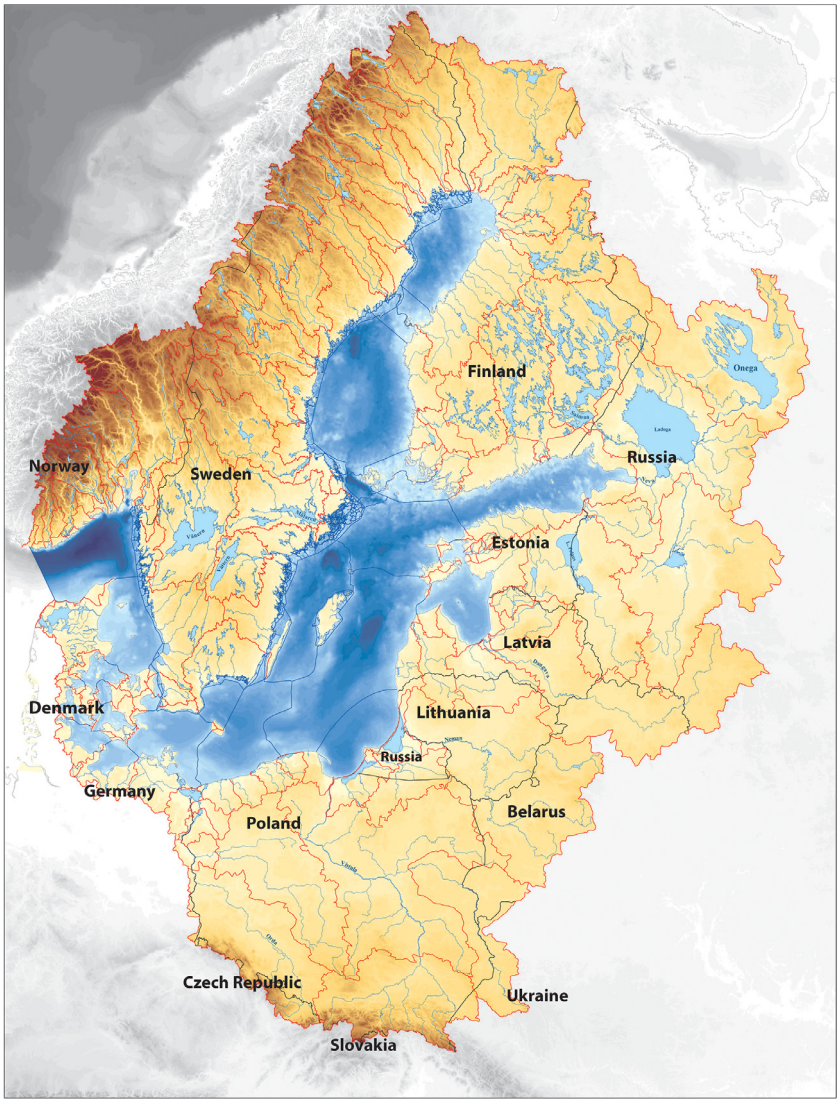

Figure 1 The Baltic Basin comprises the Baltic Sea and its drainage basin (figure courtesy of SMHI, modified by Marcus Reckermann).

entails putting oneself at risk, forgetting oneself, and opening oneself to novel interpretations that lead to new understandings. The third step, returning home, is essential to the learning process. It is not "putting oneself at risk" but returning home that is the essence of education, which entails learning to solve existing problems and foreseeing new ones, see further discussion related to the ocean and the *Odyssey* in Omstedt and Gustafsson (2022).

In this article, we will examine the BALTEX/Baltic Earth programs through the excursion and return pattern lens. The Odysseus' voyage home took a decade, and the reviewed programs were about three decades long. Participating scientists have reported many achievements in a number of books, assessments, special issues, articles and reports available on the Baltic Earth website (https://baltic.earth). Here, we discuss the overall program achievements starting from the goals at the program start, risks taken during the research journey, and knowledge development when finalizing the programs.

2. BALTEX phase I (1993—2002)

In 1990, before the start of BALTEX, the First Intergovernmental Panel on Climate Change (IPCC) Assessment Report underlined climate change as a challenge with global consequences requiring international cooperation. The Global Energy and Water Exchange (GEWEX) project, as part of the World Climate Research Programme (WCRP), was initiated in 1990, with its phase I (lasting until 2002) concentrating on the water and energy cycles. BALTEX started as a program within GEWEX to explore the regional water and energy cycles. Closing the water and energy cycles using the Baltic Sea and its drainage basin allowed a consistent way of investigating how the global and regional climate models could model these cycles in the Baltic Basin region. The program's ideas were visualized in the BALTEX I box model (Figure 2).

The goals formulated for BALTEX I were (BALTEX, 1995):

- To explore and model the various mechanisms determining the spatial and temporal variability of the energy and water budgets of the BALTEX region and this region's interactions with surrounding areas;
- to relate these mechanisms to the large-scale circulation systems in the atmosphere and oceans over the globe; and
- to develop portable methodologies to contribute to meteorology, hydrology, oceanography, climate, climate change, climate impact, and environmental research.

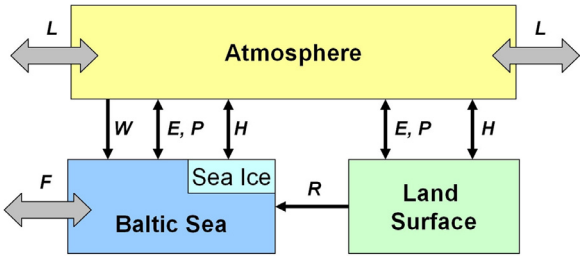

Figure 2 BALTEX I box presents a conceptual view of the coupled atmosphere, ocean, and land system in the Baltic Sea region. The arrows indicate different types of interactions between the boxes (figure courtesy of Marcus Reckermann).

The first "excursion," BALTEX phase I (1993—2002), benefitted greatly from the breakup of the Soviet Union in 1991 and from new cooperation among the 14 countries in the Baltic Sea's drainage basin (i.e., Belarus, Czech Republic, Denmark, Estonia, Finland, Germany, Latvia, Lithuania, Norway, Poland, Russia, Slovakia, Sweden, and Ukraine). The initiative was also important because it integrated scientists within meteorology, hydrology, and oceanography, and used remote sensing and modeling components. The approach was new for Baltic Basin research, in which national initiatives and marine biology research had previously dominated.

The risks of building a new science network largely concerned collecting data, involving partners, and financing issues. New working groups and data centers were formed to move the work forward. Early on, the program decided not to pay for old data; instead, all willing and relevant parties were invited to contribute by fundraising and actively participating in the network. The BALTEX research environment was friendly and open-minded, and many study conferences were held on islands in the Baltic Sea. The research involved observations from new platforms, homogenizing long-term datasets (mainly within meteorology), creating new databases, measuring and calculating components such as net precipitation and river runoff, and developing process and climate models. New weather radars were installed to cover the whole basin. Satellite data were collected, forming the basis for climate studies. In July 2000, the Öresund Bridge opened to traffic after many years of discussion, planning, and environmental studies, including observing and calculating Baltic Sea in and outflows.

In an Odyssean return after a decade of BALTEX I efforts, one of the program's essential accomplishments was building a thriving research community focused on climate change. The standards within meteorology, hydrology, and oceanography were quite different. Meteorology was leading in data checks, building databases, and creating reconstructed datasets. The disciplines in this new science community started learning to listen to and be inspired by one another, realizing the need to make quality-checked data and models available. Many scientific and technical problems were solved and reported in peer-reviewed journals. Feedback mechanisms within the system illustrated the need for coupled atmosphere—land—ocean models on the regional scale. Also, new issues emerged when it was learned that there were significant discrepancies between observed and climate-simulated water- and heat-balance components on the regional scale. For example, when coupling global to regional climate models, the water balance becomes unrealistic and often too wet. Reviews of BALTEX phase I were presented by Raschke et al. (2001), Omstedt et al. (2004), and Jacob and Omstedt (2005).

3. BALTEX phase II (2003—2012)

Anthropogenic climate change due to increased atmospheric greenhouse gas (GHG) concentrations was attract-

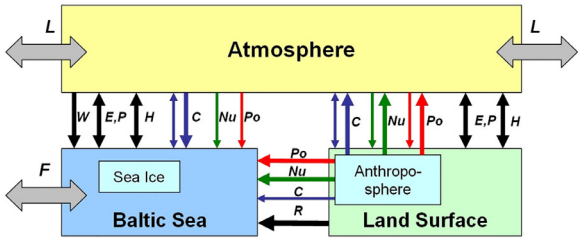

Figure 3 BALTEX II box, a conceptual view, describes the Baltic Sea region's coupled atmosphere, ocean, and land system. Here, the human role is indicated by the box labeled "Anthroposphere" (figure courtesy of Marcus Reckermann). The arrows indicate different types of interactions between the boxes.

ing increased attention in research and society. Simultaneously, concern arose about ocean acidification, regarded as the second aspect of climate warming (e.g., Gattuso and Hansson, 2011). Much of the carbon dioxide produced by human activities is absorbed in the ocean, leading to a change in the ocean acid—base balance and gradual acidification. In the Baltic Sea, a significant problem is eutrophication, accompanied by increasing areas of anoxic waters. How eutrophication and climate change interact has become a major concern. New understanding and models were needed to address the multiple stresses arising from increased GHG and nutrient levels. The BALTEX I goals were broadened to include modeling biogeochemical cycles and starting to build Earth system models (BALTEX 2005, 2006, 2009). The program ideas were visualized in the BALTEX II box (Figure 3).

The goals formulated for BALTEX II were (Grassl et al., 2004):

- To improve our understanding of energy and water cycles under changing conditions;
- to analyze climate variability and change and to provide regional climate projections over the Baltic Sea Basin for the 21st century;
- to provide improved tools for water management, with an emphasis on extreme hydrological events and long-term changes;
- to model biogeochemical cycles in the Baltic Sea Basin and transport processes within the regional Earth system under anthropogenic influences;
- to strengthen interaction with decision-makers, with an emphasis on global change impact assessments; and education and outreach at the international level.

GEWEX Phase II, 2003—2012, focused on how energy- and water-cycle processes function and quantified their contribution to climate feedback. The BALTEX phase II excursion benefitted greatly from BALTEX I results and from long-term research on eutrophication. New data on carbon dioxide in water obtained through regular ferry measurements and turbulence measurements from the atmosphere and the Baltic Sea also became available. The IPCC published its Third Assessment Report in 2001, presenting more information supporting the idea that human emissions of GHG would lead to global warming, with many consequences for human life and entailing a need for adaptation.

The scientific community addressed the new risks encountered on the second excursion of BALTEX. The network was becoming much broader, including chemistry, biology, geology, physical geography, and history researchers. Many scientists working on eutrophication had backgrounds in the International Geosphere—Biosphere Programme (IGBP), having been involved in research on global- and regional-scale interactions between Earth's biological, chemical, and physical processes and their interactions with human systems. BALTEX II became a productive meeting place for scientists working within GEWEX and IGBP. Simultaneously, a new challenge arose: the new datasets, models, and reconstructions could easily be misjudged concerning their information value, biases, and uncertainties. Data reconstructed using different methods were not homogeneous, resulting in inaccurate trends. When model outputs were compared, significant differences and open questions emerged about how to interpret results from more than one model. At the same time, atmospheric climate models' water and heat cycles turned out to be severely biased compared to observations manifesting a need for nonphysical delta change applications when forcing regional land-surface and ocean models. In general, when simulating the present climate over the BALTEX region, the climate models were too wet and had errors in the heat cycle.

A solid effort was made to establish consensus and dissensus regarding available information by forming the first BALTEX Assessment of Climate Change (BACC, 2008) involving cooperation within a broad group of scientists. BACC results were used by the Baltic Marine Environment Protection Commission, or Helsinki Commission (HELCOM), when assessing the knowledge and significance of climate change in the Baltic Sea region (HELCOM, 2007).

After the second decade of BALTEX efforts, the program's essential accomplishments included elements of interdisciplinary work. New questions and knowledge captured in long-term datasets could better address past climate conditions and access new reconstructions on the centennial scale. Earth system models were developed, but only a few could systematically resolve the carbon cycle. New observation platforms, e.g., FerryBOX data that continuously collected ship measurements, produced much higher-temporal-resolution data than traditional monitoring programs. The new observations taught the modeling community the importance of appropriate temporal and spatial scales for climate model design.

Despite marked progress in Baltic Basin research, several gaps remained in our knowledge and modeling tools. The issue of multiple stressors impinging on the Baltic Sea began attracting attention, for example, leading to the realization that efforts to combat eutrophication and climate change are closely linked. Reviews of BALTEX phase II were presented by Omstedt et al. (2014) and Reckermann et al. (2011).

4. Baltic Earth (2013—2022)

The IPCC published its Fourth Assessment Report in 2007, describing the greater certainty, compared with the 2001

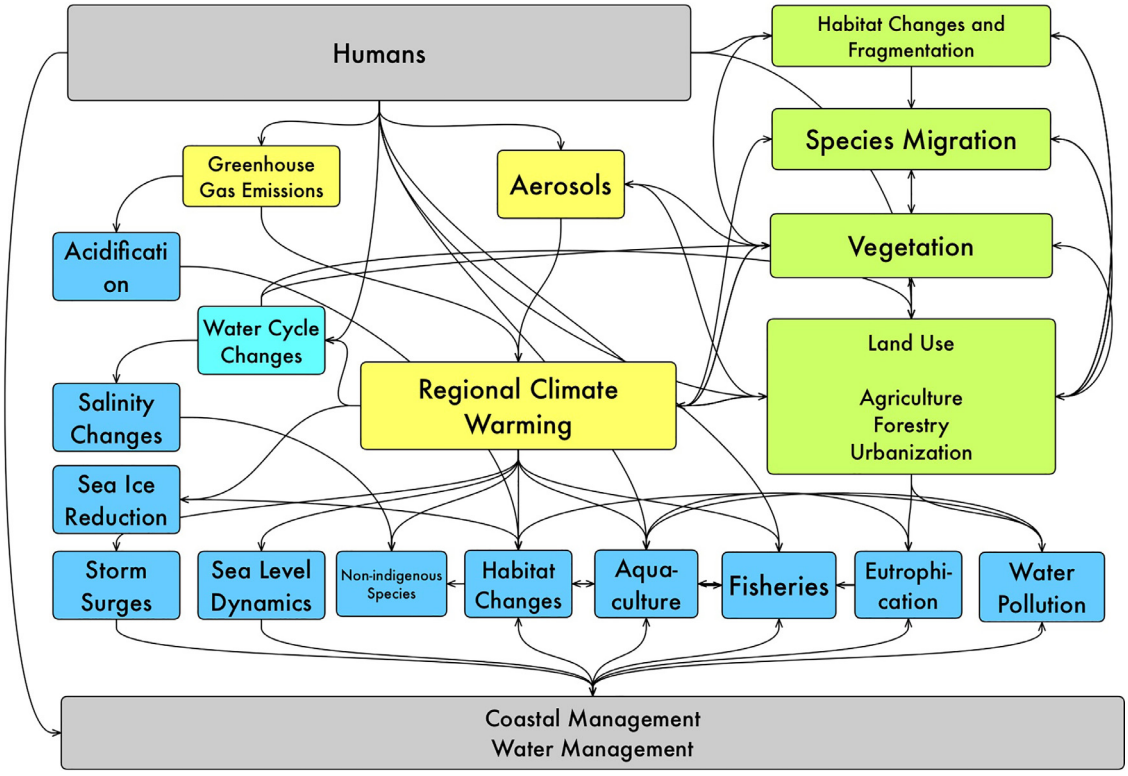

Figure 4 Baltic Earth program: a schematic illustrating different regional Earth system drivers and their interrelations. Human activities are represented by the grey boxes (figure courtesy of Marcus Reckermann).

Assessment Report, of the scientific knowledge that human activity is the main reason for present climate warming. The IPCC Fifth Assessment Report, published in 2014, delivered an even stronger message about humans' effect on global warming and that increased global warming would increase the likelihood of severe, far-reaching, and irreversible impacts. GEWEX Phase III (2013–2022) was initiated, building on the results and experience of GEWEX Phases I and II. The Future Earth program was officially announced in June 2012 at the United Nations conference on sustainable development. The program has a background in the International Geosphere–Biosphere Programme, Diversitas (Latin for diversity, aiming to apply biodiversity science for human well-being), and the International Human Dimensions Programme. Future Earth later included the Future Ocean and Future Coasts programs. A new European Baltic Sea funded program, BONUS (2010–2020), was formed to promote a better future for the Baltic Sea. The 2030 Agenda for Sustainable Development, approved in 2015 by the United Nations General Assembly, establishes a transformative economic, social, and environmental vision based on 17 different sustainability goals.

The BALTEX network was reorganized under a new name, Baltic Earth, a new program, and broadened foci (Baltic Earth Science Plan, 2017) (Figure 4). Baltic Earth inherited the scientific legacy and networks of BALTEX. The new program identified several grand challenges, in particular:

- salinity dynamics in the Baltic Sea;
- land–sea biogeochemical linkages in the Baltic Sea region;
- natural hazards and extreme events in the Baltic Sea region;
- sea level dynamics in the Baltic Sea;
- regional variability of water and energy exchanges and
- multiple drivers of regional Earth system changes.

The Baltic Earth excursion benefited greatly from the previous BALTEX I and II excursions and achievements, resulting in a focused start. The research foci were anthropogenic changes and impacts and their natural drivers, supporting a regional Earth system sciences network. A new climate assessment was conducted and published in 2015 (The BACC II Author Team, 2015). The conclusions of BACC I were confirmed by BACC II but substantially deepened and broadened. Cooperation with HELCOM developed through the formation of a Joint HELCOM/Baltic Earth Expert Network on Climate Change (EN Clim), resulting in a fact sheet published in 2021 and available on the HELCOM website.

Studies of the climate system got a significant boost from the awarding of the 2021 Nobel Prize in Physics to Klaus Hasselmann for suggesting and demonstrating approaches for dealing with the high-dimensional, complex, and inhomogeneous climate system, specifically via the stochastic climate model from 1976 and the detection of climate change and attribution of its plausible causes (von Storch and Heimbach, 2022). Although Hasselmann was not part of BALTEX

and Baltic Earth, his ideas influenced the foci of the work, leading to an emphasis on system aspects as opposed to multiple independent processes.

After the third decade of BALTEX/Baltic Earth efforts, the program's essential accomplishments included the generation of multiple assessments. In 2022, ten assessments, the so-called BEAR Reports (Baltic Earth Assessment Reports) based on the program challenges, were published in a special issue of *Earth System Dynamics* (https://esd.copernicus.org/articles/special_issue1088.html). The BEAR topics covered problems of climate change and marine ecosystems, the biogeochemical functioning of the Baltic Sea, salinity dynamics, natural hazards, extreme events, oceanographic and atmospheric regional climate predictions, human impacts, coupled regional Earth system models, sea level, and coastal erosion. The regional climate change assessments (BACC) of 2008 and 2015 were updated in this issue by Meier et al. (2022).

Increasing insights into multiple stressors, for example, fisheries, climate change, eutrophication, and land-use change, have fueled interest in addressing complex problems. While process studies—mandatory and urgently needed—are powerfully pursued by participants in Baltic Earth, the system view has attracted considerable attention, with readily available extended datasets covering recent and past changes and informing scenarios of possible futures. Specifically, the role of elevated GHG concentrations in the regional climate has been assessed. Various numerical models of the coupled atmosphere—Baltic Sea system allow climate system experimentation and the estimation of related impacts. New challenges are the separation of various signals, ranging from GHG and aerosol levels, discharge of different substances into Baltic Sea water, urbanization, and flows of goods and people, to understanding the interaction between scientifically constructed knowledge and societally and culturally constrained decision processes.

5. Education and outreach

Education and outreach at the international level have been promoted in different ways in the BALTEX/Baltic Earth programs. When these programs started, climate and climate change were not integral to the HELCOM program. Through the development of BACC and BEAR, this situation has changed.

New and other relevant publications are available via the Baltic Earth website. In the BALTEX/Baltic Earth Public Library, accessible via the web, books and articles generated through BALTEX/Baltic Earth are listed and updated. Also available on the web is documentation of relevant newsletters, special journal issues, and interviews.

BALTEX/Baltic Earth left a significant trace in *Oxford Research Encyclopedia of Climate Sciences articles on climate science*, with a dozen overview papers authored by international scholars on specific climate science topics. The articles are peer-reviewed and intended as reference material for scientists from other fields, scholars, students, and the interested public. The presently available contributions are listed on the Baltic Earth home page (https://www.baltic-earth.eu/publications/oxford_research_encyclopedia/index.php.en).

The program's multidisciplinary approach has been supported by many regional conferences. These have been designed as study conferences with sessions that combine different disciplines to promote connections among scientists with diverse backgrounds. Numerous thematic workshops have been organized on various BALTEX and Baltic Earth topics.

Capacity building has played an increasing role in Baltic Earth. Since the program's start, yearly international summer and winter schools have been organized for students and young scientists, and an international master course at Rostock University has now been established.

6. The human dimension

So far, we have focused on what was expected from the brave sailors embarking on their three excursions and on what they brought back. If we apply the CUDOS norms of Robert Merton (e.g., Grundmann, 2012) for natural science operation, personalities are hardly relevant to the findings, although they are relevant to the processes leading to them—with Klaus Hasselmann serving as a convincing case. The CUDOS norms summarize four aspects of modern science, including elements such as science is free for all and scientific validity is independent of policy. Science institutes should act for the common scientific enterprise, and scientific claims should be exposed to critical analysis.

In the case of BALTEX and Baltic Earth, a remarkable organization was built—which would not have been possible without the International Baltic Earth Secretariat (IBES), led by Hans-Jörg Isemer and later by Marcus Reckermann—financed by GKSS Research Center, Helmholtz-Zentrum Geesthacht (HZG) and Helmholtz-Zentrum Hereon.

An open and friendly research community flourished based on voluntary contributions and well-organized conferences, not on funding expectations. The ethos was not "What is in it for me?" but "What can my group and I add?" An important condition for this international approach was that almost all members of the groups had to participate not in their native tongues but using English as a lingua franca. This favored the participation of more scientists in debating and planning. In most international programs, in contrast, a significant subgroup of members with English as their mother tongue results in constrained communication, with the power relations following from such a bias in linguistic skills.

Many enthusiastic members have carried forward the community's work, some of whom participated in all three excursions. However, strong leaders were always present to identify the excursions' expectations and tasks and determine the returns' value and significance. Here one must mention the chair and co-chairs Erhard Raschke, Lennart Bengtson, Zdzisław Kaczmarek, Hartmut Grassl, Joakim Langner, Sirje Keevallik, Anders Omstedt, Hans von Storch, Markus Meier, Anna Rutgersson and Karol Kuliński. While there was a certain overrepresentation of Swedish, German, and Finnish participants in the early years, the mix developed towards a much broader representation, with many

contributions from Poland and the Baltic countries. There were also significant contributions from Russian and Belarusian members, but these pan-Baltic developments were unfortunately interrupted by the Russian aggression against Ukraine in 2022.

7. Summary and conclusions

After three decades of climate and environmental studies of the Baltic Basin within the BALTEX and Baltic Earth programs, we have seen a vast body of new scientifically constructed knowledge and new efforts to make this knowledge available to neighboring sciences and the public. Scientific development has gone from disciplinary to multidisciplinary efforts. Over the three decades of the programs, we have seen significant progress in observations and available datasets, improved models for regional studies, and increased numbers of international summer/winter schools. The programs have illustrated the need for the scientific network to navigate the European research arena while remaining independent actively. Program planning based on decadal periods has strengthened the work compared with the often shorter-term national and European research programs. The well-organized international secretariat and many dedicated scientists have made the excursions safe and successful.

The BALTEX/Baltic Earth learning process has improved our knowledge of the dynamics of the atmosphere—ocean—land climate system in the Baltic Sea region, the cycling of carbon and other substances, the region's anthropogenic climate and environmental changes, and how global warming and regional human activities can be detected outside natural variability.

Attribution studies of climate change presented in the IPCC reports, which link global climate change to rising atmospheric GHG concentrations, are well established. In the case of the Baltic Sea region, the situation is more complex: The geographic position of the Baltic Basin, marked by significant variability in large-scale atmospherically circulation and strong influence from human activities, results in unique challenges in detecting and attributing regional anthropogenic changes. Anthropogenic influences of various types are ongoing, such as air pollution and aerosol emissions, changes in large-scale atmospheric circulation, land-use change, eutrophication, coastal construction, urbanization, fisheries, and shipping. Management may fail if we do not clearly understand the different drivers and how they interact on a regional scale (Reckermann et al., 2022). However, many of these aspects can be studied using reliable, homogeneous long-term datasets describing covariation in the regional atmosphere and sea and using improved modeling tools developed over past decades. Building links to economic, social, and human sciences helps transform academic knowledge of the changing environment into a valuable basis for directing regional policies toward sustainable development paths.

Homer's words echo: "*The night passed, and the dawn came, and they sailed constantly*" — and so must we respond to the growing anthropogenic threats to our region and climate.

Acknowledgments

The Baltic Basin science community has greatly benefited from research in the international arena, for example, within WCRP, GEWEX, IPCC, the EU, and BONUS. The BALTEX/Baltic Earth program would not have been possible without the many dedicated scientists, administrating people, and institutions that enthusiastically supported the joint research mission. The International Baltic Earth Secretariat at Helmholtz-Zentrum Hereon has strongly supported the organization. We thank Marcus Reckermann for providing the figures in this article, Stephen Sanborn at Proper English for text editing, to Editorial Board and reviewers for valuable comments.

Declaration of competing interest

The authors declare that they have no known competing financial interests or personal relationships that could have appeared to influence the work reported in this paper.

References

BACC Author Team, 2008. The BALTEX Assessment of Climate Change for the Baltic Sea basin. Springer-Verlag, 1—34.

BACC II Author Team, 2015. Second Assessment of Climate Change for the Baltic Sea basin. Springer Regional Climate Studies. Springer, Cham, Heidelberg, New York, Dordrecht, London. https://doi.org/10.1007/978-3-319-16006-1

Baltic Earth Science Plan, 2017. Int. Baltic Earth Secret. Publ. No. 11. Helmholtz-Zentrum Geesthacht GmbH, Germany, 34 pp. https://archive.baltic.earth/material/Baltic_Earth_Science_Plan_2017.pdf.

BALTEX, 1995. Baltic Sea Experiment BALTEX: Initial Implementation Plan (Int. BALTEX Secret. Publ. Vol 2., 52 pp.

BALTEX, 2005. Phase II 2003—2012 Implementation plan. Int. BAL-504 TEX Secret. Publ. GKSS, Geesthacht, Germany.

BALTEX, 2006. Baltex Phase II 2003—2012. Science Framework and 501 Implementation Strategy. Int. BALTEX Secret. Publ. No. 34. 502 GKSS, Geesthacht, Germany, 90 pp.

BALTEX, 2009. BALTEX Phase II 2003—2013. Revised Objectives. Int. 499 BALTEX Secret. Publ. No. 44. GKSS, Geesthacht, Germany, 92 pp.

Chahine, M.T., 1992. The hydrological cycle and its influence on climate. Nature 359, 373—380.

Gattuso, J.-P., Hansson, L., 2011. Ocean acidification. Oxford University Press, Oxford.

Grassl, H., Gryning, S-E., Isemer, H-J., Omstedt, A., Rosbjerg, D., Rummukainen, M., 2004. Science Plan for BALTEX Phase II 2003—2012. Int. BALTEX Secret. Publ. No. 28. GKSS, Geesthacht, Germany.

Grundmann, R., 2012. "Climategate" and The Scientific Ethos. Science, Technology, & Human Values 38, 67—93.

HELCOM, 2007. Climate Change in the Baltic Sea Area — HELCOM Thematic Assessment in 2007. Baltic Sea Environ. Proc. No. 1, 49 pp.

Jacob, D., Omstedt, A., 2005. BALTEX Phase I 1993—2002: State of the Art Report. In: Int. BALTEX Secret. Publ. No. 31. GKSS, Geesthacht, Germany, 181 pp.

Meier, H.E., Kniebuch, M., Dietrich, C., et al., 2022. Climate change in the Baltic Sea region: a summary. Earth Syst. Dynam. 13, 457—593. https://doi.org/10.5194/esd-13-457-2022

Omstedt, A., Gustavsson, B., 2022. The ocean: Excursion and return. Filosofia (67) 25—40. https://doi.org/10.13135/2704-8195/7241

Omstedt, A., Elken, J., Lehmann, A., Piechura, J., 2004. Knowledge of the Baltic Sea Physics gained during the BALTEX and related programs. Prog. Oceanogr. 63, 1—28. https://doi.org/10.1016/j.pocean.2004.09.001

Omstedt, A., Elken, J., Lehmann, A., Leppäranta, M., Meier, H.E.M., Myrberg, K., Rutgersson, A., 2014. Progress in physical oceanography of the Baltic Sea during the 2003—2014 period. Prog. Oceanogr. 128, 139—171. https://doi.org/10.1016/j.pocean.2014.08.010

Raschke, E., Meywerk, J., Warrach, K., Andrea, U., Bergström, S., et al., 2001. The Baltic Sea Experiment (BALTEX): A European Contribution to the investigation of the Energy and Water Cycle over a Large Drainage Basin. B. Am. Meteorol. Soc. 82 (11), 2389—2413.

Reckermann, M., Langner, J., Omstedt, A., von Storch, H., Keevallik, S., Schneider, B., Arheimer, B., Meier, H.E.M., Hunicke, B., 2011. BALTEX — An interdisciplinary research network for the Baltic Sea region. Environ. Res. Lett. 6 (4), 045205. https://doi.org/10.1088/1748-9326/6/4/045205

Reckermann, M., Omstedt, A., Soomere, T., Aigars, J., Akhtar, N., et al., 2022. Human impacts and their interactions in the Baltic Sea region. Earth Syst. Dynam. 13, 1—80. https://doi.org/10.5194/esd-13-1-2022

Stephens, G., Polcher, J., Zeng, X., van Oevelen, P., Poveda, G., et al., 2022. The First 30 years of GEWEX. B. Am. Meteorol. Soc. 104 (1), E126—E157. https://doi.org/10.1175/BAMS-D-22-0061.1

Von Storch, H., Heimbach, P., 2022. Klaus Hasselmann: recipient of the Nobel Prize in Physics 2021. Oxford Research Encyclopedias of Climate Science. https://doi.org/10.1093/acrefore/9780190228620.013.931

Oceanologia 66 (2024) 9—25

Available online at www.sciencedirect.com

ScienceDirect

journal homepage: www.journals.elsevier.com/oceanologia

ORIGINAL RESEARCH ARTICLE

Environmental impact of water exchange blocking in a strait — a multidisciplinary study in the Baltic Sea

Taavi Liblik[a,*], Fred Buschmann[a], Enriko Siht[a], Ivan Kuprijanov[a], Germo Väli[a], Maarja Lipp[a], Ants Erm[a], Jaan Laanemets[a], Redik Eschbaum[b], Aare Verliin[b], Lauri Saks[b], Ivar Zekker[b]

[a] *Tallinn University of Technology, Tallinn, Estonia*
[b] *University of Tartu, Estonian Marine Institute, Tartu, Estonia*

Received 20 October 2022; accepted 9 June 2023
Available online 22 June 2023

KEYWORDS
Water exchange;
Environmental impact of marine structures;
Shallow sea;
Fish migration;
Baltic Sea

Abstract In this study, we report the environmental impact of water exchange blocking by a 3 km road dam built in 1896 in the shallow Väike Strait, north-eastern Baltic Sea. Using a multidisciplinary measurement campaign and numerical simulations, we show ecological conditions in the strait have considerably altered; the previously free-flowing strait now comprises two bays with separate circulation systems. Water exchange in the area close to the dam has decreased 10—12-fold. Since advection is weakened, exchange with the atmosphere and sediments has a relatively greater role in shaping water characteristics. Consequently, occasional very high sea surface temperature, salinity, and total nitrogen, and strong diurnal cycles in water temperature (>4°C) and dissolved oxygen (>4 mg l^{-1}) were observed near the dam in summer. Oxygen levels are continuously below saturation in winter and concentration occasionally drops to hypoxic levels with ice cover. Nitrogen content in sediments near the dam is 3—4 times higher than in neighboring areas. The dam also modifies sea level, wind wave and suspended matter patterns in the strait. Sediments near the dam show elevated content of hazardous substances likely associated with traffic on the dam road. The phytobenthos community near the dam is dominated by annual green algae, which massively decompose during winter. The dam likely impedes fish migration between suitable feeding and spawning areas, also there have been

* Corresponding author at: Tallinn University of Technology, Tallinn, Estonia.
E-mail address: Taavi.liblik@taltech.ee (T. Liblik).
Peer review under the responsibility of the Institute of Oceanology of the Polish Academy of Sciences.

Production and hosting by Elsevier

https://doi.org/10.1016/j.oceano.2023.06.002

fish kills caused by rapid fluctuations in sea levels, amplified by dam. The construction of new openings would alleviate negative impacts of the dam.

1. Introduction

Straits are narrow topographic features that connect two bodies of water and determine exchange flows between them (e.g., Boutov et al., 2014; Jakobsen et al., 2010; Kasai et al., 2002; Matishov and Grigorenko, 2020; Stanev et al., 2017). Straits are particularly important for physical and ecological conditions in estuarine systems, such as the Baltic Sea where, for instance, the Danish straits play a crucial role (Jakobsen, 1995; Mohrholz et al., 2015). Width, depth and other features of straits determine water characteristics in sub-basins of the Baltic Sea (Kanarik et al., 2018; Liblik et al., 2017; Lilover et al., 1998; Otsmann et al., 2001). Straits are hydrodynamically active (Kanarik et al., 2018; Otsmann et al., 2001; Raudsepp et al., 2011; Talpsepp, 2005), with strong currents generated due to differences in sea level and wind stress. As straits separate water bodies, they often contain physical, biogeochemical and biological fronts (Astok et al., 1999; Liblik et al., 2017). Constructions that change the morphology of straits, such as bridges, jetties, piers, wind farms, dams, and dredging and dumping activities, potentially impact water exchange and water characteristics in neighboring sea areas (Altunkaynak and Eruçar, 2020; Jensen et al., 2018; Lass et al., 2008; Zainal et al., 2012).

In this study, we evaluate the environmental impact of water exchange blocking in the Väike Strait, a shallow strait in the eastern Baltic Sea, located between Saaremaa and Muhu islands in the Väinameri Archipelago Sea (VAS, Figure 1). The strait is a 2–4 km wide and 20 km long shallow sea area that is blocked by a 3-km long road dam, built in 1896. Except for a small, 4-m-wide opening near Muhu Island, the road dam is closed for water exchange and, thus, divides the strait into two separate bays. The Väike Strait is part of the VAS sensitive sea area that is protected under the NATURA 2000 Habitat directive. The strait is not in a good environmental status from the eutrophication point of view (Stoicescu et al., 2018).

The dam in Väike Strait blocks horizontal mixing of the fresher and higher-nutrient-content waters of the Gulf of Riga (GoR) and the saltier and lower-nutrient-content waters of the VAS (Astok et al., 1999; Stoicescu et al., 2018). The VAS is a shallow buffer zone between the GoR, Baltic Proper (BP), mainland and islands. Prior to dam construction, the Väike Strait was part of the water exchange system between the GoR and VAS, together with five other straits (Otsmann et al., 2001); Väike and Suur Strait connect the VAS with the GoR in the south, plus there are two connections in the north and one in the west between the VAS and BP. Water flow in the straits is oscillatory, with dominant short-term periods of 13 h and 24 h (Otsmann et al., 2001) overlain by wind-driven longer-term oscillations (Talpsepp, 2005) and seasonal changes (Otsmann et al., 2001). Since Väike Strait is much shallower than Suur Strait (Figure 1), it makes a relatively small contribution to water and substance exchange between the GoR, VAS and BP (Suursaar et al., 2009).

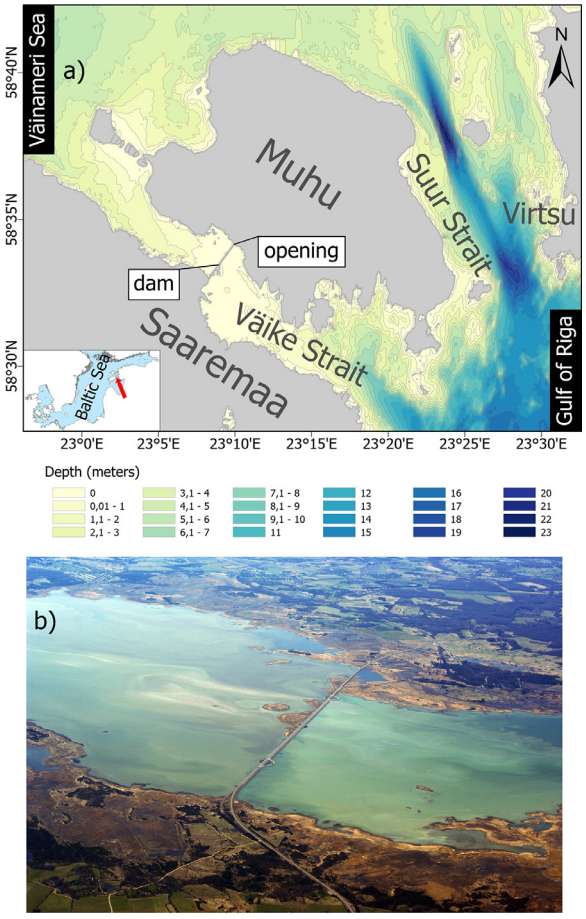

Figure 1 Bathymetry and location of the Väike Strait. (a) Bathymetry map of the Väike Strait, with inset map showing its location in the Baltic Sea. (b) Aerial photo of the 3 km road dam, viewed from Muhu to Saaremaa (photo is licensed by Estonian Land Board, 13.09.2022).

The main hypothesis of the present work is that the dam has an impact on the physical-biogeochemical and biological characteristics of the Väike Strait. Specifically, we hypothesize that due to the blocking of water exchange and horizontal mixing, other processes, such as atmospheric and benthic fluxes, have a greater influence on the characteristics of the water body. The main aim of the study is to analyze the impact of water exchange blocking

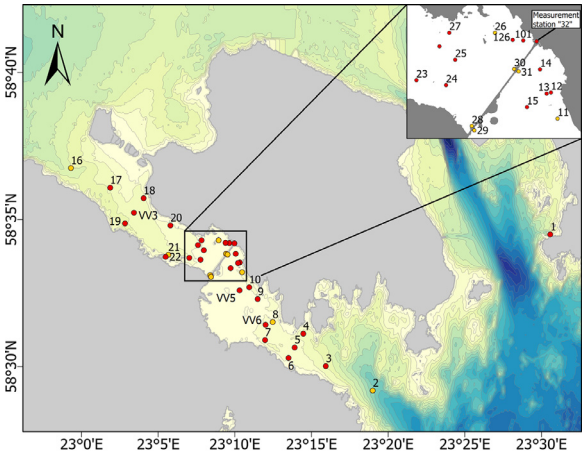

Figure 2 Bathymetry map showing location of sampling stations. In-situ measurement of seawater properties and collection of water samples for laboratory analysis was undertaken at all stations (marked red and yellow), with nutrient samples taken from a selection (marked yellow). Time-series measurements were taken below the road dam at station 32. (For interpretation of the references to colour in this figure legend, the reader is referred to the web version of this article.)

on environmental conditions in Väike Strait. To test the hypothesis and achieve the aim, we: (1) conducted field measurements of physical and biogeochemical parameters of the water column, sampled benthos and fish, and determined hazardous substances in sediment samples; (2) applied a three-dimensional numerical circulation model with high-resolution grid spacing. Thus, we provide a multidisciplinary view on the environmental effects of the anthropogenic structure.

2. Data and methods

2.1. Water column measurements

In-situ measurements of seawater properties (salinity, temperature, turbidity, chlorophyll *a* fluorescence and suspended matter concentration) were carried out simultaneously with collection of water samples for laboratory analyses (Figure 2). Six measurement campaigns were conducted between 27 July 2020 and 12 May 2021 and 186 vertical CTD profiles were recorded using a SBE 19 plus V2 SeaCAT Profiler (Sea-Bird Electronics) with a measurement interval of 4 samples per second. Measured turbidity values were converted to suspended sediment concentrations using the regression relationship between total suspended matter concentration (derived from water samples) and registered turbidity sensor readings ($r^2 = 0.67$, $p < 0.01$, $n = 47$). For nutrient analyses, 59 water samples were collected from the surface layer at 10 stations (Figure 2, yellow dots).

Samples for nutrient determination were transported to the laboratory and frozen at −20°C as soon as possible. Concentrations of dissolved nutrients were determined in the laboratory following standard spectrophotometric methods. Total nitrogen (N_{tot}), inorganic phosphate (PO_4) and the sum of nitrates and nitrites (NO_3+NO_2) were determined using a Lachat QuickChem® 8500 flow injection analyzer. Phosphates were detected at 880 nm as a complex formed after treatment with an acidic molybdate reagent and ascorbic acid solution (EVS-EN ISO 15681-1:2005). Nitrates (NO_3) were reduced to nitrites (NO_2) in a cadmium column, followed by treatment with sulfanilamide and N-(1-naphthyl)ethylenediamine, which allows detection of the azo-dye complex at 540 nm (EVS-EN ISO 13395:1999). For N_{tot}, nitrogen compounds were first digested into nitrates using potassium persulfate and ultraviolet radiation at 100°C in an automated system (EVS-EN ISO 11905-1:2003), then the procedure for determination of nitrates concentration was followed.

Total phosphorus (P_{tot}) and ammonium (NH_4) were measured manually using a Thermo Scientific™ Helios γ spectrophotometer. Phosphorus compounds first require digestion into phosphates by treatment with potassium persulfate at 121°C for 30 minutes before the concentration of phosphate is determined with the same principle as described above (Grasshoff et al., 1999, EVS-EN ISO 6878:2004). For ammonium, the seawater was treated with phenol-nitroprusside and sodium dichloroisocyanurate reagents which leads to the formation of indophenol blue complex detectable at 630 nm (Grasshoff et al., 1999).

All results are calculated and presented as elemental concentrations of phosphorus or nitrogen. The expanded measurement uncertainty and other validated parameters for the methods are continuously evaluated as a part of the accredited laboratory's quality system following EVS-EN ISO/IEC 17025.

2.2. Sediment and benthos samples

Sediment samples were collected at six locations. Stations V30 and V31 were 5 m from the dam, stations V126 and V14 were located at 560—700 m, station V05 at 5.9 km and V18 at 7.1 km distance from the dam (see Figure 2). Surface bottom sediment samples for chemical and benthos analyses were collected with a Lenz bottom sampler (modified version of an Ekman-Birge bottom grab; grip surface 0.0225 m^2). The handheld stainless-steel sediment corer was used to collect soft-bottom samples in the vicinity of the dam. The core samples were sequestered on 0—5 and 5—10 cm sediment layers. Bottom samples were collected for quantitative and qualitative characterization of benthic macrophytes and macroinvertebrates. Drop video camera transects were used to estimate the coverage of different substrate types and benthic macrophyte species. The spatial distribution of benthic macrofauna species is related to environmental disturbances, including stress caused by organic enrichment (Pearson and Rosenberg, 1978). In this study, macrozoobenthos species were classified in terms of their level of adaptability, feeding type and trophic relations (as used in long-term national monitoring of the Estonian coastal sea) to identify their sensitivity to eutrophication. Three sensitivity categories were used: (a) species typical of highly eutrophic areas; (b) species indicating moderate eutrophication; (c) species attributed to pure sea areas, potentially having the highest sensitivity to eutrophication. The data of benthos mapping is given in Appendix 2.

2.3. Fish

An ichthyological survey was conducted in the spring and autumn seasons. In spring, the survey stations consisted of a series of five monofilament bottom-set gill nets (1.8 × 30 m) with knot-to-knot mesh sizes of 42, 45, 50, 55, 60 mm. Also, one Nordic coastal multimesh gillnet (1.8 × 45 m), consisting of nine 5 m-long sections with knot-to-knot mesh sizes 30, 15, 38, 10, 48, 12, 24 60, 19 mm were added to each station. In autumn, special gill net stations consisting of 38, 40, 42, 45, 50 mm were used to detect the presence and distribution of the sea-spawning whitefish reproduction areas. Net stations were set before sunset and lifted after sunrise with a soaking time of approximately 14—15 hours. Afterwards, the fish were analysed according to the coastal fish monitoring methodology (HELCOM, 2019). Relative fish abundance (CPUE; Catch Per Unit Effort) and biomass (WPUE; Weight Per Unit Effort) in survey stations were calculated for further statistical analysis.

Fish community structure statistical analysis was conducted using ANOSIM based on the Bray-Curtis index of similarity and PRIMER 7v version for marine communities (Clarke and Gorley, 2015). A similarity percentage (SIMPER) analysis was conducted to determine the contribution of each species to the observed dissimilarities in the fish assemblage.

2.4. Numerical simulation

A three-dimensional numerical model, the General Estuarine Transport Model (GETM, Burchard and Bolding, 2002), was used to simulate hydrodynamic conditions (temperature, salinity, sea surface elevation and current velocity) both in the Väike Strait and VAS. GETM solves primitive equations with a built-in vertically adaptive coordinate scheme (Hofmeister et al., 2010; Klingbeil et al., 2018), which significantly reduces numerical mixing in the calculations (Gräwe et al., 2015). To calculate vertical mixing, GETM uses the General Ocean Turbulence Model (GOTM, Umlauf and Burchard, 2005) and the $k-\varepsilon$ scheme (Canuto et al., 2001). Horizontal sub-grid scale mixing is calculated using Smagorinsky parameterization (Smagorinsky, 1963).

A system of nested computational grids was used to model the area of interest: a 1 nautical mile grid for the whole Baltic Sea (Figure 3a), and a grid with a variable horizontal step of 100 m in the wider VAS (Figure 3b) and 25 m inside the Väike Strait (Figure 3c). The large domain Baltic Sea model uses measured sea surface elevation data from Göteborg Torshamnen station and climatological temperature and salinity profiles for Kattegat (Janssen et al., 1999) to calculate the baroclinic water exchange between the North Sea and the Baltic Sea at the open boundaries. A similar approach has been used previously to simulate the overall circulation in the Baltic Sea (Kuprijanov et al., 2021; Liblik et al., 2020). Interpolated hourly results from the coarse-resolution Baltic Sea model are used as a lateral boundary condition for the higher-resolution area.

Initial conditions for the whole Baltic Sea are based on the Copernicus Marine Service reanalysis data for 1 April 2010 and are calculated for 10 years until 31 October 2019, after which the resulting density and fields are used as input for the high-resolution model. ERA5 reanalysis is used as atmospheric boundary conditions (Hersbach et al., 2020). The freshwater input from rivers is based on the dataset prepared for the BMIP project (Gröger et al., 2022) by Väli et al. (2019), consisting of hydrological hindcast and forecast data from the E-HYPE model (Lindström et al., 2010). Parameters were calculated for the period 30 October 2019 to 31 December 2020, and the 3D data were saved as daily means.

Flow in the straits of the VAS is well related to the sea level gradients (Otsmann et al., 2001). For the model validation (see Appendix 1), we compared the simulated sea surface height with the observations in Virtsu at the Suur Strait (see Figure 1 for location). The model captured the sea level variability well ($r^2 = 0.96$, $p < 10^{-6}$, $n = 731$). The root mean square error was 6 cm and the deviation in standard deviation of the simulated and measured sea level was 1.7 cm in the Virtsu station.

To estimate the impact of the dam on water exchange between the GoR and VAS, we use quarterly and annual mean of the share of water that originated from the other side of the dam. For that, we defined salinity at the VAS side of the dam as VAS water mass salinity (S_{VAS}), and salinity at the GoR side as GoR water mass salinity (S_{GoR}). Simulated S_{VAS} was always higher than S_{GoR} in 2020. Thus, when salinity was $\leq S_{GoR}$, water was defined as 100% GoR water mass, and when salinity was $\geq S_{VAS}$, it was defined as 100% VAS water mass. When salinity was between S_{VAS} and S_{GoR}, the share of water masses was estimated linearly.

2.5. Other data

Hourly, 10-m-level wind velocities of ERA5 reanalysis data (Hersbach et al., 2020) were used in the the data analysis. Coastal temperature measurements at Virtsu, provided by the Estonian Environmental Agency, were included in data analysis.

3. Results

3.1. Water column

3.1.1. Circulation and water exchange

We use observational and numerical modelling results of the circulation to determine the impact of the dam on hydrodynamics and water exchange in the strait. Four scenarios were simulated: (DAM) the current situation (dam with 4 m opening); (DAM_28m) one 28-m-wide opening; (DAM_56m) two 28-m-wide openings; and (NO_DAM) natural condition (no dam). The numerical modelling results were validated using current measurements in the narrow channel present in the dam. The simulation results of the two openings scenario are covered in the discussion chapter.

Circulation in the strait is forced by wind and sea level variations. Sea level variability in the area is also related to wind forcing. There was a strong linear correlation between wind stress and daily transport toward VAS at transect T0 (Figure 4a). The best correlation was found using a half-day lag between wind and transport time-series and wind com-

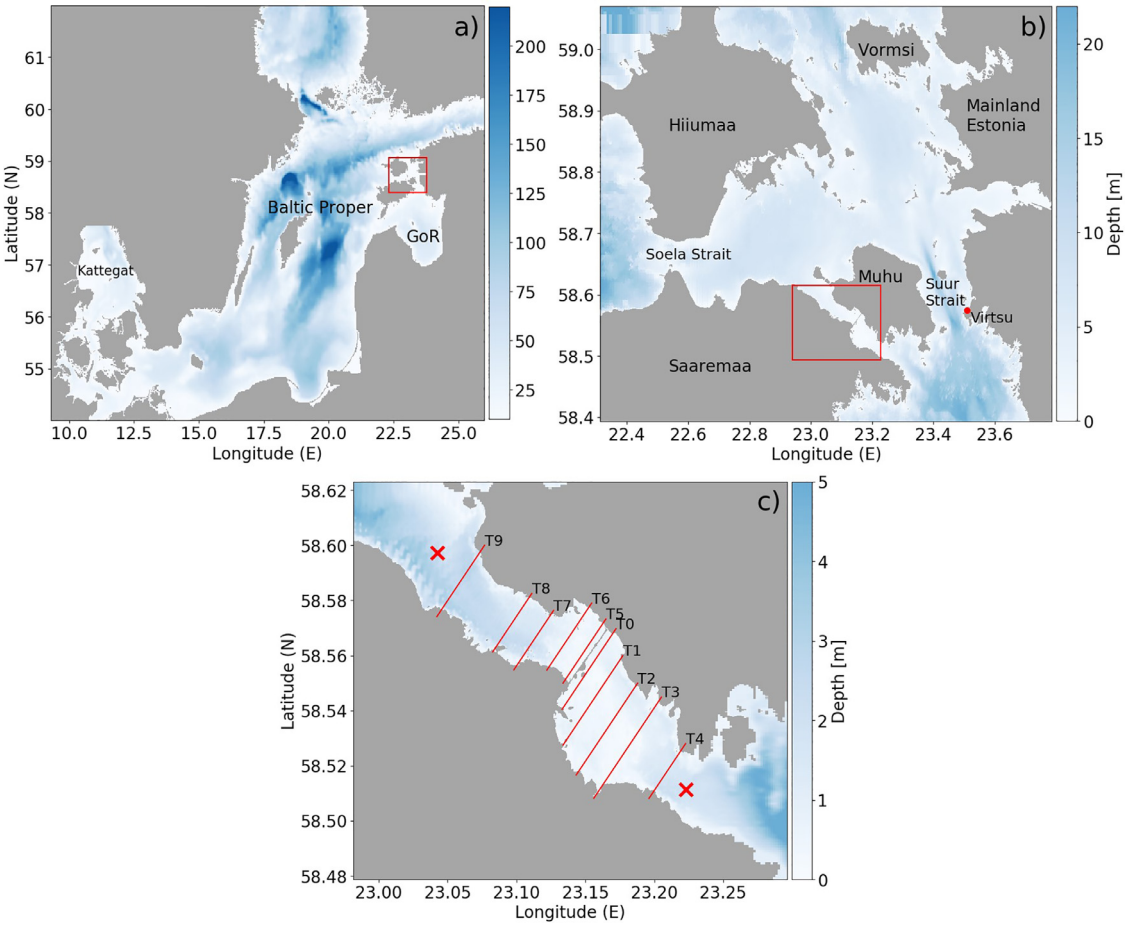

Figure 3 Nested computational grids used in numerical simulation. a) Whole Baltic Sea modelled on a 1 nautical mile grid. b) and c) Väinameri archipelago modelled with a variable horizontal step of 100 m outside the Väike Strait (b) and 25 m inside (c). T0—T9 are transects where transport and water exchange parameters were calculated and the two red crosses mark locations where salinity was determined. (For interpretation of the references to colour in this figure legend, the reader is referred to the web version of this article.)

ponent from SSW ($r^2 = 0.80$, $p < 0.01$, $n = 365$). A strong correlation ($r^2 = 0.72$, $p < 0.01$, $n = 9001$) was also detected between current measurements in the channel and wind component from SSW.

The dam has altered circulation and water exchange in the strait so that nowadays, the strait is divided into two separate bays that are almost isolated from each other. Comparison of the time series at transect T0 of simulated daily transport (Figure 4b) and cumulative transport (Figure 4c) without the dam and with the small existing opening illustrate the marked change: transport is about 100-fold higher in the no-dam situation. Note that in the existing scenario, transport through the 4 m channel is even smaller than it might be since most of the water (that passes the T0 transect) does not flow through the channel, but converges/diverges next to the dam and can be seen as high/very low water level. Transport shows seasonality related to wind forcing: flow from the GoR to VAS prevails from February to mid-March and from mid-September to the year-end (Figure 4b), with the opposite flow direction prevailing from mid-March to May. Mean annual transport without a dam is 1.2×10^6 m^3 day^{-1} toward VAS while in the last quarter of the year, it is 11×10^6 m^3 day^{-1} to the same direction. However, due to the oscillatory nature of the currents, daily transport would be much higher if the direction of flow was not considered: annual mean transport without dam would be 18×10^6 m^3 day^{-1}. More intense transport would have occurred in the last quarter (26×10^6 m^3 day^{-1}) and more modest in the second quarter (8×10^6 m^3 day^{-1}). Daily transport would have been often in the order of the volume of the strait, which is approximately 40×10^6 m^3. The latter indicates that total water exchange in the strait within one day would be quite common if it was not blocked by the dam.

To assess the impact of the dam on different parts of the strait, we compared water volume (Q), residence time (t), and residence time per volume (t_v) for 10 areas between transects T0—T9 and the dam (Figure 3c, Table 1). In the without dam case, t_v is of the same order in all areas (53—57 d km^{-3}), illustrating the natural water exchange regime through the strait. With the dam, t_v increases in all areas, with the greatest impact near the dam (t_v is 10—12-fold higher) and lesser impact away from the dam (50—100% increase in t_v).

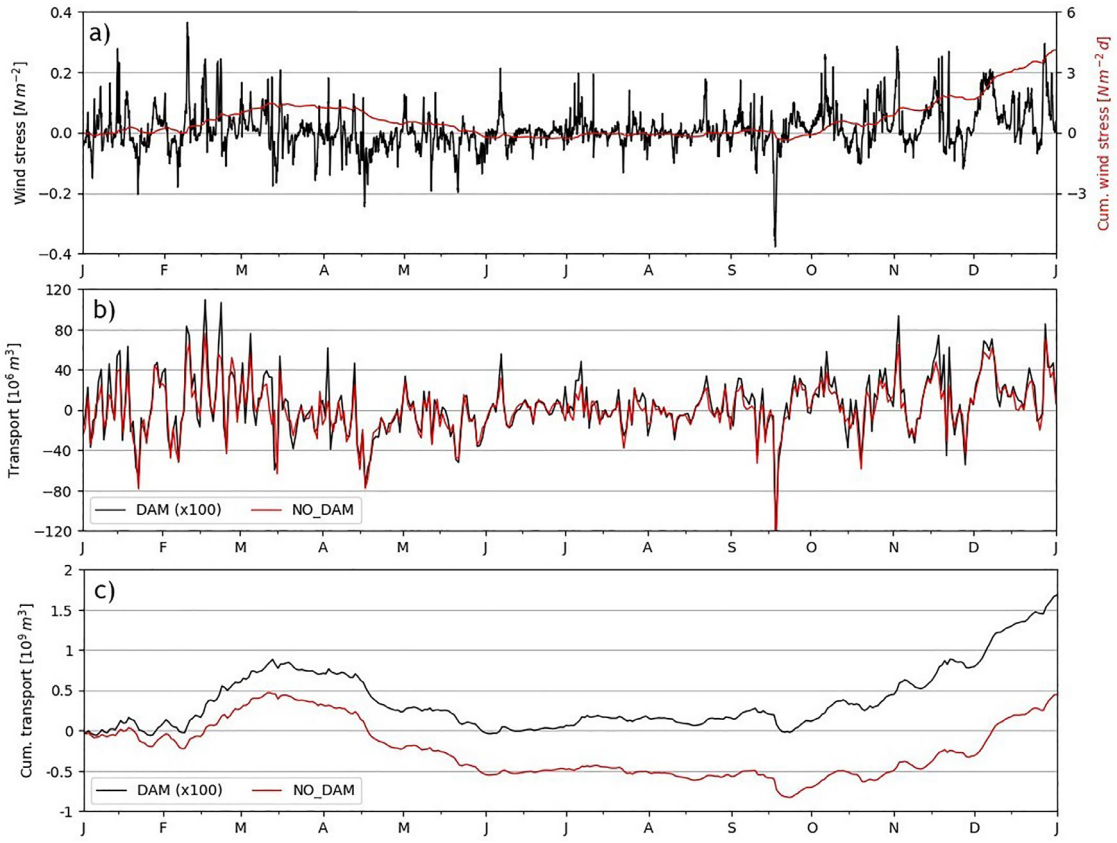

Figure 4 Wind stress from ERA-5 reanalysis data, transport and cumulative transport from GETM in 2020. Simulated transport and cumulative transport through transect T0 (see Figure 3c). Time-series DAM represents the present situation and NO_DAM the natural situation (without dam). Note that DAM time-series has been multiplied by 100.

Table 1 Comparison of transport (Q), residence time, and residence time per volume in areas between transects for the present (with dam) and natural (without dam) scenarios in the GETM simulation. Transect locations are shown in Figure 3c.

With dam	Dam-T0	T0-1	T1-2	T2-3	T3-4	Dam-T5	T5-6	T6-7	T7-8	T8-9
Q [m^3 s^{-1}]	24	64	91	109	107	17	53	98	133	132
Residence time [h]	6	8	8	6	13	4	5	8	9	29
t_V [day km^{-3}]	476	181	127	106	108	692	217	118	87	87
Without dam	**Dam-T0**	**T0-1**	**T1-2**	**T2-3**	**T3-4**	**Dam-T5**	**T5-6**	**T6-7**	**T7-8**	**T8-9**
Q [m^3 s^{-1}]	207	208	209	215	220	205	207	214	216	215
Residence time [h]	1	2	3	3	6	< 1	1	3	6	18
t_V [day km^{-3}]	56	56	55	54	53	57	56	54	54	54
	Dam-T0	**T0-1**	**T1-2**	**T2-3**	**T3-4**	**Dam-T5**	**T5-6**	**T6-7**	**T7-8**	**T8-9**
Area [m^2]	2469500	5910800	7132700	6865900	8435700	895900	3744500	3379400	4536400	11514100
Volume [m^3]	496900	1732000	2456300	2347400	5096400	232900	887100	2644600	4510200	13607900

To investigate water mass spreading from the GoR to the VAS and *vice-versa*, a quarterly and annual mean share of water mass in different parts of the strait are shown in Figure 5 for the four simulation scenarios. Under present-day conditions, GoR water mass is clearly distinguishable on the VAS side of the Muhu Island coast near the dam opening in the first and fourth quarters (DAM scenario in Figure 5), with a small showing to the opening on both sides of the strait in the second and third quarters. That the small 4-m-wide opening has such a large impact is somewhat surprising but can be explained by high hydrodynamic activity. The strong back-and-forth oscillating current through the opening continuously mixes the two water masses. In the case without the dam (NO_DAM in Figure 5), there is no strong front at the dam location: GoR water penetrates more into the VAS in the first and fourth quarter, and VAS water occupies the southeast part of the strait in the second and third quarter.

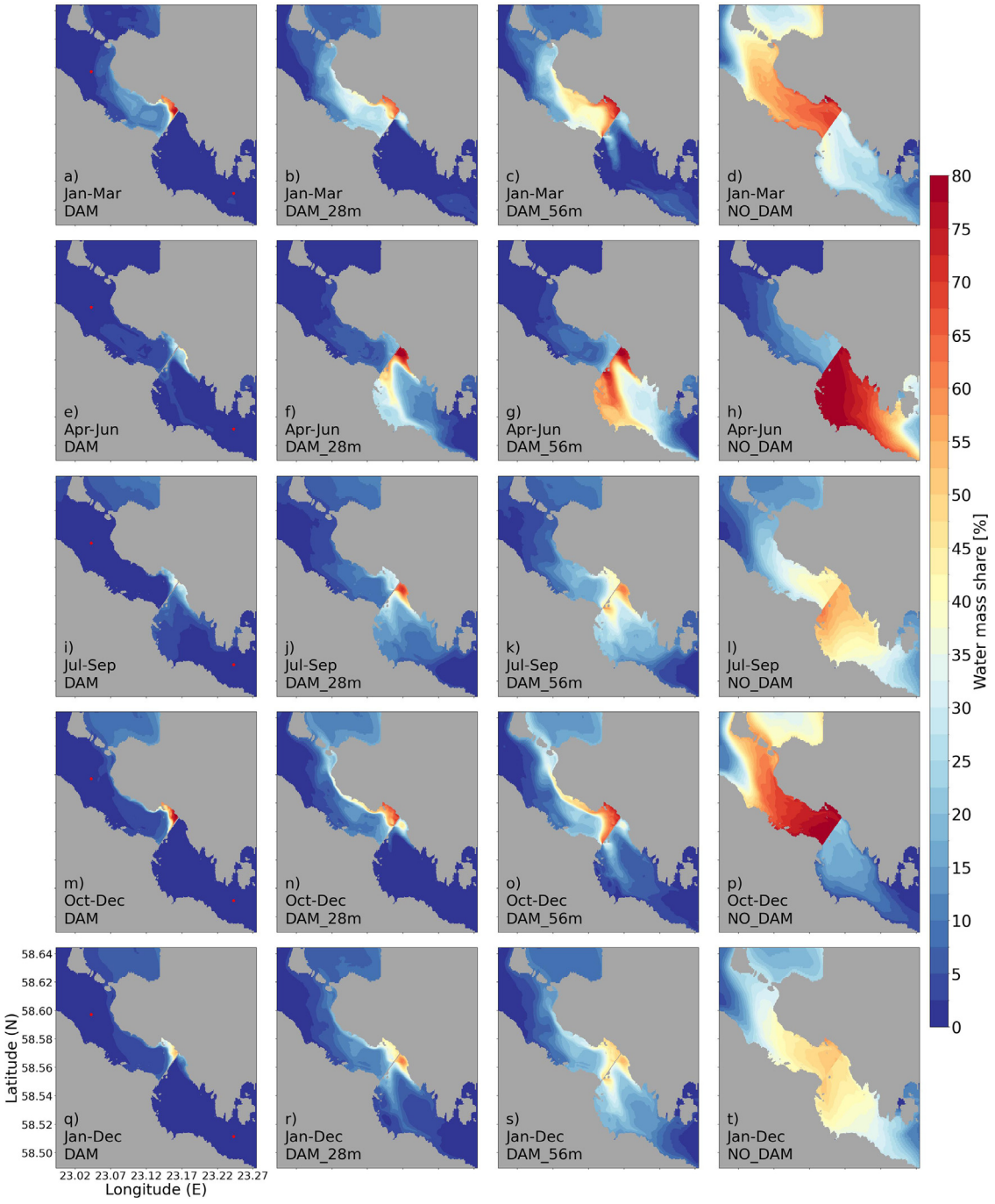

Figure 5 Comparison of water mass share under different scenarios in the GETM simulation. (a, e, i, m, q) DAM is the present (dammed) situation; (b, f, j, n, r) DAM_28m has one new 28-m-wide opening; (c, g, k, o, s) DAM56m has two 28-m-wide openings; and (d, h, l, p, t) NO_DAM has no dam. Quarterly and annual means for 2020 are presented for each scenario. The values represent the share of water mass that origins from the opposite side of the dam, e.g., 25% in the Väinameri Sea part of the strait shows that 25% of the water originates from the Gulf of Riga.

3.1.2. Spatial patterns of hydrography and biogeochemical variables

Horizontal temperature gradients, warmer near the dam and colder toward offshore, were observed in the surveys of June 2020 and May 2021 (Figure 6). These surveys were preceded by a warming period due to atmospheric heat flux. Opposite gradients (warmer offshore and colder near the dam) were observed in December 2020 (Figure 6). The phenomenon is partly natural, as shallower areas warm and cool faster, but the magnitude of the warming/cooling is probably exacerbated by the water exchange blocking effect of the dam. Complete water renewal in the strait in the case of the typical low-passed current velocity of 20 cm s^{-1} along the axis of the strait, would occur in 28 h.

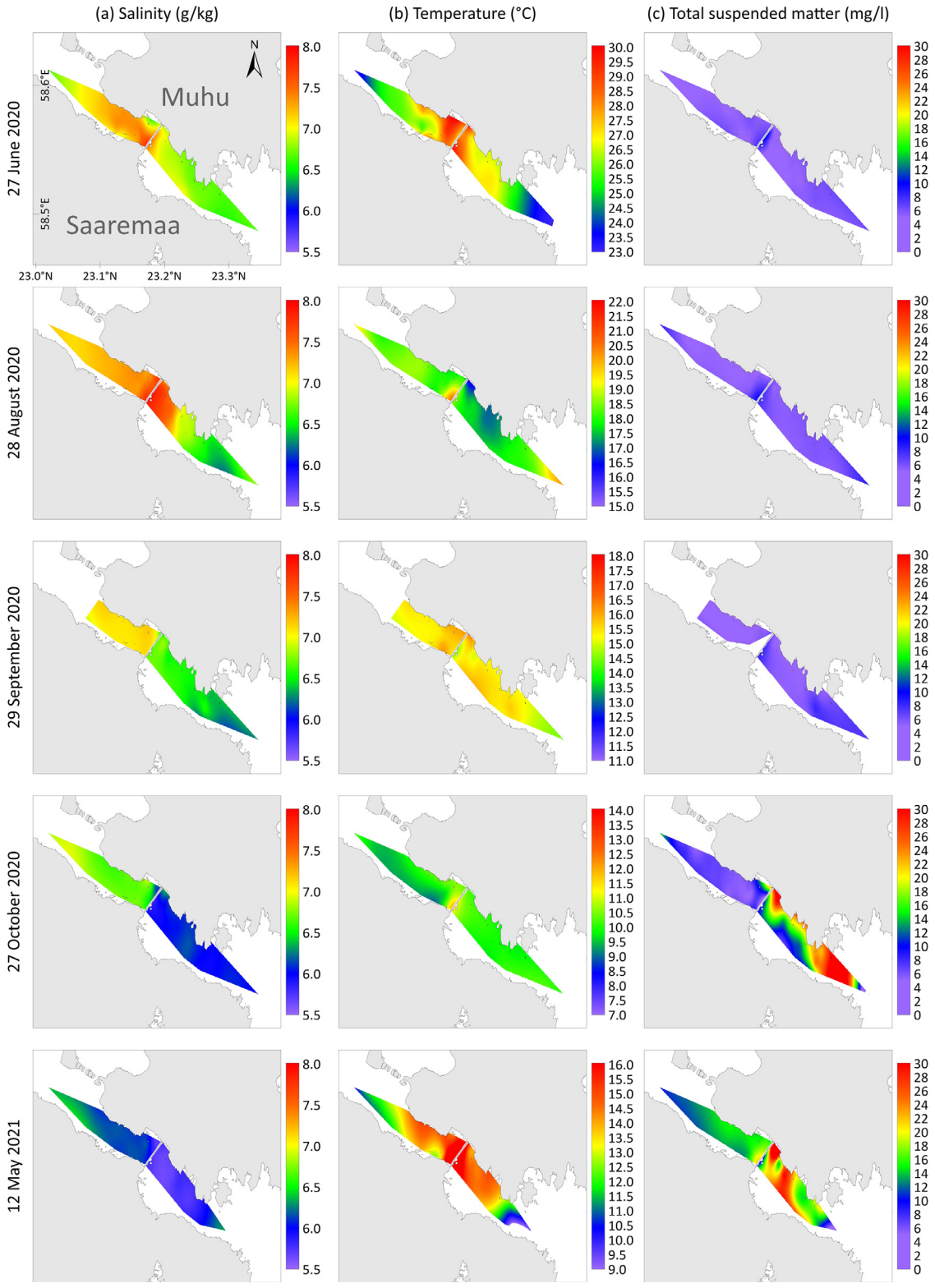

Figure 6 Salinity (a), temperature (b) and suspended matter (c) concentration observations in Väike Strait for five dates between June 2020 and May 2021.

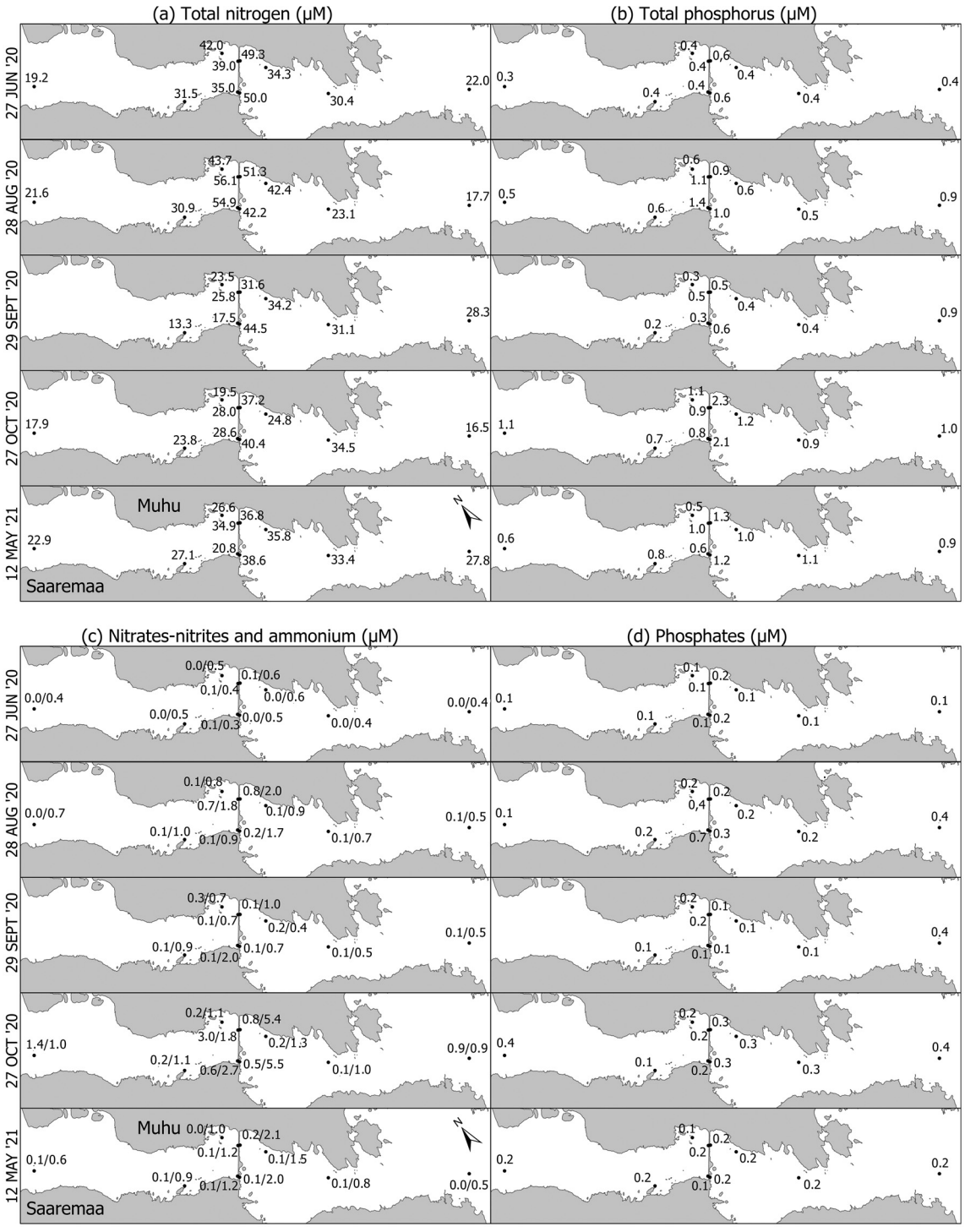

Figure 7 Observed element concentrations in the surface layer of Väike Strait for five dates between June 2020 and May 2021. (a) Total nitrogen; (b) Total phosphorous; (c) Nitrates-nitrites and ammonium; (d) Phosphates. Note that the map is tilted (north direction marked in bottom left).

Thus, even if high/low-temperature water was occasionally present in the strait without the dam, it would be rapidly flushed offshore.

Overall sea surface salinity in the strait is determined by saltier water in the VAS and fresher water in the GoR. This difference in salinity between GoR and VAS waters is observed in the strait in September and October 2020 (Figure 6). The role of the dam in impeding the horizontal mixing of the two water masses is clear (Figure 6), although, a small area of fresher GoR water can be often observed on the other side of the dam near the 4-m-wide opening. The general salinity pattern in the strait is af-

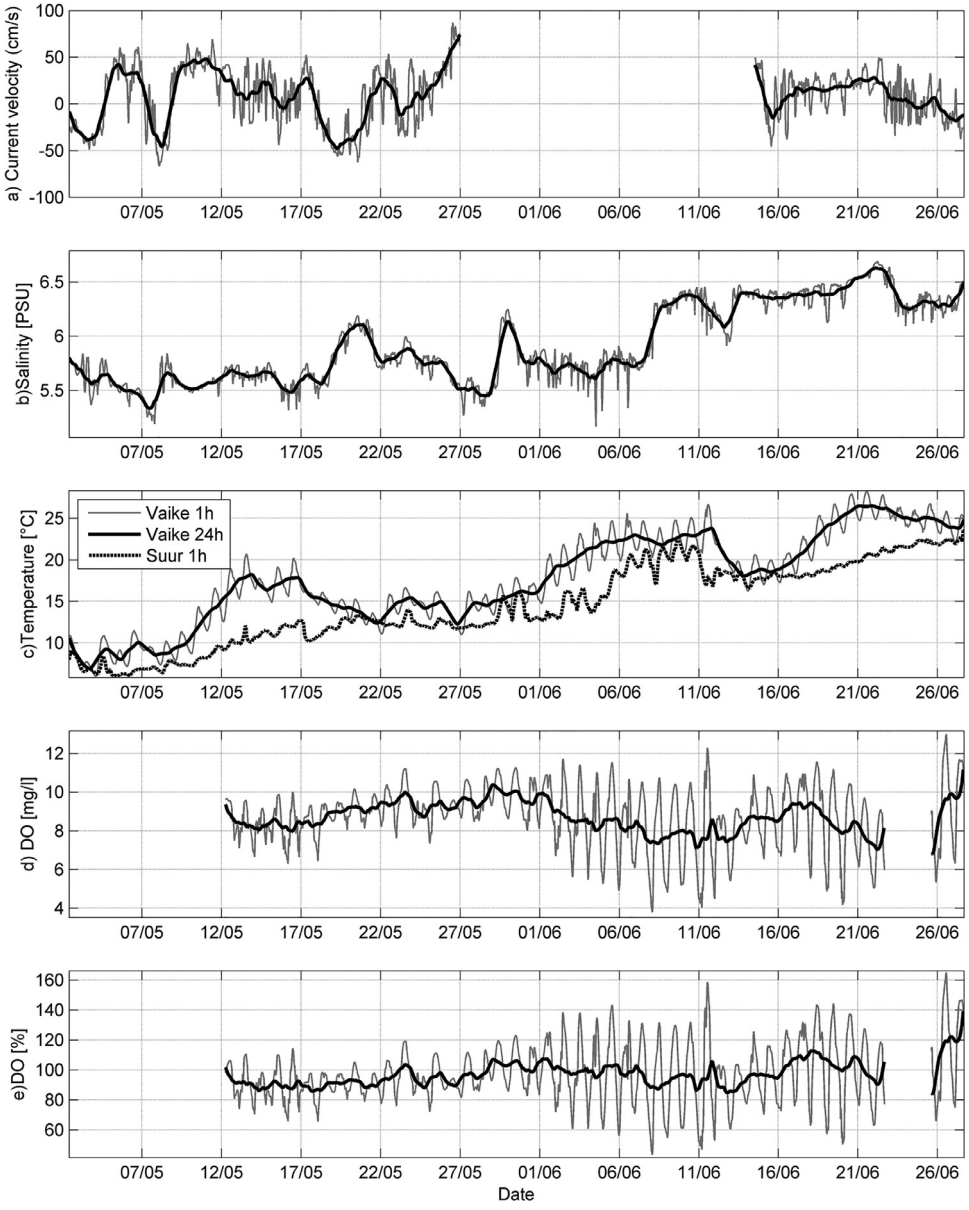

Figure 8 Time series of current velocity, salinity, temperature, dissolved oxygen (DO) concentration and saturation level measured below the dam (at station 32, see Figure 2 for location) from 5 May—27 June 2021. The temperature was also measured at the Suur Strait in Virtsu. Positive current velocity values show flow toward the Väinameri Archipelago Sea.

fected by local freshwater fluxes in summer and spring. Exceptionally high surface salinity (for the eastern Baltic Sea region, >7.5 PSU) was observed near the dam in June and August 2020, with lower salinity in the outer parts of the strait, toward the GoR (6.8—7.0 PSU) and VAS (6.2—6.5 PSU) (Figure 6). Evaporation is the likely cause of the localized salinity maximum in the shallow area. The opposite situation prevailed in May 2021, with fresher water observed near the dam compared to offshore areas of the strait (Figure 6). This is related to the seasonal terrestrial freshwater runoff maximum in spring, and precipitation in the days before the survey. Thus, weak horizontal exchange and mixing can lead to local salinity maxima/minima near the dam in the presence of evaporation and local freshwater fluxes. Such a phenomenon would hardly be seen if there was no dam.

The restricted water exchange due to the dam also impacts nutrient fields. High values of total nitrogen are observed near the dam in all surveys, compared to water at either end of the strait, particularly in summer (Figure 7a). The high total nitrogen values are mostly related to high organic nitrogen contribution that is probably the combined outcome of intense benthic primary production and weak water exchange near the dam. Total phosphorus is more variable, but still shows a tendency of higher values near the dam (Figure 7b). NH_4 values are of the same order (0.3—0.6 μM) in the whole study area in June (Figure 7c), but there are higher values (0.7—2.0 μM) near the dam in August and September, and even higher in October and December (1.8—5.5 μM and 2.8—9.0 μM, respectively). Such high values of NH_4 are not common in the eastern Baltic and can probably be linked to the intense decomposition of organic material.

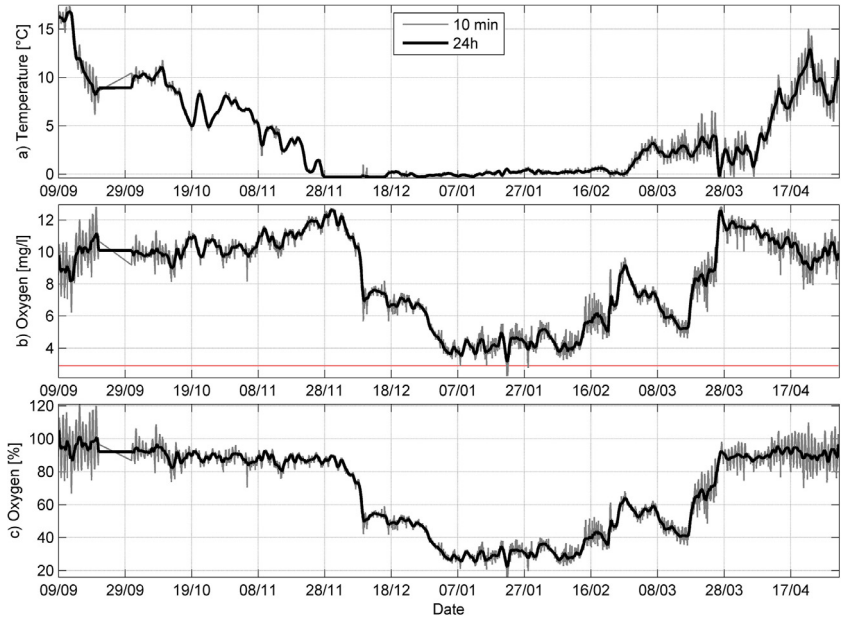

Figure 9 Time series of temperature and DO concentration and saturation level measured below the dam (at station 32, see Figure 2 for location) from 9 September 2021 to 1 May 2022. Red horizontal line in the middle panel shows the level of hypoxia (2.9 mg l^{-1}).

Nitrates-nitrites (NO_3+NO_2) and phosphates (PO_4) are very low in spring, June, and September (Figure 7c,d), which is a sign of intense primary production. Somewhat elevated values are observed in August and October, and the highest values in December. In conclusion, high concentrations of total nitrogen, phosphorus and ammonium support the physical parameters observations that indicate the impact of weak water exchange near the dam.

The dam also impacts wind waves as propagation is blocked by the dam. This in turn is reflected in the intensity of bottom sediment resuspension and suspended matter concentration in water. Suspended matter concentration is around 5—8 mg l^{-1} (Figure 6) in the whole strait in June, August and September 2020 when relatively calm conditions prevailed prior to the survey. Higher concentrations are observed in the GoR side of the strait in October 2020 (10—38 mg l^{-1}) and May 2021 (15—42 mg l^{-1}), with considerably lower concentrations in the VAS part (Figure 6). These two surveys were preceded by southerly winds of 5—10 m s^{-1} that generated waves and caused resuspension of sediments in the GoR part of the strait; resuspension did not occur in the VAS part as waves were blocked by the dam. Thus, the dam alters patterns of water transparency and sediment transport in the strait.

3.1.3. Temporal variability

Measurements recorded in the mooring station (station 32) at the 4 m dam opening in May—June 2020 and in September 2021 to 1 May 2022 show high temporal variability (Figs. 8 and 9). Positive current velocities (showing flow toward VAS) bring fresher water to the area, while the opposite flow is associated with increased salinity, with a trend of increasing salinity over the survey period. The latter coincides with a warming event, and thus is likely related to evaporation. Warming and cooling events are more rapid in Väike Strait compared to Suur Strait, which again highlights the effect of shallowness and weak water exchange in the Väike Strait. The observed diurnal temperature amplitude of 3—4 degrees is common in the strait in summer, although it is occasionally as high as 6 degrees. A very strong diurnal cycle in dissolved oxygen (DO) occurs in spring and summer; highly oversaturated values in the daytime alternate with low values (down to 4 mg l^{-1}) at night (Figure 8). The high daytime values are related to intense photosynthesis both in benthos and pelagial, and low nighttime values to respiration. The diurnal cycle was smaller during periods of lower solar radiation (not shown), e.g., from 17 May to 22 May 2021, when water temperature decreased. The strongest amplitude, up to 7—8 mg l^{-1} is during periods of strong solar radiation and warming of the water.

The diurnal cycle of temperature and oxygen weakens in autumn and gradually strengthens again in spring (Figure 9). From mid-October the oxygen content remains below saturation level, dropping to approximately 50% in early December, about one week after the first ice formation, and about 30% in early January. DO concentration ranges between 3—5 mg l^{-1} in the 1.5 month period to the end of February, and occasionally reaches hypoxia levels (2.9 mg l^{-1}).

3.2. Biota and sediments

3.2.1. Sediments

Samples collected near the dam contain a larger proportion of fine sediments, mostly aleurite, but also clay. The highest proportion of fine sediments is found in deeper layers (5—30 cm) of stations V30 and V31 (76% and 48%, respectively), with the surface layer of these stations also relatively high (44% and 36%, respectively). The other four stations have a lower proportion of fine sediments (6—18%). The higher fine sediment levels near the dam are probably a

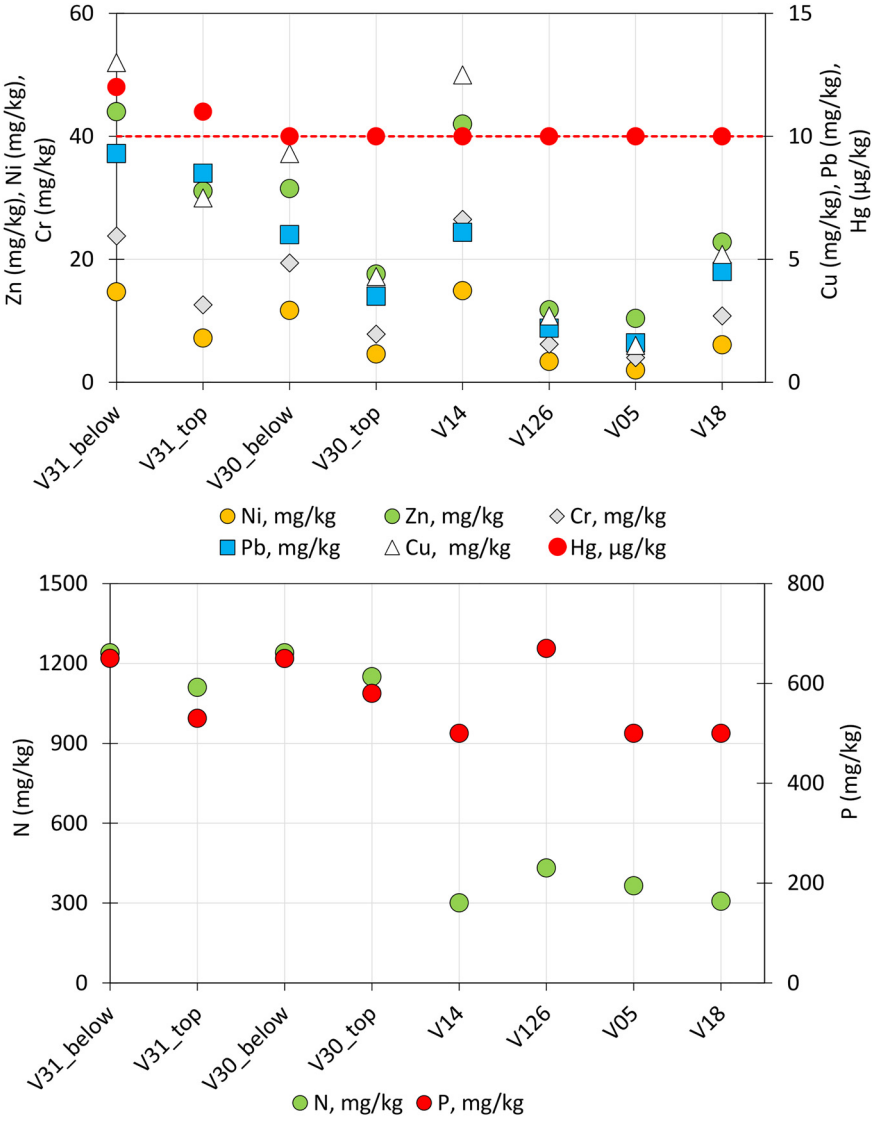

Figure 10 Heavy metals (a) and total nitrogen-phosphorus (b) concentrations in sediments. Red line marks the detection limit of Hg. The sediment top layer ("top") 0—5 cm and subsurface layer ("below") 5—10 cm are shown for stations V31 and V30. Station locations are shown in Figure 2. (For interpretation of the references to colour in this figure legend, the reader is referred to the web version of this article.)

consequence of low hydrodynamic activity and high organic matter production.

High organic matter production and sedimentation near the dam are also supported by the total nitrogen concentration in sediments. Sediments on both sides of the dam have total nitrogen concentrations of 1240 mg kg^{-1} and 1110—1150 mg kg^{-1} in the surface and deeper layer, respectively, i.e., 3—4 fold higher than in the stations farther from the dam (Figure 10). This trend was not seen in total phosphorus concentrations that are of the same order near and farther from the dam (Figure 10).

In terms of hazardous substances, heavy metals and polycyclic aromatic hydrocarbons (PAHs), no severe contamination of sediments was detected, but the highest concentrations were in the two stations near the dam (Figure 10). The highest heavy metal concentrations of the two stations near the dam are found in the deeper layer and on the GoR side of the dam. Higher values are also detected at station V14 in the GoR side. Concentrations are lowest at stations V126 and V05, and slightly higher at V18. The latter could be related to the fishing harbour in the vicinity of station V18. The only station where PAHs are higher than the detection limit (0.16 mg kg^{-1}) is at station V31 near the dam on the GoR side where the sum of 16 PAHs is 0.81 mg kg^{-1} and 1.27 mg kg^{-1} in deeper and surface layers, respectively.

3.2.2. Phyto- and zoobenthos

The phytobenthos community in the shallow area near the dam mostly comprises an annual charophyte population, sporadically occurring in combination with angiosperm plant species (Figure 11). The share of perennial species in the phytobentos community is higher further from the dam. At the end of the vegetation season, a large amount of detritus comprising remnants of annual phytobenthos settle at the bottom. The decomposition process of this substance probably causes the observed oxygen depletion

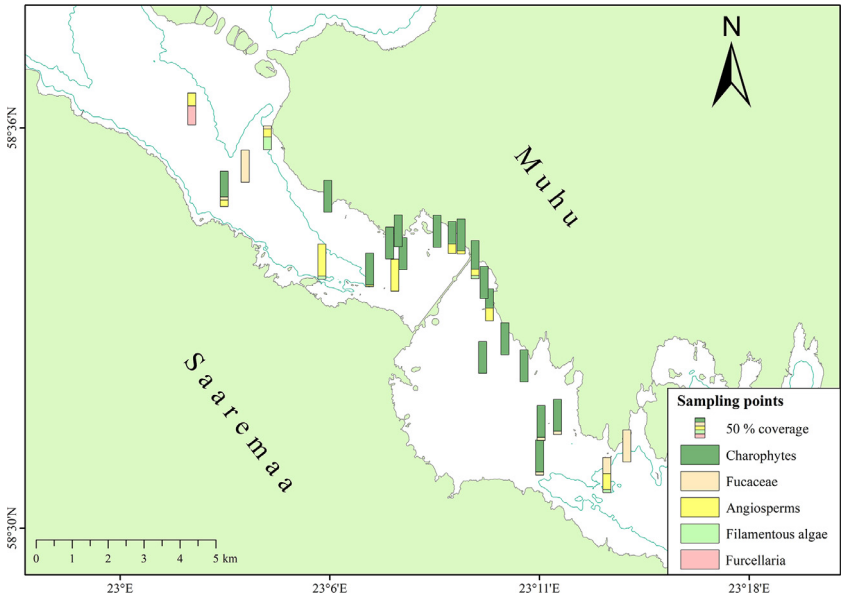

Figure 11 Phytobenthos communities in the study area.

in winter. High productivity and decomposition combined with low hydrodynamic activity have led to the formation and development of a thick mud layer in this area. The zoobenthos community is more diverse in the VAS side of the strait, with 24 zoobenthos species compared with 16 species on the GoR side. The zoobenthos community is dominated by species characteristic of moderately eutrophic water bodies. However, eight species that are typical of non-eutrophic marine areas are present on the VAS side, with only four detected on the GoR side.

3.2.3. Fish

In total, 15 fish species were caught during the autumn and spring survey. Freshwater species such as percids and cyprinids dominated both areas. Marine species such as clupeids and flounder (*Platichthys* sp.) were more present in saltier waters of the VAS.

The structure of fish assemblages (calculated on the basis of CPUE of species) was not statistically significantly different between the stations situated at the opposite sides of the dam (R=0.25; P=0.333). Low Bray-Curtis similarity value (21.86) between fish assemblages in GoR and VAS areas mainly resulted from variation in the abundance of perch (*Perca fluviatilis*) and bleak (*Alburnus alburnus*). Also, no statistically reliable difference was detected between the fish assemblage structures (calculated on the basis of WPUE of species (R=0.25; P=1.00) of GoR and VAS areas. In this case, the low Bray-Curtis similarity value (17.14) was essentially based on inter-area variation in abundances of perch and ide (*Leuciscus idus*).

The spawning areas of the sea-spawning whitefish (*Coregonus widegreni*) were found in both GoR and VAS areas during the autumn survey. This species was once one of the main targets in local fisheries but suffered a drastic decrease in abundance during the twentieth century caused mainly by overfishing, eutrophication and restricted access to spawning areas (Verliin et al., 2013).

Fish kills caused by extreme sea level fluctuations have been observed near the dam. Likewise rapid temperature rises during warm summers could cause fish kills near the dam.

4. Discussion

The dam has totally changed the hydrodynamics, water and substance exchange regime in Väike Strait. The simulation results suggest the strait was hydrodynamically active with strong currents and rapid water exchange prior to dam construction. The nearby Suur Strait provides a good analogue for the undammed situation. Suur Strait is characterized by strong currents (Suursaar et al., 2001) and the front separating GoR and VAS waters is very mobile (Astok et al., 1999), with a more intense mixing of the two water masses. The simulation results suggest water exchange in Väike Strait would be 10—12 fold faster without the dam and, with favourable conditions, water could exchange in the whole strait within a day. Today, instead of a natural strait with strong currents, two separate bays have been formed with relatively long water residence time. The impeded horizontal water exchange allows other processes, such as atmosphere and sediment fluxes, to have a relatively higher impact on the water characteristics of the strait. As a result, thermal, hydrological, biogeochemical and ecological regimes in the strait have altered, with the highest magnitude impacts closer to the dam.

More rapid warming and cooling events were observed in Väike Strait compared to the neighbouring Suur Strait. This effect is strongest near the dam, since the innermost parts of bays are the most isolated from water exchange with the open sea and are more dependent on air-sea fluxes, as has been observed in other semi-enclosed bays and fjords (Ding and Elmore, 2015; Veneranta et al., 2016). A large diurnal cycle of sea temperature was observed, occasionally up to 6°C, which is characteristic of shallow seas with limited water exchange (e.g., Beck et al., 2001). The amplitude of the diurnal temperature cycle in shallow coastal areas of the Baltic Sea has not been rigorously studied, how-

ever, our observations in the Suur Strait illustrate that other straits of the VAS do not display such large diurnal ranges.

Similar to temperature, oxygen levels also display a large diurnal cycle in Väike Strait, with the amplitude occasionally up to 6 mg l^{-1} and a saturation range of 50—140% observed near the dam. Diurnal oxygen cycles, caused by primary production during daytime and respiration and decomposition of organic material at night, with even greater magnitude have been documented in several shallow, eutrophic estuaries (Beck et al., 2001; D'Avanzo et al., 1996). In most of the Baltic, the diurnal cycle is much weaker than in Väike Strait due to water exchange and vertical mixing (Wesslander et al., 2011), and sea surface oxygen concentration does not drop significantly below saturation level. Our nighttime low oxygen observations of 0.1—0.5 m (depending on sea level) show that the air-sea oxygen flux is weaker than the oxygen consumption by respiration: this can be explained by very shallow bottom depth (0.5—1 m) near the dam and extensive benthic macrophyte coverage. The process can lead to diel hypoxia, as has been observed in other shallow marine areas (Bas-Silvestre et al., 2020; Beck et al., 2001; Tyler et al., 2009). Tyler et al. (2009) noted that nighttime hypoxic events are longer when sea temperature and daily solar insolation were higher in the previous day. Indeed, the diurnal oxygen cycle in the Väike Strait was much smaller when the weather was colder and cloudy and the sea surface temperature decreased.

Our wintertime observations revealed oxygen depletion, with concentration below 5 mg l^{-1} and occasional hypoxia (2.9 mg l^{-1}) during a 1.5 month period. Our measurements were conducted in an area that is relatively hydrodynamically active, in the small dam opening, so hypoxia could have been much worse in shallower and more remote parts of the strait (see the aerial photo in Figure 1). Hypoxia and anoxia are well-known issues in the open Baltic Sea (Carstensen et al., 2014; Liblik et al., 2018; Savchuk, 2010). Strong stratification is one of the primary obligatory conditions for oxygen depletion in the open sea, and it has also been found to be important for local, coastal hypoxia in archipelagos and enclosed bays (Dietze and Löptien, 2021; Karlsson et al., 2010; Virtanen et al., 2019; Virtasalo et al., 2005). These sites are often isolated from the open sea by topographical features (Virtanen et al., 2019) and are deep enough for seasonal thermocline formation, which impedes vertical mixing and downward transport of atmospheric oxygen. Väike Strait is very shallow (see Figure 1), particularly near the dam, thus, stratification does not play any role in oxygen deficiency here. Oxygen depletion in shallow, well-mixed areas with poor water exchange has been documented (Hsieh et al., 2021; Knight et al., 2013; Verity et al., 2006) and often eutrophication is at least partly responsible for the high oxygen consumption. Väike Strait is affected by eutrophication (Stoicescu et al., 2018), but the 10—12-fold increase in water residence time due to the dam is likely the primary reason for oxygen depletion. In other straits in the VAS such oxygen depletion has not been reported in the literature, and national monitoring data show no sign of hypoxia. Another potential contributor to low winter oxygen in Väike Strait is ice coverage, which impedes air-sea fluxes. Without the dam, the strait would, from time to time, be flushed through by oxygen-saturated water from the VAS or GoR. The low oxygen level results in various negative impacts on marine life (Breitburg, 1994; Gallo et al., 2020; Hansen et al., 2002; McCormick et al., 2022; Orio et al., 2022; Roman et al., 2012).

The results show the dam also has local impacts on salinity and nutrient fields. The dam separates the fresher and higher-nutrient-content waters of the GoR and saltier and lower-nutrient-content waters of the VAS (Astok et al., 1999; Stoicescu et al., 2018). We observed high salinity (up to 8 g kg^{-1}) near the dam in summer and while high surface salinity is common in the western Baltic Sea (Karlson et al., 2016), it is not common in the eastern Baltic. The only process that could cause such a high salinity in this area is evaporation. Indeed, we observed elevated salinity only during summertime and particularly high levels after warm periods. The fate of the higher salinity water remains unclear. If it is transported to the GoR, it could form a buoyant subsurface, submesoscale salinity maxima layer within the seasonal thermocline, as it has been observed in the open GoR (Liblik et al., 2017).

Another consequence of the low water exchange in Väike Strait is the high nitrogen content near the dam. Thus, instead of the low concentrations in waters of the VAS and high concentrations in the GoR expected from the literature, the nutrient (and salinity) field rather showed strong spatial maxima near the dam. This could cause certain macroalgae species domination (Valiela et al., 1997). Indeed, the shallow area near the dam is mostly covered by dense communities of annual charophytes. Intense charophyte production culminates in a large amount of detritus, which forms muddy bottoms, as observed near the dam.

Sediments on both sides of the dam have total nitrogen 3—4 fold higher than in the stations farther from the dam. This tendency was not seen in total phosphorus concentrations. This discrepancy could be related to the samplings done from upper and active unconsolidated sediments and a high total nitrogen level represented in the water column. The high total nitrogen in the water column could be explained by emissions from road traffic. Elevated concentrations of nitrogen dioxide at a roadside and its contribution to plant nutrition has been documented (Cape et al., 2004; Xu et al., 2019). Another explanation could be related to the dominant species of phytobenthos, charophytes, which are known as good total phosphorus accumulators. Isotopic compositions should be determined to test these hypotheses.

Elevated heavy metal and PAHs concentrations in sediments near the dam are likely related to transport on the dam road. On average, 3100 vehicles a day pass the dam according to statistics provided by Estonian Transport Administration (https://www.mnt.ee/sites/default/files/lisa_10_liiklussagedus_pohi-_ja_tugiteedel.pdf, accessed 28.02.2022). Car traffic is one of the main sources of heavy metals and PAHs in urbanized areas (Adamiec et al., 2016; Men et al., 2018), with pollution coming from exhaust gases, and from wear of tires, brakes and other car parts (Yuen et al., 2012).

According to the information from local residents, some freshwater species — mainly cyprinids — are able to migrate through the dam using the small opening near Muhu Island. However, it is very unlikely, that schools of marine species as clupeids and garfish (*Belone belone*) important to local

fisheries can navigate through that narrow and vegetation-rich channel. There are some historical sources from the beginning of the twentieth century indicating that soon after the dam was completed, a significant decrease occurred in herring and whitefish catches in the Väike Strait area (Pettai, 1984).

In the context of the goals and ecological objectives of the Baltic Sea Action Plan and keeping in mind the criteria/descriptors of the frame of the Marine Strategy Framework Directive, particularly criteria of the descriptor D7 (hydrographical conditions, Friedland et al., n.d.), we can conclude the dam has led to considerable deterioration of ecological conditions in the strait.

Our simulations examined the impact of adding one or two new 28-m-wide openings to the dam. The simulation results suggest that adding two new openings would alleviate the impact of the dam, with water exchange near the dam improving by 45% on the VAS side and 32% on the GR side. Likewise, the share of water masses that originate from the opposite side of the strait would considerably increase, both in the case of one and two new openings (Figure 5, scenarios DAM_28m and DAM_56m, respectively). Improved water exchange and share would lead to reduced diurnal cycles of temperature and salinity. Likely, the spatial maximum of salinity and temperature near the dam would be weaker during warming periods in summer. Likewise, the spatial maximum of total nitrogen near the dam would be weaker.

Openings would also enhance fish migration between the two parts, allowing different species to access more suitable feeding or spawning areas and reducing the risk of potential genetic isolation in fish populations. Also, it would reduce the probability of fish kills caused by extreme sea level fluctuations or rapid temperature rises during warm summers. As the spawning grounds of sea-spawning whitefish were present in both GoR and VAS areas, there is no cause to expect a decrease in the quality of spawning habitat after adding the new wider openings to the dam.

5. Conclusions

The dam in Väike Strait has considerably weakened water exchange and deteriorated ecological conditions. Since advection is weakened, vertical processes including exchange with atmosphere and sediments have a relatively greater role in shaping water characteristics. Consequently, occasional very high sea surface temperature, salinity, total nitrogen and total phosphorus values, and strong diurnal cycle in water temperature and dissolved oxygen were observed near the dam in summer. Oxygen levels were continuously below saturation in winter and concentration occasionally dropped to hypoxic levels with the presence of ice cover. The dam also alters sea level, wind wave and suspended matter pattern dynamics in the strait. Elevated concentrations of total nitrogen and hazardous substances in sediments were detected near the dam, along with dense beds of annual algae. The dam impedes fish migration between suitable feeding and spawning areas. The construction of two 28-m-wide openings would alleviate the negative impacts of the dam.

In conclusion, we suggest consequences of blocking water exchange should be considered in similar environments. Alleviation of negative impacts of existing dams is possible by the construction of bridges (openings).

Acknowledgements

This work was supported by the Estonian Research Council (grant no. PRG602). The study was partly financed by the Estonian Environmental Investment Centre (project number 17513). The GETM community at the Leibniz Institute of Baltic Sea Research is gratefully acknowledged for maintaining and developing the model code. The allocation of computing time on the HPC cluster by the TalTech is gratefully acknowledged.

Declaration of competing interest

The authors declare that they have no known competing financial interests or personal relationships that could have appeared to influence the work reported in this paper.

Supplementary materials

Supplementary material associated with this article can be found, in the online version, at https://doi.org/10.1016/j.oceano.2023.06.002.

References

Adamiec, E., Jarosz-Krzemińska, E., Wieszała, R., 2016. Heavy metals from non-exhaust vehicle emissions in urban and motorway road dusts. Environ. Monit. Assess. 188, 1—11. https://doi.org/10.1007/S10661-016-5377-1/FIGURES/7

Altunkaynak, A., Eruçar, S., 2020. Physical experimental investigation of the horizontal water flow patterns in the Golden Horn under different scenarios with the presence of various structures. Ocean Eng. 215, 107837. https://doi.org/10.1016/J.OCEANENG.2020.107837

Astok, V., Otsmann, M., Suursaar, Ü., 1999. Water exchange as the main physical process in semi-enclosed marine systems: the Gulf of Riga case. Hydrobiologia 393.

Bas-Silvestre, M., Quintana, X.D., Compte, J., Gascón, S., Boix, D., Antón-Pardo, M., Obrador, B., 2020. Ecosystem metabolism dynamics and environmental drivers in Mediterranean confined coastal lagoons. Estuar. Coast. Shelf Sci. 245, 106989. https://doi.org/10.1016/J.ECSS.2020.106989

Beck, N.G., Fisher, A.T., Bruland, K.W., 2001. Modeling water, heat, and oxygen budgets in a tidally dominated estuarine pond. Mar. Ecol. Prog. Ser. 217, 43—58. https://doi.org/10.3354/MEPS217043

Boutov, D., Peliz, Á., Miranda, P.M.A., Soares, P.M.M., Cardoso, R.M., Prieto, L., Ruiz, J., García-Lafuente, J., 2014. Interannual variability and long term predictability of exchanges through the Strait of Gibraltar. Glob. Planet. Change 114, 23—37. https://doi.org/10.1016/J.GLOPLACHA.2013.12.009

Breitburg, D.L., 1994. Behavioral response of fish larvae to low dissolved oxygen concentrations in a stratified water column. Mar. Biol. 120, 615—625. https://doi.org/10.1007/BF00350083

Burchard, H., Bolding, K., 2002. GETM — a general estuarine transport model. Scientific Documentation. Technical report EUR 20253 en. Tech. Rep. European Commission, Ispra, Italy.

Canuto, V.M., Howard, A., Cheng, Y., Dubovikov, M.S., 2001. Ocean turbulence. Part I: One-point closure model-momentum and heat vertical diffusivities. J. Phys. Oceanogr. 31, 1413—1426. https://doi.org/10.1175/1520-0485(2001)031⟨1413:OTPIOP⟩2.0.CO;2

Cape, J.N., Tang, Y.S., Van Dijk, N., Love, L., Sutton, M.A., Palmer, S.C.F., 2004. Concentrations of ammonia and nitrogen dioxide at roadside verges, and their contribution to nitrogen deposition. Environ. Pollut. 132, 469—478. https://doi.org/10.1016/J.ENVPOL.2004.05.009

Carstensen, J., Andersen, J.H., Gustafsson, B.G., Conley, D.J., 2014. Deoxygenation of the Baltic Sea during the last century. Proc. Natl. Acad. Sci. U. S. A. 111, 5628—5633. https://doi.org/10.1073/pnas.1323156111

Clarke, K.R., Gorley, R.N., 2015. PRIMER v7: User Manual/Tutorial. Primer-E, Plymouth.

D'Avanzo, C., Kremer, J., Wainright, S., 1996. Ecosystem production and respiration in response to eutrophication in shallow temperate estuaries. Mar. Ecol. Prog. Ser. 141, 263—274. https://doi.org/10.3354/MEPS141263

Dietze, H., Löptien, U., 2021. Retracing hypoxia in Eckernförde Bight (Baltic Sea). Biogeosciences 18, 4243—4264. https://doi.org/10.5194/BG-18-4243-2021

Ding, H., Elmore, A.J., 2015. Spatio-temporal patterns in water surface temperature from Landsat time series data in the Chesapeake Bay. U.S.A. Remote Sens. Environ. 168, 335—348. https://doi.org/10.1016/J.RSE.2015.07.009

Friedland, R., Boschetti, S., Stips, A., n.d., European Commission. Joint Research Centre., Marine Strategy Framework Directive — Review and analysis of EU Member States' 2018 reports — Descriptor 7 — permanent alteration of hydrographical conditions does not adversely affect marine ecosystems. https://doi.org/10.2760/74271

Gallo, N.D., Beckwith, M., Wei, C.L., Levin, L.A., Kuhnz, L., Barry, J.P., 2020. Dissolved oxygen and temperature best predict deep-sea fish community structure in the Gulf of California with climate change implications. Mar. Ecol. Prog. Ser. 637, 159—180. https://doi.org/10.3354/MEPS13240

Grasshoff, K., Kremling, K., Ehrhardt, M., 1999. Methods of Seawater Analysis: Third, Completely Revised and Extended Edition. Methods Seawater Anal. Third, Complet. Revis. Ext. Ed. 1—600 https://doi.org/10.1002/9783527613984

Gräwe, U., Holtermann, P., Klingbeil, K., Burchard, H., 2015. Advantages of vertically adaptive coordinates in numerical models of stratified shelf seas. Ocean Model. 92, 56—68. https://doi.org/10.1016/j.ocemod.2015.05.008

Gröger, M., Placke, M., Meier, M., Börgel, F., Brunnabend, S.-E., Dutheil, C., Gräwe, U., Hieronymus, M., Neumann, T., Radtke, H., Schimanke, S., Su, J., Väli, G., 2022. GMDD — The Baltic Sea model inter-comparison project BMIP — a platform for model development, evaluation, and uncertainty assessment. Geosci. Model Dev. Discuss. https://doi.org/10.5194/gmd-2022-160

Hansen, B.W., Stenalt, E., Petersen, J.K., Ellegaard, C., 2002. Invertebrate re-colonisation in Mariager Fjord (Denmark) after severe hypoxia. I. Zooplankton and settlement. Ophelia 56, 197—213. https://doi.org/10.1080/00785236.2002.10409499

HELCOM, 2019. Guidelines for coastal fish monitoring. https://helcom.fi/wp-content/uploads/2020/01/HELCOM-Guidelines-for-coastal-fish-monitoring-2019.pdf

Hersbach, H., Bell, B., Berrisford, P., Hirahara, S., Horányi, A., Muñoz-Sabater, J., Nicolas, J., Peubey, C., Radu, R., Schepers, D., Simmons, A., Soci, C., Abdalla, S., Abellan, X., Balsamo, G., Bechtold, P., Biavati, G., Bidlot, J., Bonavita, M., Chiara, G.De, Dahlgren, P., Dee, D., Diamantakis, M., Dragani, R., Flemming, J., Forbes, R., Fuentes, M., Geer, A., Haimberger, L., Healy, S., Hogan, R.J., Hólm, E., Janisková, M., Keeley, S., Laloyaux, P., Lopez, P., Lupu, C., Radnoti, G., Rosnay, P.de, Rozum, I., Vamborg, F., Villaume, S., Thépaut, J.-N., 2020. The ERA5 global reanalysis. Q. J. R. Meteorol. Soc. 146, 1999—2049. https://doi.org/10.1002/QJ.3803

Hofmeister, R., Burchard, H., Beckers, J.-M., 2010. Non-uniform adaptive vertical grids for 3D numerical ocean models. Ocean Model. 33, 70—86. https://doi.org/10.1016/j.ocemod.2009.12.003

Hsieh, H.H., Chuang, M.H., Shih, Y.Y., Weerakkody, W.S., Huang, W.J., Hung, C.C., Muller, F.L.L., Ranatunga, R.R.M.K.P., Wijethunga, D.S., 2021. Eutrophication and Hypoxia in Tropical Negombo Lagoon, Sri Lanka. Front. Mar. Sci. 8, 1216. https://doi.org/10.3389/FMARS.2021.678832/BIBTEX

Jakobsen, F., 1995. The major inflow to the Baltic Sea during January 1993. J. Marine Syst. 6, 227—240. https://doi.org/10.1016/0924-7963(94)00025-7

Jakobsen, F., Hansen, I.S., Ottesen Hansen, N.E., Østrup-Rasmussen, F., 2010. Flow resistance in the Great Belt, the biggest strait between the North Sea and the Baltic Sea. Estuar. Coast. Shelf Sci. 87, 325—332. https://doi.org/10.1016/j.ecss.2010.01.014

Janssen, F., Schrum, C., Backhaus, J.O., 1999. A climatological data set of temperature and salinity for the Baltic Sea and the North Sea. Dtsch. Hydrogr. Zeitschrift 51, 5—245. https://doi.org/10.1007/BF02933676

Jensen, B., Carstensen, S., Christensen, E.D., 2018. Mixing of Stratified Flow around Bridge Piers in Steady Current. J. Hydraul. Eng. 144, 04018041. https://doi.org/10.1061/(ASCE)HY.1943-7900.0001481

Kanarik, H., Tuomi, L., Alenius, P., Lensu, M., Miettunen, E., Hietala, R., 2018. Evaluating Strong Currents at a Fairway in the Finnish Archipelago Sea. J. Mar. Sci. Eng. 6 (4), 122. https://doi.org/10.3390/JMSE6040122

Karlson, B., Andersson, L.S., Kaitala, S., Kronsell, J., Mohlin, M., Seppälä, J., Willstrand Wranne, A., 2016. A comparison of FerryBox data vs. monitoring data from research vessels for near surface waters of the Baltic Sea and the Kattegat. J. Marine Syst. 162, 98—111. https://doi.org/10.1016/J.JMARSYS.2016.05.002

Karlsson, O.M., Jonsson, P.O., Lindgren, D., Malmaeus, J.M., Stehn, A., 2010. Indications of Recovery from Hypoxia in the Inner Stockholm Archipelago. Ambio 39, 486. https://doi.org/10.1007/S13280-010-0079-3

Kasai, A., Fujiwara, T., Simpson, J.H., Kakehi, S., 2002. Circulation and cold dome in a gulf-type ROFI. Cont. Shelf Res. 22, 1579—1590. https://doi.org/10.1016/S0278-4343(02)00022-5

Klingbeil, K., Lemarié, F., Debreu, L., Burchard, H., 2018. The numerics of hydrostatic structured-grid coastal ocean models: State of the art and future perspectives. Ocean Model. 125, 80—105. https://doi.org/10.1016/J.OCEMOD.2018.01.007

Knight, J.M., Griffin, L., Dale, P.E.R., Sheaves, M., 2013. Short-term dissolved oxygen patterns in sub-tropical mangroves. Estuar. Coast. Shelf Sci. 131, 290—296. https://doi.org/10.1016/J.ECSS.2013.06.024

Kuprijanov, I., Väli, G., Sharov, A., Berezina, N., Liblik, T., Lips, U., Kolesova, N., Maanio, J., Junttila, V., Lips, I., 2021. Hazardous substances in the sediments and their pathways from potential sources in the eastern Gulf of Finland. Mar. Pollut. Bull. 170, 112642. https://doi.org/10.1016/J.MARPOLBUL.2021.112642

Lass, H.U., Mohrholz, V., Knoll, M., Prandke, H., 2008. Enhanced mixing downstream of a pile in an estuarine flow. J. Marine Syst. 74, 505—527. https://doi.org/10.1016/j.jmarsys.2008.04.003

Liblik, T., Naumann, M., Alenius, P., Hansson, M., Lips, U., Nausch, G., Tuomi, L., Wesslander, K., Laanemets, J., Viktorsson, L., 2018. Propagation of Impact of the Recent Major Baltic Inflows From the Eastern Gotland Basin to the Gulf of Finland. Front. Mar. Sci. 5, 222. https://doi.org/10.3389/fmars.2018.00222

Liblik, T., Skudra, M., Lips, U., 2017. On the buoyant sub-surface salinity maxima in the Gulf of Riga. Oceanologia 59 (2), 113—128. https://doi.org/10.1016/J.OCEANO.2016.10.001

Liblik, T., Väli, G., Lips, I., Lilover, M.-J., Kikas, V., Laanemets, J., 2020. The winter stratification phenomenon and its consequences in the Gulf of Finland. Baltic Sea. Ocean Sci. 16, 1475—1490.

Lilover, M.-J., Lips, U., Laanearu, J., Liljebladh, B., 1998. Flow regime in the Irbe Strait. Aquat. Sci. 60, 253. https://doi.org/10.1007/s000270050040

Lindström, G., Pers, C., Rosberg, J., Strömqvist, J., Arheimer, B., 2010. Development and testing of the HYPE (Hydrological Predictions for the Environment) water quality model for different spatial scales. Hydrol. Res. 41, 295—319. https://doi.org/10.2166/NH.2010.007

Matishov, G.G., Grigorenko, K.S., 2020. Dynamic Mode of the Azov Sea in Conditions of Salinization. Dokl. Earth Sci. 492, 376—381. https://doi.org/10.1134/S1028334X20050141/FIGURES/4

McCormick, L.R., Levin, L.A., Oesch, N.W., 2022. Reduced Oxygen Impairs Photobehavior in Marine Invertebrate Larvae. Biol. Bull. 243 (2). https://doi.org/10.1086/717565

Men, C., Liu, R., Wang, Q., Guo, L., Shen, Z., 2018. The impact of seasonal varied human activity on characteristics and sources of heavy metals in metropolitan road dusts. Sci. Total Environ. 637—638, 844—854. https://doi.org/10.1016/J.SCITOTENV.2018.05.059

Mohrholz, V., Naumann, M., Nausch, G., Krüger, S., Gräwe, U., 2015. Fresh oxygen for the Baltic Sea - An exceptional saline inflow after a decade of stagnation. J. Marine Syst. 148, 152—166. https://doi.org/10.1016/j.jmarsys.2015.03.005

Orio, A., Heimbrand, Y., Limburg, K., 2022. Deoxygenation impacts on Baltic Sea cod: Dramatic declines in ecosystem services of an iconic keystone predator. Ambio 51, 626—637. https://doi.org/10.1007/S13280-021-01572-4/FIGURES/6

Otsmann, M., Suursaar, Ü., Kullas, T., 2001. The oscillatory nature of the flows in the system of straits and small semienclosed basins of the Baltic Sea. Cont. Shelf Res. 21, 1577—1603. https://doi.org/10.1016/S0278-4343(01)00002-4

Pearson, T., Rosenberg, R., 1978. Macrobenthic Succession in Relation to Organic Enrichment and Pollution of the Marine Environment. Oceanogr. Mar. Biol. Annu. Rev. 16, 229—311.

Pettai, E., 1984. Eesti kalanduse minevikust I [Of the history of Estonian fisheries]. Eesti Kalurite Koondis, Stockholm, 1—412.

Raudsepp, U., Laanemets, J., Haran, G., Alari, V., Pavelson, J., Kõuts, T., 2011. Flow, waves and water exchange in the Suur strait, Gulf of Riga, in 2008. Oceanologia 53 (1), 35—56. https://doi.org/10.5697/oc.53-1.035

Roman, M.R., Pierson, J.J., Kimmel, D.G., Boicourt, W.C., Zhang, X., 2012. Impacts of Hypoxia on Zooplankton Spatial Distributions in the Northern Gulf of Mexico. Estuar. Coast. 35, 1261—1269. https://doi.org/10.1007/S12237-012-9531-X

Savchuk, O.P., 2010. Large-Scale Dynamics of Hypoxia in the Baltic Sea. In: Yakushev, E. (Ed.), Chemical Structure of Pelagic Redox Interfaces. Springer, Berlin, Heidelberg, 137—160. https://doi.org/10.1007/698_2010_53

Smagorinsky, J., 1963. General Circulation Experiments with the Primitive Equations. Mon. Weather Rev. 91, 99. https://doi.org/10.1175/1520-0493(1963)091

Stanev, E.V., Grashorn, S., Zhang, Y.J., 2017. Cascading ocean basins: numerical simulations of the circulation and interbasin exchange in the Azov-Black-Marmara-Mediterranean Seas system. Ocean Dynam. 67, 1003—1025. https://doi.org/10.1007/S10236-017-1071-2

Stoicescu, S.T., Lips, U., Lips, I., 2018. Assessing the eutrophication status of Estonian marine waters. Fundam. Appl. Hydrophys. 11, 62—74. https://doi.org/10.7868/S2073667318020053

Suursaar, Ü., Kullas, T., Otsmann, M., 2009. The possible effect of re-opening of the Väike Strait (Baltic Sea): Results of high-resolution modelling. WIT Trans. Ecol. Environ. 125, 381—392. https://doi.org/10.2495/WRM090341

Suursaar, Ü., Kullas, T., Otsmann, M., 2001. The influence of currents and waves on ecological conditions of the Väinameri. Proc. Est. Acad. Sci. Biol. Ecol. 50, 231—247.

Talpsepp, L., 2005. Coherent current oscillations and water exchange in the straits of the Gulf of Riga. Oceanologia 47 (2), 115—127.

Tyler, R.M., Brady, D.C., Targett, T.E., 2009. Temporal and spatial dynamics of diel-cycling hypoxia in estuarine tributaries. Estuar. Coast. 32, 123—145. https://doi.org/10.1007/S12237-008-9108-X/FIGURES/15

Umlauf, L., Burchard, H., 2005. Second-order turbulence closure models for geophysical boundary layers. A review of recent work. Cont. Shelf Res. 25, 795—827. https://doi.org/10.1016/j.csr.2004.08.004

Väli, G., Meier, H.E.M., Placke, M., Dieterich, C., 2019. River runoff forcing for ocean modeling within the Baltic Sea Model Intercomparison Project. Meereswissenschaftliche Berichte 113. https://doi.org/10.12754/msr-2019-0113

Valiela, I., McClelland, J., Hauxwell, J., Behr, P.J., Hersh, D., Foreman, K., 1997. Macroalgal blooms in shallow estuaries: Controls and ecophysiological and ecosystem consequences. Limnol. Oceanogr. 42, 1105—1118. https://doi.org/10.4319/LO.1997.42.5_PART_2.1105

Veneranta, L., Vanhatalo, J., Urho, L., 2016. Detailed temperature mapping—Warming characterizes archipelago zones. Estuar. Coast. Shelf Sci. 182, 123—135. https://doi.org/10.1016/J.ECSS.2016.09.011

Verity, P.G., Alber, M., Bricker, S.B., 2006. Development of hypoxia in well-mixed subtropical estuaries in the Southeastern USA. Estuar. Coast. 29, 665—673. https://doi.org/10.1007/BF02784291

Verliin, A., Saks, L., Svirgsden, R., Vetemaa, M., Rohtla, M., Taal, I., Saat, T., 2013. Whitefish (*Coregonus lavaretus* (L.)) landings in the Baltic Sea during the past100 years: combining official datasets and grey literature. Adv. Limnol. 64, 133—152. https://doi.org/10.1127/1612-166X/2013/0064-0020

Virtanen, E.A., Norkko, A., Nyström Sandman, A., Viitasalo, M., 2019. Identifying areas prone to coastal hypoxia — The role of topography. Biogeosciences 16, 3183—3195. https://doi.org/10.5194/BG-16-3183-2019

Virtasalo, J.J., Kohonen, T., Vuorinen, I., Huttula, T., 2005. Sea bottom anoxia in the Archipelago Sea, northern Baltic Sea—Implications for phosphorus remineralization at the sediment surface. Mar. Geol. 224, 103—122. https://doi.org/10.1016/J.MARGEO.2005.07.010

Wesslander, K., Hall, P., Hjalmarsson, S., Lefevre, D., Omstedt, A., Rutgersson, A., Sahlée, E., Tengberg, A., 2011. Observed carbon dioxide and oxygen dynamics in a Baltic Sea coastal region. J. Marine Syst. 86, 1—9. https://doi.org/10.1016/J.JMARSYS.2011.01.001

Xu, Y., Xiao, H., Wu, D., 2019. Traffic-related dustfall and NOx, but not NH3, seriously affect nitrogen isotopic compositions in soil and plant tissues near the roadside. Environ. Pollut. 249, 655—665. https://doi.org/10.1016/J.ENVPOL.2019.03.074

Yuen, J.Q., Olin, P.H., Lim, H.S., Benner, S.G., Sutherland, R.A., Ziegler, A.D., 2012. Accumulation of potentially toxic elements in road deposited sediments in residential and light industrial neighborhoods of Singapore. J. Environ. Manage. 101, 151—163. https://doi.org/10.1016/J.JENVMAN.2011.11.017

Zainal, K., Al-Madany, I., Al-Sayed, H., Khamis, A., Al Shuhaby, S., Al Hisaby, A., Elhoussiny, W., Khalaf, E., 2012. The cumulative impacts of reclamation and dredging on the marine ecology and land-use in the Kingdom of Bahrain. Mar. Pollut. Bull. 64, 1452—1458. https://doi.org/10.1016/J.MARPOLBUL.2012.04.004

Oceanologia 66 (2024) 26—36

Available online at www.sciencedirect.com

ScienceDirect

journal homepage: www.journals.elsevier.com/oceanologia

ORIGINAL RESEARCH ARTICLE

Compound drought and heatwave events in the eastern part of the Baltic Sea region

Laurynas Klimavičius*, **Egidijus Rimkus**

Institute of Geosciences, Vilnius University, Vilnius, Lithuania

Received 28 February 2023; accepted 30 June 2023
Available online 11 July 2023

KEYWORDS
Compound climate events;
Drought;
Heatwave

Abstract Droughts and heatwaves are natural phenomena that can cause severe damage to the economy, infrastructure, human health, and agriculture, among others. However, in recent years, it has been noted that their combined effect, known as compound drought and heatwave events (CDHE), often results in even greater harm. The main aim of this study was to identify CDHEs in this region during summers from 1950 to 2022 and assess the frequency and intensity of these events. To this end, the periods of droughts and heatwaves that occurred between 1950 and 2022 were determined, and the recurrence, extent, and intensity of these phenomena were evaluated. In this study, 1-month Standard Precipitation Index (SPI) values calculated for each summer day were used to identify droughts, while heatwaves were defined as a period of five or more consecutive days when the daily maximum air temperature (T_{max}) was higher than the 90th percentile of T_{max}. Precipitation and T_{max} data (with a spatial resolution 0.25° x 0.25°) were obtained from the European Centre of Medium-Range Weather Forecast ERA-5 reanalysis dataset. The study showed that in most of the eastern part of the Baltic Sea region, the number of drought days had decreased from 1950 to 2022, while the number of heatwave days had increased significantly. In total, ten CDHEs were identified during the summers of 1950—2022. Eight of these events were recorded in 1994 or later. However, a statistically significant increase of CDHEs was found only in a small part of the study area.

* Corresponding author at: Institute of Geosciences, Vilnius University, Vilnius, Lithuania.
E-mail address: laurynas.klimavicius@chgf.vu.lt (L. Klimavičius).
Peer review under the responsibility of the Institute of Oceanology of the Polish Academy of Sciences.

Production and hosting by Elsevier

https://doi.org/10.1016/j.oceano.2023.06.010

1. Introduction

Various extreme weather phenomena have become more frequent over the last decades due to climate change. They cause damage to different areas, including residents and their living environment, infrastructure, wildlife, the economy, etc. Therefore, acquiring a better understanding of the genesis of such phenomena and their possible impacts is particularly important, as it can help not only reduce economic losses but also save lives (Rutgersson et al., 2022; Zscheischler et al., 2020a). Until the middle of the last decade, most research focused only on the impacts of individual elements of the climate system and their potential alterations in a changing climate. However, in recent years, the most significant threats and damage have occurred when several physical processes interacted simultaneously, resulting in a compound climate event (CCE) (Leonard et al., 2014; Ridder et al., 2020; Seneviratne et al., 2012; Zscheischler et al., 2020a). According to Zscheischler et al. (2018), CCEs are defined as a combination of several processes or hazards that pose social or environmental risks. Currently, CCEs are classified into four different groups: 1) preconditioned; 2) multivariate; 3) spatially compounding events; and 4) temporally compounding events (Zscheischler et al., 2020b). Recently, a lot of attention has been paid to the events that belong to the second group, namely multivariate events. These are CCEs where several different recurring processes or phenomena, acting in the same geographical location, cause an impact (Messori et al., 2021; Zscheischler et al., 2020b). Droughts and heatwaves, which are the focus of this study, are examples of such multivariate CCEs as well.

Although droughts and heatwaves cause significant damage when acting individually, during the first decades of this century, it was noted that their combined effect, defined as a compound drought and heatwave event (CDHE), often resulted in even greater harm. Furthermore, these compound events can have a negative impact even when the individual components, droughts and heatwaves, are not extreme and do not pose a significant threat (Mazdiyasni and AghaKouchak, 2015). Indeed, CDHEs cause harm to various natural systems, water resources, and the economy, and can cause natural disasters, have a negative socio-economic impact, and pose a threat to human lives (Bezak and Mikoš, 2020; Feng et al., 2020; Mukherjee and Mishra, 2020; Shi et al., 2021; Wang et al., 2022; Wu et al., 2019; Zhang et al., 2022). One of the main consequences of CDHEs is an increased risk of forest fires and tree mortality (Gazol and Camarero, 2022; Markonis et al., 2021; Rutgersson et al., 2022; Zscheischler et al., 2020a). According to a study by Gazol and Camarero in 2022, 63% of tree mortality events in Europe between 1901 and 2018 were associated with these compound events. Another area affected by CDHEs is crop production and their yield (He et al., 2022; Ribeiro et al., 2020). It has been found that globally, during the period from 1981 to 2020, more than 92% of the areas where crops were grown were affected by at least one CDHE through the vegetation season. During this period, the areas affected by extreme CDHEs increased (from 62% to 75%) along with the likelihood of recurrence of such events (from 20% to 33%) (He et al., 2022). Compound droughts and heatwaves also have a negative impact on the carbon cycle. During the 2003 drought and heatwave in Europe, gross primary productivity in Europe decreased by 30%, leading to an anomalously strong flux of carbon dioxide into the atmosphere (Ciais et al., 2005).

The damage and negative impact caused by CDHEs have become an increasingly relevant topic in recent years, as it has been observed that such events are becoming more frequent in various regions of the world. From 2000 to 2016, the number of CDHEs in various parts of the planet had increased by 1—5 events per year (Mukherjee et al., 2022). Another study found that from 1983 to 2016, the frequency (by 1—3 events per year), duration (by 2—10 days per year), and intensity of these compound events had increased in different areas of the planet. The most significant changes were recorded in the United States, the Amazon basin, Central and Northern Europe, Eastern and Central Asia, and Australia (Mukherjee and Mishra, 2020; Ridder et al., 2020). In various regions of Europe, the frequency and intensity of CDHEs have also increased since the mid-20th century (Ionita and Nagavciuc, 2021b). Such changes have been observed in Eastern Europe as well (Vyshkvarkova and Sukhonos, 2022), with the greatest increases occurring in Central Europe and the Mediterranean region, where one-third of the most intense CDHEs were recorded between 2000 and 2015 (Ionita and Nagavciuc, 2021b; Markonis et al., 2021). In another study, the main hotspots of CDHEs on the continent were found to be in Northern and Eastern Europe, Western European regions, Italy, and the Balkan Peninsula (Bezak and Mikoš, 2020). The main causes of these changes, according to the latest IPCC report, are human influence and anthropogenic climate change (Seneviratne et al., 2021).

However, despite the changing climate and an increasing interest in compound climate events at the global and European level, droughts and heatwaves in the eastern part of the Baltic Sea region have only been studied separately. The formation and recurrence of CDHEs in this area have not been analysed, making this study the first of its kind in the region. Therefore, the main goal of this study was to identify CDHEs in the eastern part of the Baltic Sea region during summers from 1950 to 2022 and assess the frequency and intensity of these events. To achieve this objective, the periods of droughts and heatwaves between 1950 and 2022 were also determined, and the recurrence, extent, and intensity of these phenomena in the eastern part of the Baltic Sea region were evaluated.

2. Data and methods

2.1. Study area and data

The eastern part of the Baltic Sea region was investigated in this study, encompassing the region from 53.5° to 60° N and from 20° to 28.5° E. This area covers the entire territory of Lithuania, Latvia, Estonia, the Kaliningrad region of Russia, the northern-eastern part of Poland, the western part of Russia, and the north-western part of Belarus (Figure 1).

According to the W. Köppen climate classification, whole study area belongs to the warm-summer humid continental climate (*Dfb*) type as the average air temperature during the coldest months of the year (December—February) falls

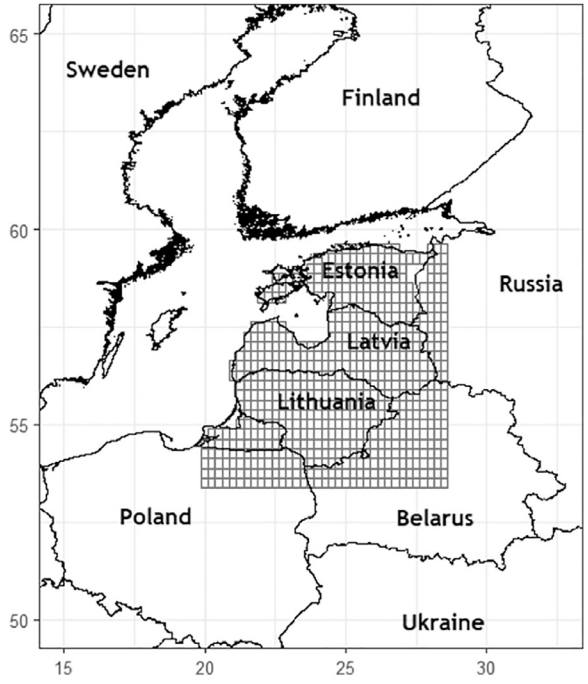

Figure 1 Map of the study area. Grey grid cells mark the territory analysed in this study.

below 0°C (Peel et al., 2007). The highest average monthly temperature in the region is recorded in July and reaches 17–18°C. The annual precipitation in the eastern part of the Baltic Sea region is 550–900 mm, with the highest amount recorded in the western part of Lithuania. The most rainfall in the study area occurs in July and August, with an average of 70–90 mm per month.

Daily data of maximum daily air temperature (T_{max}) and precipitation from 1950 to 2022 were used to identify and evaluate droughts, heatwaves, and CDHEs in the summer months in the eastern part of the Baltic Sea region. The data was obtained from the European Centre of Medium-range Weather Forecast ERA-5 reanalysis database. The grid size of the data was 0.25 × 0.25°. In total, 668 land grid cells covered the study area.

2.2. Evaluation of droughts

The SPI (Standardized Precipitation Index) was used to identify droughts during the study period (McKee et al., 1993). Daily precipitation data were used to calculate this index. The main advantage of the SPI is that it is universal and can be successfully applied to any location in the world, due to the normalisation of the precipitation data sequence during its calculation (Tsakiris and Vangelis, 2004; WMO, 2012). Finally, because of its simple calculation mechanism and applicability to various locations, the World Meteorological Organisation (WMO) recommends using this index for drought identification and evaluation (WMO, 2012). Another distinctive feature of the SPI is that it can be calculated at different time scales, from one to 48 months (WMO, 2012). However, in order to evaluate short-term changes, a 1-month time scale is typically used, as in other studies of droughts and CDHEs (He et al., 2022; Kong et al., 2020; Sharma and Mujumdar, 2017; Shi et al., 2021). SPI values range from +3 to −3. If SPI > +1, conditions are wet; when +1 > SPI > −1, average moisture conditions are identified; SPI < −1 represents dry conditions; and if SPI < −2, conditions are extremely dry (McKee et al., 1993).

In this study, 1-month SPI values were calculated for each day of the study period. Because 30 days of precipitation data are required to calculate the SPI values for June days, values of this meteorological variable for the months of May were also used. Droughts were distinguished if the SPI values were lower than −1 for at least five or more consecutive days and this condition was met in at least one third of the study area during the maximum extent of the drought. The beginning of a drought was considered when SPI values were lower than −1 in more than 10% of the points of the study area, and the end of a drought was determined when this criterion was no longer met. Drought recurrence and duration changes during the summer months were evaluated from 1950 to 2022. The statistical significance of changes was evaluated by performing a Mann-Kendall test. These changes were considered statistically significant if $p < 0.05$. The intensity of each drought was determined by calculating the median of the SPI values in the area affected by a drought. Then, during the maximum spread of each drought, the 5-day average of SPI medians was calculated and the Min-Max normalisation method was applied.

2.3. Evaluation of heatwaves

Summer daily maximum temperature data (T_{max}) were used to identify heatwaves For each summer day and each grid cell of interest, the 90th percentile of the daily maximum air temperature (T_{90}) was calculated on a 5-day moving window. A heatwave was identified if it was found that $T_{max} > T_{90}$ for at least five consecutive days and this condition was met for at least one-third of the study area. This criterion has been used in other studies (Mazdiyasni and AghaKouchak, 2015; Sharma and Mujumdar, 2017) and the method of using the 90th percentile of daily maximum temperature is widely applied in identifying heatwaves in Europe (García-León et al., 2021; Kim et al., 2018; Prodhomme et al., 2022; Rousi et al., 2022) and globally (Mukherjee et al., 2020; Perkins-Kirkpatrick and Gibson, 2017; Ridder et al., 2020). Its main advantage is that the method is relative rather than absolute, so it can be successfully applied to any location at any time of the year (Basarin et al., 2020; Ridder et al., 2020). Calculations are usually performed using various moving averages (ranging from 3 to 31 days), but the most commonly used criterion is 15 days (Geirinhas et al., 2021; Perkins-Kirkpatrick and Gibson, 2017; Sharma and Mujumdar, 2017; Wang et al., 2022). However, there is no consensus on the number of days to be considered, which also depends on the duration of the period under investigation. Since only summer months (92 days) were analysed in this study, a 5-day moving average period, which has been used in other studies (He et al., 2022), was chosen.

In this study, the start date of a heatwave was defined as a day when a heatwave was recorded in at least 10% of the grid cells based on the 90th percentile criterion. The end date of a heatwave was defined as the last day when T_{max} still satisfied this criterion. Changes in the frequency and duration of heatwaves during the study period were

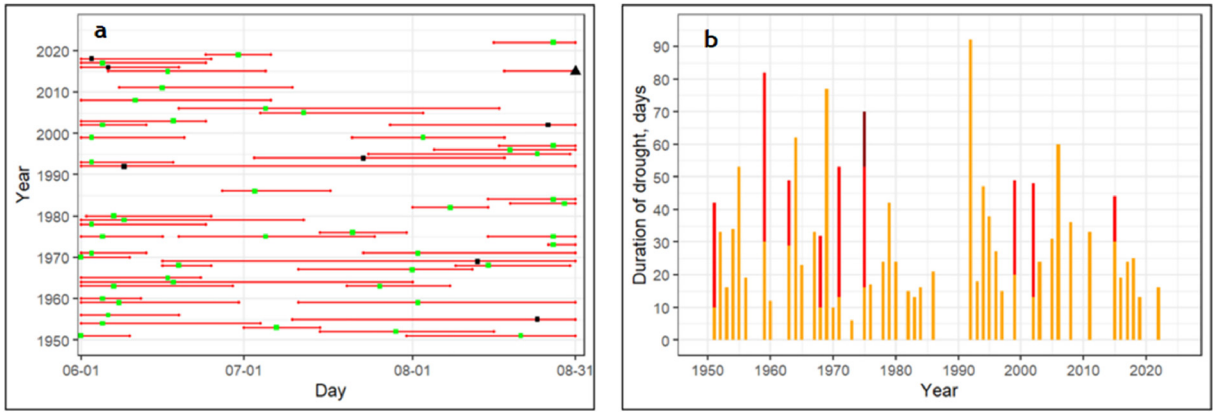

Figure 2 a) Droughts and their duration in the eastern part of the Baltic Sea region from 1950 to 2022. Squares indicate the days when each drought affected the largest part of the study area. Black squares indicate droughts whose intensity, according to the normalised 5-day SPI median average values, was greater than 0.5, while green squares indicate droughts whose intensity was less than 0.5. The black triangle indicates the date when the most intense drought reached its maximum extent. b) The duration of droughts (in days) from 1950 to 2022. The orange colour indicates the first drought in the corresponding year, red indicates the second, and dark red indicates the third.

assessed by evaluating the statistical significance of the observed changes. Heatwaves were also examined separately and assessed in each grid cell by evaluating the frequency of heatwave days and changes in the recurrence of this phenomenon over the period from 1950 to 2022. The intensity of the heatwaves was assessed by calculating the 5-day median average during the maximum spread of each heatwave and normalising the obtained values using the Min-Max method — the same principle was used in drought analysis.

2.4. Definition of CDHE

In this study, CDHEs were identified when both droughts and heatwaves reached their maximum extent in at least one-third of the studied area at the same time. The beginning of such events was considered as the day when the coincidence of these phenomena was detected in at least one-tenth of the study area points. Each CDHE lasted until the number of such grid cells no longer exceeded one-tenth of all points. The duration of each identified CDHE, the date of its maximum extent, and the percentage of the study area affected during that time were evaluated. The recurrence and duration of such events in the study area were also determined. The intensity of a CDHE was determined using the Min-Max normalization method, and the statistical significance of the changes in CDHE cases at each study grid cell was assessed by performing the Mann-Kendall test ($p < 0.05$).

3. Results

3.1. Droughts

Fifty-five droughts were identified in the eastern part of the Baltic Sea region during the period of 1950—2022 according to selected criteria (Figure 2a). The highest number of droughts (10) was identified during the period of 1970—1979 while three separate drought events were detected in the summer of 1975 (Figure 2b). Later on, there was a decrease in the number of droughts in the region — only five of them were recorded in the 1990s, and no droughts were identified in the study area between 1987 and 1991. Another period of increased drought reoccurrence was observed from 1992 to 1999, during which eight droughts were identified. In particular, in 1992, the longest drought lasting throughout the entire summer (92 days) was recorded according to selected criteria (Figure 2a). Despite this, it was noted that the number and duration of droughts decreased over the entire study period of 1950—2022 (Figure 2b). However, these changes were not statistically significant (when $p < 0.05$).

Two droughts that affected the majority of the study area were distinguished in 1955 (lasting from July 10th to August 31st) and 1994 (lasting from July 3rd to August 18th). Both of these droughts covered the entire study area at their maximum spatial extent. According to the normalised values of the 5-day median average, the most severe (intense) drought was the one that occurred at the end of the summer of 2015 (Figure 2a).

The largest number of drought days (>140 per decade) was identified in the eastern part of the study region, while the lowest number of such days (around 100) was found in the southwestern part of the study area (Figure 3a). It was calculated that the number of drought days from 1950 to 2022 had decreased in 89% of the study area's grid cells. However, statistically significant changes (when $p < 0.05$) were only found at three points in Estonia. In the majority of the study area, although the changes were negative, they were close to zero. The number of days with droughts had slightly increased only in the central part of Latvia and the southeastern edge of the study area over the 73-year period (Figure 3b).

3.2. Heatwaves

Thirty-seven heatwave events were identified in the eastern part of the Baltic Sea region from 1950 to 2022. Remarkably, heatwaves have become increasingly frequent in

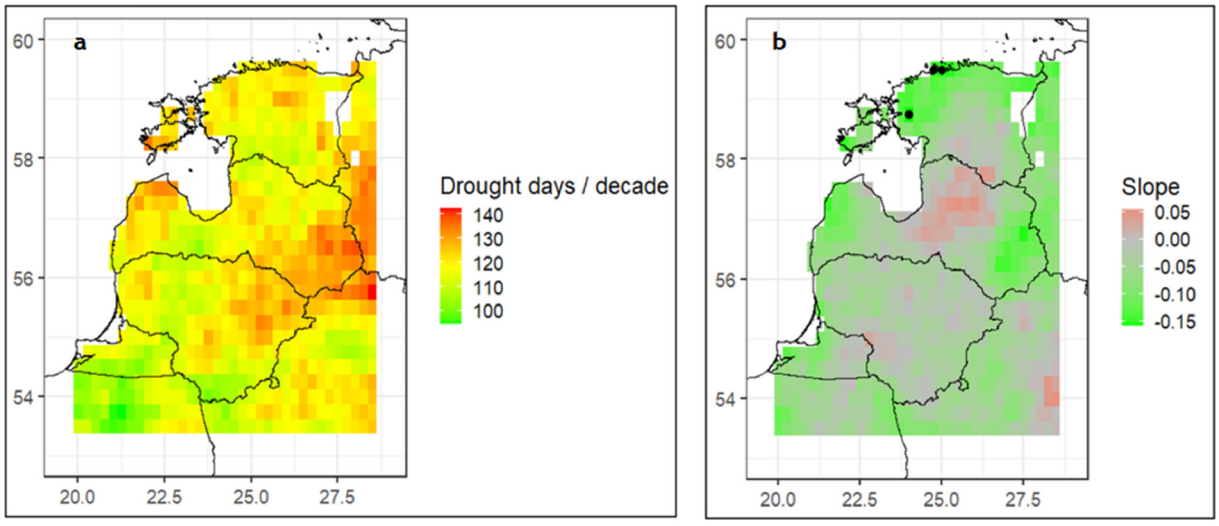

Figure 3 The number of drought days per decade in the study area (a) and the change in the number of drought days from 1950 to 2022 in each grid cell (b). Black dots indicate grid cells where the changes were statistically significant ($p < 0.05$).

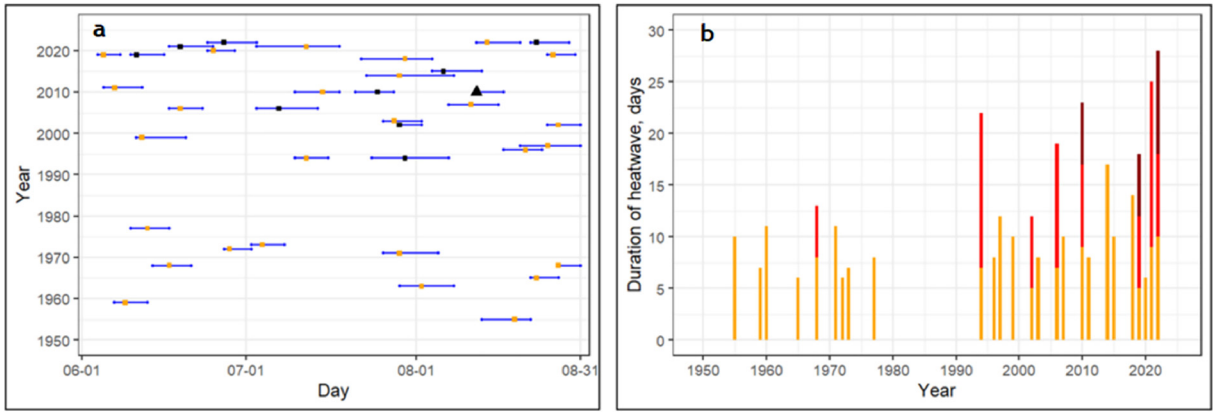

Figure 4 a) Heatwaves and their duration in the eastern part of the Baltic Sea region from 1950 to 2022. Squares indicate the days when each heatwave affected the largest part of the study area. Black squares indicate heatwaves whose intensity, according to the normalised 5-day SPI median average values, was greater than 0.5, while green squares indicate heatwaves whose intensity was less than 0.5. The black triangle indicates the date when the most intense heatwave reached its maximum extent. b) The duration of heatwaves (in days) from 1950 to 2022. The orange colour indicates the first heatwave in the corresponding year, red indicates the second, and dark red indicates the third.

recent decades. These phenomena were not identified between 1978 and 1993, whereas in the past 13 years (from 2010 to 2022), as many as 16 heatwaves have been distinguished (Figure 4a). The longest heatwave was identified in the summer of 2014. It lasted for 17 days (from July 23rd to August 8th). More heatwaves were observed in the second half of the summer (Figure 4a). It was also found that during the summers of 2010, 2019, and 2022, three heatwaves were recorded in the eastern part of the Baltic Sea region, whereas no such cases were identified prior to 2010. When assessing the changes in the frequency and duration of heatwaves from 1950 to 2022, our analyses showed that the number of days when a heatwave was identified in the entire study area during the summer season exhibited statistically significant increase (Figure 4b).

The heatwave which covered the highest number of grid cells during its maximum extent date occurred in 2021. On its peak day, June 19th, it covered the entire study area. The 2014 and 2006 heatwaves also covered almost the entire study area at their peak, with the 2014 heatwave reaching 99.85% of the study area on July 29th and the 2006 heatwave reaching 99.55% of the area on July 7th. The most severe heatwave was also identified in the 21st century, in 2010 (Figure 4a). Finally, it should be noted that of the ten most intense heatwaves, nine were recorded during the period from 2002 to 2022 (Figure 4a).

The highest number of heatwave days, when considering their occurrence in separate grid cells in the study area, was found in the northern part of the study area in Estonia. Here, the number of such cases in some places exceeded 40 per decade. The lowest number of heatwave days occurred in the southern and southwestern parts of the analysed area, where the number of such days per decade was just over 20 (Figure 5a). It was also found that the number

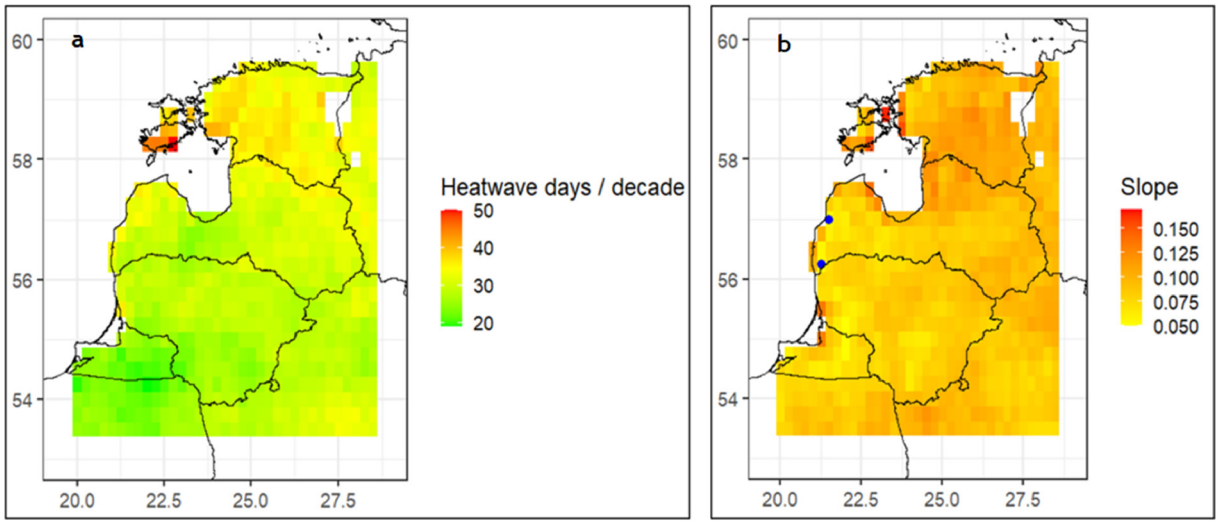

Figure 5 Heatwave days per decade in different points of the eastern part of the Baltic Sea region (a) and the change in the number of heatwave days from 1950 to 2022 in each point of the study area (b). Blue dots indicate those points where the changes were statistically insignificant (when $p > 0.05$).

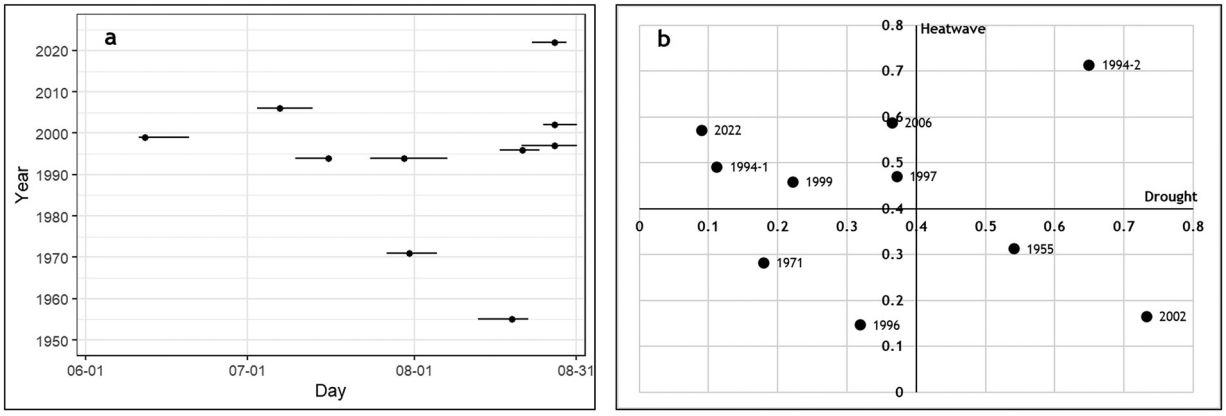

Figure 6 a) Compound drought and heatwave events (CDHE) over 1950—2022 and their duration in the eastern part of the Baltic Sea region. Black dots mark the days when the corresponding CDHE covered the largest part of the studied area. b) The intensity of each CDHE obtained by calculating the normalised SPI and $T_{max} - T_{90}$ values. 1994-1 indicates the first CDHE of that year, and 1994-2 indicates the second one.

of heatwave days from 1950 to 2022 increased throughout the whole eastern part of the Baltic Sea region, and this change was not statistically significant (when $p < 0.05$) in only two grid cells located in western Latvia. The greatest increase in the number of heatwave days over 73 years was found in coastal regions (Figure 5b).

3.3. Compound drought and heatwave events

A total of ten CDHEs (periods when a compound event was recorded in more than a third of the study area during its largest extent) were identified in the eastern part of the Baltic Sea region during the summer months of 1950—2022 (Figure 6a). The majority of these were recorded in the second half of summer, with only one CDHE identified in June (in 1999, from June 11th to 20th). Most of CDHEs (half of all cases) were recorded in the 1990s, specifically from 1994 to 1999. The year 1994 was the only year when two CDHEs were identified during the summer. The second complex event in that year was the longest of all CDHEs identified in this study, lasting for 15 days (from July 24th to August 7th) (Figure 6a). This event also covered the largest part of the study area (94.2%) and was the most intense (Figure 6b). When considering the intensity of the CDHEs, the one recorded in 2002 also stood out among all compound events. In fact, it was accompanied by the most intense drought (among those that coincided with heatwaves in at least a third of the study area points). However, the heatwave was weak, which resulted in a lower intensity of this CDHE compared to the second CDHE in 1994 (Figure 6b).

During the analysis of individual grid cells within the study area, the largest number of CDHEs (when droughts and heatwaves coincided only in individual points) during the summer months of 1950—2022 was identified in the eastern and southeastern parts of the study area, which were characterised by a high number of droughts. In these areas, the

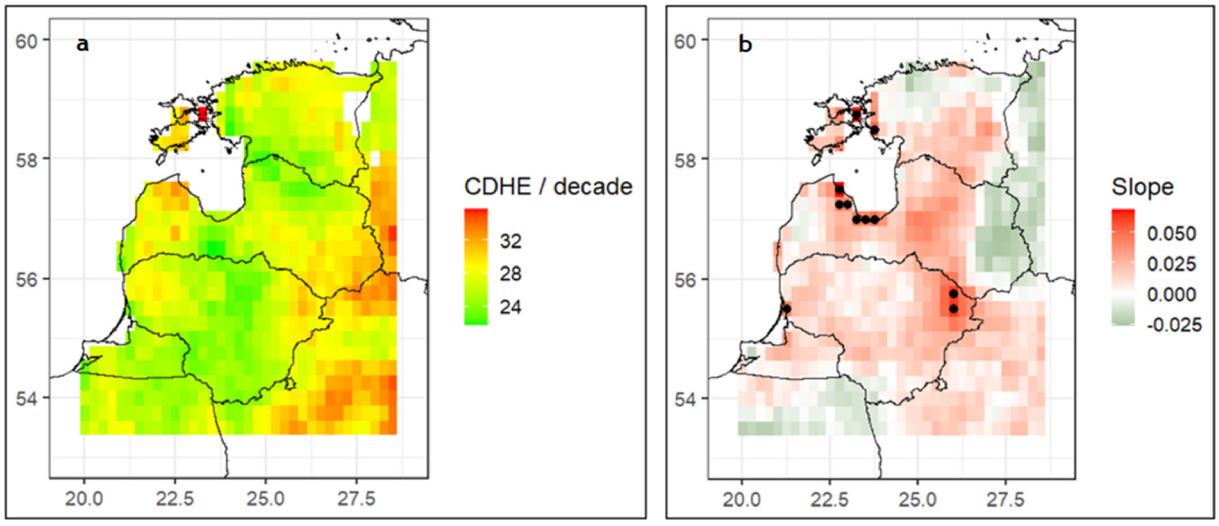

Figure 7 Number of compound drought and heatwave events (CDHE) per decade in different points of the eastern part of the Baltic Sea region (a) and changes in the number of CDHE cases from 1950 to 2022 in each point of the study area (b). Black dots indicate those grid points where the changes were statistically significant (when $p < 0.05$).

number of CDHE days in individual grid cells over the entire study period exceeded 240 (more than 33 per decade). However, the largest number of CDHEs was recorded on Muhu Island, which belongs to Estonia, where 261 CDHE days were identified from 1950 to 2022 (Figure 7a).

An analysis of the variability of CDHEs in individual points over the entire study period showed that such events were occurring more frequently in a large part of the study area. However, this change was statistically significant ($p < 0.05$) in only 1.6% of the entire study area (11 grid cells), and most of the points showing such changes are located along the coast of the Gulf of Riga (Figure 7b). Meanwhile, decreasing tendencies in the occurrence of CDHEs were observed in the northeast-eastern and southwestern parts of the study area. This was primarily due to less frequent droughts occurring in these regions (Figure 4b). However, the changes in this case were small and statistically insignificant.

4. Discussion

The main factor determining the decrease in the number of droughts since the mid-20th century in this and other studies (Jaagus and Aasa, 2018; Jaagus et al., 2022; Rimkus et al., 2013; Valiukas, 2015) was an increased amount of rainfall. However, in most cases, the changes are small and statistically insignificant. The greatest (and statistically significant) decrease in the number of drought days was observed in the northern part of the study area (Estonia), where a statistically significant increase in rainfall has been recorded since the mid-20th century (Jaagus and Aasa, 2018). Although the number of droughts has not changed significantly in various parts of the Baltic Sea region over the past few decades, their intensity has been increasing, and they have been becoming more extreme (Somorowska, 2016; Valiukas, 2015). This study confirmed these trends, with eight out of the ten of the most intense droughts identified in 1994 or later, and the most intense drought occurring in August 2015. It is predicted that in the future, due to a rapidly changing climate, the unevenness of rainfall distribution will further increase and temperatures will rise, leading to more intense droughts in the eastern Baltic Sea region as well as various regions of the world (Keršytė et al., 2015; Rimkus et al., 2020; Seneviratne et al., 2021).

In contrast to droughts, the number and duration of heatwaves increased in the eastern Baltic Sea region during the period from 1950 to 2022. Changes were statistically significant in almost the entire study area. Such trends have been observed in various parts of the world, including the eastern part of the Baltic Sea region (Awasthi et al., 2022; BACC II, 2015; Basarin et al., 2020; Seneviratne et al., 2021; Suursaar, 2022; Yoon et al., 2020). The main explanation for this is an increasing maximum daily temperature caused by climate change.

The highest number of heatwave days was identified in the northern part of the study area, which may be related to the 90th percentile method used to determine them. In the northern part of the study area (Estonia), the T_{90} values on a corresponding summer day during the study period were generally lower than in the areas further south. Therefore, when a heatwave formed and the temperature was similar throughout the study area, the T_{90} was often exceeded on more days at higher latitudes than in the southern part of the study area. The largest increase in the number of heatwave days since the mid-20th century was observed in coastal territories and the Muhu and Sarema islands.

It has been noted that the number and extremeness (the maximum area covered and intensity) of heatwave days had both increased during the study period. This was also a consequence of a warming climate. Similar trends have been observed in Poland when studying heatwaves — 11 heatwaves have been recorded since 1980, covering more than a quarter of the country's territory and lasting for at least a week. However, only one such event had been recorded prior to 1990, and more than half have occurred in the last decade (Wibig, 2021). The longest heatwaves in Poland were recorded in 1994 and 2015 (Tomczyk et al., 2020; Wibig, 2017).

All the characteristics defining the aforementioned heatwaves (number of heatwave days, intensity, covered area) are expected to increase in the future (Basarin et al., 2020; Rutgersson et al., 2022; Seneviratne et al., 2021). It has been determined that the number of heatwave days will increase by 4—34 days per season for each degree Celsius of global warming, depending on the region. The duration of heatwaves is expected to increase by 2—10 days/°C, with the greatest changes predicted to occur at lower latitudes (Perkins-Kirkpatrick and Gibson, 2017). These changes will also increase the damage caused by heatwaves. If adaptation and mitigation measures are not taken, it is likely that their impact in Europe could increase by a factor of five by 2060, compared to the historical period of 1981—2010 (García-León et al., 2021); in some areas of the Baltic Sea region, the risk of heatwaves may double by the end of this century (Rutgersson et al., 2022).

When evaluating the recurrence of CDHEs in the eastern part of the Baltic Sea region, it was observed that the vast majority of these (8 out of 10 events) were recorded from 1994 onwards. When assessing changes of CDHEs in individual grid cells, it was also found that the CDHE frequency increased in 73% of these cells during the 1950—2022 period. Similar results, indicating an increasingly frequent recurrence of CDHEs, have been obtained through studies of such events in various regions of the world and Europe (Bezak and Mikoš, 2020; Geirinhas et al., 2021; Kong et al., 2020; Mazdiyasni and AghaKouchak, 2015; Sedlmeier et al., 2018; Shi et al., 2021). However, during this study, a statistically significant increase in the occurrence of CDHEs was found in a very small area due to the decreasing frequency of droughts.

The majority of CDHEs occurred during the second half of the summers, which was closely related to the occurrences of heatwaves during the summers. The distribution of CDHEs in different points of the studied territory largely coincided with the distribution of dry days — in both cases, the most frequent occurrences of droughts and CDHEs were identified in the eastern and southeastern parts of the study area, as well as in the northwestern part of Latvia and on the islands of Muhu and Saaremaa. The most exceptional CDHE occurred between July 24 and August 7, 1994. This was the longest-lasting and the most intense event, covering the largest part of the studied territory at its maximum extent. This was also the only case when a CDHE was identified twice during the same summer (1994), which could have contributed to the extremeness of this complex event.

It is predicted that in the future, with ongoing climate change and increasing global mean temperatures, CDHEs will occur more frequently and an increase in intensity and duration will also be expected (Seneviratne et al., 2021). It has been calculated that with every degree Celsius of global warming, the duration of these complex events will increase by an average of ten days (Zhang et al., 2022). The frequency and occurrence of CDHEs in Europe will also increase in the future (Mukherjee et al., 2022; Sedlmeier et al., 2018), leading to a growing probability of negative impacts and damages. The forestry sector will be most affected, with an increased risk of forest fires and tree mortality (Feng et al., 2020; Gazol and Camarero, 2022; Seneviratne et al., 2021).

Atmospheric processes and their dynamics play a significant role in the formation of both droughts, heatwaves, and CDHE. One notable process is the prevalence of anticyclonic circulation and atmospheric blocking (Ionita et al., 2021a; Liu et al., 2020; Sousa et al., 2018; Spensberger et al., 2020). It has been observed that drought formation in the Baltic countries is almost always influenced by strong anticyclonic circulation (Rimkus et al., 2014). Similar tendencies were identified when studying the drought that affected Poland during the summer of 2019 (Ziernicka-Wojtaszek, 2021). Furthermore, it was determined that 60% of heatwaves in Central Europe during the period of 2001—2011 coincided with the formation of blocking systems (Porebska and Zdunek, 2013). However, statistically significant changes in the recurrence of such systems in the Northern Hemisphere from 1901 to 2010 have not been detected. Nevertheless, it has been observed that the duration of blocking systems is becoming longer (Wazneh et al., 2021).

The formation of droughts and/or heatwaves is also influenced by large-scale atmospheric circulation, not just local atmospheric processes. When studying the recurrence of heatwaves in Poland, it has been observed that several synoptic features play a role in their formation. These include a strong Azores high-pressure system, higher-than-usual atmospheric pressure over Central Europe, resulting in calm and sunny weather, and a strong blocking system over the North Atlantic (Wibig, 2017).

Finally, several aspects must be considered in further research. First, an important aspect that can influence the accuracy and reliability of obtained results and trends is the uncertainties and biases of the data obtained from the ERA5 database. ERA5 uses a 10-member ensemble that provides uncertainty information. However, in this case, one of the problems encountered is the lack of small-scale variability in ensemble members, and the model itself tends to have overconfidence in the uncertainty characterization (Bandhauer et al., 2022). This is because the perturbations are oriented towards large-scale dynamic variables (Hersbach et al., 2020).

However, the inaccuracies of ERA5 reanalysis data are mostly encountered in mountainous regions (e.g., in the Alps) or continents other than Europe (Bell et al., 2021; Hersbach et al., 2020; Lavers et al., 2022; Velikou et al., 2022). Only a few issues were found while analysing the performance of ERA5 in mid-latitudes. During the evaluation of extremely high temperature (above 95th percentile), it was observed that ERA5 tends to overestimate values of this variable, but the differences compared to observations are not statistically significant (Velikou et al., 2022). It was also found that random errors of precipitation data increase during the summer in mid-latitudes (Lavers et al., 2022). However, in more than 90% of cases, the variability of monthly precipitation values in Europe coincides with observations (Bell et al., 2021). Therefore, despite the shortcomings, ERA5 precipitation and temperature data are sufficiently accurate to use in mid-latitudes in Europe (Bandhauer et al., 2022; Lavers et al., 2022; Nogueira, 2020; Velikou et al., 2022).

Also, when evaluating long-term trends, it is important to emphasize that the accuracy of ERA5, like any other reanalysis data, decreases and errors increase going further

back in time. The reason for this is simple — a significantly smaller number of observations were available at the beginning of the period (1950's) compared to the past decades (Bell et al., 2021). Additionally, the number of satellite observations and their quality increased rapidly, which also plays a significant role in the accuracy of the obtained data (ECMWF, 2023).

The choice of the index used to identify droughts is also crucial. Although the SPI which was used in this study was suitable for assessing droughts in the study region, it has several limitations. The main one is that it only considers precipitation and does not take into account the effect of temperature on drought formation. As the climate changes and mean temperature rapidly increase, the latter factor will become crucial in accurately identifying droughts (Vicente-Serrano et al., 2010; WMO, 2012). It is also important to investigate the processes that lead to the formation of CDHEs in the eastern part of the Baltic Sea region and to evaluate the possible changes in CDHE characteristics in the future. This would help develop more effective adaptation and mitigation strategies and thus minimise the risks posed by CDHEs (Bezak and Mikoš, 2020; Mazdiyasni and AghaKouchak, 2015; Sedlmeier et al., 2018).

5. Conclusions

A decrease in the number of drought days was observed from 1950 to 2022 in most of the eastern part of the Baltic Sea region (89%). However, almost all these changes were statistically insignificant. Only a slight increase in the number of drought days was identified in the central part of Latvia and the southeastern outskirts of the study area. In contrast to droughts, the number and duration of heatwaves, have increased in the entire research area. The obtained changes were statistically significant in 99.7% of the study area. The extremeness of heatwaves (intensity and the area covered during their maximum extent) has also increased in the region due to rising temperatures caused by changing climate. The largest number of heatwave days was identified in the northern part of the study region and on the coast of the Baltic Sea. Ten CDHEs were identified in the eastern part of the Baltic Sea region, with eight of them recorded in 1994 or later. Moreover, an increase in the number of CDHEs was observed in 73% of the study area, but statistically significant changes were only found in 1.9% of the region. The largest positive changes were found in coastal regions, as well as in the northeastern part of Lithuania.

Declaration of competeing interest

The authors declare that they have no known competing financial interests or personal relationships that could have appeared to influence the work reported in this paper.

References

Awasthi, A., Vishwakarma, K., Pattnayak, K.C., 2022. Retrospection of heatwave and heat index. Theor. Appl. Climatol. 147 (1—2), 589—604. https://doi.org/10.1007/s00704-021-03854-z

BACC II Author Team, 2015. Second Assessment of Climate Change for the Baltic Sea Basin. Helmholtz-Zentrum Geesthacht GmbH, Germany, 501 pp.

Bandhauer, M., Isotta, F., Lakatos, M., Lussana, C., Båserud, L., Izsák, B., Szentes, O., Tveito, O.E., Frei, C., 2022. Evaluation of daily precipitation analyses in E-OBS (v19.0e) and ERA5 by comparison to regional high-resolution datasets in European regions. Int. J. Climatol. 42 (2), 727—747. https://doi.org/10.1002/joc.7269

Basarin, B., Lukić, T., Matzarakis, A., 2020. Review of biometeorology of heatwaves and warm extremes in Europe. Atmosphere 11 (12), 1—21. https://doi.org/10.3390/atmos11121276

Bell, B., Hersbach, H., Simmons, A., Berrisford, P., Dahlgren, P., Horányi, A., Muñoz-Sabater, J., Nicolas, J., Radu, R., Schepers, D., Soci, C., Villaume, S., Bidlot, J.R., Haimberger, L., Woollen, J., Buontempo, C., Thépaut, J.N., 2021. The ERA5 global reanalysis: Preliminary extension to 1950. Q. J. R. Meteorol. 147 (741), 4186—4227. https://doi.org/10.1002/qj.4174

Bezak, N., Mikoš, M., 2020. Changes in the compound drought and extreme heat occurrence in the 1961—2018 period at the european scale. Water (Switz.) 12 (12). https://doi.org/10.3390/w12123543

Ciais, P., Reichstein, M., Viovy, N., Granier, A., Ogée, J., Allard, V., Aubinet, M., Buchmann, N., Bernhofer, C., Carrara, A., Chevallier, F., De Noblet, N., Friend, A.D., Friedlingstein, P., Grünwald, T., Heinesch, B., Keronen, P., Knohl, A., Krinner, G., Loustau, D., Manca, G., Matteucci, G., Miglietta, F., Ourcival, J.M., Papale, D., Pilegaard, K., Ramball, S., Seufert, G., Soussana, J.F., Sanz, M.J., Schulze, E.D., Vesala, T., Valentini, R., 2005. Europe-wide reduction in primary productivity caused by the heat and drought in 2003. Nature 437 (7058), 529—533. https://doi.org/10.1038/nature03972

ECMWF, 2023. ERA5: uncertainty estimation Accessed on May 30th, 2023. https://confluence.ecmwf.int/display/CKB/ERA5%3A+uncertainty+estimation

Feng, Y., Liu, W., Sun, F., Wang, H., 2020. Changes of compound hot and dry extremes on different land surface conditions in China during 1957—2018. Int. J. Climatol. 41 (S1), E1085—E1099. https://doi.org/10.1002/joc.6755

García-León, D., Casanueva, A., Standardi, G., Burgstall, A., Flouris, A.D., Nybo, L., 2021. Current and projected regional economic impacts of heatwaves in Europe. Nat. Commun. 12 (1), 1—10. https://doi.org/10.1038/s41467-021-26050-z

Gazol, A., Camarero, J.J., 2022. Compound climate events increase tree drought mortality across European forests. Sci. Total Environ. 816, 151604. https://doi.org/10.1016/j.scitotenv.2021.151604

Geirinhas, J.L., Russo, A., Libonati, R., Sousa, P.M., Miralles, D.G., Trigo, R.M., 2021. Recent increasing frequency of compound summer drought and heatwaves in Southeast Brazil. Environ. Res. Lett. 16 (3). https://doi.org/10.1088/1748-9326/abe0eb

He, Y., Fang, J., Xu, W., Shi, P., 2022. Substantial increase of compound droughts and heatwaves in wheat growing seasons worldwide. Int. J. Climatol. 42 (10), 5038—5054. https://doi.org/10.1002/joc.7518

Hersbach, H., Bell, B., Berrisford, P., Hirahara, S., Horányi, A., Muñoz-Sabater, J., Nicolas, J., Peubey, C., Radu, R., Schepers, D., Simmons, A., Soci, C., Abdalla, S., Abellan, X., Balsamo, G., Bechtold, P., Biavati, G., Bidlot, J., Bonavita, M., De Chiara, G., Dahlgren, P., Dee, D., Diamantakis, M., Dragani, R., Flemming, J., Forbes, R., Fuentes, M., Geer, A., Haimberger, L., Healy, S., Hogan, R.J., Hólm, E., Janisková, M., Keeley, S., Laloyaux, P., Lopez, P., Lupu, C., Radnoti, G., de Rosnay, P., Rozum, I., Vamborg, F., Villaume, S., Thépaut, J.N., 2020. The ERA5 global reanalysis. Q. J. R. Meteorol. 146 (730), 1999—2049. https://doi.org/10.1002/qj.3803

Ionita, M., Caldarescu, D.E., Nagavciuc, V., 2021a. Compound Hot and Dry Events in Europe: Variability and Large-Scale Drivers.

Front. Clim. 3 (June), 1—19. https://doi.org/10.3389/fclim.2021.688991

Ionita, M., Nagavciuc, V., 2021b. Changes in drought features at the European level over the last 120 years. Nat. Hazards Earth Syst. Sci. 21 (5), 1685—1701. https://doi.org/10.5194/nhess-21-1685-2021

Jaagus, J., Aasa, A., 2018. Changes in drought indices in Estonia during the period of the contemporary climate warming. In: Proceedings of the 2nd Baltic Earth Conference, 11—15 June 2018. Helsingør, Denmark.

Jaagus, J., Aasa, A., Aniskevich, S., Boincean, B., Bojariu, R., Briede, A., Danilovich, I., Castro, F.D., Dumitrescu, A., Labuda, M., Labudová, L., Lõhmus, K., Melnik, V., Mõisja, K., Pongracz, R., Potopová, V., Řezníčková, L., Rimkus, E., Semenova, I., Stonevičius, E., Štepánek, P., Trnka, M., Vicente-Serrano, S.M., Wibig, J., Zahradníček, P., 2022. Long-term changes in drought indices in eastern and central Europe. Int. J. Climatol. 42 (1), 225—249. https://doi.org/10.1002/joc.7241

Keršytė, D., Rimkus, E., Kažys, J., 2015. Klimato rodiklių scenarijai Lietuvos teritorijoje XXI a. Geologija. Geografija 1 (1), 22—35. https://doi.org/10.6001/geol-geogr.v1i1.3069

Kim, S., Sinclair, V.A., Räisänena, J., Ruuhelac, R., 2018. Heat waves in Finland: Present and projected summertime extreme temperatures and their associated circulation patterns. Int. J. Climatol. 38 (3), 1393—1408. https://doi.org/10.1002/joc.5253

Kong, Q., Guerreiro, S.B., Blenkinsop, S., Li, X.F., Fowler, H.J., 2020. Increases in summertime concurrent drought and heatwave in Eastern China. Weather Clim. Extremes 28, 100242. https://doi.org/10.1016/j.wace.2019.100242

Lavers, D.A., Simmons, A., Vamborg, F., Rodwell, M.J., 2022. An evaluation of ERA5 precipitation for climate monitoring. Q. J. R. Meteorol. 148 (748), 3152—3165. https://doi.org/10.1002/qj.4351

Leonard, M., Westra, S., Phatak, A., Lambert, M., van den Hurk, B., Mcinnes, K., Risbey, J., Schuster, S., Jakob, D., Stafford-Smith, M., 2014. A compound event framework for understanding extreme impacts. WIREs Clim. Change 5 (1), 113—128. https://doi.org/10.1002/wcc.252

Liu, X., He, B., Guo, L., Huang, L., Chen, D., 2020. Similarities and Differences in the Mechanisms Causing the European Summer Heatwaves in 2003, 2010, and 2018. Earth's Future 8 (4), 1—11. https://doi.org/10.1029/2019EF001386

Markonis, Y., Kumar, R., Hanel, M., Rakovec, O., Máca, P., Kouchak, A.A., 2021. The rise of compound warm-season droughts in Europe. Sci. Adv. 7 (6), 1—8. https://doi.org/10.1126/sciadv.abb9668

Mazdiyasni, O., AghaKouchak, A., 2015. Substantial increase in concurrent droughts and heatwaves in the United States. PNAS 112 (37), 11484—11489. https://doi.org/10.1073/pnas.1422945112

McKee, T.B., Doesken, N.J., Kleist, J., 1993. The Relationship of Drought Frequency and Duration to Time Scales. In: Proceedings of the 8th Conference on Applied Climatology, 17—22 January 1993, Anaheim, CA.

Messori, G., Bevacqua, E., Caballero, R., Coumou, D., De Luca, P., Faranda, D., Kornhuber, K., Martius, O., Pons, F., Raymond, C., Ye, K., Yiou, P., Zscheischler, J., 2021. Compound climate events and extremes in the midlatitudes: Dynamics, simulation, and statistical characterization. Bull. Am. Meteorol. Soc. 102 (4), 774—781. https://doi.org/10.1175/BAMS-D-20-0289.1

Mukherjee, S., Ashfaq, M., Mishra, A.K., 2020. Compound Drought and Heatwaves at a Global Scale: The Role of Natural Climate Variability-Associated Synoptic Patterns and Land-Surface Energy Budget Anomalies. J. Geophys. Res.: Atmos. 125 (11), 0—19. https://doi.org/10.1029/2019JD031943

Mukherjee, S., Mishra, A.K., 2020. Increase in Compound Drought and Heatwaves in a Warming World. Geophys. Res. Lett. 48 (1), 1—13. https://doi.org/10.1029/2020GL090617

Mukherjee, S., Mishra, A.K., Ashfaq, M., Kao, S.C., 2022. Relative effect of anthropogenic warming and natural climate variability to changes in Compound drought and heatwaves. J. Hydrol. 605 (September 2021), 127396. https://doi.org/10.1016/j.jhydrol.2021.127396

Nogueira, M., 2020. Inter-comparison of ERA-5, ERA-interim and GPCP rainfall over the last 40 years: Process-based analysis of systematic and random differences. J. Hydrol. 583 (January), 124632. https://doi.org/10.1016/j.jhydrol.2020.124632

Peel, M.C., Finlayson, B.L., McMahon, T.A., 2007. Updated world map of the Köppen-Geiger climate classification. Hydrol. Earth Syst. Sc. 11, 1633—1644. https://doi.org/10.5194/hess-11-1633-2007

Perkins-Kirkpatrick, S.E., Gibson, P.B., 2017. Changes in regional heatwave characteristics as a function of increasing global temperature. Sci. Rep. 7 (1), 1—12. https://doi.org/10.1038/s41598-017-12520-2

Porebska, M., Zdunek, M., 2013. Analysis of extreme temperature events in central Europe related to high pressure blocking situations in 2001-2011. Meteorol. Z. 22 (5), 533—540. https://doi.org/10.1127/0941-2948/2013/0455

Prodhomme, C., Materia, S., Ardilouze, C., White, R.H., Batté, L., Guemas, V., Fragkoulidis, G., García-Serrano, J., 2022. Seasonal prediction of European summer heatwaves. Clim. Dynam. 58 (7—8), 2149—2166. https://doi.org/10.1007/s00382-021-05828-3

Ribeiro, A.F.S, Russo, A., Gouveia, C.M., Páscoa, P., Zscheischler, J., 2020. Risk of crop failure due to compound dry and hot extremes estimated with nested copulas. Biogeosciences 17 (19), 4815—4830. https://doi.org/10.5194/bg-17-4815-2020

Ridder, N.N., Pitman, A.J., Westra, S., Ukkola, A., Hong, X.Do, Bador, M., Hirsch, A.L., Evans, J.P., Di Luca, A., Zscheischler, J., 2020. Global hotspots for the occurrence of compound events. Nat. Commun. 11 (1), 1—10. https://doi.org/10.1038/s41467-020-19639-3

Rimkus, E., Kažys, J., Valiukas, D., Stankūnavičius, G., 2014. The atmospheric circulation patterns during dry periods in Lithuania. Oceanologia 56 (2), 223—239. https://doi.org/10.5697/oc.56-2.223

Rimkus, E., Maciulyte, V., Stonevicius, E., Valiukas, D., 2020. A revised agricultural drought index in Lithuania. Agric. Food Sci. 29 (4), 359—371. https://doi.org/10.23986/afsci.92150

Rimkus, E., Stonevičius, E., Korneev, V., Kažys, J., Valiuškevičius, G., Pakhomau, A., 2013. Dynamics of meteorological and hydrological droughts in the Neman River basin. Environ. Res. Lett. 8 (4). https://doi.org/10.1088/1748-9326/8/4/045014

Rousi, E., Kornhuber, K., Beobide-Arsuaga, G., Luo, F., Coumou, D., 2022. Accelerated western European heatwave trends linked to more-persistent double jets over Eurasia. Nat. Commun. 13 (1), 1—11. https://doi.org/10.1038/s41467-022-31432-y

Rutgersson, A., Kjellström, E., Haapala, J., Stendel, M., Danilovich, I., Drews, M., Jylhä, K., Kujala, P., Larsén, X.G., Halsnæs, K., Lehtonen, I., Luomaranta, A., Nilsson, E., Olsson, T., Särkkä, J., Tuomi, L., Wasmund, N., 2022. Natural hazards and extreme events in the Baltic Sea region. Earth Syst. Dynam. 13 (1), 251—301. https://doi.org/10.5194/esd-13-251-2022

Sedlmeier, K., Feldmann, H., Schädler, G., 2018. Compound summer temperature and precipitation extremes over central. Europe. Theor. Appl. Climatol. 131 (3—4), 1493—1501. https://doi.org/10.1007/s00704-017-2061-5

Seneviratne, S.I., Nicholls, N., Easterling, D., Goodess, C.M., Kanae, S., Kossin, J., Luo, Y., Marengo, J., Mc Innes, K., Rahimi, M., Reichstein, M., Sorteberg, A., Vera, C., Zhang, X., 2012. Changes in climate extremes and their impacts on the natural physical environment. In: Field, C.B., Barros, V., Stocker, T.F, Qin, D., Dokken, D.J., Ebi, K.L., Mastrandrea, M.D., Mach, K.J., Plattner, G.K., Allen, S.K., Tignor, M., Midgley, P.M. (Eds.), A Special Report of Working Groups I and II of the

Intergovernmental Panel on Climate Change (IPCC). Managing the Risks of Extreme Events and Disasters to Advance Climate Change Adaptation. Cambridge University Press, Cambridge, UK, and New York, NY, USA, 109—230.

Seneviratne, S.I., Zhang, X., Adnan, M., Badi, W., Dereczynski, C., Di Luca, A., Ghosh, S., Iskandar, I., Kossin, J., Lewis, S., Otto, F., Pinto, I., Satoh, M., Vicente-Serrano, S.M., Wehner, M., Zhou, B., 2021. Weather and Climate Extreme Events in a Changing Climate. In: Masson-Delmotte, V., Zhai, P., Pirani, A., Connors, S.L., Péan, C., Berger, S., Caud, N., Chen, Y., Goldfarb, L., Gomis, M.I., Huang, M., Leitzell, K., Lonnoy, E., Matthews, J.B.R., Maycock, T.K., Waterfield, T., Yelekçi, O., Yu, R., Zhou, B. (Eds.), Climate Change 2021: The Physical Science Basis. Contribution of Working Group I to the Sixth Assessment Report of the Intergovernmental Panel on Climate Change. Cambridge University Press, Cambridge, United Kingdom and New York, NY, USA, 1513—1766.

Sharma, S., Mujumdar, P., 2017. Increasing frequency and spatial extent of concurrent meteorological droughts and heatwaves in India. Sci. Rep. 7 (1), 1—9. https://doi.org/10.1038/s41598-017-15896-3

Shi, Z., Jia, G., Zhou, Y., Xu, X., Jiang, Y., 2021. Amplified intensity and duration of heatwaves by concurrent droughts in China. Atmos. Res. 261 (April), 105743. https://doi.org/10.1016/j.atmosres.2021.105743

Somorowska, U., 2016. Changes in drought conditions in Poland over the past 60 years evaluated by the standardized precipitation-evapotranspiration index. Acta Geophys. 64 (6), 2530—2549. https://doi.org/10.1515/acgeo-2016-0110

Sousa, P.M., Trigo, R.M., Barriopedro, D., Soares, P.M.M., Santos, J.A., 2018. European temperature responses to blocking and ridge regional patterns. Clim. Dynam. 50 (1—2), 457—477. https://doi.org/10.1007/s00382-017-3620-2

Spensberger, C., Madonna, E., Boettcher, M., Grams, C.M., Papritz, L., Quinting, J.F., Röthlisberger, M., Sprenger, M., Zschenderlein, P., 2020. Dynamics of concurrent and sequential Central European and Scandinavian heatwaves. Q. J. R. Meteorol. 146 (732), 2998—3013. https://doi.org/10.1002/qj.3822

Suursaar, Ü., 2022. Summer 2021 marine heat wave in the Gulf of Finland from the perspective of climate warming. Est. J. Earth Sci. 71 (1), 1—16. https://doi.org/10.3176/earth.2022.01

Tomczyk, A.M., Bednorz, E., Matzarakis, A., 2020. Human-biometeorological conditions during heat waves in Poland. Int. J. Climatol. 40 (12), 5043—5055. https://doi.org/10.1002/joc.6503

Tsakiris, G., Vangelis, H., 2004. Towards a Drought Watch System based on spatial SPI. Water Resour. Manage. 18 (1), 1—12. https://doi.org/10.1023/B:WARM.0000015410.47014.a4

Valiukas, D., 2015. Analysis of droughts and dry periods in Lithuania. Summary of doctoral thesis. Vilnius University.

Velikou, K., Lazoglou, G., Tolika, K., Anagnostopoulou, C., 2022. Reliability of the ERA5 in Replicating Mean and Extreme Temperatures across Europe. Water (Switz.). 14 (4). https://doi.org/10.3390/w14040543

Vicente-Serrano, S.M., Beguería, S., López-Moreno, J.I., 2010. A multiscalar drought index sensitive to global warming: The standardized precipitation evapotranspiration index. J. Clim. 23 (7), 1696—1718. https://doi.org/10.1175/2009JCLI2909.1

Vyshkvarkova, E., Sukhonos, O., 2022. Compound Extremes of Air Temperature and Precipitation in Eastern Europe. Climate 10, 133. https://doi.org/10.3390/cli10090133

Wang, C., Li, Z., Chen, Y., Li, Y., Liu, X., Hou, Y., Wang, X., Kulaixi, Z., Sun, F., 2022. Increased Compound Droughts and Heatwaves in a Double Pack in Central Asia. Remote Sens. 14 (13), 1—19. https://doi.org/10.3390/rs14132959

Wazneh, H., Gachon, P., Laprise, R., de Vernal, A., Tremblay, B., 2021. Atmospheric blocking events in the North Atlantic: trends and links to climate anomalies and teleconnections. Clim. Dynam. 56 (7—8), 2199—2221. https://doi.org/10.1007/s00382-020-05583-x

Wibig, J., 2017. Heat waves in Poland in the period 1951-2015: trends, patterns and driving factors. Meteorology Hydrology and Water Management 6 (1), 1—10. https://doi.org/10.26491/mhwm/78420

Wibig, J., 2021. Hot days and heat waves in Poland in the period 1951-2019 and the circulation factors favoring the most extreme of them. Atmosphere 12 (3). https://doi.org/10.3390/atmos12030340

WMO, 2012. Standardized Precipitation Index User Guide. WMO-No. 1090, Geneva. Accessed on February 12th, 2023. https://digitalcommons.unl.edu/cgi/viewcontent.cgi?article=1208&context=droughtfacpub

Wu, X., Hao, Z., Hao, F., Singh, V.P., Zhang, X., 2019. Dry-hot magnitude index: A joint indicator for compound event analysis. Environ. Res. Lett. 14 (6). https://doi.org/10.1088/1748-9326/ab1ec7

Yoon, D., Cha, D.H., Lee, M.I., Min, K.H., Kim, J., Jun, S.Y., Choi, Y., 2020. Recent changes in heatwave characteristics over Korea. Clim. Dynam. 55 (7—8), 1685—1696. https://doi.org/10.1007/s00382-020-05420-1

Zhang, Q., She, D., Zhang, L., Wang, G., Chen, J., Hao, Z., 2022. High Sensitivity of Compound Drought and Heatwave Events to Global Warming in the Future. Earth's Future 10 (11). https://doi.org/10.1029/2022EF002833

Ziernicka-Wojtaszek, A., 2021. Summer drought in 2019 on Polish territory — a case study. Atmosphere 12 (11). https://doi.org/10.3390/atmos12111475

Zscheischler, J., Martius, O., Westra, S., Bevacqua, E., Raymond, C., Horton, R.M., van den Hurk, B., AghaKouchak, A., Jézéquel, A., Mahecha, M.D., Maraun, D., Ramos, A.M., Ridder, N.N., Thiery, W., Vignotto, E., 2020a. A typology of compound weather and climate events. Nat. Rev. Earth Environ. 1 (7), 333—347. https://doi.org/10.1038/s43017-020-0060-z

Zscheischler, J., Van Den Hurk, B., Ward, P.J., Westra, S., 2020b. Multivariate extremes and compound events. In Climate Extremes and Their Implications for Impact and Risk Assessment. Elsevier. https://doi.org/10.1016/B978-0-12-814895-2.00004-5

Zscheischler, J., Westra, S., Van Den Hurk, B.J.J.M., Seneviratne, S.I., Ward, P.J., Pitman, A., Aghakouchak, A., Bresch, D.N., Leonard, M., Wahl, T., Zhang, X., 2018. Future climate risk from compound events. Nat. Clim. Change. 8 (6), 469—477. https://doi.org/10.1038/s41558-018-0156-3

Oceanologia 66 (2024) 37—55

Available online at www.sciencedirect.com

ScienceDirect

journal homepage: www.journals.elsevier.com/oceanologia

ORIGINAL RESEARCH ARTICLE

Seawater temperature changes in the southern Baltic Sea (1959—2019) forced by climate change

Tamara Zalewska[a,*], Bartłomiej Wilman[a], Bożena Łapeta[b], Michał Marosz[a], Dawid Biernacik[a], Agnieszka Wochna[a], Michał Saniewski[a], Agnieszka Grajewska[a], Michał Iwaniak[a]

[a] *Institute of Meteorology and Water Management — National Research Institute, Gdynia, Poland*
[b] *Institute of Meteorology and Water Management — National Research Institute, Kraków, Poland*

Received 19 February 2023; accepted 29 August 2023
Available online 19 September 2023

KEYWORDS
Sea surface temperature;
Water column temperature;
Climate change;
Long-term measurements;
Satellite data;
Reanalysis data

Abstract The study included the analysis of changes in sea surface and water column temperature and air temperature in the years 1959—2019 in the southern Baltic Sea based on in situ measurement (CTD probe), satellite data, and model data (ERA5). SST increased on average by 0.6°C per decade. Analyses at different depths showed that the highest temperature increase per decade at 0.60—0.65°C characterised the layers from 0 to 20 m. The smallest increase (0.11°C) was recorded at a depth of 70 m, below which the temperature change per decade increases again to 0.24°C. The results from satellite observations covering 1982—2019 were consistent with measurement data. The most intense water warming occured in the spring — summer (0.8—1°C per decade); in the winter, the change did not exceed 0.2°C. In the offshore area, in 1951—2020, air temperature increased by approx. 2°C, with an average increase of 0.37°C per decade. The average increase in seawater temperature in the coastal zone was 0.2°C per decade. The most intense warming characterised March to May (0.25—0.27°C). The average annual air temperature increase on the coast from 1951 to 2020 was 0.34°C per decade. The results represent an important contribution to research and prediction of changes in the marine environment caused by global climate change.

* Corresponding author at: Institute of Meteorology and Water Management — National Research Institute, Waszyngtona 42, 81—342 Gdynia, Poland.
E-mail address: tamara.zalewska@imgw.pl (T. Zalewska).
Peer review under the responsibility of the Institute of Oceanology of the Polish Academy of Sciences.

Production and hosting by Elsevier

https://doi.org/10.1016/j.oceano.2023.08.001

1. Introduction

Climate change and its massive impact on the environment and is currently one of the greatest threats and challenges for humanity. The most fundamental change is the observed increase in air temperature, resulting primarily from the greenhouse gases emitted, the consequences of which are visible at various levels of ecosystem functioning, including the marine systems. The average atmospheric concentration of carbon dioxide exceeded 410 ppm in 2019 (IPCC, 2022), and the effects of climate change have become more visible (Iles and Hegerl, 2017; IPCC, 2022; Makkonen et al., 2015). The latest Intergovernmental Panel on Climate Change (IPCC) report found that the global surface temperature in the first two decades of the 21st century (2001—2020) was 0.99°C warmer than in 1850—1900. In the period 2011—2020, it was 1.09°C higher than in the period 1850—1900, with a more significant increase in temperature over land (1.59 [1.34 to 1.83] °C) than over oceans (0.88 [0.68 to 1.01] °C) (IPCC, 2022). Scenarios for the Baltic Sea project a sea surface temperature (SST) increase of 1.2°C (0.9—1.6°C, RCP 2.6) to 3.3°C (2.6—4.1°C, RCP 8.5) by the end this century (Gröger et al., 2019; Meier and Saraiva, 2020), compared to the period 1976—2005. The Baltic Sea is a semi-enclosed, brackish regional sea with a unique large-scale gradient from temperate marine to subarctic climates and has been shown to be highly sensitive to climate change (BACC II, 2015), reflected in its being one of the fastest warming marginal seas in the world (Kniebusch et al., 2019). It is predicted that the warming trend of the Baltic Sea region will be observed continuously in the 21st century, and the impact of climate change on water transport and mixing processes will be observed in the longer term (Meier et al., 2011). In addition to climate change, the Baltic Sea is under considerable anthropogenic influence, resulting in the intensification of unfavourable processes in this area. These include eutrophication, pollution by hazardous substances, disturbed biogeochemical cycles, overfishing and ecological effect of invasive species. Climate change is likely to intensify these problems in the future (Dettinger et al., 2016). Water temperature determines the intensity of most biological and chemical processes (Brierley and Kingsford, 2009). For many fish species, the initial spawning signal is produced when the water temperature exceeds a certain threshold, and the metabolism of planktonic organisms can increase significantly as the water temperature increases (Jørgensen, 1994; Jørgensen et al., 2005). This causes changing thermal conditions to affect the timing of spring blooms, the extension of the growing season and the phytoplankton species composition (Pärn et al., 2021), with further implications for nutrient cycles and ecosystem dynamics (Klais et al., 2013). Increased primary production can lead to reduced water clarity and increased deposition of organic material, increasing oxygen consumption on the seabed and leading to oxygen depletion. These changes can affect species composition and interactions in the food web, as species that benefit from eutrophic conditions are favoured directly or by affecting habitat quality and foraging conditions (Cloern, 2001). An increase in water temperature may also directly contribute to the episodic deterioration of oxygen conditions from hypoxia, i.e., oxygen concentration below 2 mg l^{-1}, to anoxia, i.e., absolute lack of oxygen and presence of hydrogen sulphide. In addition, warmer water temperatures also increase the mineralisation rate of organic matter, which further exacerbates hypoxia (Carstensen et al., 2014; Sinkko et al., 2019; Virtanen et al., 2019). Warmer, hypoxic waters can directly affect organism mortality, changes in metabolism and growth, forced migration, habitat shrinkage, increased susceptibility to predation or changes in food availability (Diaz and Rosenberg, 2011; Levin, 2018; Pollock et al., 2007). One example observed in the Baltic Sea is the change in cod population distribution and growth (Orio et al., 2022).

Although the possible influence on climate change, at least at this stage, is limited, it is necessary to conduct research and analysis, especially in relation to changes in the thermal conditions of marine ecosystems, which are associated with a well-documented increase in air temperature (IPCC, 2022). The research must cover both the historical and contemporary contexts in order to predict future changes in temperature and assess the impact of the increase, taking into account the predicted dynamics on the functioning of the marine ecosystem, especially in terms of its effects on organisms. The research on changes in the temperature of the Baltic Sea waters conducted so far have covered various periods. The studies were based on data from multiple sources: direct measurement (e.g., Bradtke et al., 2010), modelling (Kniebusch at al., 2019) and satellite (Stramska and Białogrodzka, 2015).

The main aim of our research was to track changes in water temperature in the southern Baltic Sea in relation to global warming. Our research results are the only ones for this area showing changes in seawater temperature based on a very long series of measurement data from 1959—2019. The aim of the work was also to show the complementarity of measurement, satellite and reanalysis data. The information gained from this opens up the possibility of using various data sources in the analysis of thermal conditions in sea areas. A long-term series of measurement data has also enabled reliable analyses of temperature changes in the water column over a period of 60 years. The availability of long-term data sets has made it possible to determine the rate of seawater temperature changes in the southern Baltic Sea, taking into account different periods, coastal and offshore areas, and seasonality. The observed changes were related to climatic conditions characterised by air temperature data from measurements carried out at coastal stations and from reanalysis in offshore areas. The results of correlation studies are the basis for predicting seawater temperature changes depending on the adopted climatic scenarios, which may be of fundamental importance for research into the marine environment and adaptation activities in the southern Baltic region.

2. Material and methods

2.1. Study area

The research covers the area of the southern Baltic: sea water temperature data was obtained from surface and water column measurements and satellite data, as well as air temperature data from ERA5 re-analyses. The data come from

Figure 1 Location of the open sea and coastal stations.

measurements carried out at selected measuring stations in the open sea zone (Figure 1). Measurement data in the field of sea surface temperature and air temperature also come from measurements carried out at synoptic stations located in the coastal zone, which are part of the infrastructure of the Institute of Meteorology and Water Management — National Research Institute (Figure 1).

2.2. Measurement data

Data on water temperature are sourced from measurements carried out in the southern Baltic Sea as part of regular oceanographic and monitoring measurements carried out by the Institute of Meteorology and Water Management — National Research Institute in the years 1959—2019. The analysis used data from stations located in the open sea and territorial waters, for which the most complete data existed, enabling the most comprehensive spatial coverage and the registration of seasonal temperature changes and for which it was possible to conduct analyses of changes in the water column. It should be emphasised, however, that the time regime (months in which the measurements were carried out) was slightly different in individual years. At various depths, measurements were made using CTD probes throughout the water profile. Finally, data from eight measuring stations located in the open sea region (Figure 1) were used for the analyses. In the case of data from coastal stations, surface water temperature measurements were made daily, and the analysed data came from eight stations: Świnoujście, Międzyzdroje, Kołobrzeg, Władysławowo, Puck, Hel, Gdynia and Gdańsk (Figure 1) and cover the period 1951—2019. Data on air temperature comes from measurements carried out at four coastal stations (Świnoujście, Kołobrzeg, Hel, Gdańsk) in the period from 1951 to 2020. Air temperature measurements at synoptic stations in Poland use standard measuring sensors in accordance with WMO guidelines.

2.3. Satellite data

Satellite data provides information on the distribution of sea surface temperature in the area covered by the analyses. The study used the Baltic Sea surface temperature data series SST_BAL_SST_L4_REP_OBSERVATIONS_010_016 (Hoyer and Karagali, 2016; Hoyer and She, 2007) developed by the Danish Meteorological Institute (DMI) and made available by the Copernicus Marine Service. This series is a re-analysis of the sea surface temperature data series of the European Space Agency Climate Change Initiative (Merchant et al., 2019) and Copernicus Climate Change Service (C3S) projects covering the period from 1982 to the present. The series contains data on the daily distribution of sea surface temperature on a regular grid with a step of 0.02 × 0.02 degrees. Data from the following satellite sensors were used for its development: Advanced Very High-Resolution Radiometer (AVHRR) from NOAA-7, 9, 11, 12, 14, 15, 16, 17, 18, 19 or, Metop; Along-Track Scanning Radiometer 1 and 2 (ATSR1, ATSR2) on ERS-1 and ERS-2 respectively, Advanced Along-Track Scanning Radiometer on ENVISAT and Sea Land Surface Temperature Radiometer (SLSTR) on Sentinel-3A and 3B. To determine the sea surface temperature from satellite data, the split-window method (Walton et al., 1998) was used, using measurements of radiation in the infrared range of the spectrum, which is heavily "polluted" by cloud cover. There is often no data on sea surface temperature for the Baltic Sea area. Therefore, the optimal interpolation (OI) method was used to obtain a continuous temperature distribution (Hoyer and Kara-

gali, 2016). In order to remove the influence of daily sea surface changes due to sea heating and cooling during the day, only data from night satellite overpasses were used to prepare the time series (Hoyer and Karagali, 2016). The work uses a series of data for the years 1982—2018, for the area of the southern Baltic Sea. The average annual sea surface temperature distributions and the spatial distribution of the rate of change for the average annual sea surface temperature were calculated. The rate of change was determined as the slope of the linear regression.

To compare the sea surface temperature determined from satellite data with measurements, data from the grid mesh closest to the measurement point were used. The sea surface temperature distribution did not show abrupt changes, it was considered that with a grid size of 0.02 degrees, such an approach was sufficient to assess the suitability of the selected satellite data series for the study of the thermal characteristics of the southern Baltic Sea. In addition, all cases with ice on the surface, for which the degree of mesh coverage with ice was greater than 0.2, were excluded from the comparative analysis.

2.4. Re-analysis data

ECMWF ERA5 (source: Copernicus Climate Data Store) is one of the re-analyses currently used in climate research. It is the latest generation of ECMWF reanalysis products routinely used in climate monitoring and numerical forecasting (Qiu et al., 2023). The authors (Qiu et al., 2023) analysed its suitability to aid the calculation of evaporation ducts over the East China Sea with air temperature used as one of the variables. King et al. (2022) also confirmed the quality of ERA5 reanalysis in the context of near-surface air temperature quality over the Weddel Sea Ice Pack. ERA5 captured the air temperature variability well with very little bias for temperatures close to 0°C.

The research used data on air temperature with a spatial resolution of 0.25 × 0.25 degrees latitude/longitude and a time resolution of 3 h in the Baltic Sea area covered by the research. The time range of the analyses covered the years 1951—2019. The data were prepared and processed into a form that could be used in our further studies, particularly for the quantitative analysis of the links between meteorological conditions and oceanographic characteristics. A set of data, assigned to measurement points for water temperature measurements carried out, was prepared using the bi-linear interpolation method, a technique commonly used for processing data from a regular grid of points. The overall quality of the ERA5 reanalysis data at selected measurements points was confirmed as there was a high concordance with the other measurements used in our analysis i.e.: satellite data and in situ measurements. This fact combined with the long period of available data and fixed data assimilation method makes the ERA5 reanalysis an invaluable source of data for the analysis of the variability in thermal conditions over the long term.

2.5. Statistics

Databases were prepared to carry out statistical analyses of water temperature changes in offshore and coastal areas. In the open sea and territorial waters, data originating from stations with the most complete data sets, enabled spatial coverage and the determination of seasonal temperature changes for analyses of changes in the water column. It should be emphasised, however, that the time regime (the months in which the measurements were carried out) was slightly different in individual years, with cruises undertaken in the years 1959—2019 spanning different months. It is possible that this may impact the final characteristics of changes in the average temperature in comparisons between years where sampling campaigns were carried out. For the analysis of temperature changes in the water column, the following aggregated levels were adopted: 0, 10, 20, 30, 40, 50, 60, 70, 80, 90, 100 and 110 m. Temperature measurements were assigned to the particular levels according to the following rules: (1) if measurement depth (MD) was in the range <0; 1> assign 0 m; (2) if MD (1; 10> assign 10 m; (3) if MD (10; 20> assign 20 m, MD (20; 30> assign 30 m, (…), MD (100; 110> assign 110 m. Statistical analysis included determining basic statistical parameters: annual averages and minimum and maximum values in individual years.

Data from the ERA5 re-analysis (3h time resolution) were aggregated to daily average values to allow for comparability with other analysed variables and the calculation of statistical characteristics that were then subjected to analysis. Mean values and quantiles (5% and 95%) were compared in the statistical analysis. In addition to multi-year aggregates (1951—2020), a series of annual and seasonal values were also calculated, which enabled trends in the data to be evaluated. Directional coefficients of the trend (C/10 years) and their statistical significance ($\alpha = 0.05$) were calculated based on the F-Snedecor test.

In the case of air temperature at coastal stations, average monthly and annual values were determined at four coastal stations (Świnoujście, Kołobrzeg, Hel, Gdańsk) in the period from 1951 to 2020.

Spearman's rank correlations between seawater temperature (measured and satellite data) and air temperature at 2m altitude were also investigated in the entire offshore and coastal dataset and for each station for which data for both parameters existed (Table 1).

3. Results and discussion

3.1. Characteristics of changes in seawater temperature in the offshore zone

The analysis of long-term changes in the sea surface temperature (SST), covering the period 1959—2019, showed a statistically significant increase in mean SST in the entire area of the southern Baltic (Figure 2a). This characteristic applies to average values and maximum values (Figure 2a). In the period covered by the research, the lowest average annual SST occurred in 1964 (5.6°C), while the maximum was recorded in 2018 and amounted to 14.1°C. Similar characteristics were observed in individual areas: Bornholm Basin, Easter Gotland Basin and Gdańsk Basin, where the minimum annual averages were respectively: 4.5°C, 4.3°C and 4.2°C, while in the case of the Gdańsk Basin, the value was recorded in 1968. The warmest year, with average values of 14.1°C, 14.7°C and 15.9°C,

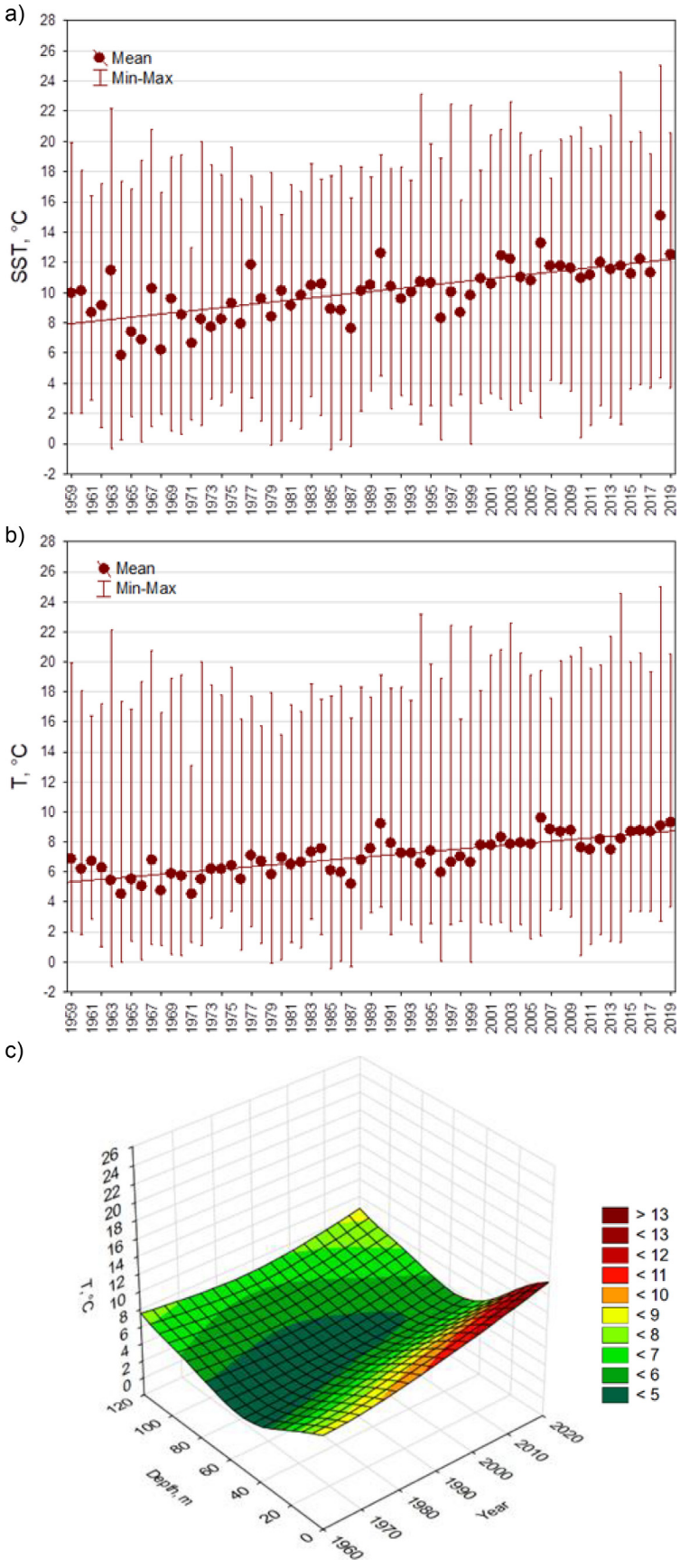

Figure 2 Seawater temperature changes in the surface layer (a) and in the entire column (b and c) with maximum and minimum values in the southern Baltic in 1959—2019 (based on data from stations: P110, P116, P1, P2, P3, P5).

Table 1 Correlation coefficients between the surface temperature of sea water (measured and satellite data) and the air temperature in the offshore zone determined by Spearman's rank method (boldface means a statistically significant relationship at the level of $p < 0.05$).

Area (station)		SST (measurement)	T2m (ERA5)
Southern Baltic (all stations)	Year	**0.196**	**0.195**
	Month	**0.591**	**0.475**
	SST (measurement)	1.000	**0.934**
	SST (satelite)	**0.989**	**0.936**
	T2m (ERA5)	**0.934**	1.000
Gdańsk Deep (P1)	SST (measurement)	1.000	**0.923**
	SST (satelite)	**0.988**	**0.930**
	T2m (ERA5)	**0.923**	1.000
Słupsk Furrow (P2)	SST (measurement)	1.000	**0.944**
	SST (satelite)	**0.994**	**0.959**
	T2m (ERA5)	**0.944**	1.000
Słupsk Furrow (P3)	SST (measurement)	1.000	**0.939**
	SST (satelite)	**0.996**	**0.953**
	T2m (ERA5)	**0.939**	1.000
Bornholm Deep (P5)	SST (measurement)	1.000	**0.948**
	SST (satelite)	**0.996**	**0.946**
	T2m (ERA5)	**0.948**	1.000
Gdańsk Basin (P110)	SST (measurement)	1.000	**0.913**
	SST (satelite)	**0.984**	**0.911**
	T2m (ERA5)	**0.913**	1.000
Gdańsk Basin (P116)	SST (measurement)	1.000	**0.913**
	SST (satelite)	**0.978**	**0.916**
	T2m (ERA5)	**0.913**	1.000
Pomeranian Bay (B13)	SST (measurement)	1.000	**0.956**
	SST (satelite)	**0.990**	**0.949**
	T2m (ERA5)	**0.956**	1.000
Pomeranian Bay (B15)	SST (measurement)	1.000	**0.940**
	SST (satelite)	**0.987**	**0.933**
	T2m (ERA5)	**0.940**	1.000
Eastern Gotland Basin (P140)	SST (measurement)	1.000	**0.955**
	SST (satelite)	**0.996**	**0.952**
	T2m (ERA5)	**0.955**	1.000

respectively, in individual basins, was 2018. Such changes are identical to the characteristics at stations located in the distinguished areas. From 1971 to 2019, in the shallow water zone (Pomeranian Bay), the sea surface temperature ranged from 6.0°C in 1972 to 13.5°C in 2003.

Taking into account the temperature change in the entire water column in the years 1959—2019, a statistically significant upward trend was also observed (Figure 2b). Changes in the average annual temperature determined based on data for the entire water column oscillated in a narrower range compared to surface waters. They varied from 4.5°C observed in 1964 and 1971 to 9.6°C in 2006. In the period covered by the study, the most noticeable increase in water temperature was recorded in the surface layer and bottom waters since the 1990s (Figure 2c). The same characteristics are visible in the temporal changes of temperature observed in the water column at selected stations representing different areas of the southern Baltic (Figure 3).

The most significant change in bottom temperature was observed in the Bornholm Deep due to the influx of warmed surface water from the North Sea introduced in the bottom layer due to higher density associated with higher salinity. In addition to the increase in temperature, an expansion of the thickness of the layer affected by the most significant changes is also observed, particularly visible in the Bornholm Basin.

The areas of influence of waters from the North Sea are related to the main water transport routes — from the Danish Straits to the Arkona Basin and through the Bornholm Gate to the Bornholm Deep. Further transport takes place through the Słupsk Furrow to the Gdańsk and Gotland Deeps. The impact of inflows, especially those with large volumes (Major Baltic Inflows), which transport highly saline water and are an essential source of oxygen, is very clearly marked, especially in the bottom layers (Meier and Kauker, 2003). As confirmed by our research, they are crucial in shaping the thermal characteristics of the bottom layers below the halocline. According to studies conducted since the 1880s, a significant decrease in the incidence of major barotropic inflows has been noted since the 1980s

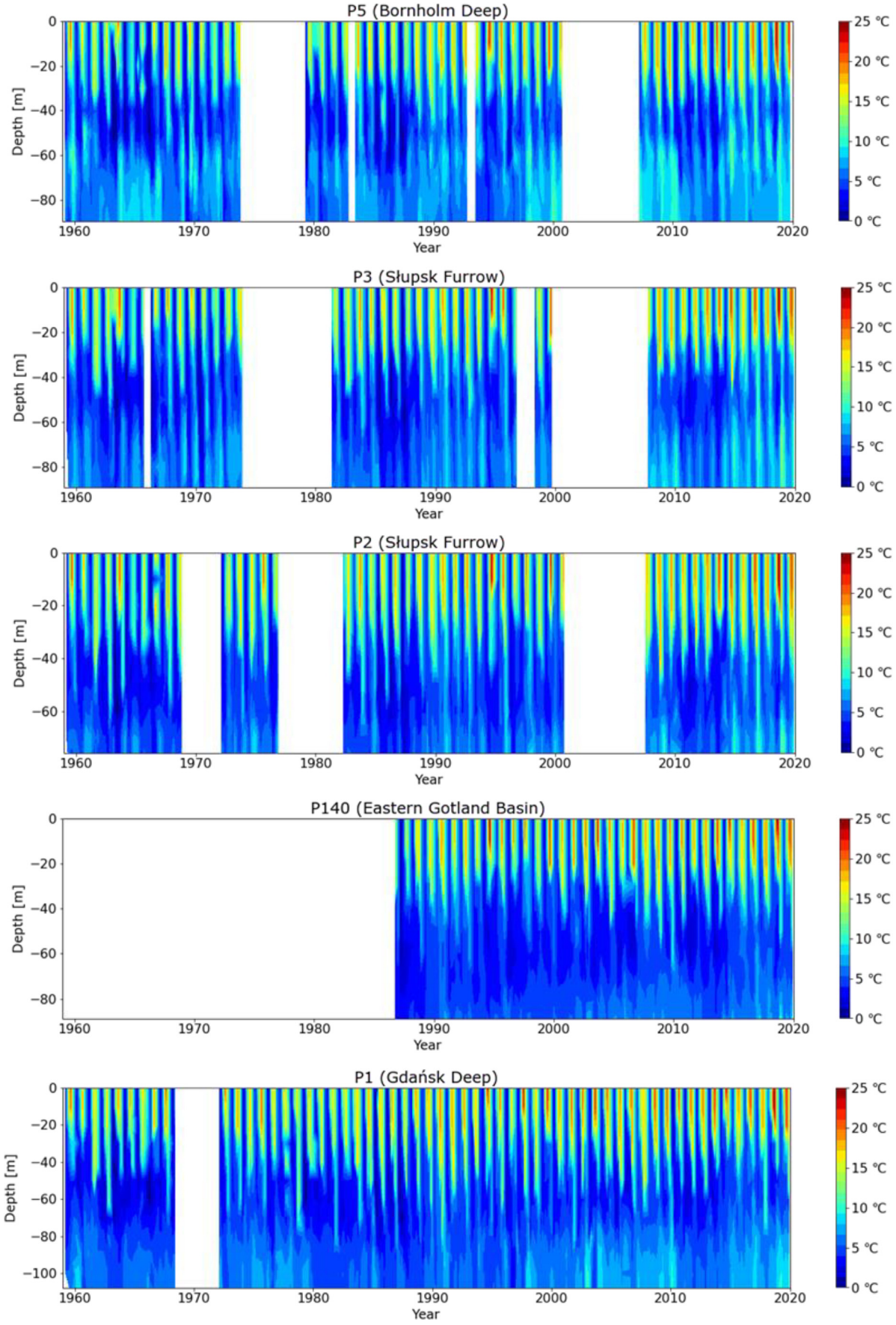

Figure 3 Seawater temperature in the water column at selected stations located in the southern Baltic in 1959—2019 (white areas — data unavailable).

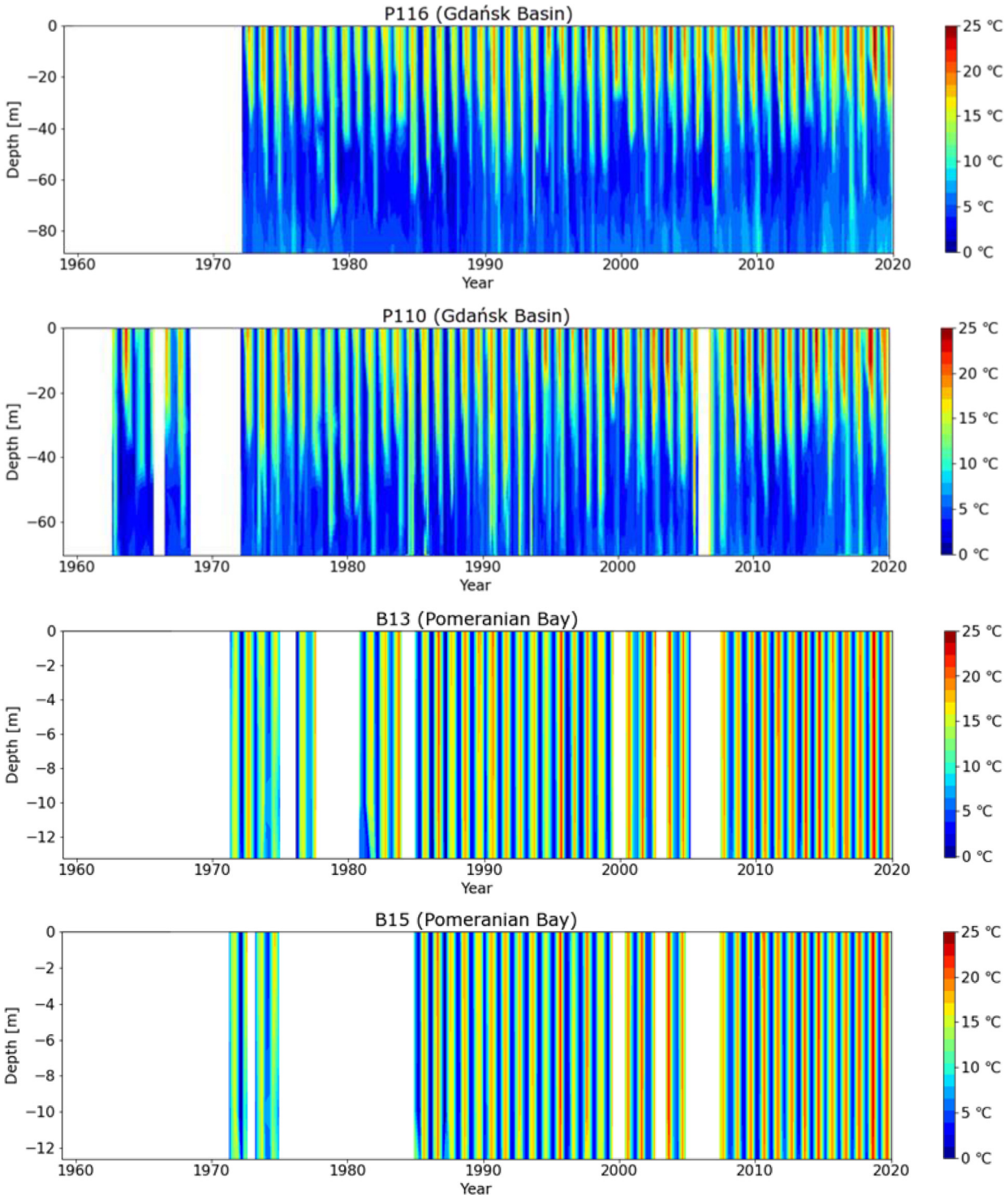

Figure 3 *Continued.*

(Fischer and Matthäus, 1996). At the same time, recent studies (taking into account that the distribution of salinity in the bottom layers does not fully confirm these observations) prove that the frequency of inflows could have been higher (Morholz, 2018). In the years 1960—1980, inflows occurred every 3—4 years, with the most significant for shaping the temperature in the Bornholm Deep taking place in the mid-1960s. This can be seen in our analysis describing characteristics of the temperature distribution in the water column (Figure 3). Subsequent Major Baltic Inflows occurred in 1993, 2003 and 2014, with the latter being the third-largest inflow in recorded history. In the area of the Bornholm Basin, a permanently higher temperature below the halocline has been observed since 2015. The same characteristics occur in the Słupsk Furrow at the P3 station and to a much lower intensity at the P2 station and

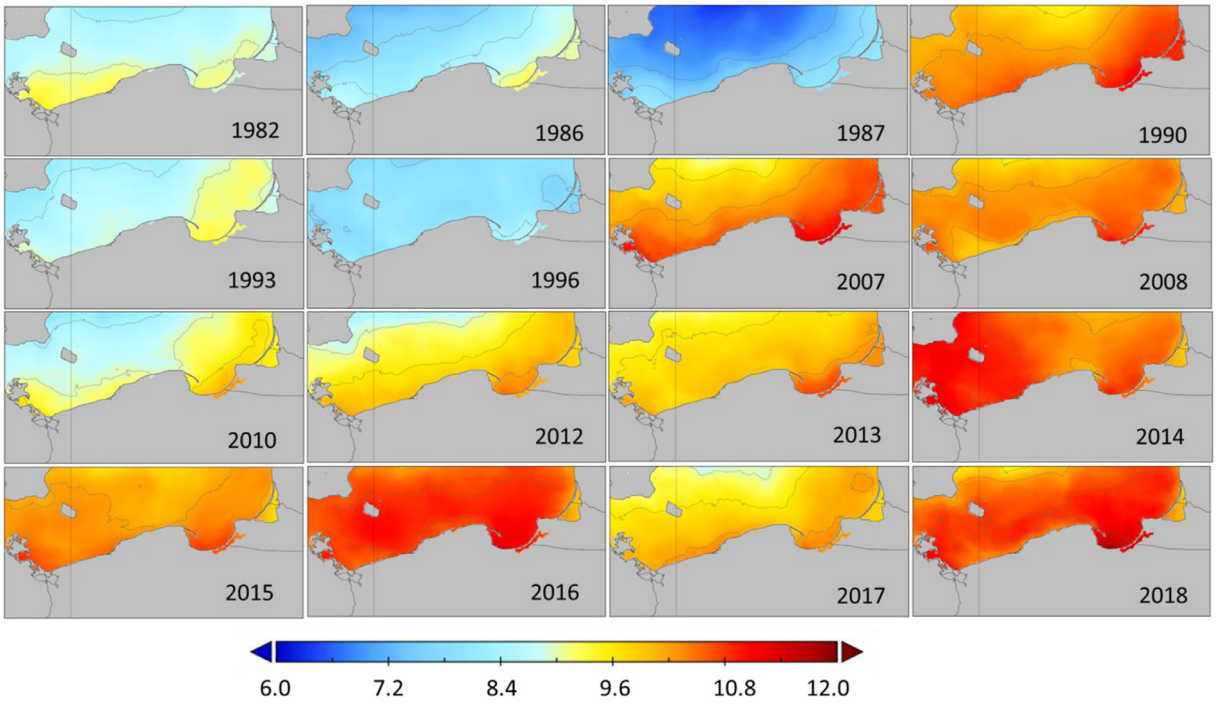

Figure 4 The average annual sea surface temperature in the southern Baltic in selected years in the period 1982—2018 based on satellite data.

in the Gdańsk Deep (P1), where the higher temperature applies to much deeper layers. Changes are least noticeable in the eastern Gotland Basin (P140) (Figure 3). An increase in the temperature of the water, both on the surface and the deeper layers of the Baltic Sea, is observed in all regions of the Baltic Sea (Høyer and Karagali, 2016; Liblik and Lips, 2019; Stramska and Białogrodzka, 2015). According to Hinrichsen et al. (2007), strong interannual variability of deep-water temperatures during the last two decades show a positive trend (an increase of 1—1.5°C). These trends are expected to continue according to the regional climate change scenarios prepared with climate models (BALTEX, 2006). Similar positive trends in deep water temperatures have also been observed in several European lakes (Dokulil et al., 2006)

The analysis of temperature changes at the stations located in the Gdańsk Basin showed that the visible impact range of the inflow waters after 2000 includes the P116 station (situated in the centre of the area). In contrast, there is no such discernible effect noted for the P110 station located in the profile of the Vistula estuary. This difference may be related to the difference in sampling depth (Figure 3). Temperature changes in shallow water areas of the Pomeranian Bay cover the entire column and their intensification is particularly visible after 2000 (Figure 3).

The analysis of surface temperature changes based on satellite data confirms the observations made based on measurement data (Figure 4). In the period covered by the study since 1982, the coldest year, as determined by average annual SST values, was 1987. From 1997 (immediately after one of the coldest periods of the average annual water temperature in 1996) surface and bottom water in the basins of the southern Baltic reached increasingly high maximum temperatures throughout the decade. However, changes in this period were not as dynamic as those observed since 2000. Apart from the year 2010, (when a decrease in temperature was recorded) in the period from 2000 to 2019 there is an intensification of warming of the southern Baltic Sea surface waters (Figure 4).

The results of calculations of temperature changes per decade also confirm the warning observations. Based on the measurement data, it was determined that SST in the southern Baltic, in 1959—2019, increased on average by 0.6°C per decade (Figure 5a), with the increase for the period 1959—1999 amounting to 0.3°C, and for the period 1980—2019 up to 0.7°C. The biggest change in the temperature of the Baltic waters compared to other sea and ocean areas was shown for the period 1982—2006 — 1.35K (Belkin, 2009a; Kniebusch et al., 2019). However, when the more extended period of 50 years is taken into account, the increase in temperature is less dynamic than in the last 30 years (Kniebusch et al., 2019), observations by our reanalysis. An increase of 0.66°C occurred over the previous 20 years.

The average rate of increase of SST per decade for the entire study period in the Gdańsk Basin was 0.60°C, in the Eastern Gotland Basin 0.58°C, in the Słupsk Furrow as much as 0.84°C, and in the Bornholm Basin 0.0.64°C. The increase in temperature in the Pomeranian Bay determined based on data for the period 1971—2019 was 0.77°C per decade (Figure 5a). An increase in water temperature values are also observed in the northern part of the Baltic Sea, although these were based on different time periods. Laakso et al. (2018) reported an increase in seawater temperatures, especially on the surface, with a rise of 0.3°C per decade for the last 100 years. Belkin et al. (2009b) re-

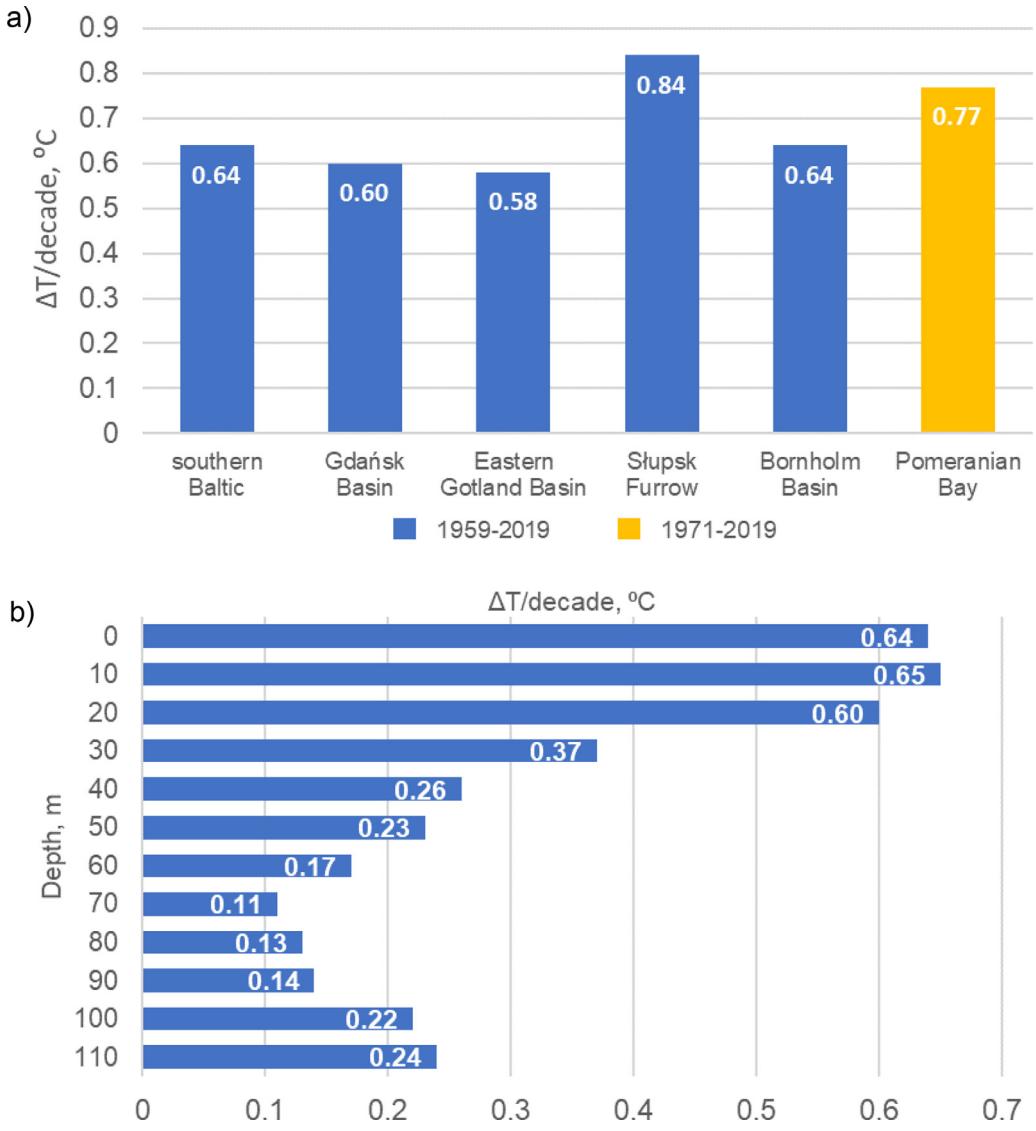

Figure 5 Change in the average seawater surface temperature per decade at selected stations (sub-basins) based on measurement data (a) and in the water column at different depths (b) based on measurement data.

ported SST changes at 1.35°C in 1982—2006 for the Baltic Sea.

Analysis of temperature changes at different depths also showed a statistically significant increase observed at all levels. However, the dynamics of this process differs depending on the depth (Figure 5b). The highest temperature increase per decade of 0.6—0.65°C characterised the layers from 0 to 20 m. The smallest increase (0.11°C) was recorded at a depth of 70 m, below which the temperature change per decade increases again to 0.24°C at a depth of 110 m (Figure 5b). The warmer surface waters from the North Sea are known to be introduced in the bottom layer, through thermohaline stratification resulting in the observed temperature distributions in the water column (Figure 3). Stratification of the water column, consisting of the three layers (upper, intermediate, and deep layer) separated by the seasonal thermocline and the permanent halocline, respectively, underpins the functioning of the Brackish Baltic Sea. The thermal stratification in the upper water layers varies seasonally in response to the annual cycle of solar heating and wind-induced mixing. In autumn and winter, the stratification is eroded by convection and strong wind mixing. A permanent halocline at 50—80 m depth separates the less saline surface water from the more saline bottom water, and during summer, a thermocline develops in the surface layer (Kullenberg, 1981). The upper layer has warmed by 0.03—0.06°C year^{-1}, and the sub-halocline deep layer is 0.04—0.06°C year^{-1} in most of the sea. The total warming trend in the Baltic has been 1.07°C for 35 years, approximately twice as high as the upper 100 m in the Atlantic Ocean (Liblik and Libs, 2019).

Decade changes in surface temperature obtained from sampling measurement data were largely confirmed by analyses of spatial satellite data. The research for the period 1982—2018 shows that the increase is observed in the entire area of the southern Baltic (Figure 6). The values of these changes range from 0.15°C to 0.60°C per decade. Slight differences in the results obtained based on measurement and

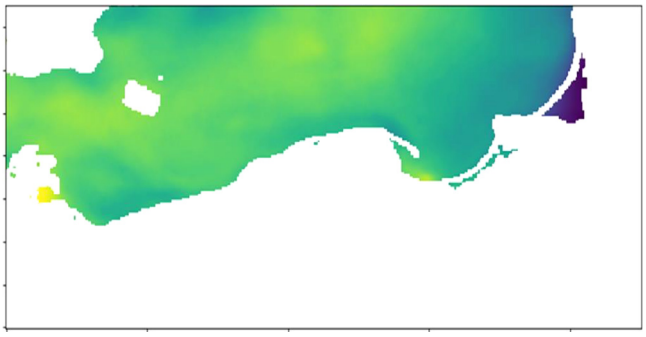

Figure 6 Change in the average sea surface temperature per decade (ΔT/decade [°C]) in the southern Baltic in 1985—2018 based on satellite data.

satellite data may result from the changing regime of measurements annually in the period covered by the analyses. Similar results based on satellite data for the period 1982—2013 were obtained by Stramska and Białogrodzka (2015). The lowest rate of sea surface temperature increase is observed in the Kursk Lagoon and the highest in the open sea area to the west and northeast of Bornholm. High trend values are also observed in the Gulf of Gdańsk, at the mouth of the Vistula.

The spatially and temporally continuous satellite data were used to determine the decadal temperature change in individual months. The most significant increase is characteristic of the months of May and June, where the temperature increase can be as much as 0.8—1°C per decade (Figure 7). A relatively significant increase in temperature is also observed in September. In the colder months of the year, the changes in temperature are typically minor. Such monthly characteristics of the decade temperature change may be related to various processes. The most obvious seems to be the increasingly frequent air temperature extremes in summer. One of the more important reasons is the higher heat capacity of waters associated with algal blooms, which also affects the transparency of waters (Kniebusch et al., 2019; Stramska and Białogradzka, 2015). This is consistent with seasonal changes in chlorophyll *a* concentration, with the most significant increase in spring and autumn. Based on data from the period 1987—2018, the average concentration of chlorophyll *a* in the Gdańsk Basin was found to be 9.4 mg m^{-3} in April, 5.5 mg m^{-3} in June and 7.6 mg m^{-3} in September. It was several times higher than that observed in the winter months (0.6—0.8 mg m^{-3}). Lower values were determined for the period 1991—2018 in the Eastern Gotland Basin: 3.7 mg m^{-3} in April, 2.5 mg m^{-3} in June, 2.4 mg m^{-3} in September and 0.6 mg m^{-3} to 1.1 mg m^{-3} in the winter months. These spatial differences are directly related to higher concentrations of nutrients in areas influenced by river waters, where eutrophication processes are much more intensive. This, in turn, is reflected in a more significant decadal increase in temperature in the waters of the Gulf of Gdańsk and the Pomeranian Bay (Figure 7). Another element that may affect the clear seasonality of the temperature increase rate is the characteristics of atmospheric circulation responsible for shaping the meteorological conditions in the Baltic Sea area: North Atlantic Oscillation (NAO) and Atlantic Multidecadal Oscillation (AMO) (e.g., Stramska and Białogradzka, 2015; Visbeck et al., 2001). Other explanations relate to the characteristics of the processes in the water column. During autumn and winter, surface cooling triggers vertical convection and cross-isopycnal mixing until the maximum density temperature is reached. Further cooling leads to the stabilisation of the water column. If the winter temperature is < 2.5°C seasonal surface warming in early spring will result in an unstable water column with convective overturning (Eiola and Stigebrandt, 1998). If the water temperature is > 2.5°C, warming leads to the development of a thermocline. In other regions, sea surface temperature (SST) changes are projected to be the largest in the Bothnian Bay and the Bothnian Sea during summer and in the Gulf of Finland during spring. According to Meier et al. (2012a), the mean summer SST will increase by about 2°C in the southern and 4°C in the northern Baltic Sea by the end of this century. The more significant warming in the north is caused at least partly by the ice-albedo feedback (Meier et al., 2012b).

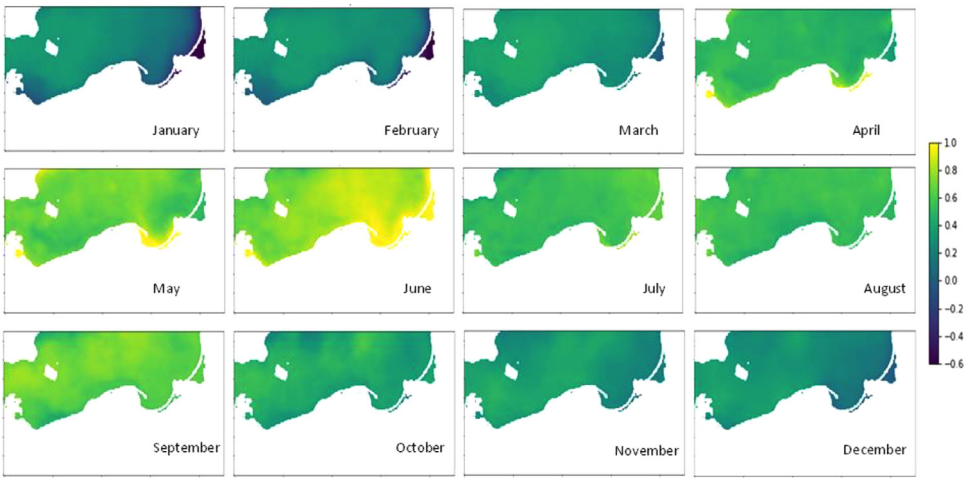

Figure 7 Change in the average sea surface temperature per decade (ΔT/decade [°C]) in the southern Baltic in months based on satellite data from 1985—2018.

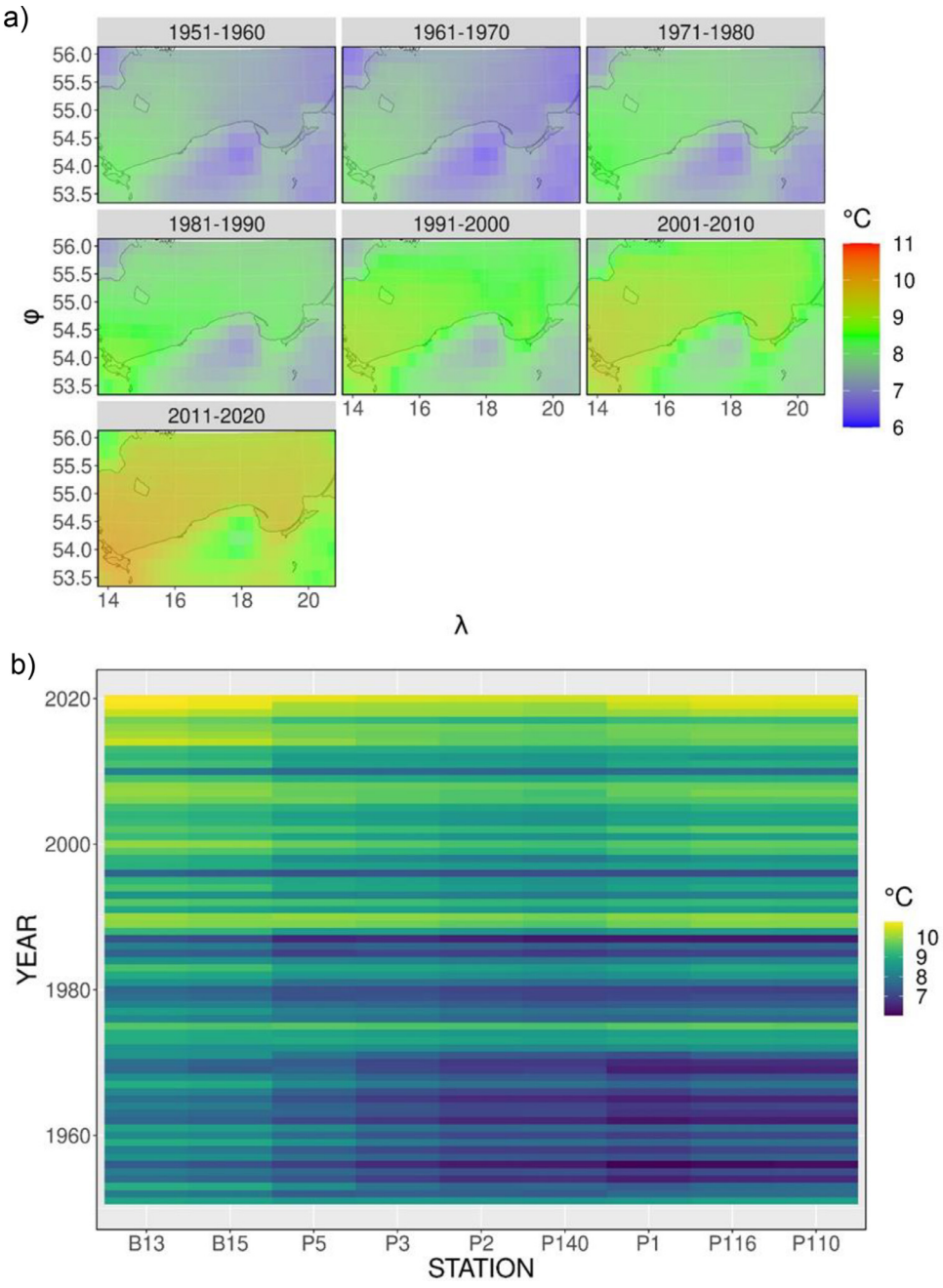

Figure 8 Mean air temperature in the southern Baltic area in decades (a) and at stations in 1951—2020 (b).

Former studies (e.g., Kniebusch et al., 2019; MacKenzie and Schiedek, 2007; Meier et al., 2012b) have shown a strong correlation between air temperature and SST. To study such a relationship in the southern Baltic, changes in thermal conditions in 1951—2020 were analysed based on data from re-analyses. Considering the average decadal temperature, an apparent increase in individual decades is observed (Figure 8a). A comparison of thermal conditions in the last decade of 2011—2020 with the period 1951—1960 shows an increase of about 2°C in the entire area. In the case of the 2011—2020 decade, which was also the warmest, the variation in the average temperature value over the southern Baltic, exceeding 9°C, was slight (Figure 8a).

Considering changes in the average annual air temperature, the years from 1951 to 1985 are visibly cooler in all locations (Figure 8b). The year 1975 was slightly warmer. Since the end of the 1980s, there has been a visible change in the characteristics of the average annual temperature. Since 2000, a clear increase in air temperature of a continuous nature has been observed in all locations. The exception was 2010, which was cooler. The variation of values between the measurement points is relatively slight and consistent with the long-term course.

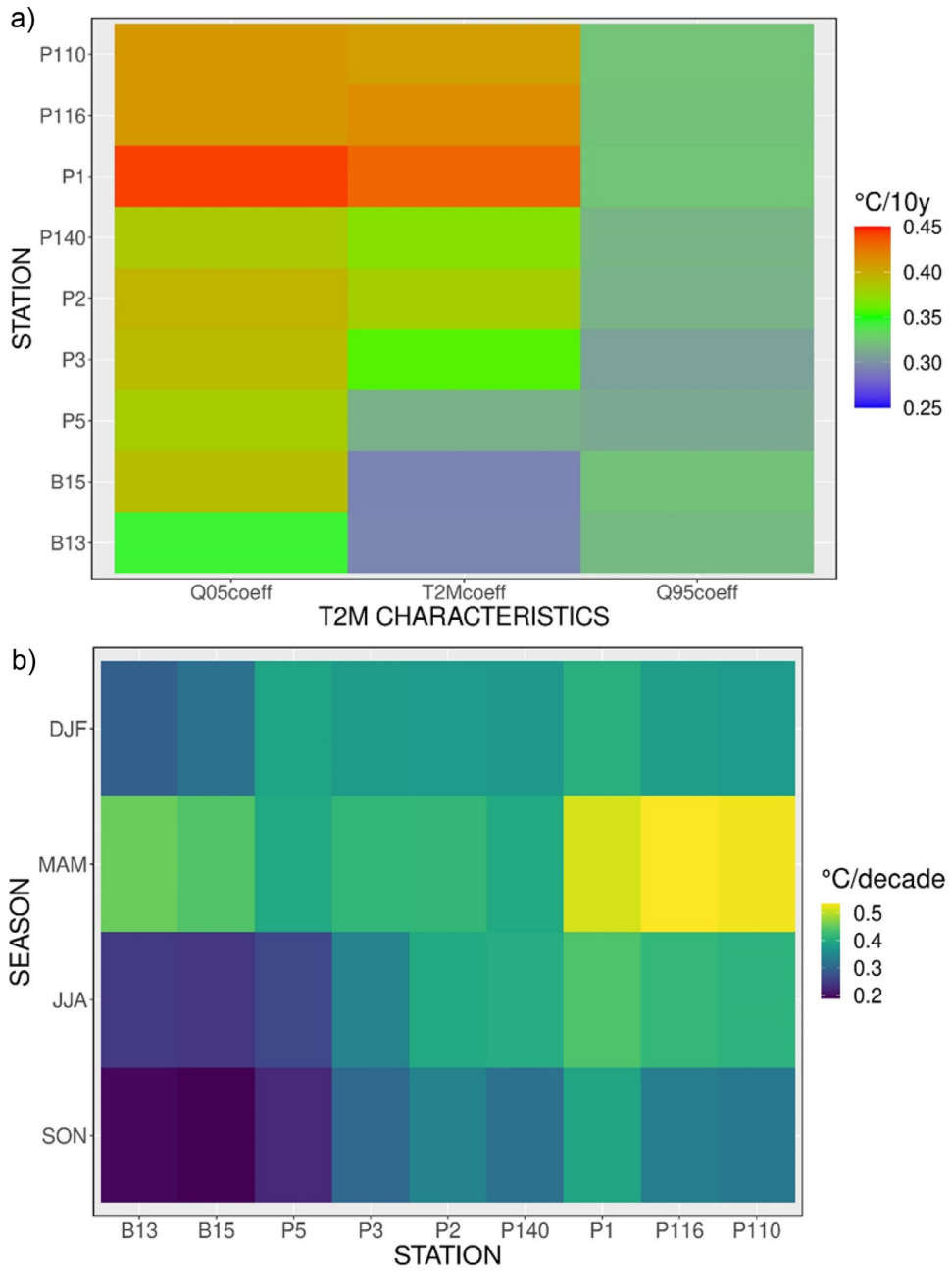

Figure 9 Directional coefficients of the trend equation (°C/10 years) of air temperature, Q05coeff — 5% quantile, T2Mcoeff — mean, Q95coeff — 95% quantile (a) and slope factors (seasonal) of the air temperature trend equation (°C/10 years) on selected stations, 1951—2020 (b).

The analysis of the directional coefficients of the air temperature trend equation clearly shows statistically significant trends in all locations (Figure 9a). The lowest average values of the decadal temperature change for the entire period 1951—2020 at the level of 0.29°C characterise the area of the Pomeranian Bay (stations B15, B13). A slightly higher value was calculated for the Bornholm Deep (0.31°C), while in the Słupsk Furrow and Eastern Gotland Basin, the decadal increase in air temperature is at the level of 0.37°C. The most remarkable changes concern the Gdańsk Basin, where the average growth rate oscillates between 0.41—0.43°C (stations P1, P116, P140) (Figure 9a). The rate of change in the case of the 5% quantile value is faster than in the case of the average values. In principle, at all points, the values of trend coefficients approach or exceed 0.4°C per decade. Slightly lower slopes of the trend equation, oscillating around 0.3°C per decade, are recorded for the 95% quantile of air temperature. In general, for all points, the picture of variability indicates a statistically significant increase in temperature in the analysed area. In contrast, in the case of the average temperature, there is a clear differentiation between the points.

Looking at the temperature changes in individual seasons, the most visible increases occur in the spring season

and concern areas located closer to the shores: the Pomeranian Bay and the Gdańsk Basin, where the decadal increase in temperature can reach even 0.5°C (Figure 9b). To a large extent, this is consistent with the observations of changes in sea surface temperature (Figure 7). Slightly lower values are recorded in winter, while the least dynamic changes occur in summer and autumn when the values of the trend coefficient are at the level of 0.2°C per decade.

Correlation studies were carried out using the Spearman rank method between the sea surface temperature determined based on measurements carried out in the period 1959—2019 satellite data for the period 1982—2019 and the air temperature from the ERA5 re-analysis for the same points in the southern Baltic region. The results showed a very strong, statistically significant relationship at $p < 0.05$ (Table 1) between the data sets. The correlation coefficient for the measurement and satellite data for the entire area is 0.989, thus confirming the complementarity and quality of data from these two sources. This value remains at a similar level for individual locations, varying from 0.978 in the Gdańsk Basin to 0.996 in the Słupsk Furrow and the Eastern Gotland Basin.

The dependence of sea surface temperature on air temperature is described by the correlation coefficient of 0.934 for all data (Table 1). There are slight differences between the areas, with the highest coefficients in the open sea: Eastern Gotland Basin — 0.955, Bornholm Basin — 0.948 and Słupsk Furrow — 0.944. The lowest correlation coefficient — 0.913 was characteristic of the stations located in the Gdańsk Basin, which is consistent with the fact that in this area, the highest increase in air temperature is observed with a similar level of SST increase as in offshore locations. Slightly different characteristics in coastal areas were also recorded along the Swedish coast and in the northern part (Bothnian Bay and Bothnian Sea and Gulf of Finland), which the authors explain by the presence of upwelling and the presence of sea ice in winter and spring isolating the surface waters from the atmosphere, respectively (Dutheil et al., 2022). Correlation studies clearly showed a statistically significant dependence of surface water temperature on year and month. Moreover, the Kruskal-Wallis test demonstrated no differences between the surface water temperature values at individual stations.

3.2. Characteristics of seawater temperature changes in the coastal zone

Sea surface temperature changes determined for the entire coastal zone measured during the period from 1951 to 2019 at eight coastal stations (Figure 10a) showed the lowest average annual temperature of 8.1°C in 1996, with the highest (10.75°C) being noted in 2019. The maximum temperature ranged from 20.7°C in 1965 to 27.3°C in 2006. The lowest annual average temperature values at east coast stations were very similar — from 7.4°C in Władysławowo to 7.8°C in Gdynia, although these occurred in different years. In Świnoujście, the lowest average annual temperature of 8.5°C occurred in 1987. The highest annual average temperature values ranged from 10.4°C in Władysławowo to 12.0°C in Puck. In the period covered by the analysis, a statistically significant increase in surface temperature was found at most stations. In Kołobrzeg and Świnoujście these changes were negligible. Temperature increases per decade in the coastal zone of the southern Baltic Sea were lower than in the offshore areas, with a value of 0.17°C determined for the entire coast (Figure 10b). The most significant changes at the level of 0.2°C were characteristic of Gdynia and Puck stations. The slightest change, apart from Kołobrzeg and Świnoujście, occurred in Gdańsk (0.12°C). Looking at changes in the annual cycle, the highest increase in surface water temperature per decade was characteristic of the months from March to May, from 0.25°C to 0.27°C (Figure 10c). In the remaining months except September (0.06°C), the SST increase was in the range of 0.11—0.16°C. In general, changes in the coastal zone are characterised by different dynamics compared with those observed in the offshore area. This difference may be related to other hydrodynamic conditions affecting heat exchange and other factors, such as the inflow of fresh water from rivers and watercourses and melting snow, which may significantly affect the temperature of surface water in the coastal zone. The lowest temperature increase per decade observed between Świnoujście and Kołobrzeg in the coastal area may result from upwelling in the Baltic Sea related to corresponding general weather conditions (Bychkova et al., 1998). Upwelling is often found to take place offshore from the Hel Peninsula (e.g., Matciak et al., 2001). According to Krężel et al. (2005), in the Hel area, the upwelling region has a spatial range of 14,000 km^{2,} while in Łeba the range is 3500 km^2, that being at most 5000 km^2 in Kołobrzeg area. According to observations, the temperature difference between upwelled deep water and surface water can reach 14 degrees, and the temperature gradient has a maximum value of 5°C per km. The Baltic Sea consists of a relatively small volume of water and changes in atmospheric conditions can impact the region quite rapidly. The mean warming trend in the sea surface temperature (SST) of 0.04—0.05°C year^{-1} has been detected in the Baltic Sea covering the period 1982—2012/13 (Høyer and Karagali, 2016; Stramska and Białogrodzka, 2015). There is an inter-annual variability in the SST (Bradtke et al., 2010), which follows the changes in air temperature (Tronin, 2017). The warming signal has been confirmed by in situ observations in coastal stations in Utö Island (Finland) (Dailidienė et al., 2011; Laakso et al., 2018).

The analysis of thermal conditions in the coastal area is based on measurement data from four synoptic stations (Figure 11a). Based on data from 70 years (1951—2020), monthly and annual averages were calculated. To determine the speed of changes, the values of the linear trend coefficient describing the increase in air temperature at the stations were calculated. The temperature values in the following five climatological normal periods were also analysed — from the multi-year period 1951—1980 to the current thirty-year period 1991—2020.

Spatial variation of the average annual air temperature on the Polish Baltic coast in 1951—2020 did not exceed 1.0°C. It was warmest in the west, with an average annual temperature of 8.5°C in Świnoujście, and the coldest in Gdańsk, where the value was 7.7°C. Considering the differences between the eastern and western parts of the coast,

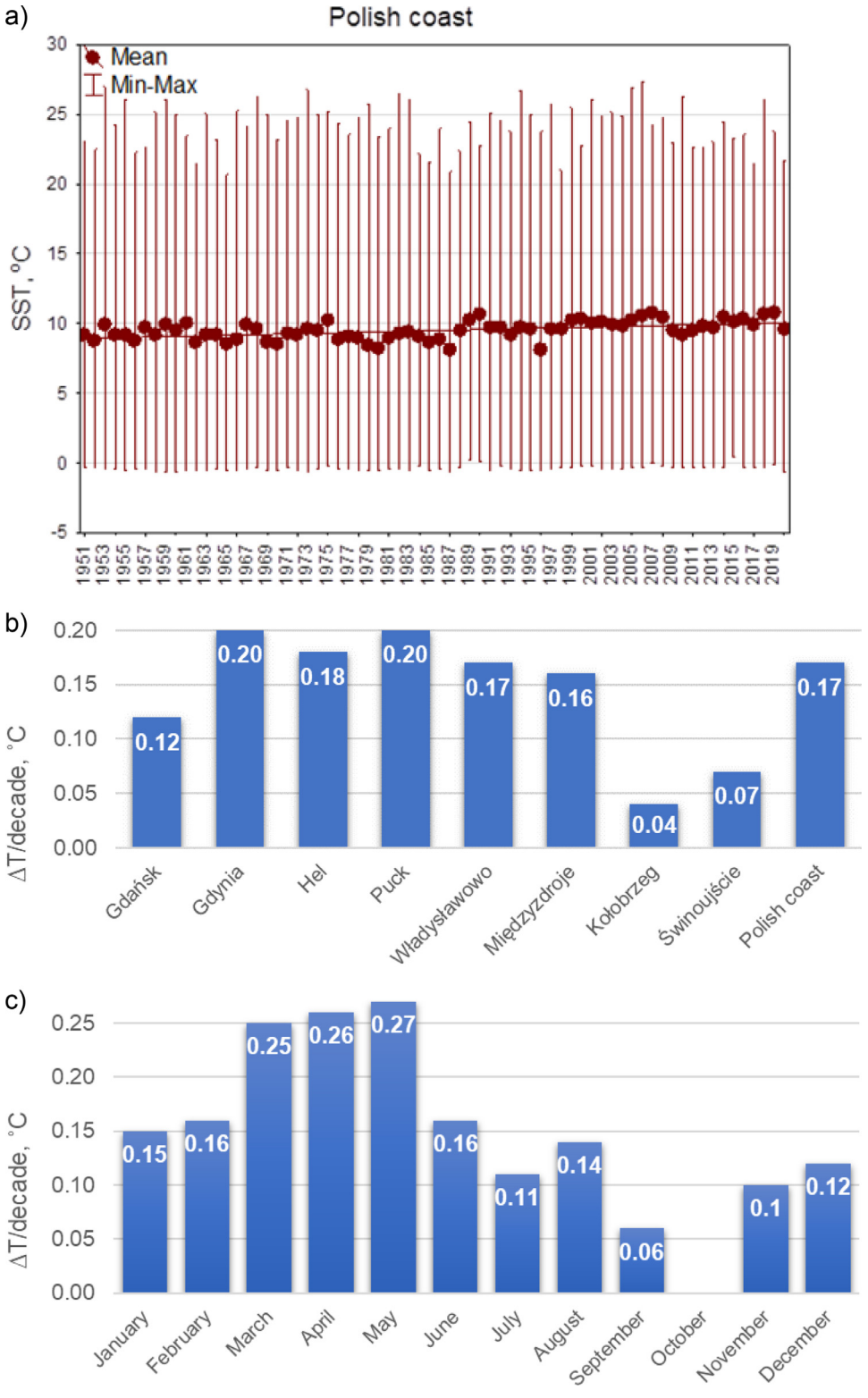

Figure 10 The average seawater surface temperature in the coastal zone of the southern Baltic Sea with minimum and maximum values in the years 1951—2019 (a) and change in the average SST per decade at coastal stations (b) and in months (c) in the southern Baltic in 1959—2019.

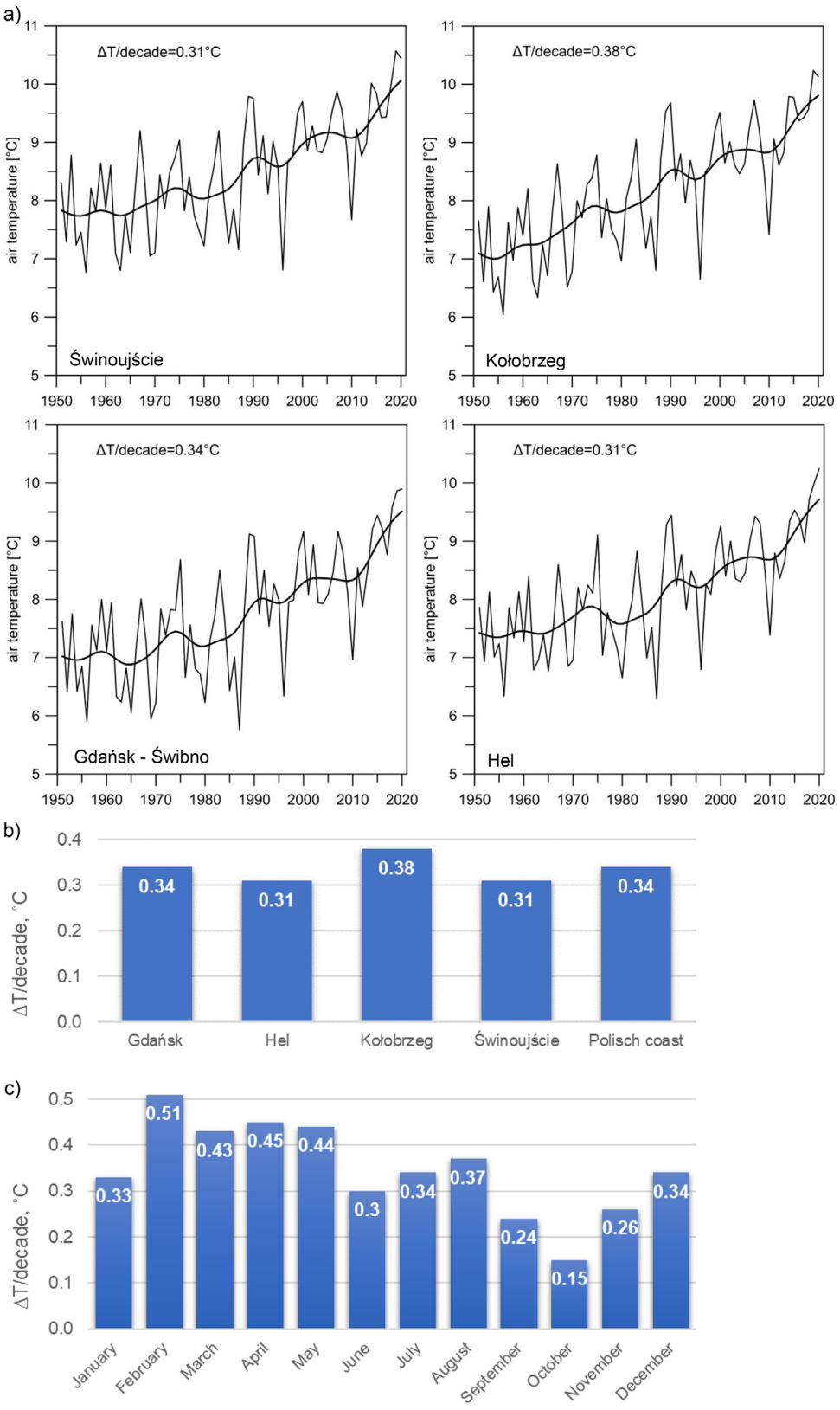

Figure 11 The average annual air temperature with a 10-year Gaussian filter in the coastal zone of the southern Baltic Sea in the years 1951—2020 (a) and change in the average temperature per decade at coastal stations (b) and in months (c) in the southern Baltic in 1951—2020.

in the west it is warmer in the months from January to August, while from September to December, the warmest station is Hel.

Inter-annual temperature fluctuations over the multiyear period were significant (Figure 11a). At all stations, the year 1956 turned out to be the coldest when the values of the average annual air temperature ranged from 5.9°C in Gdańsk to 6.8°C in Świnoujście. The last two years covered by the analysis were the warmest on the entire coast. The year 2019 was recorded as warm with the temperature from 9.9°C in Gdańsk to as much as 10.6°C in Świnoujście.

A characteristic feature of the course of the average annual air temperature on the coast in 1951—2020 was its systematic, statistically significant increase. The values of the linear trend coefficient describing the decadal changes at the stations range from 0.31°C in Świnoujście and Hel to 0.38°C in Kołobrzeg (Figure 11b). The average value of air temperature increase for the coast of Poland is 0.34°C. Taking seasonal changes into account, the fastest increase of more than 0.5°C per decade is observed at all stations in February (Figure 11c). An increase exceeding 0.4°C, also occurs in spring (March to May). A slower rate of change characterises the autumn months (September to November), with the lowest value at 0.15°C in October. The scale of this systematic increase is also visible if the air temperature over thirty-year periods is analysed. Each successive climatological normal period at all coastal stations is warmer. Temperatures in the winter months are of particular note. For the entire second half of the 20th century, negative temperatures along the whole coast were a normal phenomenon. However, since the turn of the century (1991—2020), the average for January and February (i.e. the two coldest months of the year) is negative only in Gdańsk. In July and August (the two warmest months of the year), the average temperature on the east and west coasts over the last thirty years exceeds 18.0°C. In the entire period covered by the analysis, January was the coldest month, while July was the hottest, and climatological spring is cooler than autumn on the coast of Poland.

Spearman's rank correlation studies showed a strong, statistically significant relationship between surface water and air temperature. The correlation coefficient for the entire coast was 0.921 at the significance level of $p<0.05$. In the case of individual stations, the highest values of coefficients at the level of 0.935 were found in Świnoujście and Hel, in Gdańsk it was 0.915, and the lowest value (0.908) was in Kołobrzeg, which may be related to the impact of upwelling on shaping the water temperature in this region.

4. Conclusions

Our study of changes in seawater temperature in the southern Baltic area, based on a long-term series of measurement data covering the years 1959—2019, showed a statistically significant increase. This increase is observed both in the sea surface and water column. It was determined that the temperature of the surface waters of the southern Baltic Sea in the period 1959—2019 increased on average by 0.6°C per decade, with the increase for the period 1959—1999 amounting to 0.3°C and for the period 1980—2019 as much as 0.7°C. This may indicate an intensification of the process of warming the waters of the Baltic Sea. Analyses of temperature changes at different depths showed that the dynamics at water column depths are different. The highest temperature increase per decade of 0.6—0.65°C characterised the layers from 0 to 20 m. The smallest increase (0.11°C) was recorded at a depth of 70 m, below which the temperature change per decade increases again to 0.24°C at a depth of 110 m. This is directly related to the influence of warmer surface waters from the North Sea introduced into the Baltic Sea in the bottom layer, thus shaping the conditions of thermohaline stratification.

The results of the satellite data analysis covering the period 1982—2019 were consistent with the results obtained based on direct measurements. Taking into account the spatial distribution of the decadal change in surface water temperature, the Bornholm Basin and the Słupsk Furrow areas and the area of the mouth of the Vistula in the Gulf of Gdańsk are characterised by the most significant increase. In the latter case, it may be related to the increased heat capacity resulting from the intensification of blooms and the amount of suspended matter, which is directly related to the inflow of river waters. Eutrophication processes and their effects in the form of increasing biomass are indicated as one of the reasons for the increased dynamics of seawater temperature increase in warm periods, in which the decadal increase in temperature reaches even 0.8—1°C per decade. At the same time, the change does not exceed 0.2°C per decade in winter months. The results of the correlation analysis of measurement data with satellite data showed excellent agreement; Spearman's rank correlation coefficient was 0.99 with a significance level >0.05, which indicates the possibility of using these two sources of complementary data.

Changes in seawater temperature related to atmospheric conditions, for which an increase in air temperature by approx. 2°C was recorded in the years 1951—2020. The analysis of the directional coefficients of the air temperature trend equation clearly shows significant statistical trends of change in the southern Baltic region, and the decadal changes ranged from 0.29°C in the Pomeranian Bay to 0.43°C in the Gdańsk Basin. Spearman's rank correlation coefficients were very high and ranged from 0.913 to 0.956, depending on the area.

The increase in sea surface temperature per decade in the coastal zone of the southern Baltic Sea was lower than in the offshore areas and varied from 0.12°C to 0.2°C per decade, with an average value for the entire coast of 0.2°C. Taking into account changes in the annual cycle, the highest increase in surface water temperature per decade was characteristic of the months from March to May, from 0.25°C to 0.27°C. There was also a systematic increase in the average annual air temperature on the coast from 1951 to 2020, which amounted to 0.34°C per decade.

The ongoing evaluation of the quantitative characteristics of changes in the seawater temperature, taking into account the specificity of offshore and coastal areas and the rate of atmospheric warming, is of fundamental importance for predicting changes in the functioning and processes taking place in the marine ecosystem as a result of climate change. Obtaining quantitative information from a

variety of sources is also crucial for planning adaptation measures.

Declaration of competeing interests

The authors declare that they have no known competing financial interests or personal relationships that could have appeared to influence the work reported in this paper.

Acknowledgements

The research was co-financed by the Ministry of Education and Science subsidy for the maintenance and development of research potential.

References

BACC II, 2015. Second assessment of climate change for the Baltic Sea basin. Regional climate studies. Springer, Berlin.

BALTEX, 2006. Assessment of climate change for the Baltic Sea basin — The BACC project. Summary, The BACC Lead Author Group (eds.), Int. BALTEX Secr. Publ. No 35, 26 pp.

Belkin, I.M., 2009a. Rapid warming of large marine ecosystems. Prog. Oceanogr. 81, 207—213.

Belkin, I.M., Cornillon, P.C., Sherman, K., 2009b. Fronts in large marine ecosystems. Prog. Oceanogr. 81 (1—4), 223—236.

Bradtke, K., Herman, A., Urbanski, J.A., 2010. Spatial and interannual variations of seasonal sea surface temperature patterns in the Baltic Sea. Oceanologia 52 (3), 345—362. https://doi.org/10.5697/oc.52-3.345

Brierley, A.S., Kingsford, M.J., 2009. Impacts of climate change on marine organisms and ecosystems. Current Biol. 19 (14), R602—R614.

Bychkova, V.E., Dujsekina, A.E., Fantuzzi, A., Ptitsyn, O.B., Rossi, G.L., 1998. Release of retinol and denaturation of its plasma carrier, retinol-binding protein. Fold. Des. 3 (4), 285—291.

Carstensen, J., Andersen, J.H., Gustafsson, B.G., Conley, D.J., 2014. Deoxygenation of the Baltic Sea during the last century. Proc. Nat. Acad. Sci. USA 111, 5628—5633.

Cloern, J.E., 2001. Our evolving conceptual model of the coastal eutrophication problem. Mar. Ecol. Prog. Ser. 210, 223—253.

Dailidienė, I., Baudler, H., Chubarenko, B., Navrotskaya, S., 2011. Long term water level and surface temperature changes in the lagoons of the southern and eastern Baltic. Oceanologia 53 (1-TI), 293—308. https://doi.org/10.5697/oc.53-1-TI.293

Dettinger, M., Anderson, J., Anderson, M., Brown, L.R., Cayan, D., Maurer, E., 2016. Climate change and the Delta. *San Francisco Estuary and Watershed*. Science 14 (3). https://doi.org/10.15447/sfews.2016v14iss3art5

Diaz, R.J., Rosenberg, R., 2011. Introduction to environmental and economic consequences of hypoxia. Int. J. Water Res. Develop. 27 (1), 71—82.

Dokulil, M.T., Jagsch, A., George, G.D., Anneville, O., Jankowski, T., Wahl, B., Teubner, K., 2006. Twenty years of spatially coherent deepwater warming in lakes across Europe related to the North Atlantic Oscillation. Limnol. Oceanogr. 51 (6), 2787—2793.

Dutheil, C., Meler, H.E.M., Gröger, M., Börgel1, F., 2022. Understanding past and future sea surface temperature trends in the Baltic Sea. Clim. Dynam. 58, 3021—3039. https://doi.org/10.1007/s00382-021-06084-1

Eiola, K., Stigebrandt, A., 1998. Spreading of juvenile fresh-water in the Baltic proper. J. Geophys. Res. 103 (C12), 27795—27807.

Fischer, H., Matthäus, W., 1996. The importance of the Drogden Sill in the Sound for major Baltic inflows. J. Marine Syst. 9, 137—157.

Gröger, M., Arneborg, L., Dieterich, C., 2019. Summer hydrographic changes in the Baltic Sea, Kattegat and Skagerrak projected in an ensemble of climate scenarios downscaled with a coupled regional ocean—sea ice—atmosphere model. Clim. Dynam. 53, 5945—5966. https://doi.org/10.1007/s00382-019-04908-9

Hinrichsen, H.H., Lehmann, A., Petereit, C., Schmidt, J., 2007. Correlation analyses of Baltic Sea winter water mass formation and its impact on secondary and tertiary production. Oceanologia 49 (3), 381—395.

Høyer, J.L., She, J., 2007. Optimal interpolation of sea surface temperature for the North Sea and Baltic Sea. J. Mar. Syst. 65, 1—4.

Høyer, J.L., Karagali, I., 2016. Sea surface temperature climate data record for the North Sea and Baltic Sea. J. Clim. 29, 2529—2541. https://doi.org/10.1175/JCLI-D-15-0663.1

Iles, C., Hegerl, G., 2017. Role of the North Atlantic Oscillation in decadal temperature trends. Environ. Res. Lett. 12, 114010. https://doi.org/10.1088/1748-9326/aa9152

IPCC, 2022. Climate Change 2021: The Physical Science Basis. In: Masson-Delmotte, V., Zhai, P., Pirani, A., Connors, S.L., Péan, C., Berger, S., Caud, N., Chen, Y., Goldfarb, L., Gomis, M.I., Huang, M., Leitzell, K., Lonnoy, E., Matthews, J.B.R., Maycock, T.K., Waterfield, T., Yelekçi, O., Yu, R., Zhou, B. (Eds.), Contribution of Working Group I to the Sixth Assessment Report of the Intergovernmental Panel on Climate Change. Cambridge Univ. Press, Cambridge, United Kingdom and New York, NY, USA (in press). https://doi.org/10.1017/9781009157896

Jørgensen, S.E., 1994. Models as instruments for combination of ecological theory and environmental practice. Ecol. Model. 75, 5—20.

Jørgensen, S.E., Xu, F., Salas, F., Marques, J.C., 2005. Application of indicators for the assessment of ecosystem health. In: Jørgensen, S., Xu, L., Costanza, R. (Eds.), Handbook of ecological indicators for assessment of ecosystem health, 5—65.

King, J.C., Marshall, G.J., Colwell, S., Arndt, S., Allen-Sader, C., 2022. The Performance of the ERA-Interim and ERA5 Atmospheric Reanalyses Over Weddell Sea Pack Ice. JGR Oceans 127 (9). https://doi.org/10.1029/2022JC018805

Klais, R., Tamminen, T., Kremp, A., Spilling, K., An, B.W., Hajdu, S., Olli, K., 2013. Spring phytoplankton communities shaped by interannual weather variability and dispersal limitation: mechanisms of climate change effects on key coastal primary producers. Limnol. Oceanogr. 58 (2), 753—762.

Kniebusch, M., Meier, H.E.M., Neumann, T., Börgel, F., 2019. Temperature variability of the Baltic Sea since 1850 and attribution to atmospheric forcing variables. J. Geophys. Res.-Oceans 124, 4168—4187.

Kullenberg, G., 1981. Physical oceanography in the Baltic Sea, A. Voipia (ed.), Elsevier, Amsterdam, 135—181.

Krężel, A., Ostrowski, M., Szymelfenig, M., 2005. Sea surface temperature distribution during upwelling along the Polish Baltic coast. Oceanologia 47 (4), 415—432.

Laakso, L., Mikkonen, S., Drebs, A., Karjalainen, A., Pirinen, P., Alenius, P., 2018. 100 years of atmospheric and marine observations at the Finnish Utö Island in the Baltic Sea. Ocean Sci. 14 (4), 617—632. https://doi.org/10.5194/os-14-617-2018

Levin, L.A., 2018. Manifestation, drivers, and emergence of open ocean deoxygenation. Annu. Rev Mar. Sci. 10, 229—260.

Liblik, T., Lips, U., 2019. Stratification has strengthened in the Baltic Sea—an analysis of 35 years of observational data. Front. Earth Sci. 7, 174. https://doi.org/10.3389/feart.2019.00174

MacKenzie, B.R., Schiedek, D., 2007. Long-term sea surface temperature baselines—time series, spatial covariation and implications for biological processes. J. Mar. Syst. 68, 405—420.

Makkonen, U., Saarnio, K., Ruoho-Airola, T., Hakola, H., 2015. Methods for determination of phosphate and total phosphorus in

precipitation and particulate matter, no. 2. Report Ser., Finnish Meteorol. Inst., Helsinki, Finland.
Matciak, M., Urbański, J., Piekarek-Jankowska, H., Szymelfenig, M., 2001. Presumable groundwater seepage influence on the upwelling events along the Hel Peninsula. Oceanol. Stud. 30 (3—4), 125—132.
Meier, H.E.M., Saraiva, S., 2020. Projected oceanographical changes in the Baltic Sea until 2100. [in:]. Oxford Res. Encyclopedia, Climate Sci. Oxford Univ. Press.
Meier, H.E.M., Kauker, F., 2003. Modeling decadal variability of the Baltic Sea: 2. Role of freshwater inflow and large-scale atmospheric circulation for salinity. J. Geophys. Res. 10, 3368.
Meier, H.E.M., Müller-Karulis, B., Andersson, H.C., Eilola, K., Gustafsson, B.G., Höglund, A., Hordoir, R., 2012a. Impact of climate change on ecological quality indicators and biogeochemical fluxes in the Baltic Sea: A multi-model ensemble study. AMBIO 41, 558—573.
Meier, H.E.M., Almroth-Rosell, E., 2011. Climate-related changes in marine ecosystems with a 3-dimensional coupled physical-biogeochemical model of the Baltic Sea. Clim. Res. 48 (1), 31—55. https://doi.org/10.3354/cr00968
Meier, H.E.M., Eilola, B.G., Gustafsson, I., Kuznetsov, T., Neumann, T., Savchuk, O.P., 2012b. Uncertainty assessment of projected ecological quality indicators in future climate. Rap. Oceanograf No. 112, SMHI, Norrköping, Sweden.
Merchant, C.J., Embury, O., Bulgin, C.E., Block, T., Corlett, G.K., Fiedler, E., Good, S.A., Mittaz, J., Rayner, N.A., Berry, D., Eastwood, S., Taylor, M., Tsushima, Y., Waterfall, A., Wilson, R., Donlon, C., 2019. Satellite-based time-series of sea-surface temperature since 1981 for climate applications. Sci. Data 6, 223. https://doi.org/10.1038/s41597-019-0236-x
Mohrholz, V., 2018. Major Baltic Inflow statistics — revised. Front. Mar. Sci. 5, 1—16. https://doi.org/10.3389/fmars.2018.00384
Orio, A., Heimbrand, Y., Limburg, K., 2022. Deoxygenation impacts on Baltic Sea cod: Dramatic declines in ecosystem services of an iconic keystone predator. Ambio 51, 626—637. https://doi.org/10.1007/s13280-021-01572-4
Pärn, O., Lessin, G., Stips, A., 2021. Effects of sea ice and wind speed on phytoplankton spring bloom in central and southern Baltic Sea. PloS one 16 (3), e0242637.
Pollock, M.S., Clarke, L.M.J., Dubé, M.G., 2007. The effects of hypoxia on fishes: from ecological relevance to physiological effects. Environ. Rev. 15 (NA), 1—14.
Qiu, Y., Feng, J., Zhang, Z., Zhao, X., Li, Z., Ma, Z., Zhu, J., 2023. Regional aerosol forecasts based on deep learning and numerical weather prediction. npj Clim. Atmos. Sci. 6 (1), 71. https://doi.org/10.1038/s41612-023-00397-0
Sinkko, H., Hepolehto, I., Lyra, C., Rinta-Kanto, J.M., Villnäs, A., Norkko, J., Norkko, A., Timonen, S., 2019. Increasing oxygen deficiency changes rare and moderately abundant bacterial communities in coastal soft sediments. Sci. Rep. 9, 16341.
Stramska, M., Białogrodzka, J., 2015. Spatial and temporal variability of sea surface temperature in the Baltic Sea based on 32-years (1982—2013) of satellite data. Oceanologia 57 (3), 223—235. https://doi.org/10.1016/J.OCEANO.2015.04.004
Tronin, A., 2017. The satellite-measured sea surface temperature change in the Gulf of Finland. Int. J. Remote Sens. 38 (6), 1541—1550.
Virtanen, E.A., Norkko, A., Nyström Sandman, A., Viitasalo, M., 2019. Identifying areas prone to coastal hypoxia—the role of topography. Biogeosciences 16, 3183—3195.
Visbeck, M., Hurrell, J.W., Polvani, L., Cullen, H.M., 2001. The North Atlantic Oscillation: past, present, and future. Proc. Natl. Acad. Sci. USA 98 (23), 12876—12877.
Walton, C.C., Pichel, W.G., Sapper, J.F., May, D.A., 1998. The development and operational application of nonlinear algorithms for the measurement of sea surface temperatures with the NOAA polar-orbiting environmental satellites. J. Geophys. Res.-Oceans 103 (C12), 27999—28012.

Oceanologia 66 (2024) 56—77

Available online at www.sciencedirect.com

ScienceDirect

journal homepage: www.journals.elsevier.com/oceanologia

ORIGINAL RESEARCH ARTICLE

Spatiotemporal variability of wave climate in the Gulf of Riga

Fatemeh Najafzadeh[a,*], Mikolaj Z. Jankowski[a], Andrea Giudici[a], Rain Männikus[a], Ülo Suursaar[c], Maija Viška[d], Tarmo Soomere[a,b]

[a] *School of Science, Tallinn University of Technology, Tallinn, Estonia*
[b] *Estonian Academy of Sciences, Tallinn, Estonia*
[c] *Estonian Marine Institute, University of Tartu, Estonia*
[d] *Latvian Institute of Aquatic Ecology, Riga, Latvia*

Received 28 March 2023; accepted 8 November 2023
Available online 24 November 2023

KEYWORDS
Wave climate;
Wave modelling;
In situ measurements;
SWAN;
Baltic Sea

Abstract Basic properties of wind wave climate in the Gulf of Riga, the Baltic Sea, are evaluated based on modelled wave fields, instrumentally measured and historical visually observed wave properties. Third-generation spectral wave model SWAN is applied to the entire Baltic Sea for 1990—2021 with a spatial resolution of 3 nautical miles (nmi, about 5.5 km) forced by the wind field of ERA5, to the Gulf of Riga and its entrance area with a resolution of 1 nmi (about 1.85 km), and to nearshore areas of this gulf with a resolution of 0.32 nmi (about 600 m). The calculations are performed for an idealised ice-free climate. Wave properties are represented by 36 directional and 32 frequency bins. The simulations are complemented by five sessions of instrumental measurements in the 2000s and two sets of historical visual wave observations from the island of Ruhnu and the Sõrve Peninsula for 1954—2011. Predominantly representing fetch-limited windseas, the wave climate in the gulf is milder and more intermittent than in the open Baltic Sea. The average significant wave height is mostly in the range of 0.6—0.8 m and

* Corresponding author at: Wave Engineering Laboratory, Department of Cybernetics, School of Science, Tallinn University of Technology, Ehitajate tee 5, Tallinn, 12611, Estonia.
E-mail address: fatemeh.najafzadeh@taltech.ee (F. Najafzadeh).
Peer review under the responsibility of the Institute of Oceanology of the Polish Academy of Sciences.

Production and hosting by Elsevier

https://doi.org/10.1016/j.oceano.2023.11.001

peaks at 0.82 m inside the gulf. Typical wave periods are shorter than in the Baltic proper. The spatial pattern of wave heights, with higher wave intensity in the northern and eastern parts of the basin, follows anisotropy in wind conditions. Interannual variations are highly synchronised in different parts of the gulf. Their magnitude is less than 10% of the long-term average wave height. No long-term trend has been found in significant wave height and no distinct decadal variation exists inside the gulf.

1. Introduction

Wave activity may play a particularly important role in driving coastal processes (e.g., erosion, sediment transport) in semi-enclosed marine regions, such as the Baltic Sea (Figure 1) with a total area of 435,000 km^2 (Leppäranta and Myrberg, 2009). Better knowledge of wave properties is needed in many fields, be it port construction, navigation, implementation of offshore electricity generation facilities, or arrangement of insurance (Christensen et al., 2013; Dean et al., 2008; Naulin et al., 2016; Tavakoli et al., 2023).

Several recent studies have produced a fairly good understanding of the main properties of the wave climate and its spatial variations in the Baltic Sea proper (Björkqvist et al., 2018a; Kudryavtseva and Soomere, 2017; Najafzadeh et al., 2021, 2022; Nilsson et al., 2019). During the last decade, this comprehension has been extended to cover the largest sub-basins of this water body, such as the Sea of Bothnia (Björkqvist et al., 2020), Bay of Bothnia (Dvornikov et al., 2017), Arkona Basin (Soomere et al., 2012), and the Gulf of Finland (Björkqvist et al., 2017; Giudici et al., 2023). However, the wave properties in several eastern and south-eastern parts of the sea have received less attention and information about the wave climate is scarce in these regions. Therefore, here our focus is on the wave climate of the third largest semi-sheltered sub-basin of the Baltic Sea, the Gulf of Riga (Figure 1).

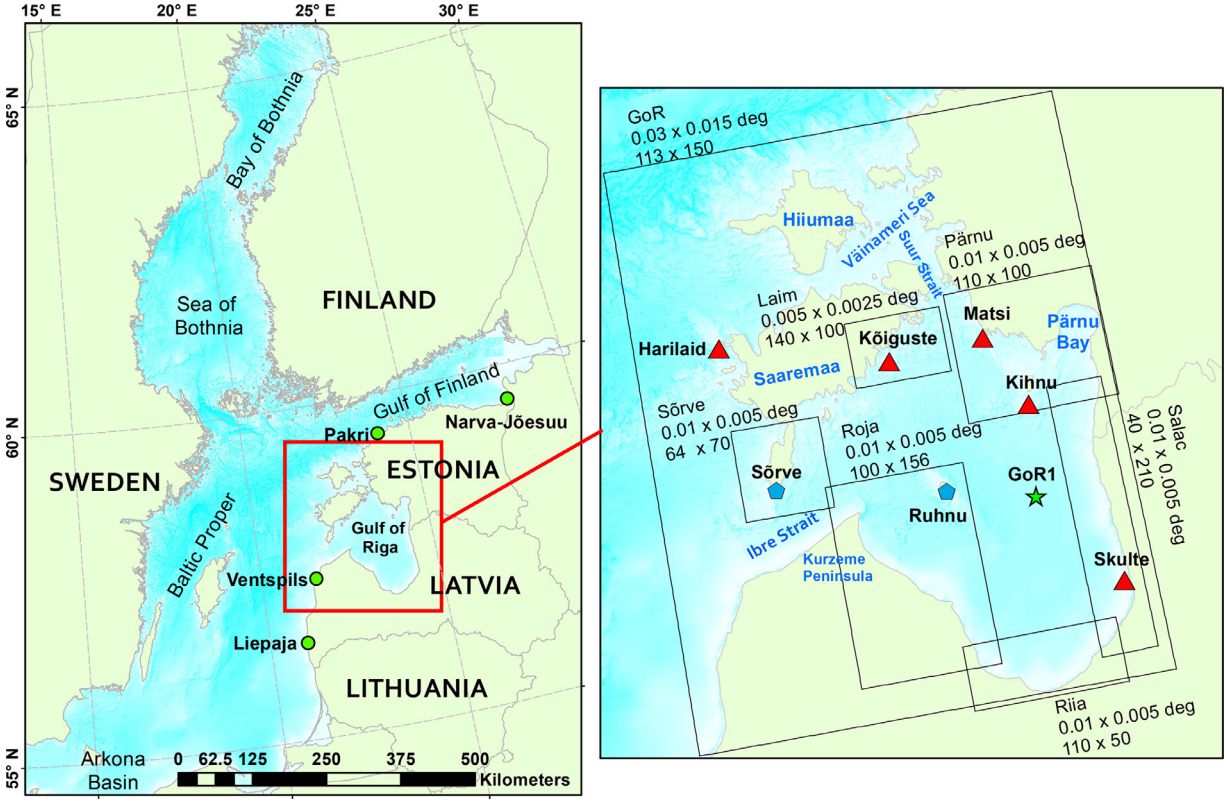

Figure 1 Map of the study area and the location scheme of visual wave observation sites in the open Baltic Sea and in the Gulf of Riga analysed in the previous research (green circles) (Hünicke et al., 2015) and the sites in the Gulf of Riga (blue pentagons). Red triangles indicate the points where short-term instrumental wave measurements are available. Green pentagram GoR1 is located in an open area of the Gulf of Riga at 23.87°E, 57.7°S. The boxes indicated nested grid areas used in the model. The numbers below the names of the grids show resolution in degrees and the number of grid cells in the East-West and North-South directions.

The water surface area of this gulf is 17,913 km^2. It has an oval-like shape with a relatively smooth geometry and covers an area of approximately 130 × 140 km (Suursaar et al., 2002). The estimated average depth from the "iowtopo2" version 3 bathymetry (Seifert et al., 2001) is 21 m and the maximum depth reaches 52 m. The 10 m isobath is located approximately 2 km from shore and the 20 m isobath is about 3.5—8 km from the shore along almost the entire Latvian part of the gulf. The northern and northeastern segment of the gulf is even shallower and contains numerous islands and islets. These regions have extensive shallow areas with depths less than 5 m. Also, there is an underwater feature called Gretagrund to the south of the island of Ruhnu. As waves in the Gulf of Riga are relatively short (Eelsalu et al., 2014), the impact of refraction on the wave propagation is comparatively small, except in the north and north-east of this waterbody and in the vicinity of Ruhnu (Männikus et al., 2022), and it is likely that in most occasions waves approach the shoreline at a relatively large angle between the wave propagation direction and the shore normal.

A first-order perception of the predominant winds in the Gulf of Riga can be retrieved from the wind recordings at the neighbouring sites that are open to the Baltic proper. Wind recordings from the island of Vilsandi (Männikus et al., 2020; Soomere and Keevallik, 2001) indicate that moderate and strong winds most frequently blow either from south-west (SW) or north-north-west (NNW). NNW winds are less frequent than SW winds but they may be the strongest (Soomere, 2001). This peculiarity is to some extent supported by an anecdotal observation of extremely high waves near the Daugava River mouth (Davidan et al., 1985). Eastern and south-eastern winds are infrequent and relatively weak (usually below 15 m/s) in the Gulf of Riga.

As the shape of the gulf is comparatively regular, the directional distribution of the local wind properties governs the main features of the wave climate in this gulf. The strongly anisotropic wind climate likely gives rise to a similar anisotropic wave climate: high waves may often occur in its eastern and southern parts and the wave regime along its western coasts is relatively mild.

Due to the semi-enclosed configuration of the gulf and the presence of shallow bays that face the direction of the strongest winds, the water level variability in this gulf is one of the largest in the entire Baltic Sea. The total historical range of water level variations can reach up to 4 m in the narrow and shallow Pärnu Bay (Jaagus and Suursaar, 2013; Männikus et al., 2019). Substantial variations in water depth may lead to notable modifications of wave properties in the relatively shallow northern part of the bay and also impact refraction, shoaling and energy dissipation in the nearshore of the rest of the bay.

The Gulf of Riga is connected to the Baltic proper via Irbe Strait. This strait, with a width of 27 km, provides a channel for waves approaching from the SW into the northern part of the gulf. The sill area between the Kurzeme Peninsula and Sõrve Peninsula is generally less than 10 m deep, except for a narrow 20—22 m deep canyon in its northwestern part. The geometry of Irbe Strait suggests that wave activity in the rest of the Baltic Sea provides a limited contribution to wave fields in the Gulf of Riga. Another outlet, Suur Strait, connects the gulf with the Väinameri (Moonsund) to the north of the Gulf of Riga. It is relatively narrow (about 4—5 km) and shallow (depths generally less than 5 m). There is very limited wave energy in the shallow Moonsund and thus waves approaching via this strait provide an insignificant contribution to the wave fields in the Gulf of Riga.

Therefore, it is likely that waves (and the parameters of the wave climate) in this basin are usually governed by the local winds and are mostly locally excited. In particular, long-period swell systems are even more infrequent and lower than the ones in the Baltic proper (Björkqvist et al., 2021). This feature provides, inter alia, a unique possibility to identify climatic changes to the meteorological forcing patterns in the gulf by analysing wave patterns or tracking wave-driven alongshore transport (Soomere et al., 2015). Such changes are usually masked by the impact of remote swell on the open ocean coasts.

Current sources of wave data, such as numerical simulations, remote sensing, and in situ measurements have been scarce in the south-eastern and eastern part of the Baltic Sea. Most of the information about wave properties and their temporal changes is extracted from a few simulations with a duration of up to 44 years (Chubarenko et al., 2012; Cieślikiewicz and Paplińska-Swerpel, 2008; Sokolov and Chubarenko, 2020), satellite altimetry and airborne laser scanning (Jahanmard et al., 2022; Kudryavtseva and Soomere, 2016), visual wave observations (Kelpšaitė et al., 2011; Pindsoo et al., 2012; Soomere, 2013) and instrumental wave measurements in the nearshore (Suursaar, 2013; 2015).

All these sources have drawbacks. The wave measurements in the Gulf of Riga are confined to short time series recorded during isolated experiments and long-term hindcasts at those point-measurement locations (Suursaar et al., 2012; Suursaar, 2015). These measurements (Figure 1) are also used to calibrate and verify the SWAN model in this study as described in more detail in Section 2.3. Wave heights retrieved from satellite altimetry are only reliable at a distance of about 0.2° from the shore in the Baltic Sea conditions (Kudryavtseva and Soomere, 2016), that is, restricted to a small area in the central part of the Gulf of Riga.

Being historically an important source of knowledge, visual wave observations inevitably contain an element of subjectivity and uncertainty (Guedes Soares, 1986; Gulev et al., 2003). They have been used to estimate the main properties of wave climate in many areas of the World Ocean in the past (Davidan et al., 1985; Hogben et al., 1986; Hogben and Lumb, 1967). Still, they often fail to properly represent complicated wave fields such as crossing seas or combinations of seas and swells (Badulin and Grigorieva, 2012; Gulev and Hasse, 1999; Orlenko et al., 1984). Observations from ships have poor spatial and temporal resolution, highly variable coverage and extensive gaps (Gulev and Grigorieva, 2006). While observations from the shore characterise only wave properties in the immediate vicinity of the site (Massel, 2013; Soomere, 2013), there have been attempts to establish a connection between visually observed wave height and instrumentally measured ones (Guedes Soares, 1986). Visual observations tend to severely underestimate wave heights compared

to offshore wave properties (Kudryavtseva et al., 2019; Plant and Griggs, 1992).

Methodical visual observations of several storm wave properties in many locations (so-called signal stations) of the Baltic Sea have existed for almost one and a half century (Rosenhagen and Tinz, 2013). Such observations have been performed systematically from the mid-1940s at numerous locations on the shores of the former USSR (Soomere, 2013) using the same routine over almost 70 years (Figure 1). Details of this routine can be found in Soomere and Zaitseva (2007) and Eelsalu et al. (2014). Their results are still the only source for the qualitative representation of the course of wave properties in many segments of the Baltic Sea (Kudryavtseva and Soomere, 2016).

The available visual wave observations in the Gulf of Riga have been critically analysed by Eelsalu et al. (2014) based on two observation sites in Estonian waters. The site on the shore of the island of Ruhnu close to the centre of gulf (Figure 1) represents the waves in this basin well except for a few situations when the island itself shelters the site. Another observation site on the eastern shore of the southern part of Sõrve Peninsula (Figure 1) is sheltered from waves approaching from the SW and NNW, which are the predominant wind directions. Thus, the Sõrve station mostly represents waves that are generated by southern and eastern winds.

The described scarcity both in time and space of in situ and visual wave measurements makes numerical models the most important and useful tool to gather insight about long-term wave information in the Gulf of Riga. Most numerical simulations performed for the Baltic Sea until about 2015 have so far had a spatial resolution of 3—4 nautical miles (nmi) (about 5.5—7 km) (Cieślikiewicz and Paplińska-Swerpel, 2008; Tuomi et al., 2011, 2014). This resolution is insufficient for resolving wave properties in in the Gulf of Riga. Some of these simulations, such as (Räämet and Soomere, 2010) have clearly insufficient spatial and temporal resolution of forcing wind data. Simulations with 3 nmi resolution have indicated that wave-driven transport of coastal sediment in the Gulf of Riga is unusually strong, may contain several convergence and divergence areas (Viška and Soomere, 2013a) and may have a different temporal course compared to that on the shores of the Baltic proper (Viška and Soomere, 2013b).

The wave regime in the Gulf of Riga has been studied numerically by Randmeri (2006) using the third-generation spectral wave model WAM with a resolution of 1 nmi and one-point winds. However, the results have not been published and are not available electronically. The newest simulations of the Baltic Sea wave fields with a spatial resolution of 1 nmi (Björkqvist et al., 2017) or even about 1 km (Nilsson et al., 2019) are focused on other aspects of the Baltic Sea wave climate.

This study attempts to evaluate the main features of the wave climate of the Gulf of Riga, first of all in terms of spatial distributions of significant wave height, its higher quantiles, and extreme wave heights. Further, the frequency of occurrence and joint distribution of wave properties are discussed. We also aim at establishing, to a first approximation, major changes in the wave climate in terms of trends in the wave height in different regions of the gulf. The analysis mostly relies on simulations of time series of wave properties with a spatial resolution of 1 nmi (about 1.85 km) for 32 years. Simulations with higher resolution have been used to validate the model against local wave data. This is done by using an updated SWAN model setup, which makes use of a nested, high-resolution (∼600 m) computational grid, to produce a new, long-term (32 years, 1990—2021) wave hindcast for the Gulf of Riga. We use all available (albeit short-term) wave measurements in this basin to evaluate the performance of the model. In addition, the outcome of simulations is compared with the historical visual wave observations.

The simulations are performed for an idealised ice-free situation. This approach does not affect comparisons of the measured and modelled data sets as measurements have been performed in ice-free time. It may lead to severe overestimation of cumulative wave properties. However, the analysis of Najafzadeh et al. (2022) in the context of the wave climate to the north of the Gulf of Riga suggests that the ignoring of seasonal sea ice insignificantly changes the classic average properties of the wave climate in the Baltic Sea. A comparison of this version of a (future) wave climate with a hindcast that takes into account seasonal ice cover in the gulf will be presented elsewhere.

2. Data and methods

2.1. Wave climate of the Gulf of Riga from visual observations

Procedures of observations of hydrometeorological parameters were unified and described in detail for the observation posts of the former Soviet Union (Guidelines, 1985). Even though the quality of observations (in terms of suitability of the location and accuracy of following the guidelines) was checked regularly, the procedures were apparently not always strictly adhered (Keevallik, 2003). A compact insight into the routine of wave observations, options of the conversion of observed properties into contemporary quantities, and shortages of the relevant procedures and data sets are presented, e.g., in Zaitseva-Pärnaste et al. (2009), Eelsalu et al. (2014), and Kudryavtseva et al. (2019).

Visual observations of wave properties tend to overestimate the wave heights (Massel, 2013) but often realistically represent the temporal course of wave intensity. The visually estimated periods of relatively long waves from ocean-going ships are slightly shorter than the instrumentally measured peak periods (Gulev and Hasse, 1998, 1999). For wave periods <7 s the observations provide estimates that almost exactly match the zero-crossing average wave periods (Davidan et al., 1985). The typical wave periods in the coastal zone of the Baltic Sea are 2—4 s (Broman et al., 2006; Soomere et al., 2012) and thus their visually observed estimates are apparently reliable.

Visual observations of the basic wave properties, such as wave direction, (optionally maximum and mean) wave height and wave period, were performed during 40 years from 1954 until 1995 at Sõrve and during about 50 years (1947—2011, with some gaps) at Ruhnu (Eelsalu et al., 2014). Gaps in observations were frequent during the entire winter and beginning of spring (December—April), and more frequently in January—March. They were associated either

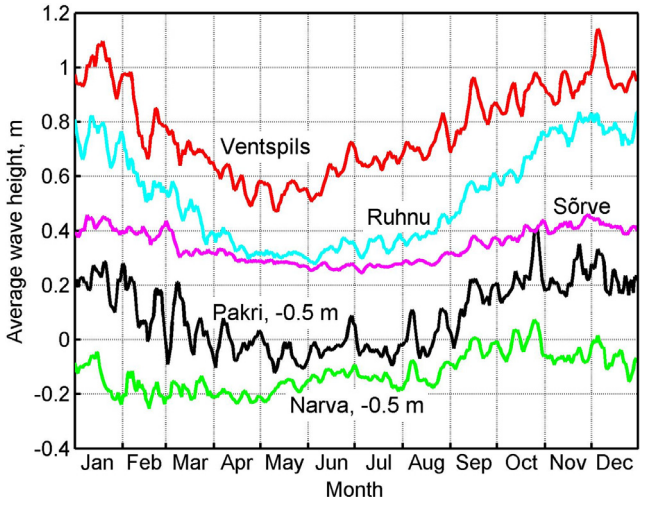

Figure 2 Seasonal variation in the average of visually observed mean wave heights for single calendar days over the period covered by the observations at Ventspils, Ruhnu, Sõrve, Pakri and Narva-Jõesuu. The records from 29 February are merged with the data from 01 March. For better visibility, the Pakri and Narva-Jõesuu data are shifted by −0.5 m concerning the other data sets. From Eelsalu et al. (2014).

with darkness or fog, or with the presence of ice cover. Sea ice is often present in the Gulf of Riga from mid-December until the end of April (Sooäär and Jaagus, 2007). Major gaps eventually because of other reasons exist in 1993–1994 in the Sõrve data set.

The long-term average wave height at the relatively open visual observation site of Ruhnu (0.52 m) is much larger than at Sõrve (0.36 m) (Eelsalu et al., 2014). The reason is that the site at Sõrve is largely sheltered from waves excited by the predominant strong winds and apparently reflects the milder wave regime characteristic to the western part of the Gulf of Riga. The wave climate in the Gulf of Riga is substantially milder than at the eastern coast of the Baltic proper but is similar to that in Narva Bay in the relatively sheltered eastern Gulf of Finland (Zaitseva-Pärnaste et al., 2011). Visually observed wave heights over 2 m are already extreme at the Sõrve station whereas at Ruhnu wave heights exceeding 4 m are not uncommon.

Visually observed wave periods at both sites are concentrated in the range of 2–4 s that are typical for coastal areas of the Baltic Sea (Broman et al., 2006; Soomere et al., 2012). Such short waves are characteristic of relatively small water bodies that are sheltered from long-period swells. Storm conditions with wave height over 2 m at Ruhnu usually have wave periods of 6–7 s. This range of wave periods is characteristic for low swells at Sõrve. Extreme wave storms at Ruhnu may have visually observed wave heights up to 4.8 m and periods 8–9 s (Eelsalu et al., 2014). This wave height represents the average of the five highest waves (not necessarily in a sequence) observed during a 5-min time in the fixed location for wave observations. According to (Guedes Soares, 1986), visually observed values exceed the significant wave height by 15–20%. Therefore, visually recorded waves of this height apparently correspond to significant wave heights about 4 m. Given also that shoaling may have contributed to the development of the wave field in the observation location, such values are not unrealistic even though wave storms of such intensity have not been instrumentally recorded yet. The directional distribution of visually observed waves has two (at Ruhnu) or three peaks (Sõrve has a tertiary peak for waves approaching from the east) and generally mirrors the two-peak directional structure of moderate and strong winds (Soomere, 2001).

The visually observed wave heights expressed on daily and weekly scales reveal considerable seasonal variation (Figure 2), characteristic to the Baltic Sea. The largest wave intensity is observed in November–January and the lowest in April–July (Eelsalu et al., 2014). This variation is much larger at Ruhnu than in the eastern more sheltered part of the gulf. The wave regime at Sõrve is much more similar to the one at Narva-Jõesuu which is also sheltered from part of predominant winds and has a long sea ice season. Interestingly, weekly variations in Figure 2 at Sõrve and Ruhnu are in counter phase on a few occasions (e.g., during the last week of January and February). These occasions reflect differences in the openness of the two sites to different directions. Also, these variations at Ruhnu are sometimes out of phase with similar variations observed at Ventspils (for instance, at the very end of October and clearly in the middle of November). Therefore, the temporal course of wave fields in the Gulf of Riga may reveal several features that do not match those in the Baltic proper.

The variations in the visually observed annual mean wave height at Ruhnu (Figure 3) have only a limited similarity with the similar course on the open coast of the Baltic proper (Liepaja) or at the entrance of the Gulf of Finland (Pakri). Ruhnu and Liepaja data sets reveal a gradual increase in wave activity from the beginning of the 1960s until the mid-1980s. However, short-term interannual variations at these locations are often not synchronised. In particular, in years with relatively low wave intensity at Liepaja and Pakri (1960, 1966 or 1976) the Ruhnu data set shows higher wave activity. The wave height at Ruhnu dropped considerably at the end of the 1980s. A possible reason for this feature is an increase in the frequency of SW winds in the region (Jaagus, 2009; Jaagus and Kull, 2011). However, problems with decreasing quality of observations during the collapse of the Soviet Union may play a role. The wave intensity at Sõrve does not show any substantial changes over the entire time of observation. This feature reflects the sheltered location of the observation site.

Despite suffering from several quality issues, visual wave observations often provide valuable information about wave properties and changes in the wave fields (Gulev and Grigorieva, 2004). Based on this information, it is safe to say that the wave climate in the Gulf of Riga is less severe than the wave regime in the eastern Baltic proper. Waves are generally lower and shorter. While wave properties in the central part of the gulf (at Ruhnu) reveal extensive interannual and decadal variations, wave observations from Sõrve show no substantial variations.

2.2. Instrumental wave measurements

In this study, we use hourly values of significant wave height H_S and peak period T_p of wave fields to validate the SWAN wave hindcast. These properties were measured

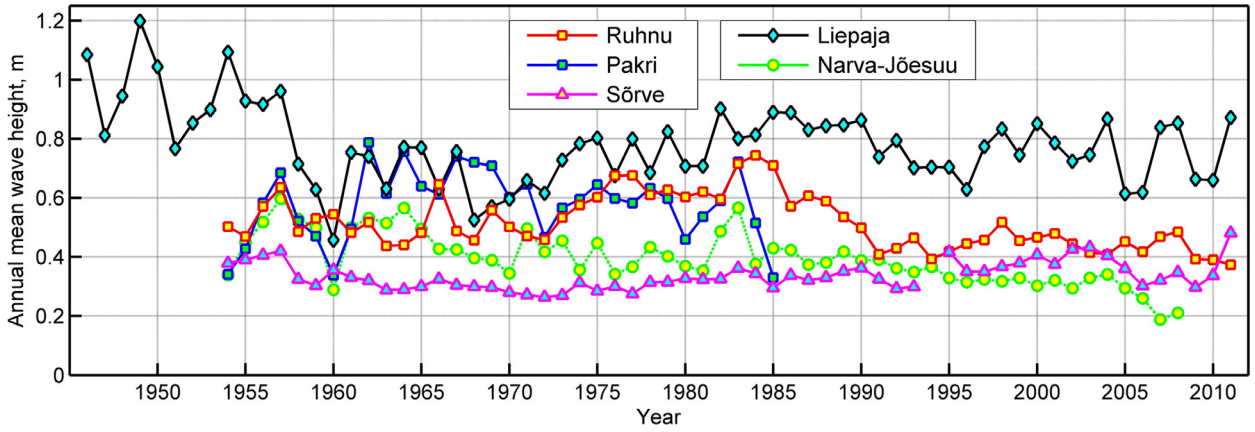

Figure 3 Annual mean visually observed wave height at visual observation sites in the Gulf of Riga (Ruhnu, Sõrve) and Liepaja, Pakri and Narva-Jõesuu. From Eelsalu et al. (2014).

Table 1 The geographical coordinates, water depth of stations, and time intervals of wave measurements in different areas of the Gulf of Riga and at Harilaid. Water depth in the corresponding grid cells of the wave model was estimated using the "iowtopo2" version 3 bathymetry (Seifert et al., 2001) and was in the range of 6—23 m.

Station	Data source	Lon. °E	Lat. °N	Depth (m)	Period of measurements (days)	Number of recordings
Kihnu	EMI	23.95	58.05	11.5	10 Sept 2012—14 May 2013 (247)	5897
Matsi	EMI	23.72	58.33	9.9	13 June—2 Sept 2011 (82)	1941
Kõiguste	EMI	23.02	58.32	12.1	2 Oct 2010—16 May 2011 (227)	5427
Harilaid	EMI	21.82	58.47	13.7	20 Dec 2006—23 May 2007 (155)	3691
					29 July 2013—3 Nov 2013 (98)	2322
Skulte	LHEI	24.36	57.32	15.9	27 July 2020—21 Apr 2021 (269)	6736

using a bottom mounted Recording Doppler Current Profiler (RDCP, RDCP-600 by Aanderaa Data Instruments) operated by Estonian Marine Institute (EMI) in four locations (Suursaar, 2015). A wave buoy (Smartbuoy) was operated at Skulte by the Latvian Institute of Aquatic Ecology (LHEI) (Figure 1, Table 1).

We do not consider recorded wave data during the ice season. For example, at Kihnu data measurements from the beginning of 2013 until April, and from 13 December 2010 at Kõiguste (Suursaar et al., 2012) included near-zero values due to ice cover. As sea ice information is not included in our simulations, we employ only the recordings that are made during the ice-free time for the model validation in the Gulf of Riga.

We also use instrumentally recorded wave data from Harilaid in winter 2006/2007 and autumn 2013 for the validation of SWAN model in the neighbourhood of the study area in the Baltic proper and to compare the properties of waves in the Baltic proper and Gulf of Riga. This site (Figure 1) is in a region where ice is formed much later than in the Gulf of Riga. As will be seen below, the presence of ice in some parts of the sea (Matsi and Skulte) did not distort the match of the modelled and measured wave properties. All time series in Table 1 provide 100% temporal coverage in the sense that the number of recorded wave properties (H_S or T_p) equals the total number of hours during the time interval covered by measurements. Skulte has the largest number of single recordings (6,736) that cover almost 9 months.

2.3. Wave model setup

Wave properties used in this study were calculated for the time frame 1990—2021 using the SWAN wave model (Booij et al., 1999), cycle III, version 41.31A. It is a third-generation phase-averaged spectral wave model developed and maintained by Delft University of Technology. We employed a three-level nested grid system in spherical coordinates (Giudici et al., 2023). It starts from the (coarse) one that covers the entire Baltic Sea between 9.3° and 30.3° E, and between 53.5° and 65.95° N with 211 × 250 cells (Figure 1). It has a resolution of 0.1° (6') in the east-west direction and 0.05° (3') in the north-south direction, equivalently, about 3 nmi. This grid is used to validate the model against measured wave data in the Baltic proper and to generate boundary conditions for the inner grid. The second (medium-resolution) grid (Figure 1) covers the Gulf of Riga and its vicinity with 113 × 150 grid cells from 21.2° to 24.59° E, and from 56.95° to 59.2° N with a resolution of 0.03° in the east-west direction and 0.015° in the North-South direction. The third level (fine) grids were constructed along the coastline of the gulf. Their resolutions follow the appearance of the geometry and bathymetry of the gulf. The southern side of the Gulf of Riga has a more

or less straight coastline where the resolution of approximately 600 m is enough to replicate spatial variations in the wave properties. The northern side of the gulf and the entire Moonsund have a complicated shape and irregular bathymetry. Hence, grids with a resolution of approximately 300 m were employed (Figure 1).

Extensive calibration of the model was performed using instrumentally measured wave time series from several subbasins of the Baltic Sea (Giudici et al., 2023). The following parameters were addressed: whitecapping coefficient, bottom friction-induced energy dissipation, depth-induced wave breaking, nonlinear transfer of wave energy through three-wave interactions, and the wind drag coefficient. The aim was to reach a model version that would provide acceptable results for the entire Baltic Sea, Gulf of Finland, Gulf of Riga, and for high-resolution nearshore grids along the eastern shore of the Baltic Sea in moderate and strong wind conditions. These parameters were iteratively adjusted in order to maximize the accuracy of the model in selected storms.

The resulting model was used with the following options: the whitecapping coefficient $\delta = 1$ (Pallares et al., 2014; Rogers et al., 2003), the bottom friction coefficient 0.038 m^2/s^3 (Zijlema et al., 2012); the parameters for the depth-induced wave breaking source term $\alpha = 1$ and $\gamma = 0.73$. Wind drag parameterisation was taken from (Wu, 2012), as suggested by Björkqvist et al. (2018a). The default parameters for whitecapping from (Komen et al., 1984) led to the most acceptable results. The presence of currents, varying water levels and seasonal ice-cover was ignored. Further discussion of model details and the rationale behind the configuration choices is detailed in (Giudici et al., 2023) and verification of the model is provided in Section 3.1.

The information about water depths in the Baltic proper was taken from Baltic Sea Bathymetry Database (Baltic Sea Hydrographic Commission, 2013) (http://data.bshc.pro/legal/). The bathymetry data for the Gulf of Riga was received from Estonian Transport Administration and Latvian Institute of Aquatic Ecology. The resolution of input bathymetry data varied between 50 and 200 m in Estonian waters. In the Latvian waters the input data was coarser: the resolution was 500…1000 m in deeper areas and about 300 m along the coastline. The constructed fine grids thus make full use of the bathymetry data in the Latvian waters and further increase in the resolution of the wave model is not practical.

The wave model was run on this nested grid system in non-stationary mode. For wind forcing, we utilized ERA5 reanalysis, which is a state-of-the-art global atmospheric reanalysis developed by the European Centre for Medium-Range Weather Forecasts (ECMWF). The fifth-generation data set produced by ECMWF from 1979 onwards undergoes trimestral updates. In our study, we employed data that slightly extend beyond the latest WMO climatological standard normals of 1991−2020. Compared to its precursors, ERA5 incorporates a more recent version of the ECMWF Integrated Forecast System model (IFS 41r2, ECMWF, 2006) with increased temporal output, horizontal and vertical resolutions (1 h, 0.25°, and 137 vertical levels, respectively). Additionally, it includes various improvements to different parameterisations (e.g., convection and microphysics) and to the data assimilation scheme (Hersbach et al., 2018).

3. Results

3.1. Comparison of significant wave heights

We have validated the modelled H_S and T_p against all available instrumental wave measurements in and near the study area (Figure 1; Table 2). Since the model hindcast does not include the ice cover, the in situ measurements during the ice season that started from 13 December 2010 at Kõiguste, are eliminated from the validation. Therefore, 1658 single

Table 2 Measured wave properties, bias (measurement minus model), root mean square deviation (RMSD), and correlation coefficient of the wave model at measurement sites at Harilaid and in the Gulf of Riga. The upper row presents estimates for the entire duration of recordings while the lower row represents situations with measured $H_S > 0.5$ m.

Site	H_S (m)					T_p (s)			
	Grid (Figure 1)	ρ	Bias (m)	RMSD (m)	Measured mean H_S (m)	ρ	Bias (s)	RMSD (s)	Measured mean T_p (s)
Kihnu (2012/2013)	Pärnu	**0.92**	−0.23	0.30	0.67	0.40	0.51	1.21	4.88
		0.83	−0.19	0.28	1.00				
Matsi (2011)	Pärnu	**0.92**	−0.19	0.24	0.31	0.31	0.83	1.43	4.44
		0.71	−0.12	0.23	0.82				
Kõiguste (2010)	Laim	**0.89**	−0.29	0.35	0.42	0.20	1.04	1.75	4.99
		0.80	−0.18	0.25	0.94				
Harilaid (2006/2007)	GoR	**0.93**	−0.35	0.41	0.57	0.62	0.18	1.42	5.55
		0.86	−0.39	0.48	1.03				
Harilaid (2013)	GoR	**0.91**	−0.16	0.27	0.56	0.56	−0.41	1.46	4.30
		0.89	−0.12	0.27	0.99				
Skulte (2020/2021)	GoR	**0.91**	0.02	0.19	0.49	0.21	0.36	2.49	3.91
		0.88	0.47	0.62	1.16				
Skulte (2020/2021)	Salac	**0.92**	0.03	0.20	0.49	0.20	0.38	2.51	3.91
		0.89	0.52	0.67	1.16				

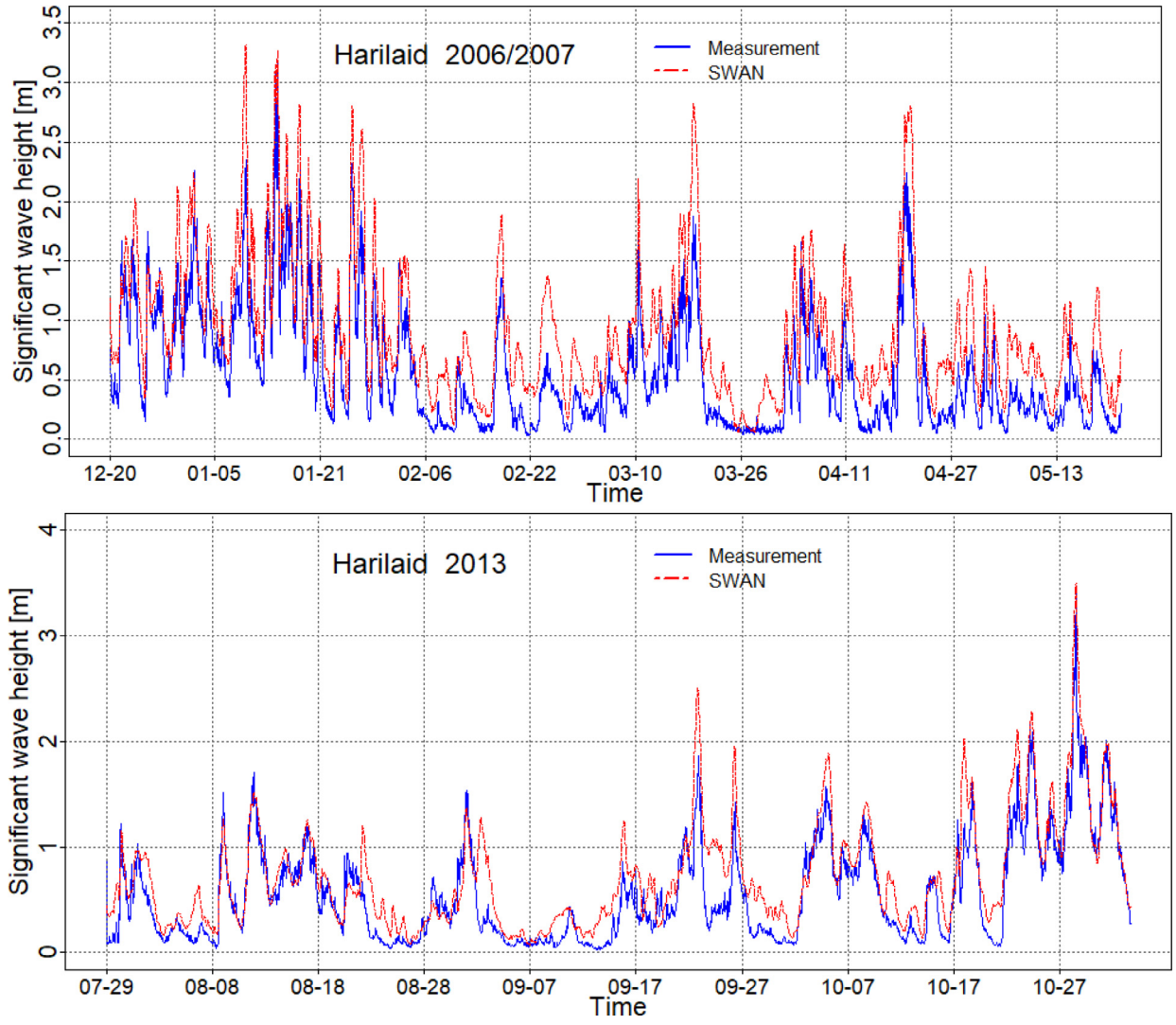

Figure 4 Time series of measured (blue) and modelled (red) significant wave height at Harilaid (Figure 1) in the north-eastern Baltic proper from December 2006 to May 2007 (upper panel) and in July—October 2013 (lower panel).

measurements were used for this purpose. At Kihnu, the wave data after 10 January 2013 include zeros due to the presence of ice cover. These recordings are also omitted from the validation. Thus, 2869 single measurements were employed. The whole data sets at Harilaid, Matsi, and Skulte are recorded during the ice-free period.

The performance of the model in the Baltic proper (equivalently, the quality of information about waves that propagate into the Gulf of Riga from the open Baltic Sea) is estimated using RDCP data at a location in the eastern Baltic proper to the north of the entrance to this gulf (Harilaid, Figure 4).

This location is fully open to the predominant winds and represents well the wave properties in the area for most wind conditions (Suursaar, 2013, 2015). The hindcast for this location is retrieved from a relatively coarse 1 nmi Gulf of Riga grid that also covers the neighbouring areas of the Baltic proper. The match of measured and modelled data is generally good with a correlation coefficient of 0.91—0.93. The modelled wave height almost always follows the course of measured wave heights. Relative large discrepancies occur between 28 August and 07 September 2013 (Figure 4). The main source of mismatch is probably the influence of complicated bathymetry (including indented coastline, presence of islets, rocks and shallows), which are not ideally captured in the model bathymetry.

The model tends to overestimate wave heights. The average bias (measurement minus model) over the entire period of measurements is —0.35 m in 2006—2007 and —0.16 m in 2013. The root mean square difference (RMSD) varied from 0.41 m to 0.27 m in these years, respectively. The fairly good match at this measurement site in the light of similar estimates of Björkqvist et al. (2018a) suggests that the employed model configuration and wind information are suitable for reconstructing the wave properties at the entrance to the Gulf of Riga.

The wave data in three measurement locations in the northern Gulf of Riga (Figure 5) were retrieved using an RDCP over a range from a few to several months (Table 1). The match of modelled and measured data is better for a

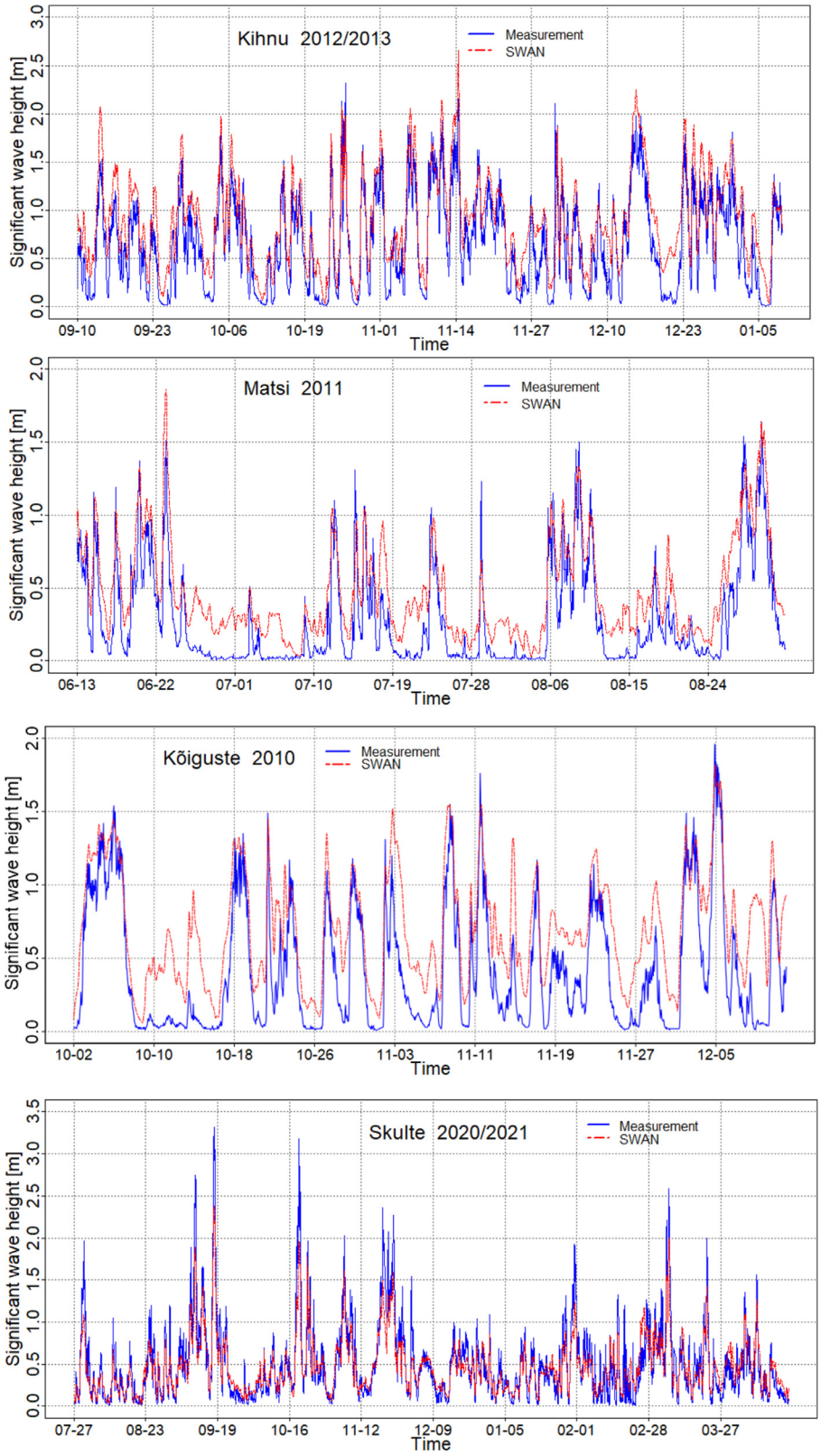

Figure 5 Comparison of the measured (blue) and modelled (red) significant wave height at Kihnu in 2012, Matsi in 2011, Kõiguste in 2010, and Skulte in 2020/2021.

finer-resolution wave model at Kihnu and Matsi. The correlation coefficients for these stations from the grid size of 0.32 nmi (~600 m, grid called Pärnu) are about 0.92. The bias is lower, in the range of −0.19 to −0.23 m. The RMSD is in the range of 0.24—0.30 m, which is almost the same as for simulations of Björkqvist et al. (2017) for the Gulf of Finland.

The match is less satisfactory for the relatively sheltered area at the south-eastern coast of Saaremaa. The hindcast with the fine spatial resolution (grid called Laim, ~0.32 nmi, Figure 1) at Kõiguste had a variable match, with the correlation coefficient, bias and rsmd 0.89, −0.29 and 0.35 cm, respectively. The typical mismatch of peaks of wave heights is 10—20 cm at these locations. Higher wave conditions (H_S > about 0.5 m) are reproduced more satisfactorily. Similar to the situation at Harilaid, it is likely that the established differences mainly stem from the complicated bathymetry and geometry of the vicinity of measurement locations. The indented coastline and the presence of islets are accompanied here by numerous rocks and shallows that are not reflected in the existing seabed maps. They are thus often overlooked by the model bathymetry but may sill lead to local variations in wave properties depending on the wave periods and directions.

The situation is different in the southern part of the gulf where in situ wave data are derived from buoy measurements. On average, the hindcast slightly underestimates wave heights (the measurement-model bias is positive) in this part of the Gulf of Riga, at Skulte. The overall course of wave heights is reproduced adequately but the model does not always follow the peak wave heights. The latter feature becomes evident from the comparison of modelled and measured wave situations with $H_S > 0.5$ m. Interestingly, the quality of reproduction of higher waves is better or the same as the replication of all wave conditions at Harilaid, Matsi and Kõiguste while higher waves are reproduced poorly at Skulte. This kind of discrepancy calls for further research and analysis. A comparison of results for the 1 nmi and 0.32 nmi grids at Skulte (Table 2) suggests that the inability of reproduction of relatively severe wave conditions at Skulte does not stem from the insufficient spatial resolution of the inner grid in the area with complicated geometry and bathymetry apparently for the same reasons as discussed above. There is also relatively large bias of reconstructed and measured peak periods (Table 2). These properties have a satisfactory match at Harilaid in the Baltic proper but are poorly correlated in the Gulf of Riga.

3.2. Statistical properties of significant wave heights

The shape of scatter plots of measured and modelled wave heights in the interior of the Gulf of Riga (Figure 6: Kõiguste, Matsi, Kihnu, and Skulte) signals that even though the overall bias between the data sets is fairly small, single values of wave heights can still differ considerably. The correlation coefficients for the two data sets are around 0.92 (Table 2). The relevant Theil-Sen regression coefficients are slightly lower, on the order of 0.91. In four locations the modelled wave heights are slightly overestimated and at Kõiguste several measured wave conditions are much lower than the associated modelled values. On the contrary, modelled wave heights starting from H_S about 0.5 m are systematically larger than the associated measured values at Skulte. The average bias for such waves is also about 0.5 m (Table 2). The difference between these values increases with the increase in the wave height.

The overall shape of the empirical probability distributions of measured wave heights at all sites in the Gulf of Riga (Figure 7) are characteristic of similar distributions in sheltered coastal areas of the eastern Baltic Sea (Soomere, 2005). About half of the measured wave heights are very low, below 0.25 m, at relatively sheltered Matsi and Kõiguste. This is a typical feature of very sheltered sea areas, such as bays deeply cut into mainland. This part of the distribution is wider at Skulte and Harilaid where more than half of wave events have H_S below 0.5 m. Accordingly, the median H_S is below 0.5 m at Matsi and Kõiguste while it reaches about 0.7 m at Kihnu. Somewhat surprisingly, the median H_S is below 0.5 m also at Skulte even though this area is open to the predominant wind and waves in the Gulf of Riga. The situation is greatly different at Kihnu. The record in this site has a much larger proportion of situations with $H_S > 1$ m whereas the frequency of occurrence of wave heights from 0.25 to 1.25 m varies insignificantly.

The similar distributions for modelled waves are greatly different and resemble analogous distributions in smaller but more open sub-basins of the Baltic Sea such as the Arkona Basin (Soomere et al., 2012). They all qualitatively follow a 2-parameter Weibull distribution with a narrow peak at wave heights 0.25—0.5 m at Matsi and Skulte, at 0.5—0.75 m at Harilaid, and a much wider distribution at Kihnu and Kõiguste. While systematic mismatch of these distributions at the relatively sheltered Matsi and Kõiguste locations may be associated with the complexity of geometry and bathymetry in their neighbourhood, the reasons for the described differences at Kihnu and Harilaid remain unclear. The relevant distributions for Harilaid show also a certain mismatch: the measured data contain a much larger amount of very low waves than the modelled data. As a similar difference is also evident at Skulte, it could be a specific feature of the Gulf of Riga wave climate that is not resolved by the used combination of the SWAN model and its forcing. To understand what exactly causes the described mismatch of modelled and measured wave regimes, wave measurements with better temporal resolution and possibly resolving single waves with periods down to a few tenths of seconds are apparently necessary.

A comparison of visually observed wave heights with their modelled counterparts is not straightforward for several reasons (see Soomere, 2013 and Kudryavtseva et al., 2019 for the relevant discussion). Still, it is natural to expect a qualitative match of statistical properties of observed wave heights and periods with modelled ones as well as some similarity in the course of average wave properties.

The distributions of visually observed wave heights at Ruhnu and Sõrve in the past (Eelsalu et al., 2014) resemble this distribution for measured wave heights at Skulte. Both historical distributions contain about 40% of very low waves (wave height below 0.5 m) and 35% of waves in the range of 0.5—1 m (Eelsalu et al., 2014). These differences more likely stem from the features of visual observations rather than from ignoring the ice cover in simulations.

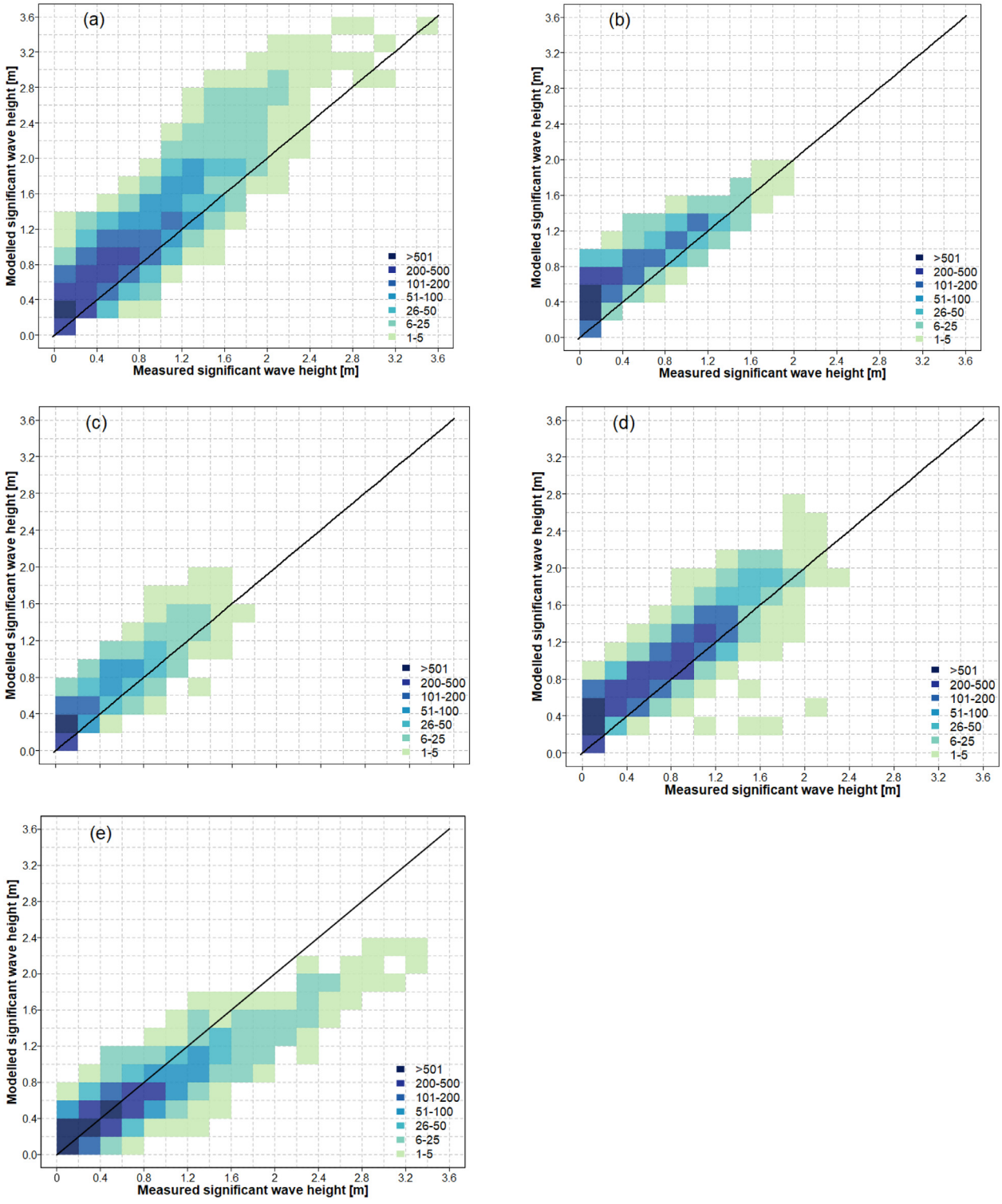

Figure 6 Comparison of the measured and modelled significant wave heights for Harilaid (a), and four measurement sites located in the interior part of the Gulf of Riga; Kõiguste (b), Matsi (c), Kihnu (d), and Skulte (e).

Direct comparisons of visually observed wave properties with similar instrumental records are complicated on the latitudes of the Gulf of Riga. During relatively calm spring and autumn often three observations per day is possible. Therefore, the calmer part of the wave climate is properly reproduced in the observations. However, most wave storms occur during the autumn and winter seasons with relatively limited daylight time when often only one observation per day is possible. It is thus highly likely that a large part of heavy wave conditions are missing from observation records. This perception is supported by the outcome of a comparison of visually observed wave heights

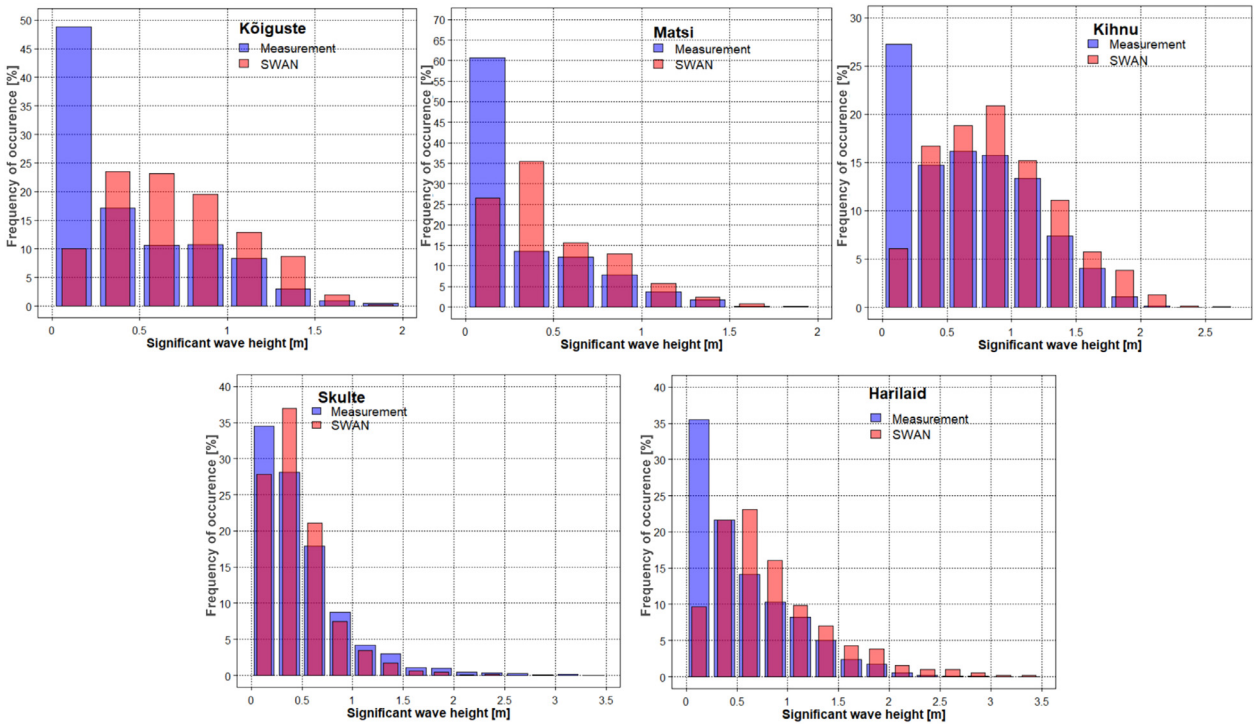

Figure 7 The empirical probability of occurrence of measured (blue) and modelled (red) wave situations at Harilaid and in four locations in the Gulf of Riga. The modelled data sets only represent the time interval covered by observations.

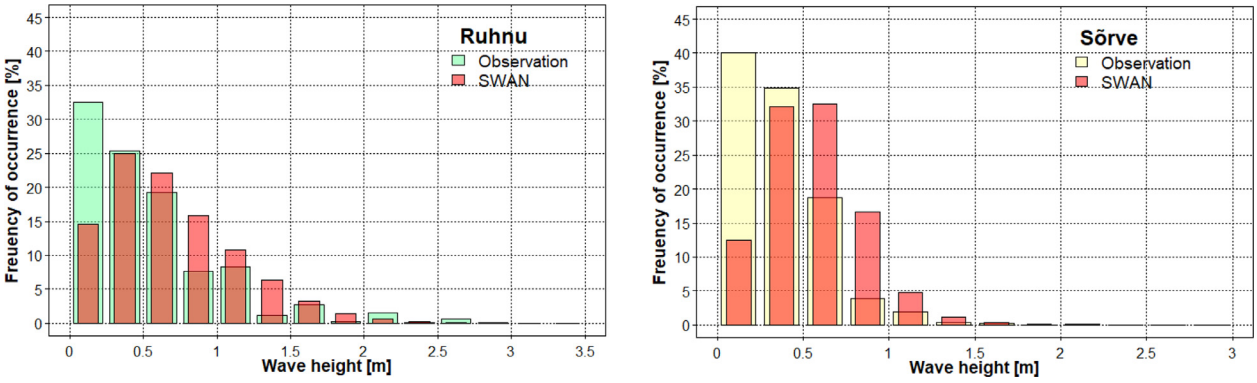

Figure 8 Comparison of the frequency of occurrence of all modelled significant wave heights and visually observed wave heights at Ruhnu (green) and Sõrve (yellow). Bars in the distributions of visually observed wave properties show the simple arithmetic mean of all observations in a single day (Eelsalu et al., 2014). As diurnal variations of wave parameters are almost negligible in the Baltic Sea (Soomere et al., 2012), it is likely that the daily average wave heights adequately represent the wave regime at the sites in question.

from the Caspian Sea shores with satellite-derived wave heights. A direct comparison of the visually observed and satellite-derived wave height records is almost meaningless as it reveals a discrepancy that is larger than the typical wave height. The RMSD between the two sets of records ranges from 0.8 m to 1.1 m in the Caspian Sea conditions (Kudryavtseva et al., 2019) where the average wave height is around 1 m (Lebedev and Kostianoy, 2008). The situation could be a little bit better in comparisons of visually observed and numerically modelled wave heights.

However, Kudryavtseva et al. (2019) demonstrate that already monthly averages of visually observed wave heights may reasonably correlate with the outcome of satellite-derived information. This feature suggests that a comparison of visually observed wave properties averaged over longer periods with the outcome of numerical simulations may provide reliable additional information about wave climate and its changes.

It is expected that visual observations from the shore provide systematically lower wave heights compared to various estimates of offshore or even nearshore wave heights (unless waves exert strong shoaling). This feature is likely more pronounced for our simulations that ignore the presence of sea ice. This difference is about 50% of the modelled wave heights (Figure 9). Even though there is some similarity in the course of the annual average of visually observed

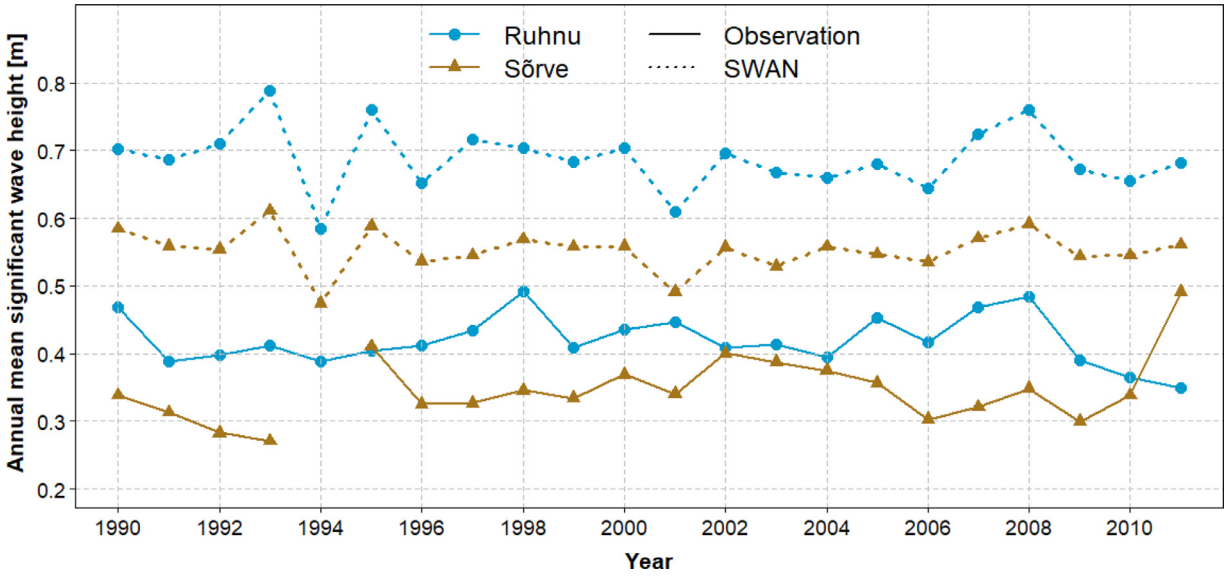

Figure 9 Annual average of visually observed and modelled wave height at Ruhnu and Sõrve.

and modelled wave heights at Ruhnu and Sõrve, the match of these two data sets is poor. Similar to the above, it is likely that the mismatch largely stems from the shortages of visual wave observations.

3.3. Peak periods

The empirical probability distributions of wave periods in the Gulf of Riga exhibits a bell-shape curve around the modal value, resembling a more or less symmetric, Gaussian-like pattern around its maximum (which is also typical for the ocean waves; e.g., Massel, 2013). The most frequent recorded periods are 3—4 s at Skulte, 3—5 s at Matsi and 4—5 s at Kihnu and Kõiguste. The modelled distributions are skewed towards shorter periods at all locations in the interior of the gulf and also considerably underestimate wave periods, especially at Kõiguste. Wave data at Skulte contain numerous estimates of peak periods >10 s. The relevant wave heights are very small. The average wave height of wave fields with peak periods ≥10 s is about 11 cm. For an observer, this is an almost perfectly calm sea surface. As even higher periods are unrealistic, wave fields with periods ≥12 s have been omitted in the analysis.

The distributions of measured and modelled periods match each other well at Harilaid in the Baltic proper. Both distributions resemble the typical shape of such distributions in the Baltic proper. It is therefore likely that the model used in this study appropriately reconstructs the statistics of wave periods in the open part of the gulf and that the mismatch of the modelled and measured periods stems from the inability of this model to replicate wave properties in the northern part of the gulf that has complicated bathymetry and geometry.

The distribution of modelled wave periods in the interior of the Gulf of Riga, first of all at Skulte (Figure 10) matches well the distributions extracted from visual observations (Figure 11). The visually observed wave periods are concentrated between 2 and 4 s both in Sõrve and Ruhnu (Eelsalu et al., 2014). This distribution is narrow and negatively skewed at Sõrve but wider and positively skewed at Ruhnu (Eelsalu et al., 2014). It is likely that the latter feature reflects local wave conditions in the vicinity of the Sõrve observation site. Wave periods longer than 6 s are very rare in the visually observed and modelled data but abundant in the RDCP data. Likely, such occasions are very low-wave situations that originate from the Baltic proper. As such wave conditions are not easy to recognise by the naked eye, they have not been recorded in visual observations.

The performed analysis signals that even though there may be considerable differences in average properties and in the shape of statistical distributions that reflect the wave climate, the performed simulations satisfactorily replicate the course of wave heights in single locations and provide reasonable estimates of average wave heights throughout measurement campaigns. The match of simulated and recorded wave periods is poor; however, the typical values of periods and the shape of distributions of wave periods are replicated adequately.

3.4. Spatial variations in the wave climate

We start the description of the simulated idealised wave climate in the Gulf of Riga from the patterns of long-term average significant wave height (H_S) in its different regions. The wave climate in this water body is milder than in the neighbouring areas of the Baltic proper (Figure 12). As expected based on the properties of predominant winds in the region, waves are systematically higher in the central and eastern parts of the gulf. While the East-West asymmetry is fairly modest, the South-North asymmetry is much more pronounced. Most of the interior of the gulf has long-term average H_S between 0.7 and 0.8 m while the neighbouring Baltic proper regions have it in the range of 1.1—1.2 m (that matches the estimates of Björkqvist et al., 2018a). The area with highest waves, with the average H_S slightly over 0.8 m and a maximum of 0.82 m, is located between islands of Ruhnu and Kihnu and is centered at 30°E, 58°N. The mean

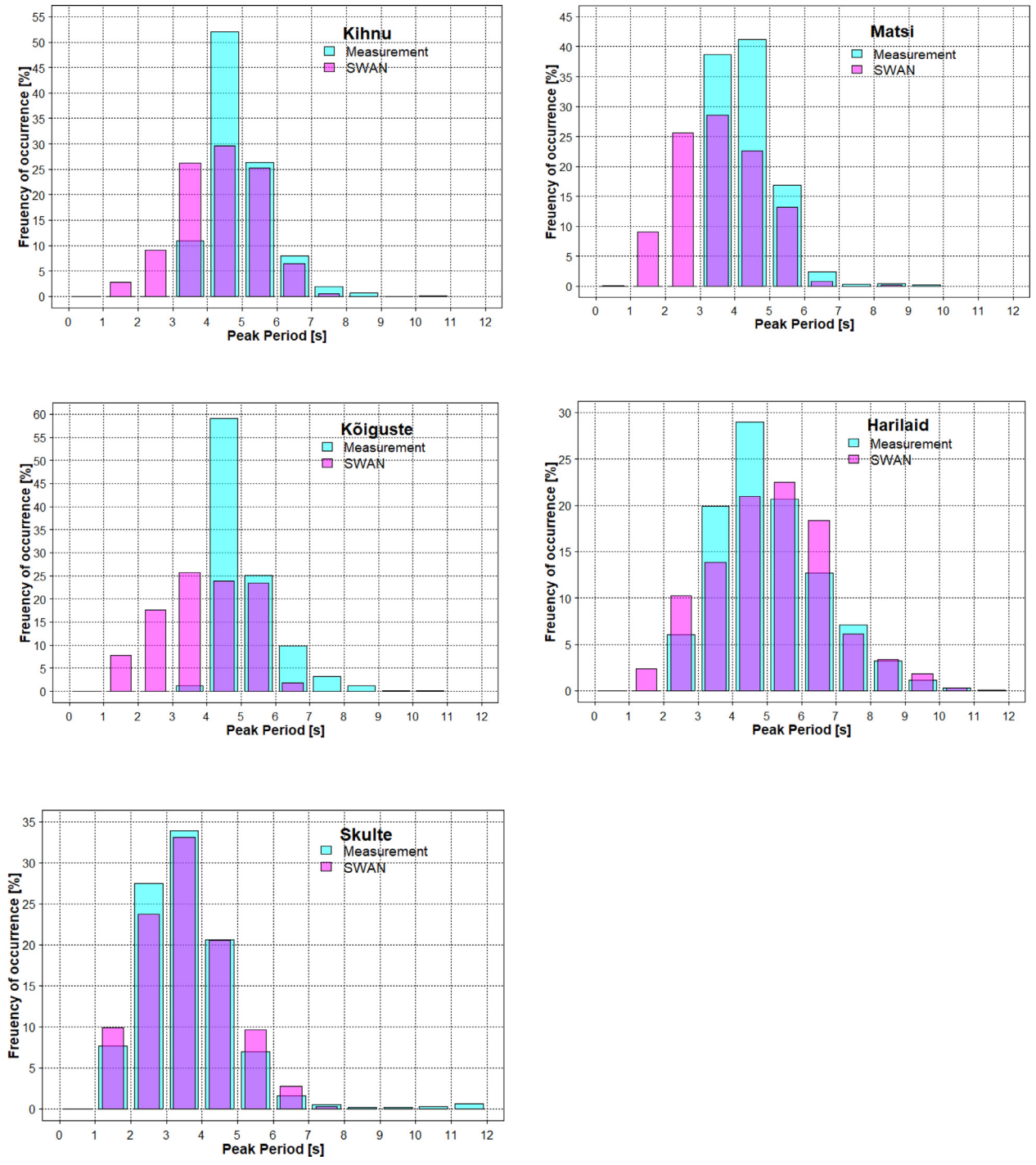

Figure 10 Empirical probability distributions of measured (blue) and observed (red) peak periods in five measurement locations. As the RDCP pressure sensor does not recognise wave periods of shorter waves when deployed to larger depths, wave periods below 2—3 s (depending on deployment depth) are not directly represented in the instrument output at Kihnu, Matsi, Kõiguste, and Harilaid.

H_S is below 0.7 m in the southern part of the gulf to the south of latitude 57°30′N.

The appearance of this map (Figure 12) suggests that moderate and strong SW winds are clearly more frequent than north-western or NNW winds. The calmest region is located near Jurmala at the southern bayhead of the Gulf of Riga. The mean H_S is smaller near the south-western shore compared to the situation near the eastern shore of the gulf. A relatively low average H_S in Pärnu Bay apparently reflects two features. First of all, it mirrors wave attenuation over a relatively shallow seabed in the entrance region of the bay. Secondly, Pärnu Bay is geometrically sheltered for most wave directions. It is likely that high waves penetrate into this bay only for a few wind directions that create the largest water levels in the bay (Suursaar et al., 2002).

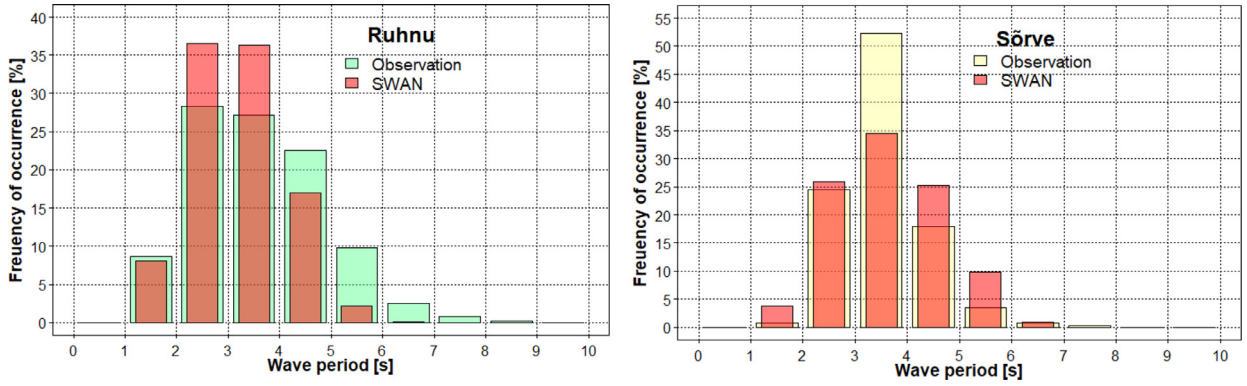

Figure 11 Empirical probability distributions of the frequency of occurrence of observed wave periods at Ruhnu (green) and Sõrve (yellow) (Eelsalu et al., 2014). The colour code is the same as for Figure 8.

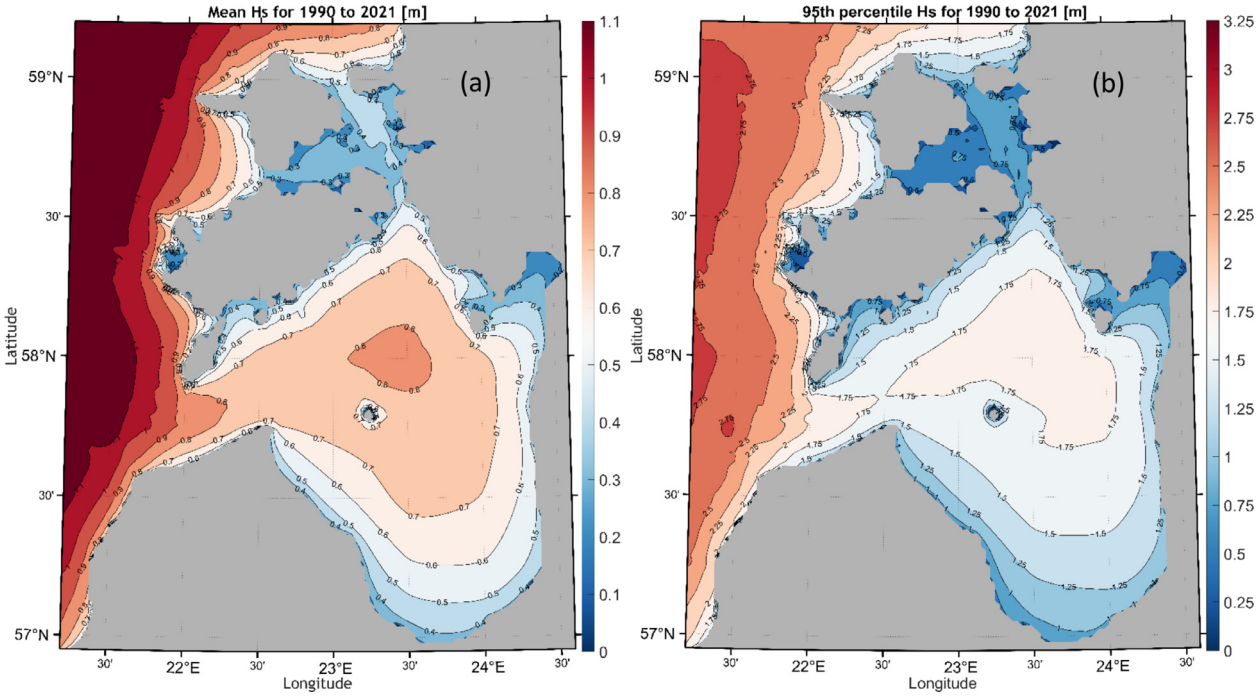

Figure 12 Spatial distribution of the long-term mean H_S (a) and the 95 percentile of H_S (b) in 1990—2021 evaluated using the GoR grid with a resolution of about 1 nmi (Figure 1).

The spatial distribution of higher quantiles of wave heights is slightly more asymmetric in the East-West direction than the above distribution of average wave heights. The area with 95 percentiles lower than 1.5 m (Figure 12) is much wider near Kurzeme Peninsula near the eastern shore of the gulf and extends to the shore of the island of Kihnu. The North-South asymmetry is also more pronounced and high waves are common in the entire northern segment of the gulf. The relevant thresholds (1.75—1.9 m, with a maximum of 1.91 m) are lower than in the neighbouring regions of the Baltic proper where they extend above 2.75 m. The estimates of Björqkvist et al. (2018a) for 1965—2005 led to a similar spatial distribution of 95 percentiles, with values over 2 m between Ruhnu and Kihnu.

The similar distribution for 99 percentiles is similar to the one for 95 percentiles. Typical values of this threshold exceed 2.2 m in the northern and northeastern parts of the gulf and reach over 2.4 m in the northeast, with a maximum of 2.48, while they are close to 4 m in the neighbouring Baltic proper. The estimates of Björqkvist et al. (2018a) again led to a similar spatial distribution of 99 percentiles but with values over 2.5 m in the area where our simulations indicated 2.25—2.5 m.

Wave conditions during extreme storms may be even more severe. It is likely that the January 2005 storm Erwin/Gudrun (Soomere et al., 2008) that created exceptional water levels in the Gulf of Riga (Suursaar et al., 2006) excited wave fields with significant wave heights well over 4

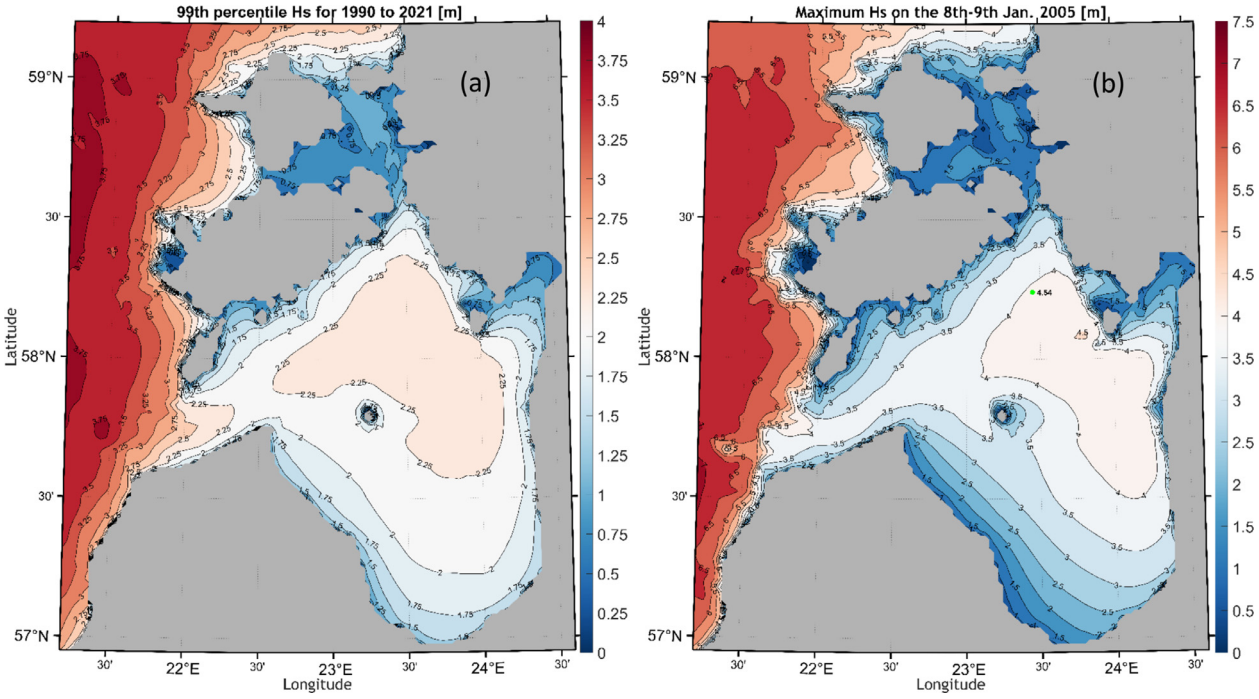

Figure 13 Spatial distribution of the 99 percentile of wave heights in 1990—2021 (a) and maximum wave heights on January 08—09, 2005 wave storm (b).

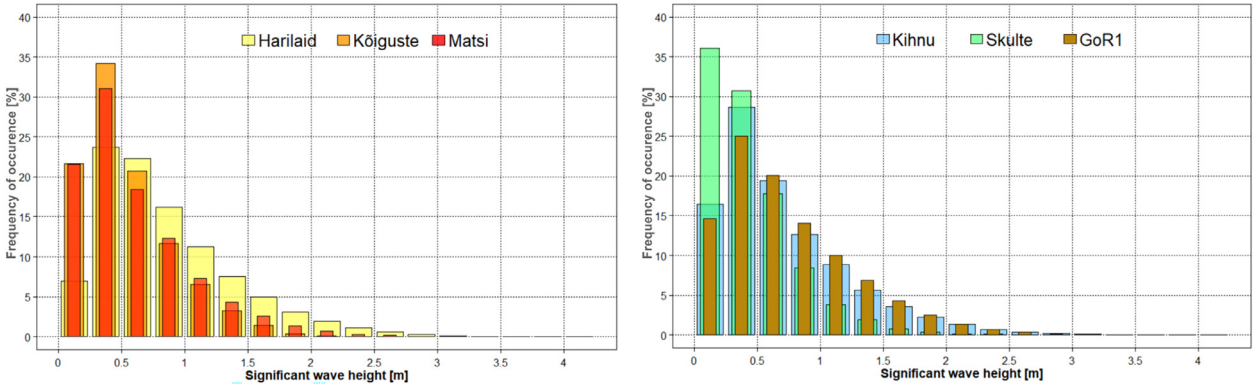

Figure 14 Frequency distributions of modelled H_S at six locations in 1990—2021.

m in the entire eastern part of the gulf, with a maximum of slightly over 4.5 m near the island of Kihnu and in the north of the gulf (Figure 13). These values are clearly smaller than the maximum H_S 6.2 m that was estimated to occur in the Gulf of Riga on 2 November 1969 within the modelled time period of 1965—2006 (Björqkvist et al., 2018b).

3.5. Frequency of occurrence of wave heights and periods

Long-term distributions of the frequency of occurrence of wave fields with different H_S (Figure 14) have the same overall shape in all locations of measurements, except at Skulte where the proportion of wave fields with H_S <0.25 m is clearly higher than in other locations. These locations evidently reflect well wave properties in different parts of the gulf. They all follow a 2-dimensional Weibull distribution. The overall shape of the realisations of this distribution is narrower than similar distributions in the Baltic proper (incl. Harilaid) but still clearly wider than similar ones in sheltered nearshore regions (Soomere, 2005). The median H_S is below 0.5 m, and is closest to 0.5 m at the most open location Skulte. Calm situations, with H_S not exceeding 0.25 m cover about 17—30% of the time in the Gulf of Riga against 7% at Harilaid. The probability of having waves with $H_S > 1$ m varies from 23% at Kihnu down to 7% at Skulte. Wave fields with $H_S > 2$ m occur with a probability of about 1% and $H_S > 3$ m are very rare.

The majority of wave fields have peak periods in the range of 2—5 s, with periods 3—4 s being the most frequent (Figure 15). Waves are thus systematically shorter in

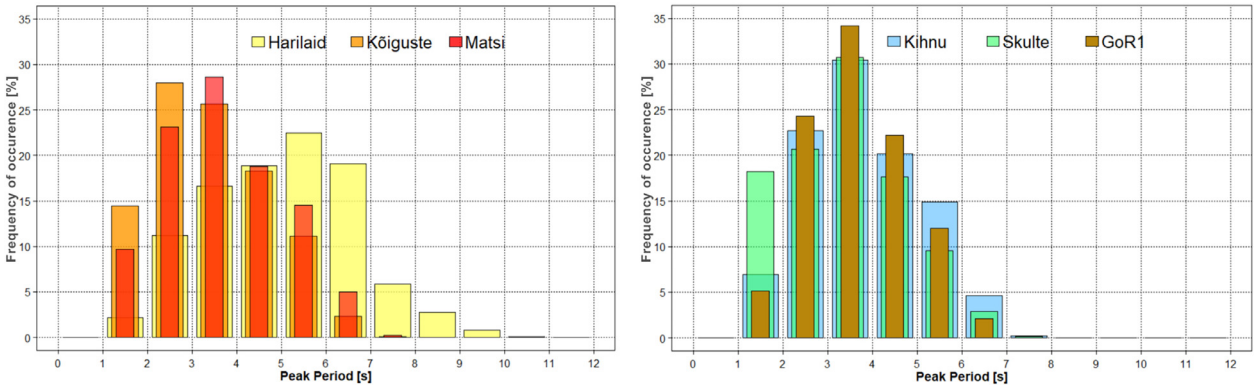

Figure 15 The frequency distribution of modelled wave periods at six in situ measurement sites.

the Gulf of Riga compared to the neighbouring segments of the Baltic proper where the predominant wave periods are 4—7 s.

3.6. Joint distribution of significant wave height and mean period

The joint distribution of visually observed wave heights and periods roughly matches the fully developed wave conditions at Ruhnu but to some extent reflects such distributions for swell-dominated regions at Sõrve (Eelsalu et al., 2014). The simulated data sets provide additional details to this feature. Wave conditions at all sites reveal the presence of two different sets of wave conditions (Figure 16). The properties of the majority of wave fields almost exactly follow the properties of fully developed wave fields with a Pierson-Moskowitz spectrum. The highest waves of this set have slightly longer periods than the corresponding fully developed seas (except for GoR1). The other set of wave conditions has periods much longer than the waves with the same height but with a Pierson-Moskowitz spectrum. As the wave height is mostly below 0.5 m in such situations, they likely reflect waves created in a remote area; possibly in the Baltic proper.

These distributions provide a simple estimate of the combinations of wave heights and periods in the most extreme storms. These combinations likely match the ones for fully developed wave systems with a Pierson-Moskowitz spectrum. For example, at Kihnu extreme wave conditions with a H_S close to 4 m are likely to have a period of 6.5 s.

3.7. Long-term variations

The simulations shed some light on the interannual variability in wave properties. The addressed time interval 1990—2021 contains several implications of rapid climate change in the region. In particular, systematic changes have been observed in the parameters of the generalised extreme value distribution for water level extremes (Kudryavtseva et al., 2021). Such shifts are likely associated with similar shifts in the drivers of water level, including wind properties. However, the simulations were presented for the hypothetical ice-free case, even if the ice was actually present on the sea. In reality, some of the variability would come from actual variations in ice cover.

The course of annual average modelled H_S is qualitatively similar in all addressed locations (Figure 17). The magnitude of interannual variations in the H_S is about 20% (±10%) from the long-term mean at all sites. The level of such variations was larger in 1990—1997 and 2007—2020. Interannual variations are highly synchronised in different parts of the gulf and near the entrance of the gulf (Harilaid), Importantly, there exists no systematic decrease or increase in the annual average H_S over the considered time interval. On the one hand, this conjecture is consistent with the perception that (scalar) wind properties in the Baltic Sea region have not massively changed during many decades (BACC, 2015). On the other hand, this feature also signals that some wave properties of the Gulf of Riga, at least the average H_S in this basin, may be disconnected from changes to these parameters in the Baltic proper, as noted in (Viška and Soomere, 2013a).

4. Discussion

In general, the simulations of wave time series in the Gulf of Riga clearly expressed some heterogeneity in the wave conditions (Figures 12—13). Wave intensity is relatively large in its central, northeastern and eastern regions. This is consistent with the perception that the majority of moderate and strong winds blow from the southwest in this region (Soomere and Keevallik, 2001). It is however somewhat unexpected that the wave climate of the southern part of this water body is milder than in the north-east also in terms of higher quantiles of wave heights. NNW winds are less frequent but they have the longest fetch and thus have the potential to generate severe waves in the south of this water body. Spatial distributions of wave properties (Figures 12—13) suggest that this potential has not been systematically realized in 1990—2021. Instead, westerly winds have become more frequent (Bierstedt et al., 2015).

The used wave model has been first of all tuned for neighbouring water bodies, such as the Baltic proper or the Gulf of Finland. It tends to show poorer performance than, e.g., in the Gulf of Finland (Giudici et al., 2023) even if applied in a much finer resolution. This feature partially reflects difficulties with a representation of wave properties in regions with highly variable bathymetry, similar to gaps in the performance of wave models in archipelagos

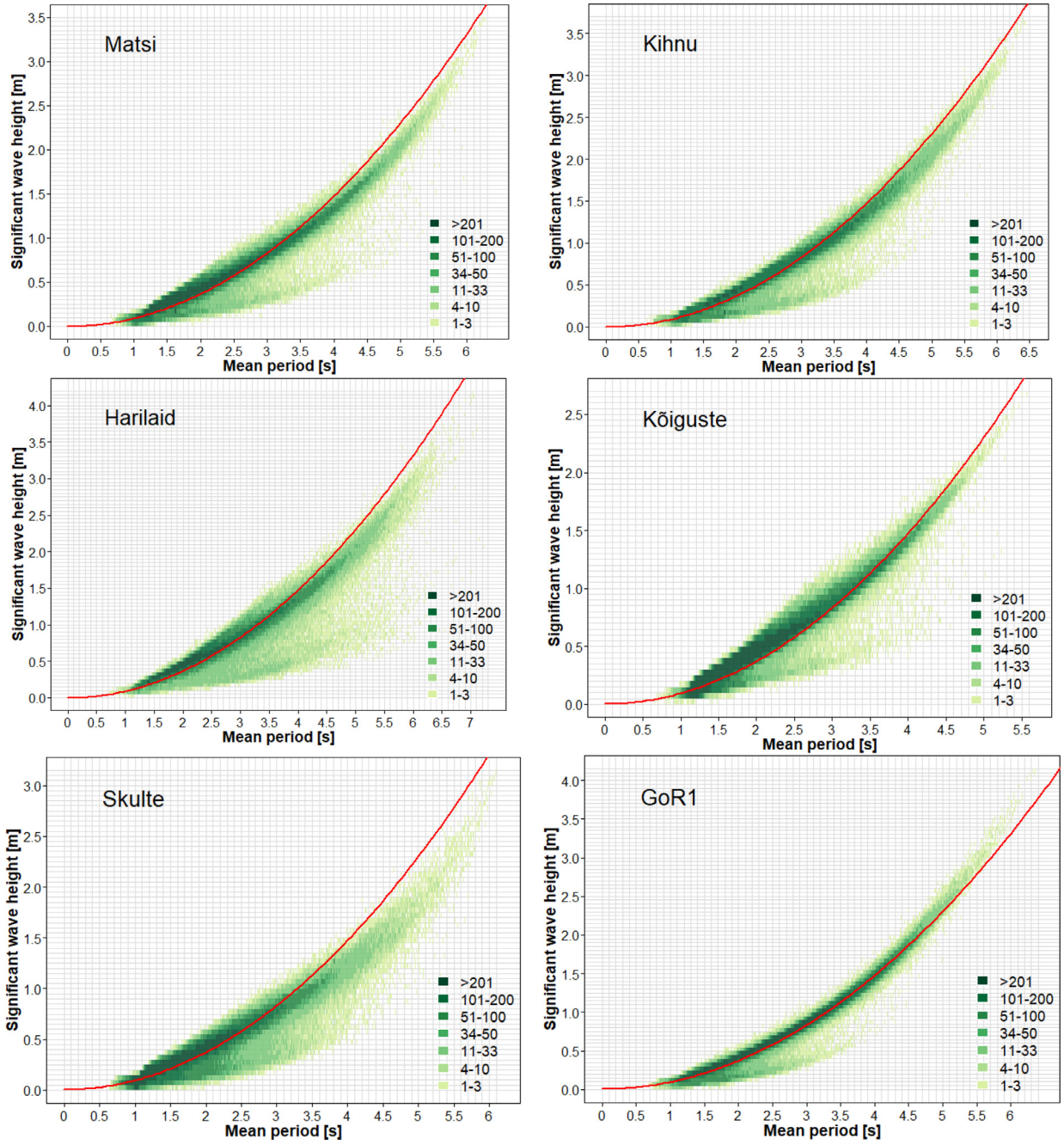

Figure 16 Joint distribution of modelled H_S and mean period. The width of classes of the mean period (T_{02}) is 0.01 s and 0.05 m for H_S. The red line shows the SWH of the fully developed wave systems with the Pierson-Moskowitz spectrum for the given mean period.

(Björkqvist et al., 2018b) where the performance of the wave model depends on the wind direction and apparently on the openness of the particular location towards specific directions. It is particularly evident at Kõiguste where the duration of measured wave storms often differed from the hindcast one. Part of this difference may result from the properties of the device (RDCP), and some from generalisation of the irregular bathymetry in the shallow, archipelago-like sea area. The match is much better in the fully open location of Skulte where a waverider buoy was used for wave measurements.

Historical visual observations considerably underestimate the long-term average wave height and provide a distorted estimate of the probability of occurrence of waves of different heights. This distribution overestimates the proportion of almost calm seas, especially in the relatively sheltered location of Sõrve. The match of the interannual course of the measured and modelled data sets is also poor.

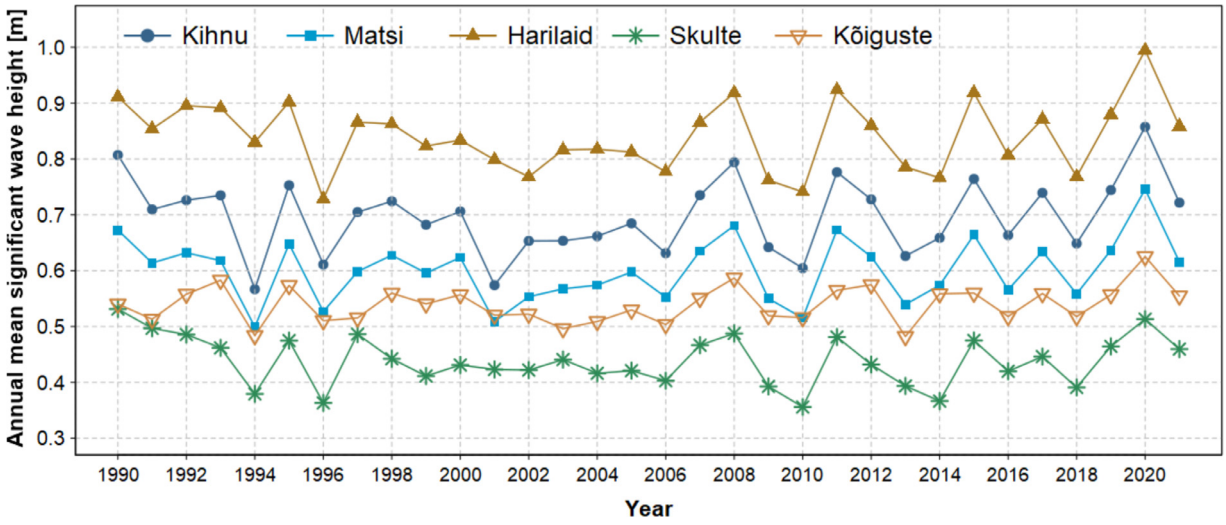

Figure 17 Time series of annual mean modelled H_S at five sites in the Gulf of Riga.

In contrast, the distribution of the observed wave periods matches well the similar distributions generated from modelled data.

Changing properties of wind wave fields are one of the markers of manifestations of climate change over seas and oceans (Charles et al., 2012; Dodet et al., 2010). Time series of common climatic variables (such as wind speed or sea surface temperature) extend back over substantial time intervals (BACC, 2008). Water level time series extend back over almost two and a half centuries in the Baltic Sea (Ekman, 1999). The longest instrumentally measured wave time series only covers a few decades. In this context, visually observed data serve as one of a few options to identify climate changes in the past even though the quality of such records is low. The sets of visually observed wave data are consistent with the hindcast in terms of the magnitude of interannual variations in wave intensity and the absence of any long-term trend in the wave height in the 1990s and 2000s.

A major limitation of the performed numerical simulations and the relevant discussion is the use of an idealised ice-free approach. The Gulf of Riga is at least partially ice-covered each winter in the contemporary climate. Ignoring ice leads to systematic overestimation of cumulative wave energy and its flux on the latitudes of the Gulf of Riga (Najafzadeh et al., 2022). This approach may also lead to major differences in spatial distributions of wave properties in strong storms in partially ice-covered seas (Tuomi et al., 2019) and thus to distortions of spatial distributions of higher quantiles of wave heights. This assumption, however, does not erode the validity of comparison of wave reconstructions with in situ measurements in ice-free times.

Another limitation is the use of constant water level in wave simulations. The Gulf of Riga often experienced large variations in the water level. Both preconditioning (filling first the entire Baltic Sea and then the Gulf of Riga with excess water during some storms) (Männikus et al., 2019) and local changes in water level in the nearshore may impact wave heights. As the Gulf of Riga has a fairly regular shape, with relatively narrow and shallow nearshore, it is likely that changes to the overall water level in the gulf do not add any detectable variation to the wave properties in most of the gulf area.

The situation is more complicated in the nearshore and, in particular, in the narrow and shallow Pärnu Bay. The historic total range of water level variations has reached 4 m (+2.75, −1.25 m) in this bay (Jaagus and Suursaar, 2013) and has apparently exceeded 3 m along most of the eastern shore of the gulf (Männikus et al., 2019). However, extreme events are rare. The water level usually stays within ±50 cm in the entire gulf (Männikus et al., 2019) and the impacts are mostly confined to specific sections of the shore. For example, it has been argued that somewhat higher waves could have been reached Pärnu Bay during extreme storm Gudrun in 2005 (Suursaar et al., 2006).

The relevant effects may to some extent affect the properties of waves in the nearshore, mostly via alterations of refraction, shoaling and bottom-driven loss of energy. These effects first become evident in terms of changes to the wave impact on the shore and wave-driven sediment transport. It is likely, similar to the eastern shore of the Baltic proper, that high waves often approach part of the shores of the Gulf of Riga at large angles between the wave approach direction and shore normal. A decrease in the intensity of refraction in deeper water may amplify this feature. Therefore, the development of local instabilities of the coastline (Ashton et al., 2001) is likely in some segments of this water body. For this reason, it is important to describe not only the general properties of the wave climate of the Gulf of Riga in more detail but also adequately evaluate the directional distribution of severe wave conditions in future research.

5. Conclusions

Wave climate in the Gulf of Riga is considerably milder than in the Baltic proper, Gulf of Bothnia or Gulf of Finland and comparable to that of the Arkona Basin. The long-term average modelled significant wave height is mostly in the range

of 0.7—0.8 m. Wave periods are predominantly 2—5 s and thus systematically shorter than in the Baltic proper. Wave fields are usually fully saturated wind seas or (in the northern part) contain low swells generated in the Baltic proper.

The modelling exercise suggests that the threshold of significant wave height that occurs with a probability of 5% (95 percentiles) is lower than 1.5 m near the Kurzeme peninsula but reaches 1.75—1.9 m in the central, northern and eastern parts of the gulf. The typical values of the threshold for waves that occur with a probability of 1% exceed 2.2 m in the northern and northeastern parts of the gulf and reach over 2.4 m in the northeast. The modelled significant wave height reached well over 4 m in the entire eastern part of the during the January 2005 storm Erwin/Gudrun.

The wave climate varies spatially; the waves are higher and longer in the eastern part of the gulf. Modelled extreme wave heights may reach 4—5 m, with periods up to 7—8 s.

Although historical visual wave observations from the shore underestimate wave heights, they still have a reasonable correlation with simulations in terms of wave periods and interannual variability in wave heights.

There was a substantial interannual variability in the mean wave height without any systematic trend or distinct decadal-scale variation in the wave heights in 1990—2021.

Declaration of competing interests

The authors declare that they have no known competing financial interests or personal relationships that could have appeared to influence the work reported in this paper.

Acknowledgements

The research was co-supported by the Estonian Research Council (grants PRG1129 and PRG1471), and the European Economic Area (EEA) Financial Mechanism 2014—2021 Baltic Research Programme (grant EMP480).

References

Ashton, A., Murray, A.B., Arnault, O., 2001. Formation of coastline features by large—scale instabilities induced by high-angle waves. Nature 414 (6861), 296—300. https://doi.org/10.1038/35104541

Badulin, S.I., Grigorieva, V.G., 2012. On discriminating swell and wind-driven seas in Voluntary Observing Ship data. J. Geophys. Res.-Oceans 117 (C11), C00J29. https://doi.org/10.1029/2012JC007937

Baltic Sea Hydrographic Commission, 2013. Baltic Sea Bathymetry Database Version 0.9.3. (Downloaded on 15.02.2020 from http://data.bshc.pro/on).

Bierstedt, S.E., Hünicke, B., Zorita, E., 2015. Variability of wind direction statistics of mean and extreme wind events over the Baltic Sea region. Tellus A 67, 29073. https://doi.org/10.3402/tellusa.v67.29073

Björkqvist, J.V., Kanarik, H., Johansson, M.M., Tuomi, L., 2018b. A wave forecast for the Helsinki archipelago in the Gulf of Finland. 2018 IEEE/OES Baltic International Symposium (BALTIC), June 12—15. Klaipeda, Lithuania. https://doi.org/10.1109/BALTIC.2018.8634863

Björkqvist, J.V., Lukas, I., Alari, V., van Vledder, P.G., Hulst, S., Pettersson, H., Behrens, A., Männik, A., 2018a. Comparing a 41-year model hindcast with decades of wave measurements from the Baltic Sea. Ocean Eng. 152, 57—71. https://doi.org/10.1016/j.oceaneng.2018.01.048

Björkqvist, J.-V., Pärt, S., Alari, V., Rikka, S., Lindgren, E., Tuomi, L., 2021. Swell hindcast statistics for the Baltic Sea. Ocean Sci. 17, 1815—1829. https://doi.org/10.5194/os-17-1815-2021

Björkqvist, J.V., Rikka, S., Alari, V., Männik, A., Tuomi, L., Pettersson, H., 2020. Wave height return periods from combined measurement-model data: a Baltic Sea case study. Nat. Hazards Earth Syst. Sci. 20 (12), 3593—3609. https://doi.org/10.5194/nhess-20-3593-2020

Björkqvist, J.V., Tuomi, L., Fortelius, C., Pettersson, H., Tikka, K., Kahma, K.K., 2017. Improved estimates of nearshore wave conditions in the Gulf of Finland. J. Marine Syst. 171, 43—53. https://doi.org/10.1016/j.jmarsys.2016.07.005

Booij, N., Ris, R.C., Holthuijsen, L.H., 1999. A third-generation wave model for coastal regions: 1. Model description and validation. J. Geophys. Res.-Oceans 104 (C4), 7649—7666. https://doi.org/10.1029/98JC02622

Broman, B., Hammarklint, T., Rannat, K., Soomere, T., Valdmann, A., 2006. Trends and extremes of wave fields in the north-eastern part of the Baltic Proper. Oceanologia 48 (S), 165—184.

Charles, E., Idier, D., Delecluse, P., Deque, M., Le Cozannet, G., 2012. Climate change impact on waves in the Bay of Biscay. France. Ocean Dynam. 62 (6), 831—848. https://doi.org/10.1007/s10236-012-0534-8

Christensen, E.D., Johnson, M., Sørensen, O.R., Hasager, C.B., Badger, M., Larsen, S.E., 2013. Transmission of wave energy through an offshore wind turbine farm. Coast. Eng. 82, 25—46. https://doi.org/10.1016/j.coastaleng.2013.08.004

Chubarenko, B.V., Leitsina, L.V., Esiukova, E.E., Kurennoy, D.N., 2012. Model analysis of the currents and wind waves in the Vistula Lagoon of the Baltic Sea. Oceanology 52 (6), 748—753. https://doi.org/10.1134/S000143701206001X

Cieślikiewicz, W., Paplińska-Swerpel, B., 2008. A 44-year hindcast of wind wave fields over the Baltic Sea. Coast. Eng. 55, 894—905. https://doi.org/10.1016/j.coastaleng.2008.02.017

Davidan, I.N., Lopatoukhin, L.I., Rozhkov, V.A., 1985. Wind Waves in the World Oceans. Gidrometeoizdat, Leningrad (in Russian).

Dean, R.G., Walton, T.L., Hatheway, D., 2008. Wave setup in U.S. flood insurance studies. Coast. Eng. 5, 926—974. https://doi.org/10.1142/9789814277426_0081

Dodet, G., Bertin, X., Taborda, R., 2010. Wave climate variability in the North-East Atlantic Ocean over the last six decades. Ocean Model. 31 (3—4), 120—131. https://doi.org/10.1016/j.ocemod.2009.10.010

Dvornikov, A.Y., Martyanov, S.D., Ryabchenko, V.A., Eremina, T.R., Isaev, A.V., Sein, D.V., 2017. Assessment of extreme hydrological conditions in the Bothnian Bay, Baltic Sea, and the impact of the nuclear power plant "Hanhikivi-1" on the local thermal regime. Earth Syst. Dynam. 8 (2), 265—282. https://doi.org/10.5194/esd-8-265-2017

ECMWF, 2006. IFS Documentation — Cy41r2. Operational Implementation 8 March 2016. Part IV: Physical Processes. Accessed on Fabruary 7th, 2023, https://www.ecmwf.int/en/elibrary/79697-ifs-documentation-cy41r2-part-iv-physical-processes.

Eelsalu, M., Org, M., Soomere, T., 2014. Visually observed wave climate in the Gulf of Riga. The 6th IEEE/OES Baltic Symposium Measuring and Modeling of Multi-Scale Interactions in the Marine Environment, May 26—29, 6887829. IEEE Conference Publications, 10. https://doi.org/10.1109/BALTIC.2014.6887829

Ekman, M., 1999. Climate changes detected through the world's longest sea level series. Glob. Planet. Change 21 (4), 215—224. https://doi.org/10.1016/S0921-8181(99)00045-4

Giudici, A., Jankowski, M.Z., Männikus, R., Najafzadeh, F., Suursaar, Ü., Soomere, T., 2023. A comparison of Baltic Sea wave

properties simulated using two modelled wind data sets. Estuar. Coast. Shelf Sci. 290, 108401. https://doi.org/10.1016/j.ecss.2023.108401

Guedes Soares, C., 1986. Assessment of the uncertainty in visual observations of wave height. Ocean Eng. 13 (1), 37—56. https://doi.org/10.1016/0029-8018(86)90003-X

Guidelines, 1985. Guidelines for Hydrometeorological Stations and Posts. Meteorological observations at stations. Leningrad: Gidrometeoizdat 3 (1), 300 pp. (in Russian).

Gulev, S.K., Grigorieva, V., 2004. Last century changes in ocean wind wave height from global visual wave data. Geophys. Res. Lett. 31 (24), L24302. https://doi.org/10.1029/2004GL021040

Gulev, S.K., Grigorieva, V., 2006. Variability of the winter wind waves and swell in the North Atlantic and North Pacific as revealed by the Voluntary Observing Ship data. J. Clim. 19 (21), 5667—5685. https://doi.org/10.1175/JCLI3936.1

Gulev, S.K., Grigorieva, V., Sterl, A., Woolf, D., 2003. Assessment of the reliability of wave observations from voluntary observing ships: insights from the validation of a global wind wave climatology based on voluntary observing ship data. J. Geophys. Res.-Oceans 108 (C7), 3236.

Gulev, S.K., Hasse, L., 1998. North Atlantic wind waves and wind stress fields from voluntary observing ship data. J. Phys. Oceanogr. 28, 1107—1130. https://doi.org/10.1175/1520-0485(1998)028⟨1107:NAWWAW⟩2.0.CO;2

Gulev, S.K., Hasse, L., 1999. Changes of wind waves in the North Atlantic over the last 30 years. Int. J. Climatol. 19 (10), 1091—1117. https://doi.org/10.1002/(SICI)1097-0088(199908)19:10⟨1091::AID-JOC403⟩3.0.CO;2-U

Hersbach, H., Bell, B., Berrisford, P., Biavati, G., Horányi, A., Muñoz Sabater, J., Nicolas, J., Peubey, C., Radu, R., Rozum, I., Schepers, D., Simmons, A., Soci, C., Dee, D., Thépaut, J.-N., 1979 to present. Copernicus Climate Change Service (C3S). Climate Data Store (CDS). https://doi.org/10.24381/cds.bd0915c6

Hogben, N., Dacunka, N.M.C., Olliver, G.F., 1986. Global Wave Statistics. Unvin Brothers, London.

Hogben, N., Lumb, F.E., 1967. Ocean Wave Statistics; a statistical survey of wave characteristics estimated usually from Voluntary Observing Ships sailing along the shipping routes of the world. H.M.S.O, Ministry of Technology, National Physical Laboratory, London, 263 pp.

Hünicke, B., Zorita, E., Soomere, T., Skovgaard Madsen, K., Johansson, M., Suursaar, Ü., 2015. Recent change — sea level and wind waves. In: The BACC II Author Team, Second Assessment of Climate Change for the Baltic Sea Basin. Regional Climate Studies. Springer, 155—185. https://doi.org/10.1007/978-3-319-16006-1_9

Jaagus, J., 2009. Long-term changes in frequencies of wind directions on the western coast of Estonia. In: Kont, A., Tõnisson, H. (Eds.), Climate Change Impact on Estonian Coasts. Publication 11/2009. Tallinn: Institute of Ecology, Tallinn University, 11—24 (in Estonian).

Jaagus, J., Kull, A., 2011. Changes in surface wind directions in Estonia during 1966—2008 and their relationships with large-scale atmospheric circulation. Est. J. Earth Sci. 60, 220—231. https://doi.org/10.3176/earth.2011.4.03

Jaagus, J., Suursaar, Ü., 2013. Long-term storminess and sea level variations on the Estonian coast of the Baltic Sea in relation to large-scale atmospheric circulation. Est. J. Earth Sci. 62 (2), 73—92. https://doi.org/10.3176/earth.2013.07

Jahanmard, V., Varbla, S., Delpeche-Ellmann, N., Ellmann, A., 2022. Retrieval of directional power spectral density and wave parameters from airborne LiDAR point cloud. Ocean Eng. 266, 112694. https://doi.org/10.1016/j.oceaneng.2022.112694

Keevallik, S., 2003. Possibilities of reconstruction of the wind regime over Tallinn Bay. Proc. Estonian Acad. Sci. Eng. 9 (3), 209—219. https://doi.org/10.3176/eng.2003.3.04

Kelpšaitė, L., Dailidienė, I., Soomere, T., 2011. Changes in wave dynamics at the south-eastern coast of the Baltic Proper during 1993—2008. Boreal Environ. Res. 16 (Supplement A), 220—232.

Komen, G.J., Hasselmann, S., Hasselmann, K., 1984. On the existence of a fully developed wind-sea spectrum. J. Phys. Oceanogr. 14 (8), 1271—1285. https://doi.org/10.1175/1520-0485(1984)014⟨1271:OTEOAF⟩2.0.CO;2

Kudryavtseva, N., Kussembayeva, K., Rakisheva, Z.B., Soomere, T., 2019. Spatial variations in the Caspian Sea wave climate in 2002—2013. Est. J. Earth Sci. 68 (4), 225—240. https://doi.org/10.3176/earth.2019.16

Kudryavtseva, N., Soomere, T., 2017. Satellite altimetry reveals spatial patterns of variations in the Baltic Sea wave climate. Earth Syst. Dynam. 8 (3), 697—706. https://doi.org/10.5194/esd-8-697-2017

Kudryavtseva, N., Soomere, T., Männikus, R., 2021. Non-stationary analysis of water level extremes in Latvian waters, Baltic Sea, during 1961—2018. Nat. Hazards Earth Syst. Sci. 21 (4), 1279—1296. https://doi.org/10.5194/nhess-21-1279-2021

Kudryavtseva, N.A., Soomere, T., 2016. Validation of the multi-mission altimeter wave height data for the Baltic Sea region. Est. J. Earth Sci. 65 (3), 161—175. https://doi.org/10.3176/earth.2016.13

Lebedev, S.A., Kostianoy, A.G., 2008. Integrated use of satellite altimetry in the investigation of the meteorological, hydrological, and hydrodynamic regime of the Caspian Sea. Terr. Atmos. Ocean. Sci. 19 (1—2), 71—82. https://doi.org/10.3319/TAO.2008.19.1-2.71(SA)

Leppäranta, M., Myrberg, K., 2009. Physical Oceanography of the Baltic Sea. Springer Science & Business Media, Praxis, Berlin, Heidelberg. https://doi.org/10.1007/978-3-540-79703-6

Männikus, R., Soomere, T., Kudryavtseva, N., 2019. Identification of mechanisms that drive water level extremes from in situ measurements in the Gulf of Riga during 1961—2017. Cont. Shelf Res. 182, 22—36. https://doi.org/10.1016/j.csr.2019.05.014

Männikus, R., Soomere, T., Najafzadeh, F., 2022. Refraction may redirect waves from multiple directions into a harbour: a case study in the Gulf of Riga, eastern Baltic Sea. Est. J. Earth Sci. 71 (2), 80—88. https://doi.org/10.3176/earth.2022.06

Männikus, R., Soomere, T., Viška, M., 2020. Variations in the mean, seasonal and extreme water level on the Latvian coast, the eastern Baltic Sea, during 1961—2018. Estuar. Coast. Shelf Sci. 245, 106827. https://doi.org/10.1016/j.ecss.2020.106827

Massel, S.R., 2013. Ocean Surface Waves: Their Physics and Prediction, 2nd edn. World Scientific, New Jersey, London, Singapore, 692 pp.

Najafzadeh, F., Kudryavtseva, N., Soomere, T., 2021. Effects of large-scale atmospheric circulation on the Baltic Sea wave climate: application of the EOF method on multi-mission satellite altimetry data. Clim. Dynam. 57 (11), 3465—3478. https://doi.org/10.1007/s00382-021-05874-x

Najafzadeh, F., Kudryavtseva, N., Soomere, T., Giudici, A., 2022. Effect of ice cover on wave statistics and wave-driven processes in the northern Baltic Sea. Boreal Environ. Res. 27, 97—116. http://www.borenv.net/BER/archive/pdfs/ber27/ber27-097-116.pdf.

Naulin, J.P., Moncoulon, D., Le Roy, S., Pedreros, R., Idier, D., Oliveros, C., 2016. Estimation of insurance-related losses resulting from coastal flooding in France. Nat. Hazards Earth Syst. Sci. 16, 195—207. https://doi.org/10.5194/nhess-16-195-2016

Nilsson, E., Rutgersson, A., Dingwell, A., Björkqvist, J.-V., Pettersson, H., Axell, L., Nyberg, J., Stromstedt, E., 2019. Characterization of wave energy potential for the Baltic Sea with focus on the Swedish Exclusive Economic Zone. Energies 12 (5), 793. https://doi.org/10.3390/en12050793

Orlenko, L.R., Lopatukhin, L.I., Portnova, G.L. (Eds.), 1984, Studies of the Hydrometeorological Regime of Tallinn Bay. Gidrometeoizdat, Leningrad, 152 pp. (in Russian).

Pallares, E., Sánchez-Arcilla, A., Espino, M., 2014. Wave energy balance in wave models (SWAN) for semi-enclosed domains—Application to the Catalan coast. Cont. Shelf Res. 87, 41—53. https://doi.org/10.1016/j.csr.2014.03.008

Pindsoo, K., Soomere, T., Zujev, M., 2012. Decadal and long-term variations in the wave climate at the Latvian coast of the Baltic Proper. In: Proceedings of the IEEE/OES Baltic 2012 International Symposium "Ocean: Past, Present and Future. Climate Change Research, Ocean Observation & Advanced Technologies for Regional Sustainability,". May 8—11, Klaipėda, Lithuania. IEEE https://doi.org/10.1109/BALTIC.2012.6249160

Plant, N.G., Griggs, G.B., 1992. Comparison of visual observations of wave height and period to measurements made by an offshore slope array. J. Coast. Res. 8 (4), 957—965.

Räämet, A., Soomere, T., 2010. The wave climate and its seasonal variability in the northeastern Baltic Sea. Est. J. Earth Sci. 59 (1), 100—113. https://doi.org/10.3176/earth.2010.1.08

Randmeri, R., 2006. Description of the wave climate of the Gulf of Riga using the WAM wave model. MSc Thesis. Tallinn University.

Rogers, W.E., Hwang, P.A., Wang, D.W., 2003. Investigation of wave growth and decay in the SWAN model: Three regional-scale applications. J. Phys. Oceanogr. 33 (2), 366—389. https://doi.org/10.1175/1520-0485(2003)033⟨0366:IOWGAD⟩2.0.CO;2

Rosenhagen, G., Tinz, B., 2013. New historical data of the southern Baltic Sea coasts. In: Reckermann, M., Köppen, S. (Eds.), 7th Study Conference on BALTEX, 10—14 June 2013, Borgholm, Island of Öland, Sweden, 84 Conference Proceedings, International BALTEX Secretariat, Publication No. 53.

Seifert, T., Tauber, F., Kayser, B., 2001. A high-resolution spherical grid topography of the Baltic Sea—revised edition. Baltic Sea Science Congress 2001, Nov. 25—29.

Sokolov, A.N., Chubarenko, B.V., 2020. Temporal variability of the wind wave parameters in the Baltic Sea in 1979—2018 based on the numerical modeling results. Phys. Oceanogr. 27 (4), 352—363. https://doi.org/10.22449/1573-160X-2020-4-352-363

Sooäär, J., Jaagus, J., 2007. Long-term changes in the sea ice regime in the Baltic Sea near the Estonian coast. Proc. Estonian Acad. Sci. Eng. 13 (3), 189—200.

Soomere, T., 2001. Extreme wind speeds and spatially uniform wind events in the Baltic Proper. Proc. Estonian Acad. Sci. Eng. 7 (3), 195—211. https://doi.org/10.3176/eng.2001.3.01

Soomere, T., 2005. Wind wave statistics in Tallinn Bay. Boreal Environ. Res. 10 (2), 103—118. http://www.borenv.net/BER/archive/pdfs/ber10/ber10-103.pdf

Soomere, T., 2013. Extending the observed Baltic Sea wave climate back to the 1940s. J. Coast. Res. Special Issue 65, 1969—1974. https://doi.org/10.2112/SI65-333

Soomere, T., Behrens, A., Tuomi, L., Nielsen, J.W., 2008. Wave conditions in the Baltic Proper and in the Gulf of Finland during windstorm Gudrun. Nat. Hazards Earth Syst. Sci. 8 (1), 37—46. https://doi.org/10.5194/nhess-8-37-2008

Soomere, T., Bishop, S.R., Viška, M., Räämet, A., 2015. An abrupt change in winds that may radically affect the coasts and deep sections of the Baltic Sea. Clim. Res. 62, 163—171. https://doi.org/10.3354/cr0126

Soomere, T., Keevallik, S., 2001. Anisotropy of moderate and strong winds in the Baltic Proper. Proc. Estonian Acad. Sci. Eng. 7 (1), 35—49. https://doi.org/10.3176/eng.2001.1.04

Soomere, T., Weisse, R., Behrens, A., 2012. Wave climate in the Arkona Basin, the Baltic Sea. Ocean Sci. 8 (2), 287—300. https://doi.org/10.5194/os-8-287-2012

Soomere, T., Zaitseva, I., 2007. Estimates of wave climate in the northern Baltic Proper derived from visual wave observations at Vilsandi. Proc. Estonian Acad. Sci. Eng. 13 (1), 48—64. https://doi.org/10.3176/eng.2007.1.02

Suursaar, Ü., 2013. Locally calibrated wave hindcasts in the Estonian coastal sea in 1966—2011. Est. J. Earth Sci. 62 (1), 42—56. https://doi.org/10.3176/earth.2013.05

Suursaar, Ü., 2015. Analysis of wave time series in the Estonian coastal sea in 2003—2014. Est. J. Earth Sci. 64 (4), 289—304. https://doi.org/10.3176/earth.2015.35

Suursaar, Ü., Kullas, T., Aps, R., 2012. Currents and waves in the northern Gulf of Riga: measurement and long-term hindcast. Oceanologia 54 (3), 421—447. https://doi.org/10.5697/oc.54-3.421

Suursaar, Ü., Kullas, T., Otsmann, M., 2002. A model study of the sea level variations in the Gulf of Riga and the Väinameri Sea. Cont. Shelf Res. 22 (14), 2001—2019. https://doi.org/10.1016/S0278-4343(02)00046-8

Suursaar, Ü., Kullas, T., Otsmann, M., Saaremäe, I., Kuik, J., Merilain, M., 2006. Cyclone Gudrun in January 2005 and modelling its hydrodynamic consequences in the Estonian coastal waters. Boreal Environ. Res. 11 (2), 143—159. https://www.borenv.net/BER/archive/pdfs/ber11/ber11-143.pdf

Tavakoli, S., Khojasteh, D., Haghani, M., Hirdaris, S., 2023. A review on the progress and research directions of ocean engineering. Ocean Eng. 272, 113617. https://doi.org/10.1016/j.oceaneng.2023.113617

The BACC Author Team, 2008. Assessment of climate change for the Baltic Sea basin. Springer Science & Business Media, Berlin, Heidelberg, 473 pp.

The BACC II Author Team, 2015. Second Assessment of Climate Change for the Baltic Sea Basin. Regional Climate Studies. Springer, Cham, Heidelberg, New York, Dordrecht, London. https://doi.org/10.1007/978-3-319-16006-1

Tuomi, L., Kahma, K.K., Pettersson, H., 2011. Wave hindcast statistics in the seasonally ice-covered Baltic Sea. Boreal Environ. Res. 16 (6), 451—472. http://www.borenv.net/BER/archive/pdfs/ber16/ber16-451.pdf

Tuomi, L., Kanarik, H., Björkqvist, J.V., Marjamaa, R., Vainio, J., Hordoir, R., Höglund, A., Kahma, K.K., 2019. Impact of ice data quality and treatment on wave hindcast statistics in seasonally ice-covered seas. Front. Earth Sci. 7, 166. https://doi.org/10.3389/feart.2019.00166

Tuomi, L., Pettersson, H., Fortelius, C., Tikka, K., Björkqvist, J.-V., Kahma, K.K., 2014. Wave modelling in archipelagos. Coast. Eng. 83, 205—220. https://doi.org/10.1016/j.coastaleng.2013.10.011

Viška, M., Soomere, T., 2013a. Long-term variations of simulated sediment transport along the eastern Baltic Sea coast as a possible indicator of climate change. In: Reckermann, M., Köppen, S. (Eds.), 7th Study Conference on BALTEX, 10—14 June 2013, Borgholm, Island of Öland, Sweden. International BALTEX Secretariat, Publication No. 53, 99—100.

Viška, M., Soomere, T., 2013b. Simulated and observed reversals of wave-driven alongshore sediment transport at the eastern Baltic Sea coast. Baltica 26 (2), 145—156. https://doi.org/10.5200/baltica.2013.26.15

Wu, J., 2012. Wind-stress coefficients over sea surface from breeze to hurricane. J. Geophys. Res.-Oceans 87 (C12), 9704—9706. https://doi.org/10.1029/JC087iC12p09704

Zaitseva-Pärnaste, I., Soomere, T., Tribštok, O., 2011. Spatial variations in the wave climate change in the eastern part of the Baltic Sea. J. Coast. Res. Special Issue 64, 195—199. https://www.jstor.org/stable/26482160

Zaitseva-Pärnaste, I., Suursaar, Ü., Kullas, T., Lapimaa, S., Soomere, T., 2009. Seasonal and long-term variations of wave conditions in the northern Baltic Sea. J. Coast. Res. Special Issue 56, 277—281. https://www.jstor.org/stable/25737581

Zijlema, M., van Vledder, G.P., Holthuijsen, L.H., 2012. Bottom friction and wind drag for wave models. Coast. Eng. 65, 19—26. https://doi.org/10.1016/j.coastaleng.2012.03.002

Oceanologia 66 (2024) 78—90

Available online at www.sciencedirect.com

ScienceDirect

journal homepage: www.journals.elsevier.com/oceanologia

ORIGINAL RESEARCH ARTICLE

Submesoscale processes in the surface layer of the central Baltic Sea: A high-resolution modelling study

Germo Väli[a,*], H.E. Markus Meier[b], Taavi Liblik[a], Hagen Radtke[b], Knut Klingbeil[b], Ulf Gräwe[b], Urmas Lips[a]

[a] *Department of Marine Systems, Tallinn University of Technology, Tallinn, Estonia*
[b] *Leibniz Institute for Baltic Sea Research Warnemünde (IOW), Rostock, Germany*

Received 25 March 2023; accepted 16 November 2023
Available online 30 November 2023

KEYWORDS
Ocean Modelling;
Submesoscale;
Kinetic energy;
Rossby numbers;
GETM;
Baltic Sea

Abstract A high-resolution model with a horizontal resolution of 250 m was used to analyze the surface eddy fields and the distribution of kinetic energy in the Baltic Sea. The results indicate a close relationship between the wind speed and the kinetic energy at the surface and the vertically averaged kinetic energy in the sea, and a lagged correlation between the kinetic energy at the surface and the eddy field. The spatial patterns of kinetic energy indicate more energetic currents in the western and southern parts of the Baltic Sea. The distribution of vorticity is inhomogeneous and differs significantly between sea areas. Submesoscale features are also inhomogeneously distributed and occur more frequently in the Gdańsk Basin, the Gulf of Finland, and the western part of the northern Baltic proper.

1. Introduction

The Baltic Sea, located in Northern Europe, has strong horizontal and vertical gradients, complex circulation and complex transport pathways (e.g., Leppäranta and Myrberg, 2009; Meier and Kauker, 2003). The long-term mean circulation in the sea is cyclonic and characterized by large-scale basin-wide gyres (e.g., Elken and Matthäus, 2008; Meier, 2007). The water exchange regime is governed by the estuarine circulation, which is maintained by the salt-water flux from the North Sea, including the large sporadic inflows, hence called the Major Baltic Inflows (MBIs, e.g., Fischer and Matthäus, 1996; Matthäus and Franck, 1992; Mohrholz et al., 2015), and by the large input of riverine

* Corresponding author at: Department of Marine Systems, Tallinn University of Technology, Tallinn, Estonia.
E-mail address: germo.vali@taltech.ee (G. Väli).
Peer review under the responsibility of the Institute of Oceanology of the Polish Academy of Sciences.

Production and hosting by Elsevier

https://doi.org/10.1016/j.oceano.2023.11.002

waters. The short-term variability of the circulation and current structure is shaped by variable atmospheric forcing, estuarine circulation reversals, various mesoscale processes etc.

Nutrients from rivers are partly trapped in the coastal zone or exchanged with offshore areas through horizontal advection and mixing (e.g., Eilola et al., 2012; Holtermann et al., 2020). Likewise, the strong pycnoclines impede the vertical mixing of nutrients and other substances. The role of mesoscale processes on the horizontal and vertical fluxes has been highlighted in the Baltic (Laanemets et al., 2009; Lass et al., 2010; Lips et al., 2009), but the role of submesoscale features is not clear. Recent studies in other regions have highlighted the importance of submesoscale processes in horizontal and vertical transport (e.g., Ito et al., 2021; Tippenhauer et al., 2021). Thus, the role of fluxes in the submesoscale might be important in the Baltic as well.

Mesoscales characterised by the spatial length scales in the order of 10 km are well known and studied in the Baltic Sea from the 1980s (Aitsam et al., 1984). Most common mesoscale features are in the form of fronts and eddies due to upwellings and downwellings or freshwater spread in the sea (e.g., Laanemets et al., 2005; Lips et al., 2009; Lips et al., 2016c) having a considerable impact to the biological fields in the Baltic Sea (e.g., Kononen et al.,1999; Nausch et al., 2009).

High-resolution remote sensing, observations and model simulations have revealed a considerable amount of variability and motions in the so-called submesoscale range (e.g., Barkan et al., 2019; Brannigan et al., 2017; McWilliams, 2016; Thomas et al., 2008) in the surface layers. These motions are characterised by the Rossby number and bulk Richardson number on the order of one (Thomas et al., 2008) and horizontal length scales on the order of 1 km. Recent high-resolution simulations in the Baltic Sea have shown that the submesoscale features occur as filaments or eddies with high relative vorticity (e.g., Chrysagi et al., 2021; Väli et al., 2017; Zhurbas et al., 2022), while both the observations and simulations suggest that the submesoscale structures in the Baltic Sea are strongly connected to the mesoscale flow field (Lips et al., 2016a; Salm et al., 2023; Väli et al., 2017).

Eddy activity in the Baltic Sea has been studied either by specific observational experiments such as PEX-86 (Elken et al., 1987), remote sensing (Kahru et al., 1990; Karimova et al., 2012) or numerical simulations (e.g., Onken et al., 2019; Vortmeyer-Kley et al., 2019; Zhurbas et al., 2019a,b). The aim of PEX-86 was to observe the large-scale non-uniformity of temperature, salinity and phytoplankton fields and frontal activity in the central Baltic Sea in general (Kahru et al., 1990; Suursaar et al., 2021). The presence of warm and cold eddies in the Baltic Sea was observed from SAR images (Karimova et al., 2012). Vortmeyer-Kley et al. (2019) counted the number of eddy structures and their lifetime in the Baltic Sea using the results of a 600 m resolution model, while Zhurbas et al. (2019a) compared the simulated surface fields with satellite images and Zhurbas et al. (2019b) focused on the different properties of cyclonic and anticyclonic eddies.

The aim of this paper is to analyse the general statistical properties of eddy activity at the sea surface in different areas of the Baltic Sea, focusing on the statistical presence of submesoscale features, i.e., Rossby numbers in the order of 1. The outcome of the present paper will allow to design targeted measurement campaigns and focused numerical simulations in the areas where the activity of submesoscale processes is high. These areas might be important for intensified horizontal mixing and matter fluxes.

The paper is structured as follows: Sections 2 and 3 describe the methods and results, respectively, and Section 4 discusses the main findings of the study. Finally, the conclusions are presented. For an evaluation of the model results, the reader is referred to the supplementary material.

2. Material and methods

2.1. Model setup

2.1.1. General description

In this study, the General Estuarine Transport Model (GETM; Burchard and Bolding, 2002) was used. GETM is a hydrostatic, three-dimensional primitive equation model (Klingbeil et al., 2018) that has embedded adaptive vertical coordinates (Hofmeister et al., 2010; Gräwe et al., 2015), which together with the used Superbee advection scheme reduces numerical mixing in the simulations (Klingbeil et al., 2014).

The vertical mixing in the GETM is calculated with the General Ocean Turbulence Model (GOTM; Burchard and Bolding, 2001), which is based on a two-equation k-ε scheme with an algebraic closure of the second moment (Canuto et al., 2001). The horizontal turbulence (viscosity and diffusion) is calculated using a Smagorinsky-type parameterisation (Smagorinsky, 1963).

2.1.2. Description of the setup

A high-resolution nested model was constructed for the main part of the Baltic Sea comprising the Arkona Basin (AB), the Bornholm Basin (BB), the Gdańsk Basin (GdB), the Eastern Gotland Basin (EGB), the Northern Gotland Basin (NGB), the Western Gotland Basin (WGB), the Gulf of Riga (GoR), and the Gulf of Finland (GoF) (see Figure 1). In the model domain, the horizontal grid spacing is 250 m, which permits submesoscale processes. Sixty vertically adaptive layers were used. The maximum layer thicknesses in the two uppermost layers amounted to 0.5 m.

A 9-year simulation from 2010 to 2018 was carried out. Open boundaries are used in the western and northern parts of the model domain. A one-way nesting approach was used. At the lateral boundaries, results from a 2 km Baltic Sea model with a 1-hourly resolution for sea surface height and 3-hourly resolution for salinity, temperature and current profiles were spatially and temporally interpolated onto the grid of the high-resolution model. The coarse resolution model run started on 01.04.2009 and used the Copernicus Marine Service reanalysis product "BALTICSEA_REANALYSIS_PHYS_003_008" for the initial temperature and salinity conditions. The details of the coarse resolution model can be found in Radtke et al. (2020).

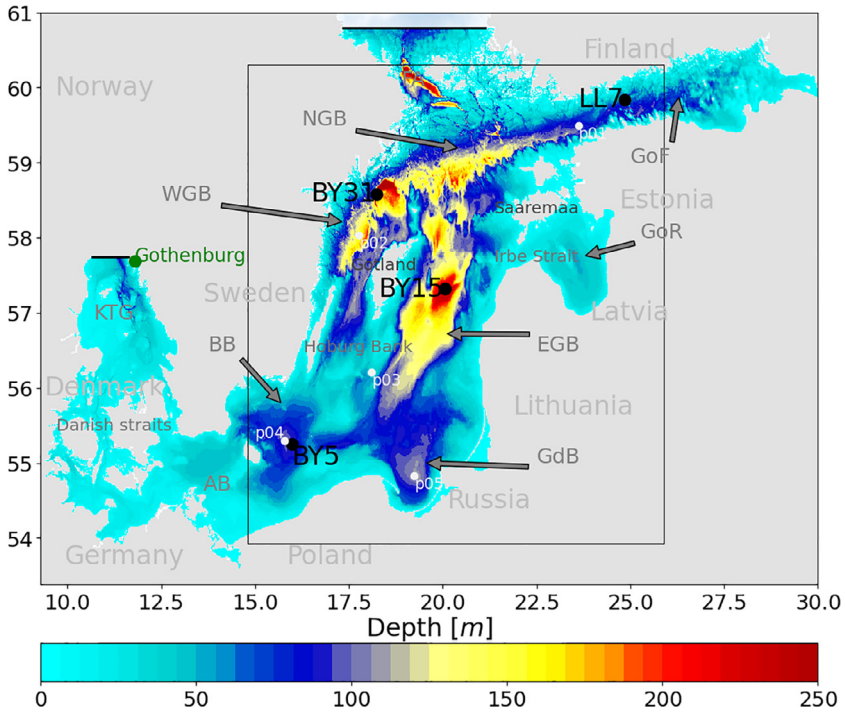

Figure 1 The nested model domain in the simulations. The location of the open boundaries (thick black lines), offshore monitoring stations BY5, BY15, BY31 and LL7 (large black dots), virtual time-series locations (small white dots) and abbreviations for different basins (AB = Arkona Basin, BB = Bornholm Basin, GdB = Gdańsk Basin, EGB = Eastern Gotland Basin, NGB = Northern Gotland Basin, WGB = Western Gotland Basin, GoR = Gulf of Riga, GoF = Gulf of Finland, KTG = Kattegat) are shown. The area used for the spatial averaging in the study is indicated by the black box.

The momentum and heat fluxes were calculated from the output of the regional reanalysis data set UERRA-HARMONIE with a spatial resolution of 11 km and a temporal resolution of 1 hour. The long-term, high-quality and high-resolution dataset was originally produced within the FP7 project UERRA (Uncertainties in Ensembles of Regional Re-Analyses, http://www.uerra.eu/) and is part of the Copernicus Climate Change Service (C3S, https://climate.copernicus.eu/copernicus-regional-reanalysis-europe) (Gröger et al., 2022).

The freshwater input to the Baltic Sea was produced for the Baltic Model Intercomparison Project (BMIP; Gröger et al., 2022) based on the E-HYPE (Lindström et al., 2010) hindcast and forecast products (Väli et al., 2019). The Baltic Sea dataset includes 91 rivers, while 56 were used for the high-resolution model runs. The freshwater input is treated in the model as a change in the sea surface height due to the discharged water volume at every model time step. The river water salinity is fixed at 0.05 g/kg, but the river water temperature is assumed to be the same as the ambient temperature in the corresponding grid cell. To avoid numerical instabilities in the model, we used three grid cells for every river around the river mouth location and eight cells for the largest river (Neva).

The high-resolution run started with the initial condition at rest where the sea surface height was set to zero. The initial temperature and salinity fields were taken at a vertical resolution of 10 m from the coarse-resolution model results for 30.12.2009 and interpolated to the high-resolution model grid. Adjustment of wind-driven currents is expected within 10 days (Krauss and Brügge, 1991; Lips et al., 2016b), but geostrophic adjustment may take several years (Meier, 2007).

Temperature and salinity observations from selected long-term monitoring stations and sea surface height measurements from coastal tide gauges were used to evaluate the model results. The simulation shows a positive bias in surface layer salinities, while bottom salinities are simulated more accurately. Overall, salinity is simulated satisfactorily. Sea surface elevations in the main sub-basins are well captured, while near the open boundary, the bias and phase lag are relatively high, and the observed variability is underestimated. Details on model evaluation can be found in the supplementary material.

2.2. Statistical methods

The parameters used in this study are the total kinetic energy calculated from the zonal and meridional flow components u and v as $(u^2+v^2)/2$ in the surface layer (SKE) and the water column (VKE; vertically averaged value). The maximum thickness of the first layer was limited to 0.5 m, so the values varied from 1/15 m at the coast to about 0.5 m in the open sea. The Rossby number, i.e., the vertical component of the relative vorticity divided by the Coriolis parameter f ($Ro = (\partial v/\partial x - \partial u/\partial y)/f$), is used to characterise the eddy activity. The changes in stratification are shown by the potential energy anomaly (PEA; Simpson and Bowers, 1981 and

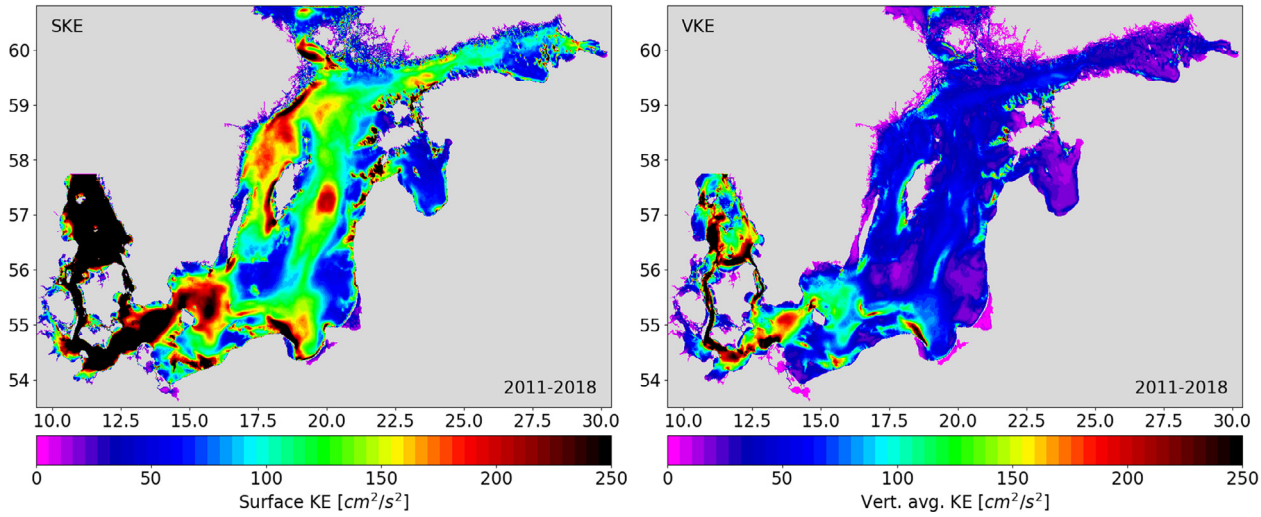

Figure 2 Mean surface (left) and vertically averaged (right) kinetic energy during 2011–2018.

Simpson et al., 1990):

$$PEA = \frac{1}{h}\int_{-h}^{0}(\rho_A - \rho)\,gzdz,\ \rho_A\frac{1}{h}\int_{-h}^{0}\rho zh \tag{1}$$

where h is the depth of the water column, ρ is the density at depth z, ρ_A is the average density in the water column, and g is the gravitational acceleration.

We will present spatial distributions of the average and the 1st, 10th, 50th, 90th and 99th percentiles of the studied parameters, SKE and Ro. Simulated parameters were available with the following temporal resolution:

- surface current components as snapshot values every 7.2 hours;
- 3D density and current field as daily means;
- wind field with a 1-hour resolution (forcing dataset).

To account for the effects of both anticyclonic and cyclonic eddies, the squared Rossby number Ro^2 was used instead of Ro in the averaging.

For the evaluation of the model, the following statistical parameters were calculated:

(1) The relative error of the standard deviation $RE = (\sigma_{obs}\text{-}\sigma_{mod})/\sigma_{obs}\ ^*100$, where σ_{obs} is the standard deviation of observations and σ_{mod} is the standard deviation of simulations.
(2) The Pearson correlation coefficient r.
(3) The mean absolute bias $MAB = \frac{1}{N}\sum_{i=1}^{N}|o_i - m_i|$, where o_i and m_i are the observed and modelled values at i^{th} time-moment, N the number of measurements.
(4) The root mean square deviation $RMSD = \sqrt{\frac{1}{N}\sum_{i=1}^{N}(o_i - m_i)^2}$.

3. Results

3.1. Eddy activity in the surface layer

3.1.1. General spatial variability

The long-term mean distributions of SKE and VKE show a large spatial variability in the Baltic proper (Figure 2). The highest values for SKE and VKE are found in the southern (AB and BB) and western (KTG) parts of the Baltic Sea, but remarkably high values are also calculated in the northwestern Baltic Sea near the Swedish coast. Some high-energy sites are also found near the east coast of the Baltic proper, but, in general, kinetic energies tend to be higher in deeper areas. As the GoR is relatively enclosed compared to other sea regions, we found much lower values for both SKE and VKE in this basin.

The long-term mean values of the PEA and the squared Rossby number are shown in Figure 3. Similar to the kinetic energies, the stratification strength is large in deep regions. The eddy activity, characterised by the root mean square of the Rossby number, is greatest in the western Baltic Sea, but high values are also found in the GoF, BB, NGB and WGB in areas with high kinetic energy.

3.1.2. Temporal variability

Here, we present the time series for quantities obtained from spatial averaging over the central Baltic Sea (black box in Figure 1).

The spatially averaged time series of total kinetic energy and Rossby number squared show some interannual variability and no trend. The time series of SKE and Ro are weakly correlated in summer (r=0.374; see Supplementary Material for details) but strongly correlated in winter (r=0.749). The overall correlation is moderate (r=0.525).

The seasonal variability of kinetic energy in the Baltic Sea is large (Figure 4). The maxima of SKE and VKE occur in winter, while the minima are in late spring. VKE tends to be low throughout the summer, while SKE is relatively high during the summer season compared to the spring minimum. The squared wind speed, characterizing the work done on the sea surface, qualitatively shows the same seasonal pattern as VKE – smallest values in summer, largest in late autumn and winter. The different behaviour of SKE and VKE can be explained by the seasonal changes in stratification. This is because the PEA is lowest in winter and highest in summer, mostly due to the development of the seasonal thermocline. The seasonal variability of the Rossby number

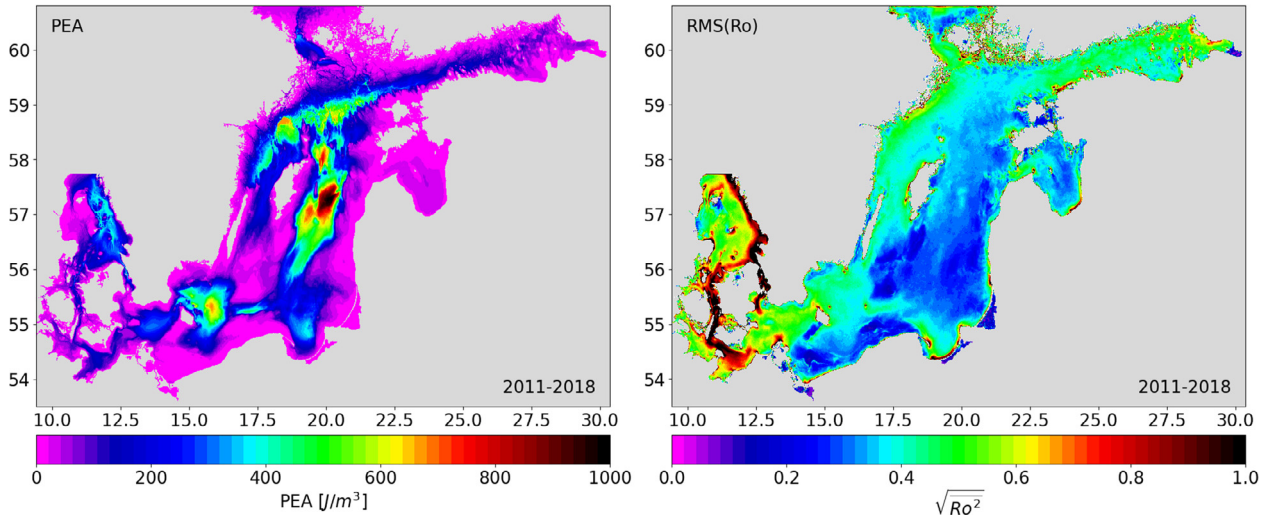

Figure 3 Mean potential energy anomaly (PEA) and root mean square Rossby number during 2011—2018.

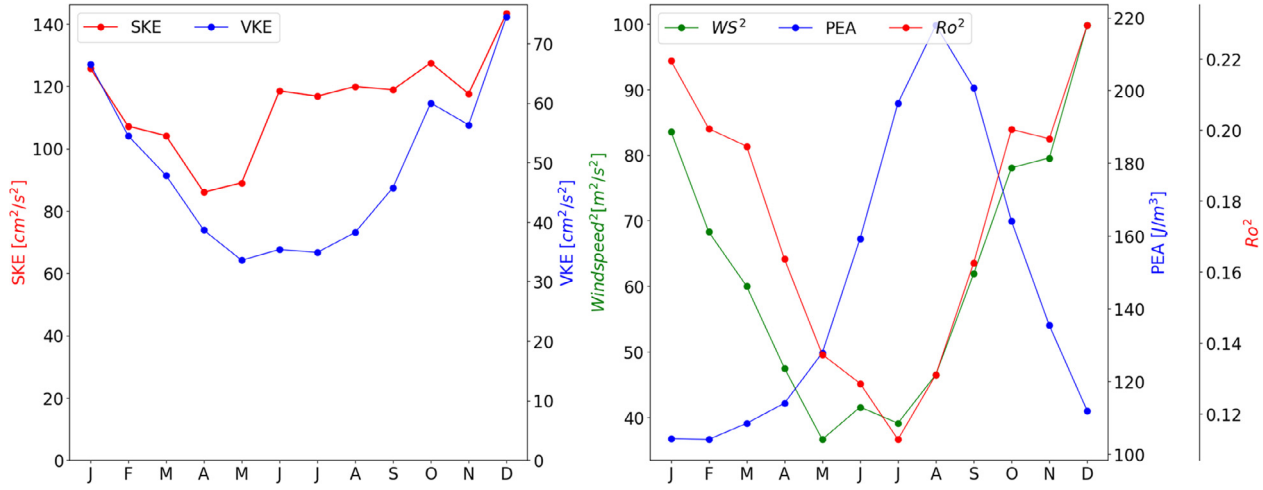

Figure 4 The annual cycle of the spatially averaged surface kinetic energy (SKE), potential energy anomaly (PEA), squared wind speed (WS^2) and squared Rossby number values (Ro^2) as well as the vertically averaged kinetic energy (VKE) in the region 14.7—25.9°E and 54.1—60.3°N.

is also high — the eddy activity reaches minimum values in July and the annual maximum in December. However, the annual cycles of kinetic energies and Rossby number are shifted in the Baltic proper (Figure 4). Both SKE/VKE and Rossby number squared are highest from October to February, while the minima for SKE and VKE occur in late spring, i.e., April—May, and for the Rossby number throughout the summer from June to August. The correspondence between the VKE and wind work is high.

3.1.3. Spatial patterns of seasonality

Figure 5 summarises the seasonality in the spatial distribution of kinetic energy. VKE is much larger in winter in all regions. The same applies to SKE, even if the relative change is much smaller, and the difference between the high-energy areas (along the southern coast and some other places) and the low-energy areas is more pronounced in winter than in summer. The high-energy hotspots include, for example, the Swedish coast in NGB, WGB, and BB (see Figure 1 for the location of the basins), the entrance to the GoR, etc. Interestingly, the SKE is reduced in winter compared to summer in some regions, such as the south-eastern part of the Baltic proper and the coastal areas in the southern part of the GoF.

Figure 6 shows the seasonal changes in stratification and eddy activity. As expected, the PEA is lower in the Baltic Sea areas with depths shallower than the permanent halocline depth (50—70 m) throughout the year. This contrast is especially prominent in winter since the water column in shallow areas is convectively mixed down to the seabed due to the large-scale cooling of the sea.

The vorticity is significantly greater in winter than in summer in all areas of the Baltic Sea. The seasonal signal is smaller along the southern coast of the Bornholm Basin and the Gdańsk Basin, in the eastern Baltic proper, and in the area south of Gotland, where root mean square values of the Rossby number remain below 0.3 even in winter. The increase of Ro by more than 0.2 from summer to winter up to values larger than 0.5 is revealed in other regions (e.g., NGB).

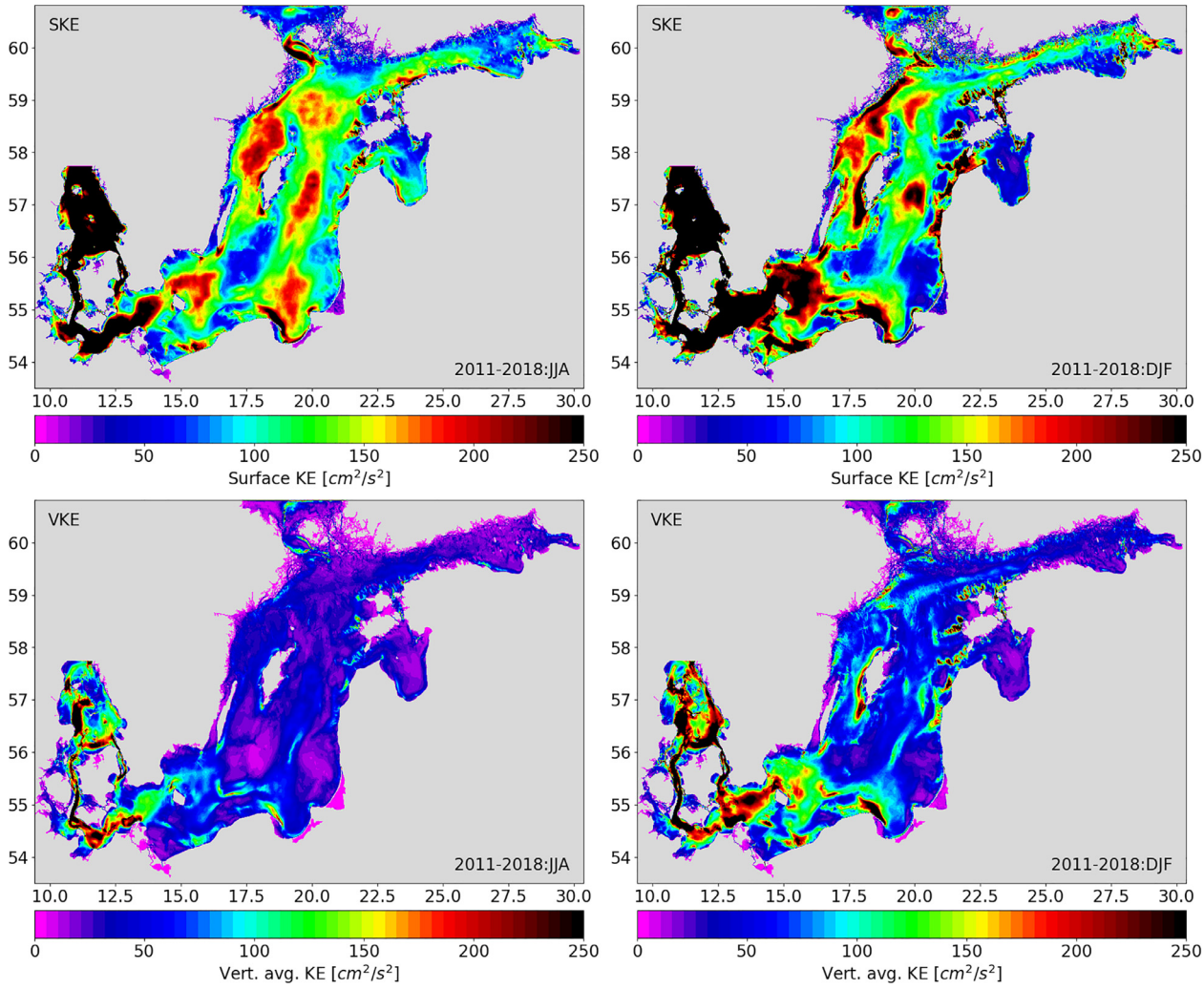

Figure 5 Mean surface (top) and vertically averaged (bottom) kinetic energy during summer (left) and winter (right).

3.2. Probability distribution patterns

The probability density functions (pdfs) of SKE and the Rossby number in five analysed basins during 2010—2018 show large differences between the basins (Figure 7). SKE appears to have the largest values in the NGB and BB, and the smallest values above the Hoburg Bank, located south of Gotland Island (PO3; see Figure 1). Similarly, the distribution of the Rossby number is much broader in the NGB and GoF, while the pdf is sharpest above the Hoburg Bank, where absolute values rarely exceed 1.

The spatial distributions of the SKE percentiles for winter and summer and the whole year are shown in Figure 8. The SKE tends to be the largest in the Kattegat, but significant differences are also seen in other sea areas. For example, larger SKE values for all presented percentiles are found in the NGB, GoF, BB and AB than in other parts of the model area.

The highest SKE values for the 10th percentile are found in the Kattegat, while the corresponding values in the Baltic proper do not exceed 25 cm^2 s^{-2}. Interestingly, the 10th percentile values are also large in the BB and NGB, while the values in the GoR are much smaller. Similar spatial patterns are also found for the median (50th percentile), 90th and 99th percentiles. In addition to the large-scale patterns of the SKE, the 99th percentiles tend to be larger along the Baltic Sea coasts, e.g., near the eastern coasts of the EGB, eastern and south-western coasts of the GoR, and the coasts of the western and central GoF.

The winter and summer values of SKE are in the same order of magnitude, although there are exceptions. For example, 10th percentiles in the GoR are close to zero in winter, while values in summer are around 10 cm^2 s^{-2}. The differences between summer and winter SKEs are most pronounced in the 99th percentiles, which tend to be larger in winter over much of the southern Baltic Sea, the NGB and the WGB. Furthermore, in the GoF, the 99th percentiles are larger along the northern than the southern coast in winter, while larger along the southern than the northern coast in summer.

The eddy activity in the Baltic Sea, measured by the Rossby number, is spatially variable (Figure 9). The 10th percentiles are negative in the northern part of the Baltic proper and the Kattegat, while the values tend towards zero in the central Baltic Sea. The 90th and 99th percentiles also have larger positive values in the northern part of the Baltic

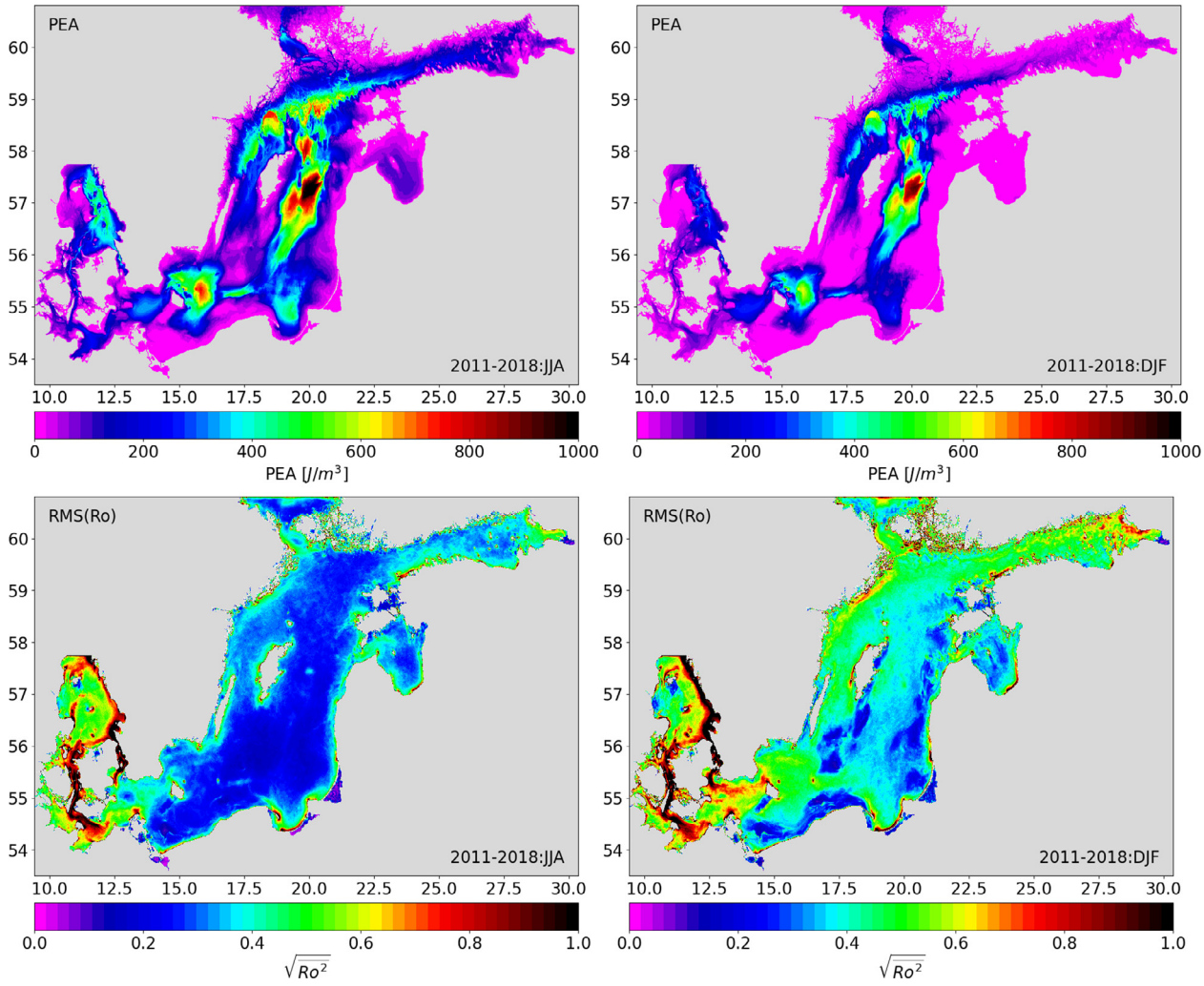

Figure 6 Mean stratification strength or Potential Energy Anomaly (PEA) (top) and root mean square Rossby number (bottom) in summer (left) and winter (right).

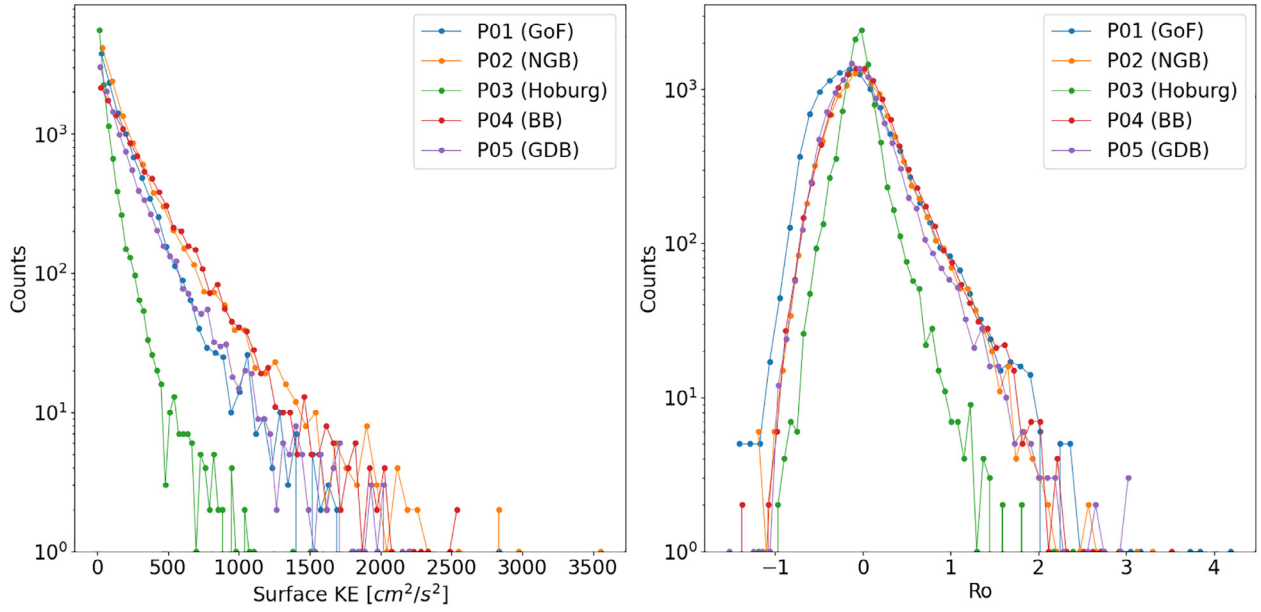

Figure 7 Histograms of surface kinetic energy (SKE) (left) and Rossby number (Ro) (right) in different regions of the Baltic Sea. Selected locations are shown in Figure 1.

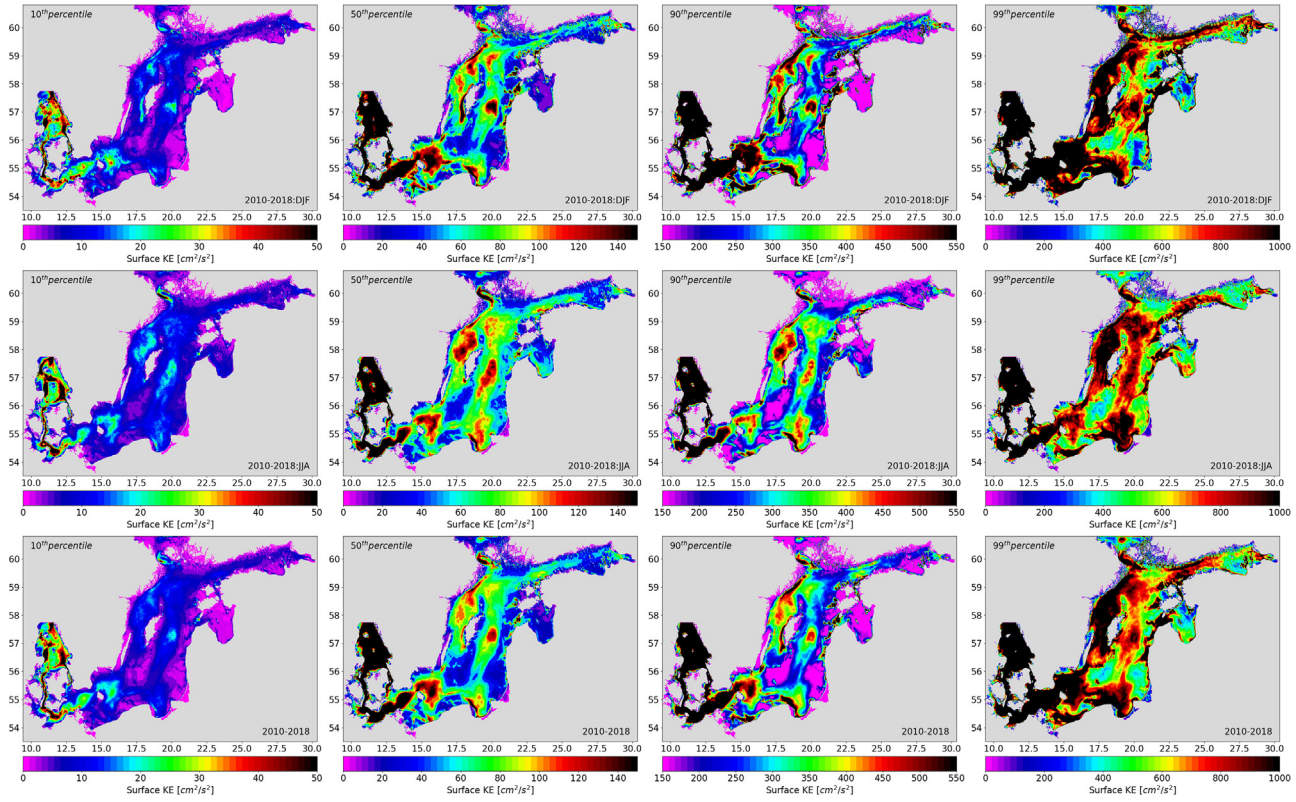

Figure 8 Kinetic energy distribution in the surface layer for winter (DJF), summer (JJA) and the whole year in 2010—2018, corresponding to 10th, 50th, 90th and 99th percentiles in the SKE probability density function.

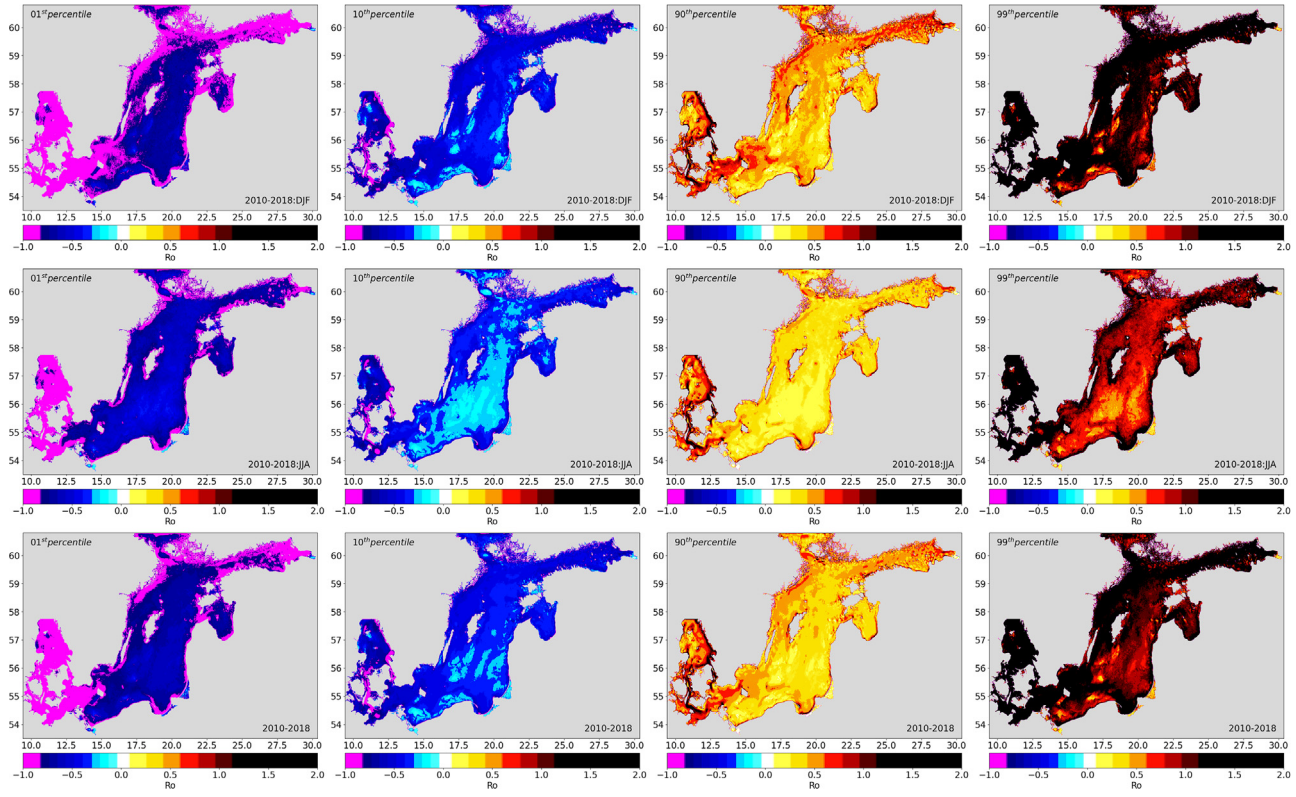

Figure 9 Rossby number distribution in the surface layer for winter (DJF), summer (JJA) and the whole year in 2010—2018, corresponding to 1st, 10th, 90th and 99th percentiles in the Ro probability density function.

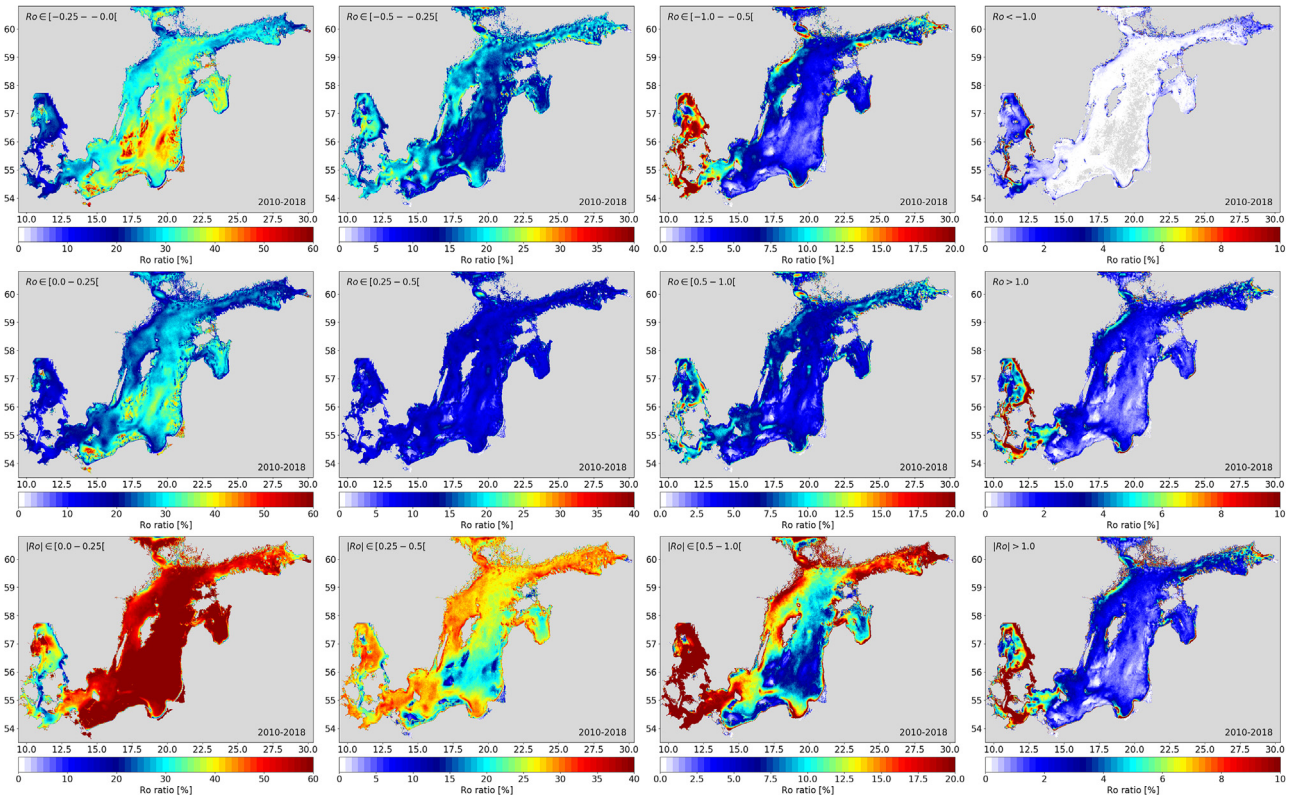

Figure 10 Spatial distributions of the occurrence of different ranges in Rossby number and its absolute value in the surface layer for the annual mean in 2010—2018.

proper and smaller positive values in the central part of the sea. For all percentiles, the absolute values of the Rossby number are smaller in summer than in winter. Similarly to the SKE, the absolute Rossby number maxima have locally larger values along the coasts. Also, larger SKE values are revealed in the western, relatively deep and narrow part of the GoF, while they are much smaller in the deep areas of the EGB.

Figure 10 shows the relative coverage of the sea surface with eddies with different Rossby numbers. Selected ranges with absolute values in [0, 0.25], [0.25, 0.5], [0.5, 1.0] and [1.0, …] indicate no eddy activity, weak eddy activity, moderate eddy activity and strong (submesoscale/ageostrophic) eddy activity, respectively. The southern Baltic Sea, i.e., the area between Gotland Deep and GdB, generally shows less eddy activity than the other regions. On the other hand, relatively large eddy activity is observed in the northern parts of the Baltic proper, i.e., the GoF and along the Swedish coast in the NGB. Somewhat greater activity is also found in the BB and GdB. It is noteworthy that the occurrence of strong anticyclonic or cyclonic (submesoscale or ageostrophic) eddies characterised by $|Ro| > 1$ is relatively low in the Baltic Sea, as the frequency of values above 1 is less than 4% in most of the sea area.

3.3. Seasonal variability of submesoscale activity in the surface layer

The occurrence of Rossby numbers in different areas during summer and winter is shown in Supplementary Material (Figures S08 and S09). In summer, the sea surface is mostly covered by weak eddies with absolute values of Ro smaller than 0.25. In the NGB, the proportion of eddies with Ro greater than 0.25 and less than 0.5 is at least 20%, reaching more than 35% in the GoF and along the Swedish coast. Strong eddies with absolute values of Ro greater than 0.5 are more common in GdB, GoF, parts of GoR and NGB along the Swedish coast. In other regions, the temporal share of strong eddies ($|Ro| > 0.5$) is less than 7%.

In winter, eddies tend to be stronger. The proportion of moderate eddies increases in all areas, and the tendency towards mesoscale and submesoscale eddies ($|Ro| > 0.5$) also increases. In the GoF, their occurrence increases to 5% compared to 3% in summer.

4. Discussion

The spatial patterns of kinetic energy indicate much stronger currents in the southern and western parts of the Baltic proper, both at the surface and throughout the water column. Nevertheless, relatively high values are also found in the western part of the NGB, mainly along the coasts, which can be explained by energetic boundary currents (e.g., Jędrasik and Kowalewski, 2019; Liblik et al., 2022).

The seasonality of the kinetic energy is closely related to the annual cycle of the wind (e.g., Lizuma et al., 2013) in the region, as also found earlier, indicating that mainly wind-driven currents are prevailing (Krauss and

Brügge, 1991). Stratification has a decisive influence on the vertical distribution of the currents. Relatively high SKE values are characteristic in the months with a seasonal thermocline, although the wind speeds are relatively low. Observations from the GoF (Suhhova et al., 2018) and also from other regions (Lilover et al., 1998; Lass et al., 2003) support this finding about the layered flow systems.

The spatial distribution of the root mean squared Rossby number indicates higher vorticity in the western Baltic Sea (KTG, AB, northern part of BB) but also in the western part of NGB, WGB and overall in GoF and GdB. In the entrance area (western Baltic proper), eddy activity is most likely caused by strong jet-like currents in the narrow Danish straits, which eventually produce baroclinic instabilities and high Rossby numbers in the AB. The occurrence of moderate eddies reduces significantly in the BB due to dilution and intensive mixing of inflowing saltier water with ambient water in BB. In addition, as observed, the small and moderate inflows from the North Sea are only able to ventilate the halocline of BB and do not reach other basins of the Baltic Sea (e.g., Meier et al., 2006). On the other hand, we detected some increase in the eddy activity of the surface layers in the Stolpe Channel (channel from BB towards EGB), where observations and model simulations have indicated strong sub-surface eddy activity (e.g., Zhurbas et al., 2004; Zhurbas et al., 2012). The surface eddies in the Stolpe Channel could be formed due to instabilities in the dense gravitational flow similar to the Irbe Strait, where Lips et al. (2016c) have noticed propagation and bifurcation of mesoscale eddies entering the GoR.

Eddy activity in the GoF, GdB and the western part of the NGB can be explained by wind-induced upwelling events that generate coastal jets during their active phase (e.g., Laanemets et al., 2011; Väli et al., 2017, 2018) and eventually form eddies due to baroclinic instabilities in the fronts and filaments. The above-mentioned locations are known for intensive upwelling (e.g., Kowalewski and Ostrowski, 2005; Lehmann et al., 2012; Väli et al., 2011). Another interesting site for increased eddy activity is the Irbe Strait, known as the semi-permanent front between the GoR and the central Baltic Sea (Lips et al., 1995). Lilover et al. (1998) and Otsmann et al. (2001) demonstrated the pulsating nature of the flow regime in the Irbe Strait with ADCP measurements. More recently, Liblik et al. (2022) have shown the quasi-permanent flow regime characterised by very persistent and high current velocities along the island of Saaremaa, which may explain higher vorticity values along the western Saaremaa coast.

On the seasonal scale, a time lag is found between the Rossby number, kinetic energy, and wind field during the decay period in spring and no delay during the increase period in autumn. The time lag is about two months, as the minimum of the mean squared Rossby number occurs in June, but SKE and wind speed squared minima are found in April and May. Since the lifetime of eddies can be several weeks (e.g., Väli et al., 2017; Vortmeyer-Kley et al., 2019), such a long delay between the active forcing and eddy field can only be explained by the prolongation of the eddy field by the merging of individual eddies (e.g., Cui et al., 2019; Morvan et al., 2019; Väli and Zhurbas, 2021) or decomposing of larger and stronger eddies into smaller and weaker eddies which take longer than the lifetime of individual eddies.

The aim of this study was to analyze the spatio-temporal statistics of eddies on the seasonal time scale, while other studies focus more on individual eddies in the central Baltic Sea using high-resolution modelling (e.g., Onken et al., 2019; Vortmeyer-Kley et al., 2019; Zhurbas et al., 2019a,b) or are based on remote sensing data (e.g., Karimova et al., 2012). We have identified the hotspots of relative vorticity, indicating the locations where the meso- and submesoscale eddies and structures are more frequent in the central Baltic Sea during different seasons. Furthermore, the distribution of Ro is right-skewed, indicating that more cyclonic than anticyclonic strong eddies ($|Ro|>1$) exist. Similar findings have also been reported in other studies (e.g., Thomas et al., 2008; Shcherbina et al., 2013; Zhurbas et al., 2019a,b). Väli et al. (2017) explained the positive skewness with the conversion of potential vorticity. It is possible to pull the isopycnals infinitely far apart (the only limit is the sea depth) and, thus, not limit the vorticity. At the same time, it is not possible to compress them infinitely (relative vorticity is limited to $-f$). Another explanation for the dominance of the cyclonic eddies is the unstable nature of anticyclonic and stable nature of cyclonic flows (Hoskins and Bretherton, 1972; Shcherbina et al., 2013).

The overall proportion of weak vorticity ($|Ro| < 0.25$) is relatively large in most areas of the central Baltic Sea. An exception is the Kattegat, where strong baroclinic currents probably have large horizontal gradients and vorticity. In areas with a high occurrence of very weak or no eddies, the share of medium and large vorticity values is much lower. For example, the proportion of $|Ro|$ in the range [0.25, 1.0) in the southern EGB is less than 30%. Structures with high vorticity ($|Ro|>1$) are more common along coastlines or in the GoF and the western part of the NGB in summer, characterized by higher kinetic energy and in the GdB.

Earlier studies have shown that the presence of mesoscale features is necessary to produce submesoscale structures. This has already been shown in Väli et al. (2017), where the submesoscale structures were created during the relaxation of the upwelling in the GoF. Lips et al. (2016a) also demonstrated the presence of submesoscale structures using high-resolution ferrybox observations following upwelling events that produce high variations in temperature and salinity along the transect. Recently, Salm et al. (2023) found the presence of submesoscale structures in high-resolution glider observations generated at the mesoscale front in the GoF. Our results suggest that submesoscale structures are not expected to have the same probability everywhere in the Baltic Sea and are rare, for example, in the offshore areas of the EGB. The lifetime of submesoscale structures under real conditions will be investigated in future studies. Our findings will help to design targeted in-situ observational and numerical experiments in specific regions, where the occurrence of the submesoscale processes is higher than the average.

5. Conclusions

The spatiotemporal distributions of kinetic energy and Rossby number are highly inhomogeneous for different parts of the Baltic Sea, and both fields have large seasonal

variability. The highest values for SKE are in the southern- and westernmost parts of the Baltic proper, but relatively high values are also in the NGB and GoF.

Seasonally averaged Rossby numbers indicate stronger eddies (increased eddy activity) during winter and weaker (reduced eddy activity) during summer everywhere in the Baltic Sea. The eddy activity is the largest in areas with high SKE.

The seasonal cycles of the averaged Rossby number, on the one hand, and SKE, VKE and WS^2, on the other hand, show a time lag of about two months during the decay period (spring) and no delay during the increase period (summer). The latter does not apply to SKE. The lime lag (2 months) is longer than the ordinary lifetime of eddies (in the order of days in the Baltic Sea), suggesting the generation of new, smaller and weaker eddies during the decay of large eddies.

The submesoscale features spatially differ. Some regions have |Ro| larger than one more often than others. The asymmetric distribution of strong submesoscale eddies with more cyclonic and less anticyclonic eddies, as also shown earlier, is confirmed. The largest occurrence of mainly cyclonic submesoscale structures is found in the Kattegat and the Danish Straits, as well as the AB and along the coasts (most pronounced in the NGB and GdB). In these areas, the most mesoscale activity has also been found. However, anticyclonic eddies dominate here. Targeted future investigations in specific hot-spot areas of submesoscale processes will be designed based on the presented findings.

Declaration of competing interest

The authors declare that they have no known competing financial interests or personal relationships that could have appeared to influence the work reported in this paper.

Acknowledgements

The presented research is part of the Baltic Earth programme (Earth System Science for the Baltic Sea region, see http://baltic.earth, last access: 2 February 2023) and the new focus programme on “Shallow Water Processes and Transitions to the Baltic Scale” at the Leibniz Institute of Baltic Sea Research Warnemünde (https://www.io-warnemuende.de/stb-shallow-water-processes.html, last access: 11 February 2023). Furthermore, the study is a contribution to the BMBF-funded project CoastalFutures (03F0911E). The HLRN supercomputer centre in Göttingen is gratefully acknowledged for the computational and storage resources (project mvk00075). G.V., T.L., and U.L. were supported by the Estonian Research Council (project PRG602) and G.V. with several scholarships from the Leibniz Institute of Baltic Sea Research Warnemünde. K.K. gratefully acknowledges the financial support from the Collaborative Research Centre TRR 181 “Energy Transfers in Atmosphere and Ocean” (project 274762653), funded by the German Research Foundation (DFG).

Supplementary materials

Supplementary material associated with this article can be found, in the online version, at https://doi.org/10.1016/j.oceano.2023.11.002.

References

Aitsam, A., Hansen, H.-P., Elken, J., Kahru, M., Laanemets, J., Pajuste, M., Pavelson, J., Talpsepp, L., 1984. Physical and chemical variability of the Baltic Sea: a joint experiment in the Gotland basin. Cont. Shelf Res. 3, 291—310.

Barkan, R., Molemaker, M.J., Srinivasan, K., McWilliams, J.C., D’Asaro, E.A., 2019. The Role of Horizontal Divergence in Submesoscale Frontogenesis. J. Phys. Oceanogr. 49, 1593—1618. https://doi.org/10.1175/JPO-D-18-0162.1

Brannigan, L., Marshall, D.P., Naveira Garabato, A.C., Nurser, A.J.G., Kaiser, J., 2017. Submesoscale Instabilities in Mesoscale Eddies. J. Phys. Oceanogr. 47, 3061—3085. https://doi.org/10.1175/JPO-D-16-0178.1

Burchard, H., Bolding, K., 2001. Comparative Analysis of Four Second-Moment Turbulence Closure Models for the Oceanic Mixed Layer. J. Phys. Oceanogr. 31, 1943—1968. https://doi.org/10.1175/1520-0485(2001)031⟨1943:CAOFSM⟩2.0.CO;2

Burchard, H., Bolding, K., 2002. GETM — a general estuarine transport model. Scientific Documentation, Technical report EUR 20253 en., Tech. Rep. European Commission, Ispra, Italy, https://op.europa.eu/en/publication-detail/-/publication/5506bf19-e076-4d4b-8648-dedd06efbb38/language-en/format-PDF/source-281672731 (last access: 3 March 2023).

Canuto, V.M., Howard, A., Cheng, Y., Dubovikov, M.S., 2001. Ocean turbulence, Part I: One-point closure model-momentum and heat vertical diffusivities. J. Phys. Oceanogr. 31, 1413—1426. https://doi.org/10.1175/1520-0485(2001)031⟨1413:OTPIOP⟩2.0.CO;2

Chrysagi, E., Umlauf, L., Holtermann, P., Klingbeil, K., Burchard, H., 2021. High-resolution simulations of submesoscale processes in the Baltic Sea: The role of storm events. J. Geophys. Res.-Oceans 126 (3), e2020JC016411.

Cui, W., Wang, W., Zhang, J., Yang, J., 2019. Multicore structures and the splitting and merging of eddies in global oceans from satellite altimeter data. Ocean Sci. 15, 413—430. https://doi.org/10.5194/os-15-413-2019

Eilola, K., Rosell, E.A., Dieterich, C., Fransner, F., Höglund, A., Meier, H.E.M., 2012. Modeling Nutrient Transports and Exchanges of Nutrients Between Shallow Regions and the Open Baltic Sea in Present and Future Climate. AMBIO 41, 586—599. https://doi.org/10.1007/s13280-012-0322-1

Elken, J., Matthäus, W., 2008. Baltic Sea oceanography. In: Regional Climate Studies, Assessment of climate change for the Baltic Sea Basin. Annex A 1, 379—385.

Elken, J., Pavelson, J., Talpsepp, L., 1987. Dynamics and water mass distribution at the southern Gotland Basin (polygon studies). In: Proc. 15th CBO, Copenhagen, 136—144.

Fischer, H., Matthäus, W., 1996. The importance of the Drogden Sill in the Sound for major Baltic inflows. J. Marine Syst. 9 (3—4), 137—157.

Gräwe, U., Holtermann, P., Klingbeil, K., Burchard, H., 2015. Advantages of vertically adaptive coordinates in numerical models of stratified shelf seas. Ocean Model. 92, 56—68. https://doi.org/10.1016/j.ocemod.2015.05.008

Gröger, M., Placke, M., Meier, H.E.M., Börgel, F., Brunnabend, S.-E., Dutheil, C., Gräwe, U., Hieronymus, M., Neumann, T., Radtke, H., Schimanke, S., Su, J., Väli, G., 2022. The Baltic Sea Model Intercomparison Project (BMIP) — a platform for model development, evaluation, and uncertainty assessment.

Geosci. Model Dev. 15, 8613—8638. https://doi.org/10.5194/gmd-15-8613-2022

Hofmeister, R., Burchard, H., Beckers, J.-M., 2010. Non-uniform adaptive vertical grids for 3D numerical ocean models. Ocean Model. 33, 70—86. https://doi.org/10.1016/j.ocemod.2009.12.003

Holtermann, P., Prien, R., Naumann, M., Umlauf, L., 2020. Interleaving of oxygenized intrusions into the Baltic Sea redoxcline. Limnol. Oceanogr. 65, 482—503.

Hoskins, B.J., Bretherton, F.P., 1972. Atmospheric frontogenesis models: Mathematical formulation and solution. J. Atmos. Sci. 29 (1), 11—37.

Ito, D., Suga, T., Kouketsu, S., Oka, E., Kawai, Y., 2021. Spatiotemporal evolution of submesoscale filaments at the periphery of an anticyclonic mesoscale eddy north of the Kuroshio Extension. J. Oceanogr. 77, 763—780. https://doi.org/10.1007/S10872-021-00607-4/FIGURES/14

Jędrasik, J., Kowalewski, M., 2019. Mean annual and seasonal circulation patterns and long-term variability of currents in the Baltic Sea. J. Marine Syst. 193, 1—26.

Kahru, M., Leppänen, J.-M., Nõmmann, S., Passow, U., Postel, L., Schulz, S., 1990. Spatio-temporal mosaic of the phytoplankton spring bloom in the open Baltic Sea in 1986. Mar. Ecol. Prog. Ser. 66, 301—309.

Karimova, S.S., Lavrova, O.Y., Solov'ev, D.M., 2012. Observation of Eddy Structures in the Baltic Sea with the Use of Radiolocation and Radiometric Satellite Data. Izv. Atmos. Ocean. Phy. 48, 1006—1013. https://doi.org/10.1134/S0001433812090071

Klingbeil, K., Lemarié, F., Debreu, L., Burchard, H., 2018. The numerics of hydrostatic structured-grid coastal ocean models: State of the art and future perspectives. Ocean Model. 125, 80—105 .

Klingbeil, K., Mohammadi-Aragh, M., Gräwe, U., Burchard, H., 2014. Quantification of spurious dissipation and mixing — Discrete Variance Decay in a Finite-Volume framework. Ocean Model. 81, 49—64. https://doi.org/10.1016/j.ocemod.2014.06.001

Kononen, K., Huttunen, M., Kanoshina, I., Laanemets, J., Moisander, P., Pavelson, J., 1999. Spatial and temporal variability of a dinoflagellate-cyanobacterium community under a complex hydrodynamical influence: a case study at the entrance to the Gulf of Finland. Mar. Ecol. Prog. Ser. 186, 43—57.

Kowalewski, M., Ostrowski, M., 2005. Coastal up-and downwelling in the southern Baltic. Oceanologia 47 (4), 453—475.

Krauss, W., Brügge, B., 1991. Wind-produced water exchange between the deep basins of the Baltic Sea. J. Phys. Oceanogr. 21, 373—384. https://doi.org/10.1175/1520-0485(1991)021⟨0373:WPWEBT⟩2.0.CO;2

Laanemets, J., Pavelson, J., Lips, U., Kononen, K., 2005. Downwelling-related mesoscale motions at the entrance to the Gulf of Finland: observations and diagnosis. Oceanol. Hydrobiol. Stud. 34 (2), 15—36.

Laanemets, J., Väli, G., Zhurbas, V., Elken, J., Lips, I., Lips, U., 2011. Simulation of mesoscale structures and nutrient transport during summer upwelling events in the Gulf of Finland in 2006. Boreal Environ. Res. 16, 15—26.

Laanemets, J., Zhurbas, V., Elken, J., Vahtera, E., 2009. Dependence of upwelling-mediated nutrient transport on wind forcing, bottom topography and stratification in the Gulf of Finland: Model experiments. Boreal Environ. Res. 14 (1), 213—225.

Lass, H.U., Mohrholz, V., Nausch, G., Siegel, H., 2010. On phosphate pumping into the surface layer of the eastern Gotland Basin by upwelling. J. Marine Syst. 80 (1—2), 71—89.

Lass, H.U., Prandke, H., Liljebladh, B., 2003. Dissipation in the Baltic proper during winter stratification. J. Geophys. Res. 108, 3187. https://doi.org/10.1029/2002JC001401

Lehmann, A., Myrberg, K., Höflich, K., 2012. A statistical approach to coastal upwelling in the Baltic Sea based on the analysis of satellite data for 1990—2009. Oceanologia 54 (3), 369—393. https://doi.org/10.5697/OC.54-3.369

Leppäranta, M., Myrberg, K., 2009. Circulation. In: Physical Oceanography of the Baltic Sea. Springer, Berlin, Heidelberg, 131—187.

Liblik, T., Väli, G., Salm, K., Laanemets, J., Lilover, M.-J., Lips, U., 2022. Quasi-steady circulation regimes in the Baltic Sea. Ocean Sci. 18, 857—879. https://doi.org/10.5194/os-18-857-2022

Lilover, M.J., Lips, U., Laanearu, J., Liljebladh, B., 1998. Flow regime in the Irbe Strait. Aquatic Sci. 60, 253—265.

Lindström, G., Pers, C., Rosberg, J., Strömqvist, J., Arheimer, B., 2010. Development and testing of the HYPE (Hydrological Predictions for the Environment) water quality model for different spatial scales. Hydrol. Res. 41, 295—319. https://doi.org/10.2166/nh.2010.007

Lips, I., Lips, U., Liblik, T., 2009. Consequences of coastal upwelling events on physical and chemical patterns in the central Gulf of Finland (Baltic Sea). Cont. Shelf Res. 29, 1836—1847.

Lips, U., Kikas, V., Liblik, T., Lips, I., 2016a. Multi-sensor in situ observations to resolve the sub-mesoscale features in the stratified Gulf of Finland. Baltic Sea. Ocean Sci. 12, 715—732. https://doi.org/10.5194/os-12-715-2016

Lips, U., Lilover, M.J., Raudsepp, U., Talpsepp, L., 1995. Water renewal processes and related hydrographic structures in the Gulf of Riga. EMI Report Ser. 1, 1—34.

Lips, U., Zhurbas, V., Skudra, M., Väli, G., 2016b. A numerical study of circulation in the Gulf of Riga, Baltic Sea, Part I: Whole-basin gyres and mean currents. Cont. Shelf Res. 112, 1—13. https://doi.org/10.1016/J.CSR.2015.11.008

Lips, U., Zhurbas, V., Skudra, M., Väli, G., 2016c. A numerical study of circulation in the Gulf of Riga, Baltic Sea. Part II: Mesoscale features and freshwater transport pathways. Cont. Shelf Res. 115, 44—52.

Lizuma, L., Avotniece, Z., Rupainis, S., Teilans, A., 2013. Assessment of the present and future offshore wind power potential: A case study in a target territory of the Baltic Sea near the Latvian coast. Sci. World J. 2013, 126428. https://doi.org/10.1155/2013/126428

Matthäus, W., Franck, H., 1992. Characteristics of major Baltic inflows — a statistical analysis. Cont. Shelf Res. 12, 1375—1400.

McWilliams, J.C., 2016. Submesoscale currents in the ocean. P. Roy. Soc. A-Math. Phy. 472 (2189), 20160117.

Meier, H.E.M., 2007. Modeling the pathways and ages of inflowing salt- and freshwater in the Baltic Sea. Estuar. Coast. Shelf Sci. 74, 610—627. https://doi.org/10.1016/j.ecss.2007.05.019

Meier, H.E.M., Feistel, R., Piechura, J., Arneborg, L., Burchard, H., Fiekas, V., Golenko, N., Kuzmina, N., Mohrholz, V., Nohr, C., Paka, V.T., 2006. Ventilation of the Baltic Sea deep water: A brief review of present knowledge from observations and models. Oceanologia 48 (S), 133—164.

Meier, H.E.M., Kauker, F., 2003. Modeling decadal variability of the Baltic Sea: 2. Role of freshwater inflow and large-scale atmospheric circulation for salinity. J. Geophys. Res. 108 (C11), 3368. https://doi.org/10.1029/2003JC001799

Mohrholz, V., Naumann, M., Nausch, G., Krüger, S., Gräwe, U., 2015. Fresh oxygen for the Baltic Sea - An exceptional saline inflow after a decade of stagnation. J. Marine Syst. 148, 152—166. https://doi.org/10.1016/j.jmarsys.2015.03.005

Morvan, M., L'Hégaret, P., Carton, X., Gula, J., Vic, C., de Marez, C., Sokolovskiy, M., Koshel, K., 2019. The life cycle of submesoscale eddies generated by topographic interactions. Ocean Sci. 15, 1531—1543. https://doi.org/10.5194/os-15-1531-2019

Nausch, M., Nausch, G., Lass, H.U., Mohrholz, V., Nagel, K., Siegel, H., Wasmund, N., 2009. Phosphorus input by upwelling in the eastern Gotland Basin (Baltic Sea) in summer and its effects on filamentous cyanobacteria. Estuar. Coast. Shelf Sci. 83, 434—442.

Onken, R., Baschek, B., Angel-Benavides, I.M., 2019. Very high-resolution modelling of submesoscale turbulent patterns and processes in the Baltic Sea. Ocean Sci. Discuss (in review). https://doi.org/10.5194/os-2019-44

Otsmann, M., Suursaar, Ü., Kullas, T., 2001. The oscillatory nature of the flows in the system of straits and small semienclosed basins of the Baltic Sea. Cont. Shelf Res. 21 (15), 577—1603. https://doi.org/10.1016/S0278-4343(01)00002-4

Radtke, H., Brunnabend, S.-E., Gräwe, U., Meier, H.E.M., 2020. Investigating interdecadal salinity changes in the Baltic Sea in a 1850—2008 hindcast simulation. Clim. Past 16, 1617—1642. https://doi.org/10.5194/cp-16-1617-2020

Salm, K., Liblik, T., Lips, U., 2023. Submesoscale variability in a mesoscalefront captured by a glider mission in the Gulf of Finland, Baltic Sea. Front. Mar. Sci. 10, 984246. https://doi.org/10.3389/fmars.2023.984246

Shcherbina, A.Y., D'Asaro, E.A., Lee, C.M., Klymak, J.M., Molemaker, M.J., McWilliams, J.C., 2013. Statistics of vertical vorticity, divergence, and strain in a developed submesoscale turbulence field. Geophys. Res. Lett. 40 (17), 4706—4711. https://doi.org/10.1002/grl.50919

Simpson, J.H., Bowers, D.G., 1981. Models of stratification and frontal movements in shelf seas. Deep-Sea Res. 28, 727—738.

Simpson, J.H., Brown, J., Matthews, J., Allen, G., 1990. Tidal straining, density currents and mixing in the control of estuarine stratification. Estuar. Coast. 13, 125—132.

Smagorinsky, J., 1963. General circulation experiments with the primitive equations: I. The basic experiment. Mon. Weather Rev. 91, 99—164. https://doi.org/10.1175/1520-0493(1963)091⟨0099:GCEWTP⟩2.3.CO;2

Suhhova, I., Liblik, T., Lilover, M.-J., Lips, U., 2018. A descriptive analysis of the linkage between the vertical stratification and current oscillations in the Gulf of Finland. Boreal Environ. Res. 23, 83—103.

Suursaar, Ü., Elken, J., Belkin, I.M., 2021. Fronts in the Baltic Sea: A Review with a Focus on Its North-Eastern Part. The Handbook of Environmental Chemistry. Springer, Berlin, Heidelberg https://doi.org/10.1007/698_2021_813

Thomas, L., Tandon, A., Mahadevan, A., 2008. Submesoscale processes and dynamics. Am. Geophys. Union Geophys. Monogr. Ser. 177, 17—38. https://doi.org/10.1029/177GM04

Tippenhauer, S., Janout, M., Chouksey, M., Torres-Valdes, S., Fong, A., Wulff, T., 2021. Substantial Sub-Surface Chlorophyll Patch Sustained by Vertical Nutrient Fluxes in Fram Strait Observed With an Autonomous Underwater Vehicle. Front. Mar. Sci. 8, 605225. https://doi.org/10.3389/fmars.2021.605225

Väli, G., Meier, H.E.M., Placke, M., Dieterich, C., 2019. River runoff forcing for ocean modeling within the Baltic Sea Model Intercomparison Project. Meereswiss. Ber., Warnemünde 113, 1—25. https://doi.org/10.12754/msr-2019-0113

Väli, G., Zhurbas, V., 2021. Seasonality of Submesoscale Coherent Vortices in the Northern Baltic Proper: A Model Study. Fundamentalnaya i Prikladnaya Gidrofizika 14 (3), 122—129. https://doi.org/10.7868/S2073667321030114

Väli, G., Zhurbas, V., Laanemets, J., Elken, J., 2011. Simulation of nutrient transport from different depths during an upwelling event in the Gulf of Finland. Oceanologia 53 (1-TI), 431—448.

Väli, G., Zhurbas, V., Lips, U., Laanemets, J., 2017. Submesoscale structures related to upwelling events in the Gulf of Finland, Baltic Sea (numerical experiments). J. Marine Syst. 171, 31—42. https://doi.org/10.1016/j.jmarsys.2016.06.010

Väli, G., Zhurbas, V., Lips, U., Laanemets, J., 2018. Clustering of floating particles due to submesoscale dynamics: a simulation study for the Gulf of Finland. Baltic Sea 11, 21—35. https://doi.org/10.7868/s2073667318020028

Vortmeyer-Kley, R., Holtermann, P.L., Feudel, U., Gräwe, U., 2019. Comparing Eulerian and Lagrangian eddy census for a tide-less, semi-enclosed basin, the Baltic Sea. Ocean Dynam. 69, 701—717. https://doi.org/10.1007/s10236-019-01269-z

Zhurbas, V., Elken, J., Paka, V., Piechura, J., Väli, G., Chubarenko, I., Golenko, N., Shchuka, S., 2012. Structure of unsteady overflow in the Słupsk furrow of the Baltic Sea. J. Geophys. Res. 117, 4027. https://doi.org/10.1029/2011JC007284

Zhurbas, V., Stipa, T., Mälkki, P., Paka, V., Golenko, N., Hense, I., Sklyarov, V., 2004. Generation of subsurface cyclonic eddies in the southeast Baltic Sea: Observations and numerical experiments. J. Geophys. Res. 109, C05033. https://doi.org/10.1029/2003JC002074

Zhurbas, V., Väli, G., Kostianoy, A., Lavrova, O., 2019b. Hindcast of the mesoscale eddy field in the Southeastern Baltic Sea: Model output vs satellite imagery. Russian J. Earth Sci. 19, 1—17. https://doi.org/10.2205/2019ES000672

Zhurbas, V., Väli, G., Kuzmina, N., 2019a. Rotation of floating particles in submesoscale cyclonic and anticyclonic eddies: a model study for the southeastern Baltic Sea. Ocean Sci. 15, 1691—1705. https://doi.org/10.5194/os-15-1691-2019

Zhurbas, V., Väli, G., Kuzmina, N., 2022. Striped texture of submesoscale fields in the northeastern Baltic Proper: Results of very high-resolution modelling for summer season. Oceanologia 64 (1), 1—21. https://doi.org/10.1016/J.OCEANO.2021.08.003

Oceanologia 66 (2024) 91—98

Available online at www.sciencedirect.com

ScienceDirect

journal homepage: www.journals.elsevier.com/oceanologia

ORIGINAL RESEARCH ARTICLE

Changes in cloudiness contribute to changing seasonality in the Baltic Sea region

Piia Post[a,*], **Margit Aun**[b]

[a] *Institute of Physics, University of Tartu, Tartu, Estonia*
[b] *Tartu Observatory, University of Tartu, Tõravere, Estonia*

Received 3 April 2023; accepted 16 November 2023
Available online 8 December 2023

KEYWORDS
Northern Europe;
Cloud fraction;
Seasonal shift;
Shortwave irradiance;
Baltic Sea

Abstract In the Baltic Sea region, a significant increase in solar radiation has been detected during the past half-century. Changes in shortwave irradiance are associated with atmospheric transparency and cloudiness parameters like cloud fraction and albedo. One of the most important reasons for day-to-day changes in cloudiness is the synoptic-scale atmospheric circulation; thus, we look for reasons for solar radiation trends due to changes in atmospheric circulation. We analysed regional time series and trends from satellite-based cloud climate data record CLARA-A2 for the Baltic Sea region in 1982—2018. As the rise in solar radiation depends on the seasonally averaged values of total fractional cloud cover (CFC), surface incoming shortwave radiation (SIS) and occurrences of circulation types were analysed. We show that the shift in seasonality connected to the earlier accumulated sums of SIS is at least partly explained by the changes in synoptic-scale atmospheric circulation.

1. Introduction

Ecosystems have evolved to adapt to seasonal changes in temperature and light. Economic sectors such as energy, agriculture, water resources, fisheries, and tourism heavily rely on the distribution of incoming solar shortwave radiation. Nature and its cycles have utilised instantaneous solar flux, and nowadays, humans increasingly harness solar energy in real-time and as it becomes available. In recent years, there has been an increased interest in renewable energy due to the need to plummet GHG emissions. The unit costs of solar energy sources have reduced by 85% from 2010 to 2019 (IPCC, 2022), and in 2022, for example, solar energy capacity increased by over 20% (IRENA, 2023).

* Corresponding author at: Institute of Physics, University of Tartu, Tartu, Estonia.
E-mail address: piia.post@ut.ee (P. Post).
Peer review under the responsibility of the Institute of Oceanology of the Polish Academy of Sciences.

Production and hosting by Elsevier

https://doi.org/10.1016/j.oceano.2023.11.004

Therefore, a detailed understanding of how and why solar energy is distributed during a whole year on a regional scale is needed.

The variation in solar radiation at the top of the atmosphere is relatively small compared to the amount reaching the Earth's surface. The surface incoming shortwave radiation depends on atmospheric conditions. Changes in shortwave irradiance are associated with atmospheric transparency and cloudiness parameters like cloud fraction and albedo. There have been decadal-scale trends in shortwave irradiance, with a decrease in the 1950s to 1980s and an increase afterwards in many regions of Europe (Ohvril et al., 2009; Parding et al., 2016; Pfeifroth et al., 2018; Post and Aun, 2020; Russak, 2009; Sanchez-Lorenzo et al., 2015; Wild et al., 2005). The switch from dimming to a brightening phase during the early 1980s is usually attributed to a decline in aerosol emissions (Ohvril et al., 2009; Wild et al., 2005).

Northern Europe's dimming and brightening periods are often associated with large-scale atmospheric circulation through the North Atlantic Oscillation (Pfeifroth et al., 2018; Russak, 2009). The link between circulation and shortwave radiation is frontal cloudiness. The phase and position of the North Atlantic Oscillation describe the westerlies' strength and location in the broad North Atlantic sector. The storm track of midlatitude cyclones, the main reason for frontal cloudiness, is associated with the position of westerlies. NAO link to storm track is a monthly scale relationship and works better for the cold half-year. Concerning solar radiation, the significance of a warm half-year is amplified in higher latitudes because of the extremely low radiative fluxes experienced during winter. Thus, employing synoptic-scale weather patterns becomes a sensible approach in these regions.

Sfîcă et al. (2021) have shown an essential link between atmospheric circulation and cloud cover using the daily scale atmospheric circulation patterns in 1981—2014. Parding et al. (2016) constructed empirical models of SW irradiance to relate daily synoptic-scale atmospheric circulation in northern Europe to the radiative climate in spring and summer. They summarise that in both seasons, a decrease in anticyclonic and an increase in cyclonic weather patterns over northern Europe contributed to the dimming from the 1960s to 1990. At the same time, they conclude that large-scale atmospheric circulation is not the only important factor in SW radiation variability in northern Europe.

Observed shifts in seasonal cycles have become an important research topic as the lengths and timing of the thermal seasons impact nature and human practices. Researchers agree that winter is shorter, spring and summer in Europe start earlier, and the last one lasts longer (e.g. Jaagus et al., 2003; Park et al., 2018; Peña-Ortiz et al., 2015; Ruosteenoja et al., 2020). The exact seasonal shifts in days depend on the latitude and the thresholds used to define the seasons. Park et al. (2018) find that the summer onset has advanced more than the delay of summer withdrawal. For the Northern Europe domain regional average, they found the summer onset to be 18 days earlier and the withdrawal 12 days later in 2012 than in 1953 by trendline. These are the second largest shifts in Northern Hemisphere regions.

A significant seasonality change has been detected in the Baltic Sea. Kahru et al. (2016) showed that the annual cycle of several environmental characteristics of the Baltic Sea has changed during the last half-century. The summer season starts earlier, and the productive season lasts longer. They found that starting from March, more incoming shortwave irradiance cumulates, which increases sea temperature, and several biota-connected phenomena have shifted to earlier dates.

Building on the findings of previous studies, we aim to look for reasons for changes in seasonality in the Baltic Sea region's atmosphere, which may pose problems in the ecosystems and human practices. We start from changes in SIS and hypothesise that the changes here are due to changes in cloudiness. The next step is associating changes in cloudiness with changes in atmospheric circulation. The trends in atmospheric circulation are hypothesised to be a complementary reason for seasonal shifts. While looking for seasonal shifts, it is reasonable to describe the mechanisms on a daily scale. We use the synoptic-scale atmospheric circulation patterns as the temporal and spatial scales should be coherent.

2. Data and methods

2.1. Cloud and shortwave radiation data

We analyse cloud cover and incoming shortwave radiation changes over the Baltic Sea region using daily data from EUMETSAT's CLARA-A ed. 2.1 dataset (Karlsson et al., 2020) from Satellite Application Facility on Climate Monitoring (CM SAF). This extended dataset covers 01.01.1982—30.06.2019 and is specially prepared for climatological research. While our research area covers latitudes higher than 60°N, we chose the dataset from the AVHRR sensor onboard polar-orbiting NOAA and METOP satellites. We use daily mean cloud fraction cover (CFC) with a 0.25° × 0.25° grid. CFC is the fraction of cloudy pixels per grid square (point) compared to the total number of analysed pixels in the grid square (Karlsson et al., 2020). CFC unit is per cent. Surface incoming shortwave radiation (SIS, units W/m^2) data is from the same dataset CLARA-A ed. 2.1. We use the daily mean SIS in the same 0.25° × 0.25° grid.

2.2. Atmospheric circulation data

We use synoptic-scale atmospheric circulation patterns to describe atmospheric circulation on the daily temporal scale. We chose Jenkinson-Collison circulation patterns (Jenkinson and Collison, 1977; Post et al., 2002) from various methods due to the simplicity of interpretation and flexibility in sensitivity studies. Jenkinson-Collison circulation patterns (JCTs) were calculated for all days between 1979 and 2018 using gridded mean sea level pressure data of ERA5 reanalysis (Hersbach et al., 2020) at noon UTC with the cost733class software package (Philipp et al., 2016). We use the version with ten types (Philipp et al., 2014). There are eight directional types, with names showing the prevailing airflow direction: W, NW, N, NE, E, SE, S, SW, and two

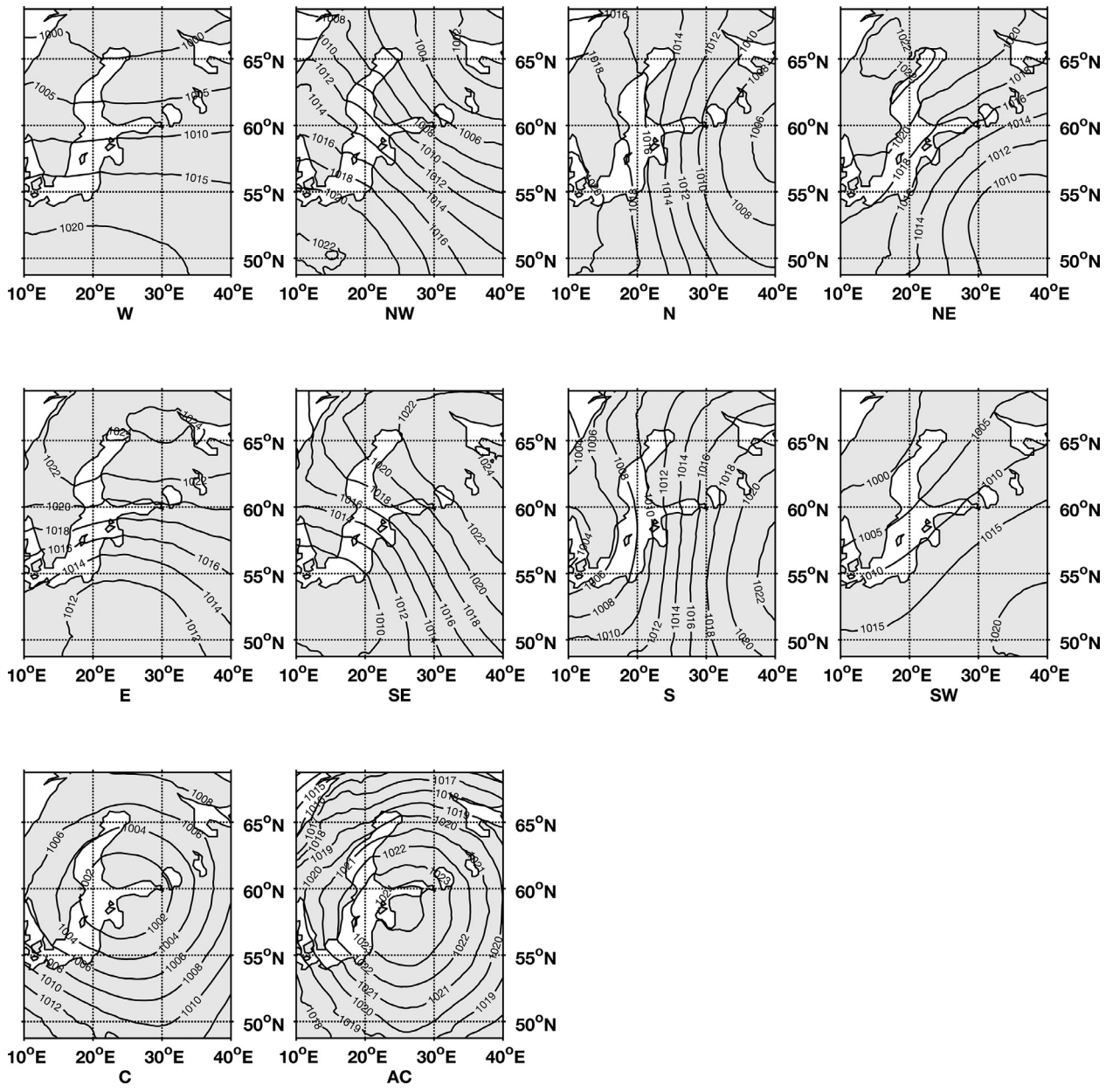

Figure 1 Maps of 10 Jenkinson-Collison (JCT) circulation patterns that are centred 58.75°N, 25°E. Cloudy types are S, SW, and C; clear types are E, SE, and AC.

types connected to the air pressure system in the centre of the area: cyclonic (C) and anticyclonic (AC). The JCT circulation pattern maps centred at 58.75°N, 25°E are presented in Figure 1. The correlation between the daily CFC and the occurrence of various circulation patterns was calculated to find the cloudy and clear types. Based on these calculations, the S, SW and C types were detected as cloudy and NE, E and AC as clear sky. Other types did not give such a clear correlation and were left out of the analysis. The occurrences for cloudy (Figure 2) and clear sky (Figure 3) types are summed up and correlated to the cloud fraction. Pixels over the Baltic Sea and the land are shown separately in scatterplots, and the correlation is slightly better over the land than the sea. The conclusion was that the land and sea pixels should not be differentiated from the atmospheric circulation viewpoint.

2.3. Methods

As our research aims to associate the seasonality changes with possible reasons, we analyse long-term changes in cloud cover, radiation, and atmospheric circulation. For that, we calculate seasonal values of CFC, SIS and JCT frequencies for 37 years (1982—2018) and look for temporal changes. The study area includes the Baltic Sea and surrounding countries from 52 to 70°N and 5 to 32°E. The climate of the region is characterised by four distinct seasons. Instead of the common 3-month seasons, we use 6-

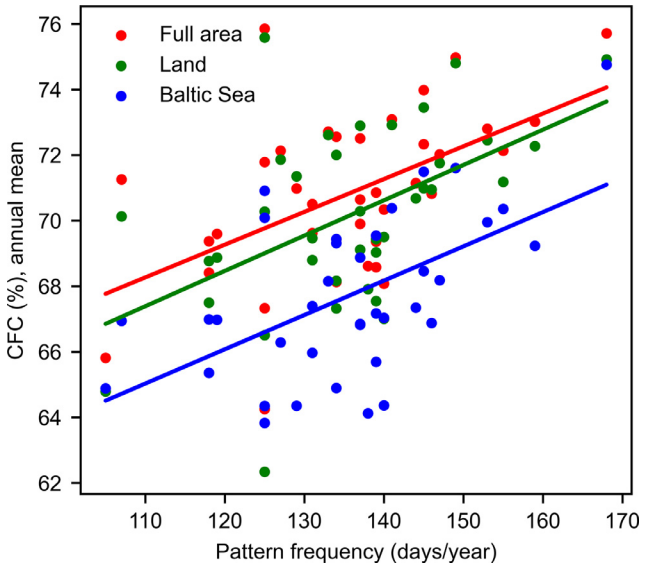

Figure 2 Annual mean CFC vs cloudy JCT pattern (S, SW and C) frequency for individual years, separately for the sea and land pixels.

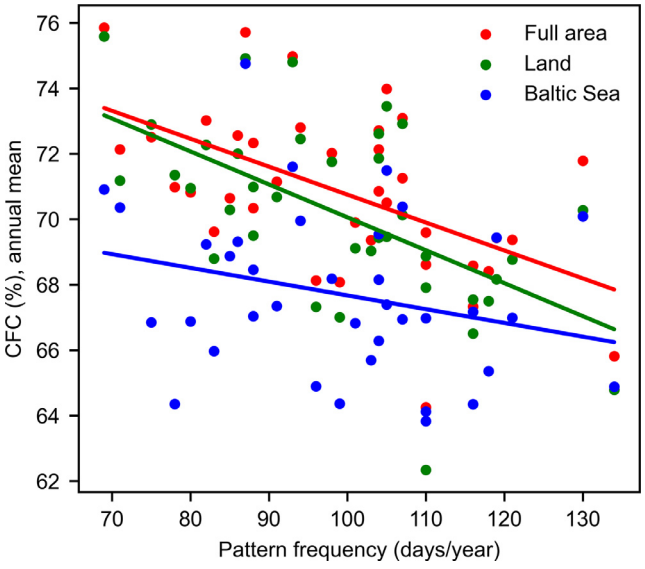

Figure 3 Annual mean CFC vs clear JCT pattern (NE, E and AC) frequency for individual years, separately for the sea and land pixels.

month seasons: spring is January—June (JFMAMJ), summer April—September (AMJJAS), fall July—December (JASOND), and winter October—March (ONDJFM). The first reason for using 6-month seasons is the high interannual variability in atmospheric circulation in high latitudes. JCT classification classifies all days of a year into easily interpretable synoptic types using the same thresholds. Therefore, in 3-month winters, clear types do not occur in some years. Prolonging the season filters the results, and we can show robust outcomes. Another possibility would have been to calculate the running mean over the years to eliminate missing values. The second reason is that nature accumulates the signal from the environment for relatively long periods, supporting the idea of longer seasons. It would have been possible to show just two seasons, the warm and the cold, but knowing what happens in transition seasons is essential.

For every season, sums for SIS and frequencies of JCT patterns were found. For cloud cover, six-month averages were found. The mean of daily CFC (in %) and the sum of SIS (in W/m^2) were found for each pixel and averaged over the area. We also examined the differences between cloud cover over the Baltic Sea and land area. We applied masks to select only the desired area and used the same methods on previously described data.

A linear trend was calculated for all seasons and analysed with the Mann-Kendall test (Kendall, 1975; Mann, 1945). We considered the statistical significance level 0.05.

3. Results

3.1. Long-term changes in the sums of SIS and CFC

As the region is located at relatively high latitudes, the sums of SIS per particular six-month period vary substantially with seasons. There is about seven times more radiation available during summer compared to winter. The long-term means are 30475 W/m^2 (std. 2099 W/m^2) vs 4243 W/m^2 (std. 793 W/m^2). The amount of radiation has increased in time in all seasons; all rates are significant but not equal (Figure 4, Table 1). The largest trend is in summer, and the smallest is in winter, meaning the warm season gets longer from both sides due to higher incoming radiation. While the trend for spring is more prominent than for fall, it leads to an earlier start of the warm season compared to a later ending. It shifts the midsummer earlier.

Now, we ask if this shift in seasons is associated with the changes in cloud cover. Cloudiness shows high interannual variability in the study area, but in general, there are most

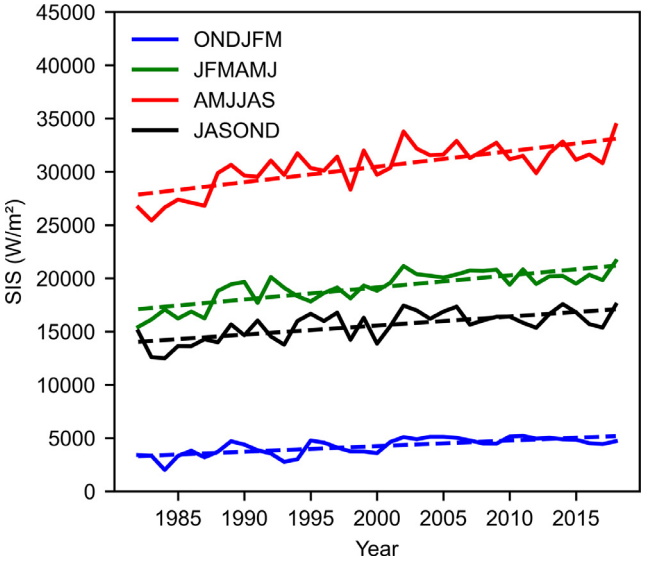

Figure 4 Six-month sums of daily mean SIS and SIS trendlines from CMSAF data in the Baltic Sea region for four seasons (1982—2018). All trends are significant and shown in Table 1.

Table 1 Slope values for linear regression lines added to seasonal changes in SIS, CFC and frequency of JCT patterns. A significant trend based on the Mann-Kendall test is shown in bold according to the *p* values in the bracket.

Variable	ONDJFM	JFMAMJ	AMJJAS	JASOND
SIS [(W/m^2)/year]	**45.66 (p < .001)**	**114.48 (p < .001)**	**134.82 (p < .001)**	**85.80 (p < .001)**
CFC [%/year]	**−0.13 (p = .0023)**	**−0.14 (p < .001)**	**−0.18 (p < .001)**	**−0.15 (p = .0012)**
CFC Baltic Sea [%/year]	−0.05 (p = .20)	−0.11 (p = .058)	−0.13 (p = .058)	−0.06 (p = .23)
CFC land [%/year]	**−0.15 (p = .0016)**	**−0.16 (p < .001)**	**−0.23 (p < .001)**	**−0.17 (p = .0019)**
JCT clear [days/year]	0.15 (p = .40)	0.09 (p = .52)	0.23 (p = .088)	0.25 (p = .12)
JCT cloudy [days/year]	0.00 (p = .89)	−0.09 (p = .49)	**−0.20 (p = .049)**	−0.10 (p = .58)

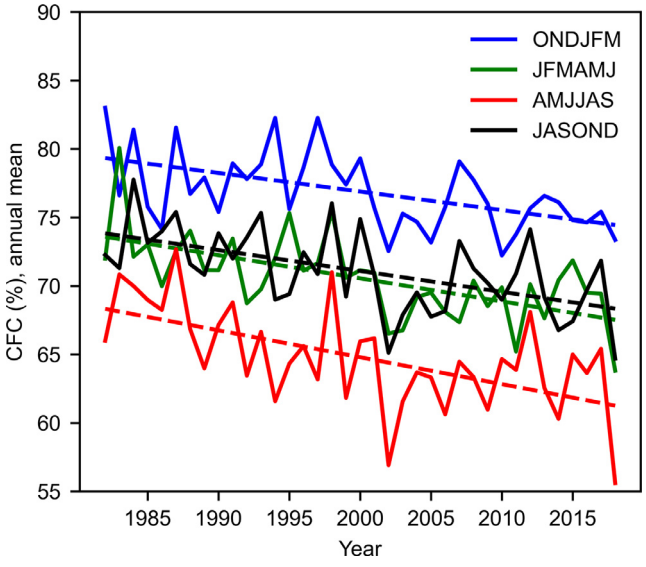

Figure 5 Six-month means of daily CFC and CFC trendlines from CMSAF data in the Baltic Sea region for four seasons (1982–2018). All trends are significant and shown in Table 1.

clouds in winter and least in summer (Figure 5). The mean for CFC in winter is 76.9% (std. 2.8%), and in summer, 64.8% (std. 3.7%). It means that while the radiation flux at the top of the atmosphere is the smallest in winter, the cloudiness also contributes to winter's already low radiative fluxes. Although the year-to-year variability is high, there are also statistically significant long-term changes. As expected, the trends for CFC are opposite compared to SIS – all trends are negative and statistically significant according to the Mann-Kendall test (see Table 1). It has become clearer in the Baltic Sea area, in summer more than in fall, spring and winter. While the clouds appear only in case of enough moisture in the air, then from here follows, there is less moisture transport to the area, especially in summer.

The cloud amount also depends on the underlying surface, and it changes seasonally if there are more or fewer clouds over the sea than over the continent (Figure 6). In summer, this contrast is the best pronounced. There are fewer clouds over the sea than over the land. The same is valid for spring. The most negligible contrast is in fall, but in winter, there are more clouds over the sea than on the land.

We also looked at the trends over the sea and land separately to detect a possible difference in the shift of seasons. Still, all trends in cloudiness are negative (Figure 7), but the trend over the land is always bigger than over the Baltic Sea. For winter and fall, the trends over the sea are marginal (Table 1); here, the summer trend is the largest. The cloudiness has significantly decreased in summer and spring over the land. This means the contrast in cloudiness between the land and the sea decreases over time.

3.2. Changes in atmospheric circulation

Daily time series of JCT patterns calculated from ERA5 reanalysis mean sea level pressure data were used to show the variability in synoptic-scale atmospheric circulation. Cyclonic, southern, and southwestern circulation types are overcast and fully overcast days, while anticyclonic, northeastern, and eastern types are clear or almost clear days. A load of clear types is 22–93 days per season and 43–102 days for cloudy patterns. Indeed, many days fall into types that do not exhibit a clear correlation with cloudiness. The clear patterns (Figure 8) and overcast patterns (Figure 9) show a sizeable interannual variability, but the tendencies coincide with the trends in CFC. Clear patterns become more frequent, and cloudy patterns become less frequent for all seasons. The biggest rise is in autumn clear types. The slightest increase for clear types is in spring, and there is no decrease for cloudy types in winter. The only statistically significant trend here is the reduction of cloudy types in summer.

4. Discussion

We have shown that the Baltic Sea area gets more shortwave radiation during all seasons, but summer's rise is the biggest. It could be one reason for the warm season's ear-

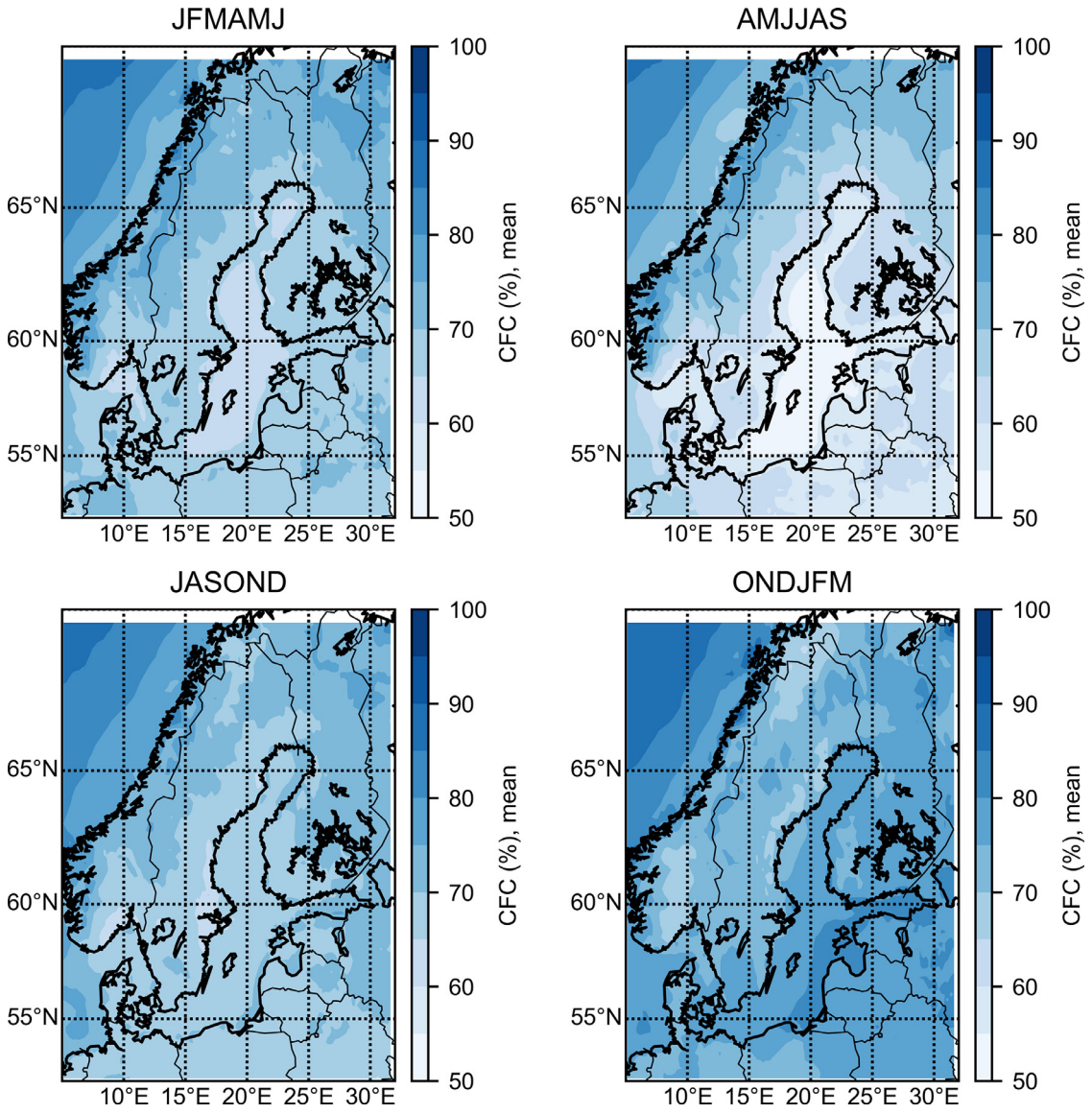

Figure 6 Six-month means of daily CFC from CMSAF data in the Baltic Sea region for four seasons (1982—2018).

lier onset and later withdrawal over the Baltic Sea area. The reason is fewer clouds in summer due to clearer circulation patterns. The CFC and the SIS are highly correlated, varying in opposite phases. At the same time, the interannual variability is much higher for cloudiness and even higher for occurrences of circulation types. It is a robust result. Due to the very high variability of circulation patterns, we sum up all daily level characteristics over six-month periods, averaging the details out. Nevertheless, the seasons' results could also be distinguished for winter and autumn, which was impossible if accumulation started just from the beginning of the calendar year, as in Kahru et al. (2016).

We have included a land area of up to 70°N in our research area, compared to Kahru et al. (2016), who showed that the warm season starts earlier and lasts longer over the Baltic Sea only. We, therefore, could not use the same satellite data as Kahru et al. (2016) for SIS and CFC, while for such high latitudes, it is not reasonable to use data from geostationary satellites. The new result here is that the summer season has prolonged over the land even more than over the sea. While the summer cloudiness over the sea was lower than over the land, the faster decrease in cloudiness over the land makes this contrast less with time. There are fewer clouds over the sea than over the land in summer and more in winter, which is connected to local environmental properties. We conclude from the result that no essential differences existed between the correlations with circulation type frequencies over the land and sea. One reason could be connected to convective cloudiness, which is more probable over the land in summer months, while towards fall, convection gets more probable over the Baltic Sea shallow areas.

Why is the cloud amount decreasing in time? On one side, it could be connected to the overall global temperature rise. Then, more moisture is needed for air to get saturated. Over the sea, there should always be enough

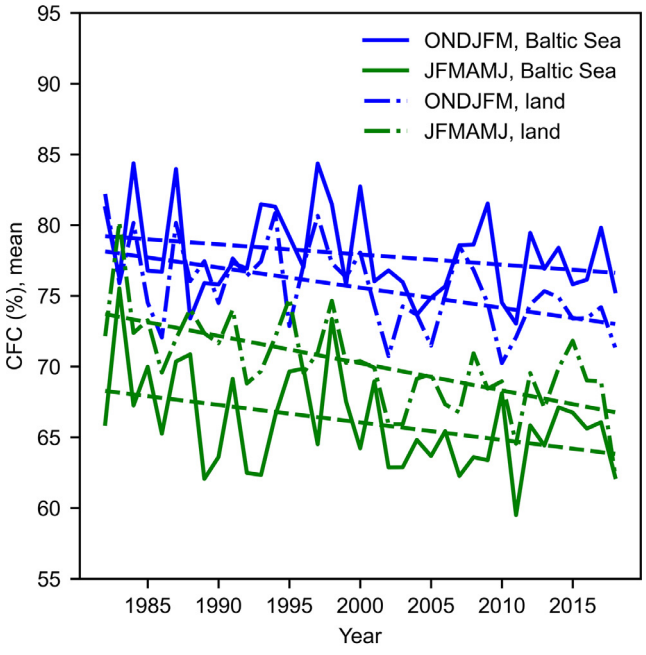

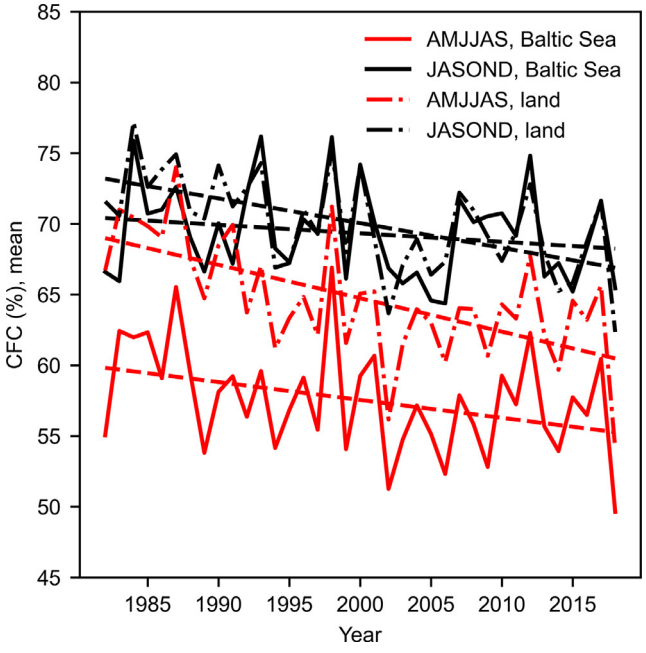

Figure 7 Six-month means of daily CFC and CFC trendlines from CMSAF data for four seasons (1982–2018), separately for the sea and land pixels. All trends are significant for the land and not significant for the sea pixels.

water to evaporate, but the land areas may undergo intermittent arid conditions in different years. Another potential explanation is linked to interdecadal variability in atmospheric circulation patterns, which have accounted for the observed interdecadal fluctuations in SIS and cloud cover (Parding et al., 2016). Of course, both drivers can also work together. The clearing in the last tens of years should not give an understanding that this trend is forever.

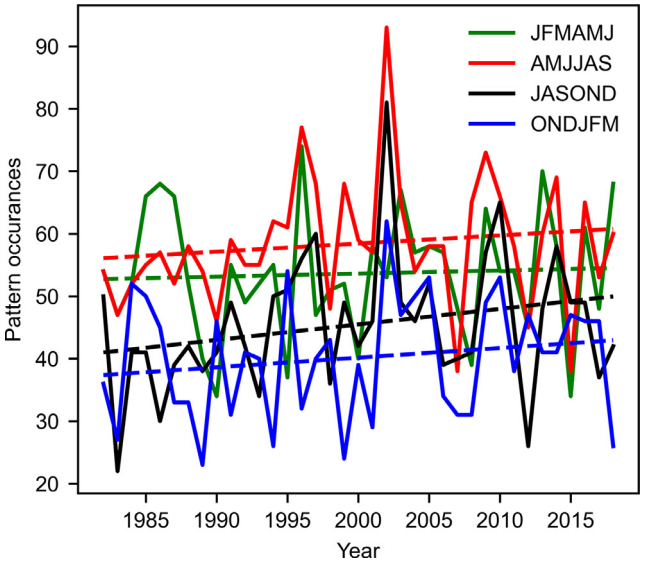

Figure 8 Six-month sums of clear JCT patterns for four seasons (1979–2018). All trends are not significant.

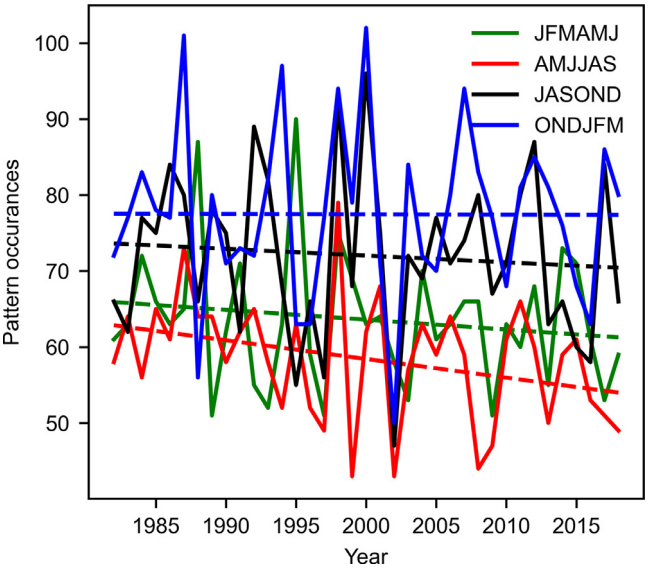

Figure 9 Six-month sums of cloudy JCT patterns for four seasons (1979–2018). All trends are negative; the only significant one is for summer.

5. Conclusions

We show that the changes in synoptic-scale atmospheric circulation at least partly explain longer and earlier summers in the Baltic Sea area. While looking at the land and the Baltic Sea separately, we found that the speed of the season shifts over the land area is even faster than over the sea. This shift is reasoned by the increased surface incoming shortwave radiation in all seasons, but the most rapid growth has happened in summer. This SIS increase is at least partly due to the decrease in total cloudiness, which is also valid for all four seasons, with the fastest drop in summer. The variability of synoptic-scale atmospheric circulation patterns explains at least partly why the cloudiness has

decreased. There are more clear circulation patterns and less cloudy patterns. The upcoming research will involve categorising cloud cover into grades ranging from nearly clear to overcast. The aim is to investigate whether the reduction in CFC results from fewer clouds on many days or if there is a decline in the number of days with cloud cover. The other interesting theme is connected to local factors in cloud development.

Declaration of competing interest

The authors declare that they have no known competing financial interests or personal relationships that could have appeared to influence the work reported in this paper.

Acknowledgements

The research presented in this study is part of the Baltic Earth program (Earth System Science for the Baltic Sea region; see https://www.baltic.earth, last access: March 31, 2023). We are grateful to the EUMETSAT's Satellite Application Facility on Climate Monitoring for the data and software.

Cost733class was compiled by the community of COST Action 733 Harmonisation and Applications of Weather Type Classifications for European Regions.

This research has been supported by the Estonian Research Council (grant no. PRG1726).

References

Hersbach, H., Bell, B., Berrisford, P., et al., 2020. The ERA5 global reanalysis. Q. J. R. Meteorol. Soc. 146, 1999–2049. https://doi.org/10.1002/qj.3803

IPCC, 2022. Summary for Policymakers. In: Shukla, P.R., Skea, J., Slade, R., Al Khourdajie, A., van Diemen, R., McCollum, D., Pathak, M., Some, S., Vyas, P., Fradera, R., Belkacemi, M., Hasija, A., Lisboa, G., Luz, S., Malley, J. (Eds.), Climate Change 2022: Mitigation of Climate Change. Contribution of Working Group III to the Sixth Assessment Report of the Intergovernmental Panel on Climate Change. Cambridge University Press, Cambridge, UK and New York, NY, USA. https://doi.org/10.1017/9781009157926.001

IRENA, 2023. Renewable capacity statistics 2023, available at Renewable capacity statistics 2023 (irena.org) last access: 30 March 2023.

Jaagus, J., Truu, J., Ahas, R., Aasa, A., 2003. Spatial and temporal variability of climatic seasons on the east European plain in relation to large-scale atmospheric circulation. Clim. Res. 23, 111–129.

Jenkinson, A.F., Collison, F.P., 1977. An initial climatology of gales over the North Sea. Synoptic Climatol. Branch Memorandum, No. 62. Meteorological Office, Bracknell.

Kahru, M., Elmgren, R., Savchuk, O.P., 2016. Changing seasonality of the Baltic Sea. Biogeosciences 13, 1009–1018. https://doi.org/10.5194/bg-13-1009-2016

Karlsson, K.-G., Anttila, K., Trentmann, J., Stengel, M., Solodovnik, I., Meirink, J.F., Devasthale, A., Kothe, S., Jääskeläinen, E., Sedlar, J., Benas, N., van Zadelhoff, G.-J., Stein, D., Finkensieper, S., Håkansson, N., Hollmann, R., Kaiser, J., Werscheck, M., 2020. CLARA-A2.1: CM SAF cLoud, Albedo and surface RAdiation dataset from AVHRR data – Edition 2.1, Satellite Application Facility on Climate Monitoring. https://doi.org/10.5676/EUM_SAF_CM/CLARA_AVHRR/V002_01

Kendall, M.G., 1975. Rank Correlation Methods, 4th edn., Charles Griffin, London.

Mann, H.B., 1945. Non–parametric test against trend. Econometrica 13 (3), 245–259. https://doi.org/10.2307/1907187

Ohvril, H., Teral, H., Neiman, L., Kannel, M., Uustare, M., Tee, M., Russak, V., Okulov, O., Jõeveer, A., Kallis, A., Ohvril, T., Terez, E.I., Terez, G.A., Gushchin, G.K., Abakumova, G.M., Gorbarenko, E.V., Tsvetkov, A.V., Laulainen, N., 2009. Global dimming and brightening versus atmospheric column transparency, Europe, 1906–2007. J. Geophys. Res.-Atmos. 114, D00D12. https://doi.org/10.1029/2008JD010644

Parding, K.M., Liepert, B.G., Hinkelman, L.M., Ackerman, T.P., Dagestad, K., Olseth, J.A., 2016. Influence of Synoptic Weather Patterns on Solar Irradiance Variability in Northern Europe. J. Climate 29, 4229–4250. https://doi.org/10.1175/JCLI-D-15-0476.1

Park, B., Kim, Y., Min, S., Lim, E., 2018. Anthropogenic and Natural Contributions to the Lengthening of the Summer Season in the Northern Hemisphere. J. Climate 31, 6803–6819. https://doi.org/10.1175/JCLI-D-17-0643.1

Peña-Ortiz, C., Barriopedro, D., García-Herrera, R., 2015. Multidecadal Variability of the Summer Length in Europe. J. Climate 28, 5375–5388. https://doi.org/10.1175/JCLI-D-14-00429.1

Pfeifroth, U., Bojanowski, J.S., Clerbaux, N., Manara, V., Sanchez-Lorenzo, A., Trentmann, J., Walawender, J.P., Hollmann, R., 2018. Satellite-based trends of solar radiation and cloud parameters in Europe. Adv. Sci. Res. 15, 31–37. https://doi.org/10.5194/asr-15-31-2018

Philipp, A., Beck, C., Esteban, P., Kreienkamp, F., Krennert, T., Lochbihler, K., Lykoudis, S.P., Pianko-Kluczynska, K., Post, P., Alvarez, D.R., Spekat, A., 2014. cost733class-1.2 User guide. University of Augsburg, Augsburg, Germany.

Philipp, A., Beck, C., Huth, R., Jacobeit, J., 2016. Development and Comparison of Circulation Type Classifications Using the COST 733 Dataset and Software. Int. J. Climatol. 36, 2673–2691. https://doi.org/10.1002/joc.3920

Post, P., Aun, M., 2020. Changes in satellite-based cloud parameters in the Baltic Sea region during spring and summer (1982–2015). Adv. Sci. Res. 17, 219–225. https://doi.org/10.5194/asr-17-219-2020

Post, P., Truija, V., Tuulik, J., 2002. Circulation weather types and their influence on temperature and precipitation in Estonia. Boreal Environ. Res. 7 (3), 281–289.

Ruosteenoja, K., Markkanen, T., Räisänen, J., 2020. Thermal seasons in northern Europe in projected future climate. Int. J. Climatol. 40, 4444–4462. https://doi.org/10.1002/joc.6466

Russak, V., 2009. Changes in solar radiation and their influence on temperature trend in Estonia (1955–2007). J. Geophys. Res.-Atmos. 114, D00D01. https://doi.org/10.1029/2008JD010613

Sanchez-Lorenzo, A., Wild, M., Brunetti, M., Guijarro, J.A., Hakuba, M.Z., Calbó, J., Mystakidis, S., Bartok, B., 2015. Reassessment and update of long-term trends in downward surface shortwave radiation over Europe (1939–2012). J. Geophys. Res.-Atmos. 120, 9555–9569. https://doi.org/10.1002/2015JD023321

Sfîcă, L., Beck, C., Nita, A.-I., Voiculescu, M., Birsan, M.-V., Philipp, A., 2021. Cloud cover changes have been driven by atmospheric circulation in Europe during the last decades. Int. J. Climatol. 41 (Suppl. 1), E2211–E2230. https://doi.org/10.1002/joc.6841

Wild, M., Gilgen, H., Roesch, A., Ohmura, A., Long, C.N., Dutton, E.G., Forgan, B., Kallis, A., Russak, V., Tsvetkov, A., 2005. From Dimming to Brightening: Decadal Changes in Solar Radiation at Earth's Surface. Science 308, 847–850. https://doi.org/10.1126/science.1103215

Oceanologia 66 (2024) 99—110

Available online at www.sciencedirect.com

ScienceDirect

journal homepage: www.journals.elsevier.com/oceanologia

ORIGINAL RESEARCH ARTICLE

The use of Argo floats as virtual moorings for monitoring the South Baltic Sea

Małgorzata Merchel*, Waldemar Walczowski, Daniel Rak, Piotr Wieczorek

Institute of Oceanology, Polish Academy of Sciences, Sopot, Poland

Received 24 February 2023; accepted 10 January 2024
Available online 2 February 2024

KEYWORDS
Argo floats;
Virtual mooring;
Baltic Sea;
Temperature;
Salinity

Abstract The Argo float measurement network is increasingly effectively covering internal seas and shelf areas. In this paper, a specific approach to using Argo floats as 'virtual moorings' within the conditions of the Baltic Sea is presented. Following a series of successful deployments with standard configurations, it was decided that the settings forcing the float to stay at the bottom between profiles should be tested. This significantly reduced the drift of the float and allowed measurements to be made in a limited water area for a longer time. The data obtained from Argo floats used as virtual mooring can be a valuable source for monitoring and analysing the hydrology of individual basins of the Baltic Sea. The results show that the temporal and spatial variability of the observed fields of temperature, salinity, and other properties of seawater is very high. More data are needed to correctly determine the mean properties of the basins and their temporal variability. Therefore, Argo floats can be a source of efficient and inexpensive hydrographic data for shallow seas such as the Baltic.

1. Introduction

The seas and oceans affect all aspects of our lives. Shipping, fishing, sports and tourism are the zones of activity where the importance of the ocean is obvious. However, these impacts are often more difficult to observe or measure, which can lead to limited social awareness of their effects. The influence of the ocean on climate and its changes caused by human activities is an important aspect of oceanographic research. More than 25% of the carbon released by burning fossil fuels is dissolved in the ocean, the ocean absorbs and stores more than 90% of the ex-

* Corresponding author at: Institute of Oceanology, Polish Academy of Sciences, Sopot, Poland.
E-mail address: merchel@iopan.pl (M. Merchel).
Peer review under the responsibility of the Institute of Oceanology of the Polish Academy of Sciences.

Production and hosting by Elsevier

https://doi.org/10.1016/j.oceano.2024.01.002

cess heat that reaches the Earth due to the greenhouse effect (Rhein et al., 2013). Ocean heat content is growing rapidly. Warming is not only affecting the surface layers, but the temperature of the deep ocean layers is also rising gradually (Desbruyères et al., 2017; Levitus et al., 2012; Merchel and Walczowski, 2020; Purkey and Johnson, 2010; Roemmich et al., 2015).

100 years of observations at the Finnish Utö Atmospheric and Marine Research Station show changes in the atmosphere and water temperature of this part of the Baltic Sea. The increase in seawater temperature on the surface is 0.3°C per decade for the last 100 years at the station. In a deeper layer, the increase is lower. The temperature of the atmosphere has increased at a rate of 0.4°C per decade during the last 35 years, which is significantly lower than in the land area (Laakso et al., 2018). However, a 32-year (1982—2013) satellite data series shows a trend in sea surface temperature (SST) that generally exceeds 0.04°C per year, and even around 0.06°C per year in the Gulf of Finland (Stramska and Białogrodzka, 2015). Various climate change scenarios used in numerical modelling also predict significant environmental changes for the Baltic Sea region (Christensen et al., 2022; Meier et al., 2022). Based on 30 years of simulation time, the average increase in the surface temperature of the Baltic Sea by 2.9°C was already predicted in 2004 (Döscher and Meier, 2004). Contemporary analyses indicate a warming of the Baltic Sea surface waters by 0.4—0.6°C per decade since the 1980s, but the trend is accelerating (Meier et al., 2022). Changes in the seasonal cycle of heat transfer between the atmosphere and the water surface are also predicted. Changes in the average water temperature of the Baltic Sea are closely related to changes in the temperature of the atmosphere. However, during climate change, these processes do not have to run in parallel, due to changes in the surface heat balance (Omstedt and Hansson, 2006).

The greatest changes are taking place in the northern part of the Baltic, but the South Baltic is also subject to strong anthropogenic pressure. The summer sea surface temperature (SST) will increase by approximately 4°C in the northern parts of the Baltic Sea and by approximately 2°C in the southern part near the end of this century. These changes cause an increase in sea level and affect marine biogeochemistry. Therefore, it is necessary, among others, to develop and maintain monitoring and observation activities of the marine environment (HELCOM, 2013). An efficient observation system is required to observe the rapid changes in the hydrosphere. A large amount of global data is obtained through satellite observations. Unfortunately, the data are only for the surface of the ocean and are not able to provide information about the ocean interior. Oceanographic vessels provide surface-to-bottom measurements, but the coverage by these measurements is not sufficient. Moorings are rarely placed and most do not provide real-time information; the data from them reaches the users after a long time. The only global oceanographic measurement network providing near-real-time (NRT) data is the Argo system.

The Argo programme was developed in the late 1990s. The input for growth was the World Ocean Circulation Experiment (WOCE) programme. 290 Autonomous Lagrangian Circulation Explorer (ALACE) floats were used during the programme (Davis et al., 1992). ALACE floats used the principle of neutral buoyancy invented by Swallow in the mid-1950s to observe currents at particular depths (Swallow, 1955). Today, the Argo Programme is a major component of both the Global Ocean Observing System (GOOS) and the Global Climate Observing System (GCOS). Almost 4000 core Argo floats cover deep oceans, each profile the water column to a depth of 2000 m every 10 days. All data collected by Argo floats are freely available through Global Data Assembly Centres (GDACs), after automatic Real-Time Quality Control (RTQC) within 24 hours of transmission. After performing Delayed-Mode Quality Control (DMQC) within a year of data collection, the Argo system provides high-quality data that can be used for science.

This revolution in deep-ocean observation is slowly spreading to the marginal and shelf seas. Argo reached the Mediterranean Sea the fastest (Notarstefano et al., 2021), while Finnish and Polish oceanographers used it in the Baltic Sea (Haavisto et al., 2018; Roiha et al., 2018; Siiriä et al., 2018; Walczowski et al., 2020). In recent years, the launching of the Argo in the Baltic Sea has also been carried out by German oceanographers. Years of experience in the South Baltic allow us to conclude that Argo floats are an efficient and inexpensive source of hydrographic data from this reservoir. In the 11 years between 2012 and December 2022, 50 floats were deployed in the Baltic Sea (Figure 1). They provided 8378 temperature and salinity versus depth (CTD) profiles. Equipping traditional CTD floats with a dissolved oxygen (DO) sensor has significantly enriched the measurements. By the end of December 2022, 4352DO profiles were made (Table 1).

In this paper, we present a specific way of using Argo floats in the conditions of the Baltic Sea. The work was carried out as part of the Euro-Argo Research Infrastructure Sustainability and Enhancement (Euro-Argo RISE) project funded by the Horizon2020 programme. The objective of Euro-Argo RISE was: 'to enhance and extend the capabilities of the Argo network to provide essential ocean observations to answer new societal and scientific challenges and support:

1) ocean and climate change research,
2) climate change monitoring (characterizing the climate change impact on the ocean physics and chemistry,
3) seasonal and climate change forecasting by improving the 4D description of the ocean state,
4) ocean analysis and forecasting and associated ocean services, including Copernicus Services (Pouliquen, 2018).'

When planning experiments in the Baltic Sea, the hypothesis was made that it is possible to keep floats in a limited water area for a longer time and that it will give even better results than data from the free drift of floats. A series of experiments were carried out that confirmed the hypothesis. The data obtained have enriched our knowledge of the Baltic Sea and are available on the CORIOLIS website (https://www.coriolis.eu.org/).

2. Argo working conditions in the South Baltic

In the Baltic, Argo encounters conditions are completely different from those of the deep ocean. These are:

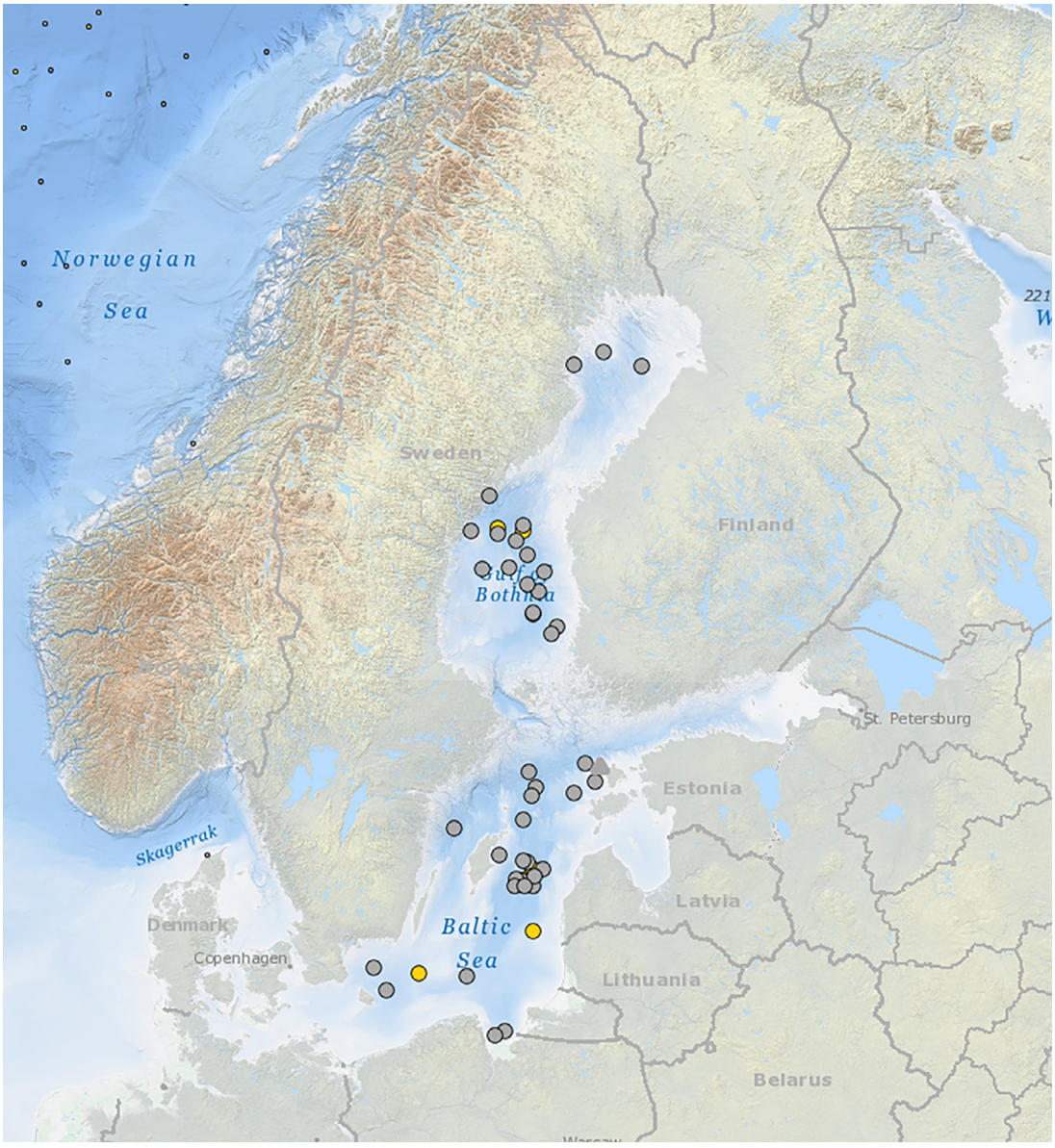

Figure 1 Positions of active (yellow circles) and inactive (grey circles) Argo floats in the Baltic Sea in January 2023.

Table 1 Countries that deployed Argo floats in the Baltic Sea in 2012—2022.

Country	Institution	Deployment year	Number of deployed floats	Number of CTD cycles	Number of DO cycles
Finland	FMI	2012	32	4160	1620
Poland	IOPAN	2016	11	3075	1589
Germany	ICBM, BSH	2021	7	1143	1143

- strong density gradients → float needs to be balanced to match the expected densities of the target area,
- heavy ship traffic and fishing activity → increased risk of damage or entanglement of the float,
- seasonal ice cover → ice avoidance algorithms needed,
- shallow depths → possibility of bottom contact,
- proximity to the coast → floats can be recovered and redeployed after maintenance.

Furthermore, the Baltic conditions require different procedures for Delayed-Mode Quality Control (DMQC) of the data than for floats operated in the deep oceans (Klein et al., 2022; Wong et al., 2022). Despite the problems mentioned above, the experience gained in the use of Argo floats in the South Baltic Sea has demonstrated the usefulness of this technology (Walczowski et al., 2020). During the analyses carried out as part of the Euro-Argo

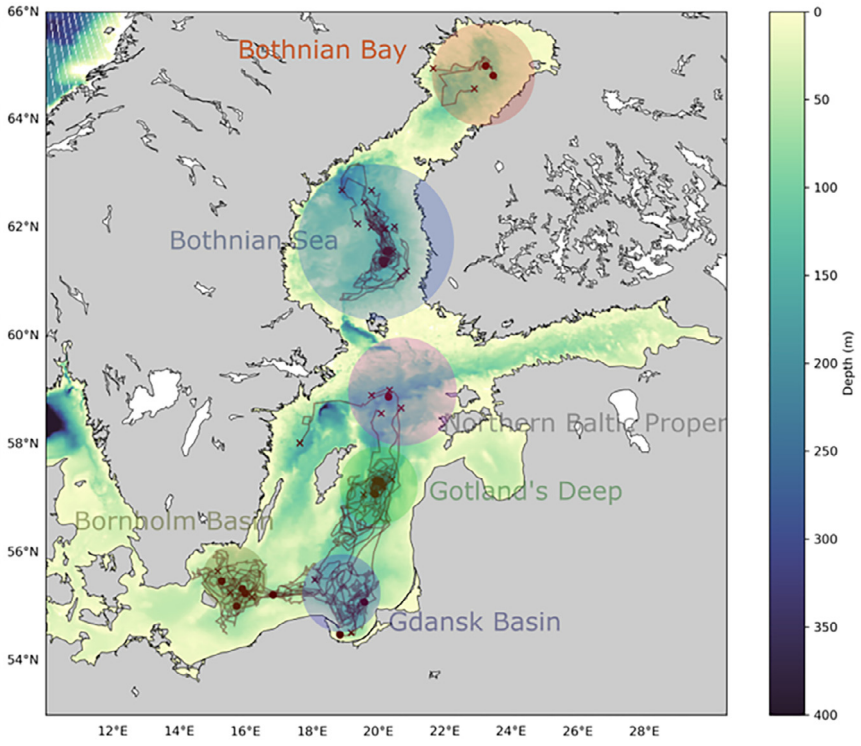

Figure 2 Deep basins of the Baltic Sea and typical float routes (Siiriä et al., 2020).

RISE and Argo-Poland projects, we came to the conclusion that for good coverage of the Baltic Sea, at least seven floats continuously working in deep basins are needed (Euro-Argo ERIC, 2017; Siiriä et al., 2020). Floats should work in the Bornholm Basin, Gdańsk Basin, Gotland Deep, Northern Baltic Proper, Bothnian Sea and Bothnian Bay (Figure 2).

The problem we experience in the southern part of the Baltic Sea is the fast drift of floats. The device deployed in the Bornholm Basin (WMO 3902110), within a few months, passes through the Slupsk Channel to the Gdańsk Basin. Here, the float usually makes several anticyclonic loops, and after next drifts northward to the Eastern Gotland Basin. In this region, the float remains longer time (Figure 3, red dots). To limit the movement of floats between basins, they can be recovered and redeployed. However, this is a quite costly and time-consuming procedure. Therefore, it was decided to test the 'bottom parking' technique, which could solve these problems.

A typical float in the deep ocean (core Argo), between the performing of profiles with a frequency of 10 days, drifts at the so-called 'parking depth', usually 1000 m. Contact with the bottom is avoided. Such a float can work for up to 5 years; after the batteries are used up, the float sinks. With a measurement frequency of 10 days, a standard core Argo can perform up to 180 profiles to a depth of 2000 m. In the shallow and small Baltic Sea, the frequency of measurements could and should be increased. During the Baltic missions, we used different measurement frequencies, from 6 hours to 5 days. Finally, we experimentally established a profiling period of 2 days and a parking depth of 40—50 m, as optimal for monitoring needs. These parameters can be changed during the ongoing mission. If the float uses a two-way Iridium transmission, it allows us to change the setting of the float during its lifetime. Contrary to the ocean, in the shallow Baltic (average depth 55 m), it is impossible to avoid contact of the float with the bottom. Initial concerns about the possibility of the floats getting stuck in the sediments did not come true (Walczowski et al., 2020). That is why we decided to test settings that force the float to stay on the bottom between profiles. It was assumed that this would reduce the drift of the device and allow measurements to be made in a limited body of water.

Another technique of using a free-floating device for measuring in a limited area is used by seaglider operators. Appropriate piloting of the device allows for profiling the water column in an area with a limited diameter. The size of this region is strongly dependent on the dynamics of the ocean. This use of a glider is referred to as a 'virtual mooring' because it can provide data similar to data with a mooring anchored to the bottom (Nakamura et al., 2007; Rudnick et al., 2004). Japanese oceanographers even used the technique of leaving the glider at the bottom for a certain period and resuming measurements (Asakawa et al., 2016). The main difference between gliders and Argo floats is that the control of the glider is possible by changing its buoyancy, centre of gravity, or lifting surfaces, whereas with Argo floats, we only can adjust their buoyancy. When moving up or down due to the change in buoyancy, the glider can 'glide' in a horizontal direction. This movement can be controlled by the remote operator. The movement of the Argo is controlled only in the vertical direction, and horizontally the device drifts with the moving water. The name 'virtual mooring' in the case of Argo does not mean the same thing as in the case of a glider, but it seems to be the most appro-

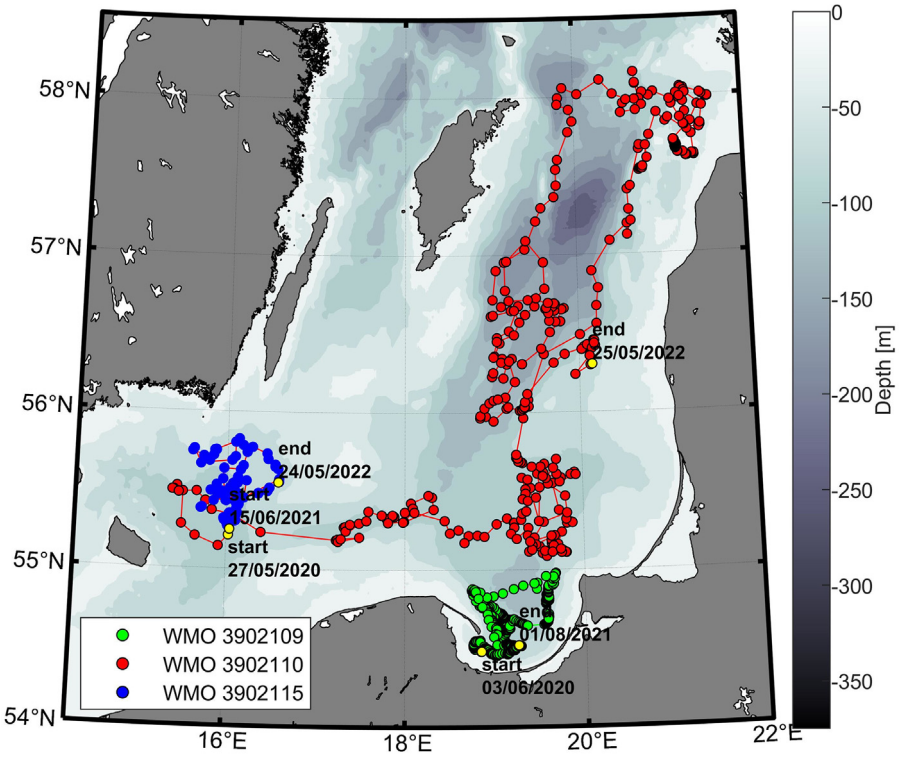

Figure 3 Trajectories of three Argo floats: red dots — typical trajectory of the float deployed in the Bornholm Basin, green dots — 'virtual mooring' in the Gdańsk Basin, blue dots — 'virtual mooring' in the Bornholm Basin.

priate. To limit the drift of the floats in the time between measurements, the parking depth was set higher than the maximum depth of the reservoir. This caused the float to 'anchor' to the bottom and minimise drift.

Experiments aimed at holding a float in a limited area of the Gotland Deep (WMO 6902014, 6902019, 6902020) were previously performed by Finnish oceanographers (Siiria et al., 2018). In contrast to the attempts described in this article, the contact of the float with the bottom was avoided for fear of getting stuck. The position of the float in a limited body of water was maintained by anticyclonic bottom circulation. These tests also gave a positive effect, but the float operated in a much larger area of the Gotland Deep, as in our experiments. The authors conclude that measurements in a circle with a radius of 40 km give a valuable time series for the needs of analyses of seasonal variability of the Baltic Sea basin under study.

3. Data and methods

The first float used as a 'virtual mooring' was deployed by IOPAN in June 2020. Float WMO 3902109 (Figure 3, green dots) worked from 03 June 2020 to 01 August 2021. The measurement region covered the Gdańsk Basin, and all measurements were located within a circle with a radius of 30 km (Figure 4). Initially, profiling was performed every 12 hours, and from 20 August 2020 (profile no. 153) the frequency was changed to once a day.

The float did not stay in one place; apparently, the anchorage to the bottom was not strong enough. The average drift velocity between measurements was 1.36 cm s^{-1}. However, there have been a few episodes where there have been one-time rapid movements of the float, even at a speed of 14.9 cm s^{-1} on February 25 and 12.9 cm s^{-1} on March 15 (marked in Figure 4 as green asterisks). In the period 19 May—2 June, there was a quick transfer of the float from the western to the eastern part of the Gdańsk Deep (marked in Figure 4 as yellow asterisks). The maximum speed reached 9.8 cm s^{-1}. Although significant one-time displacements in February and March could be attributed to fishing activities, the longer period of increased float velocity in May/June was likely caused by natural factors. However, the speed of the floats is better characterised by the median, which is 0.84 cm s^{-1}. Both the mean and median for this float are much lower than for free-drift floats (WMO 3901110), which are 21.4 cm s^{-1} and 13.1 cm s^{-1}, respectively.

The systematic measurements lasted for more than a year, and the float performed 500 CTD profiles. Data have been subjected to Real-Time Quality Control (RTQC) used for Argo floats in general (Wong et al., 2022) and Delayed-Mode Quality Control (DMQC) specific to hydrographic conditions in the Baltic Sea (Klein et al., 2022). Only the profiles collected during the float's ascent were used for further processing. The temperature and salinity values were averaged at intervals (Figure 5). Processed data made it possible to reconstruct the annual cycles of temperature and salinity at various depths.

High seasonal variability of temperature in the upper layer was observed (Figure 5). The salinity of the upper layer was less variable; low salinity, below 6.0 observed during the initial phase of the measurements, was due to the

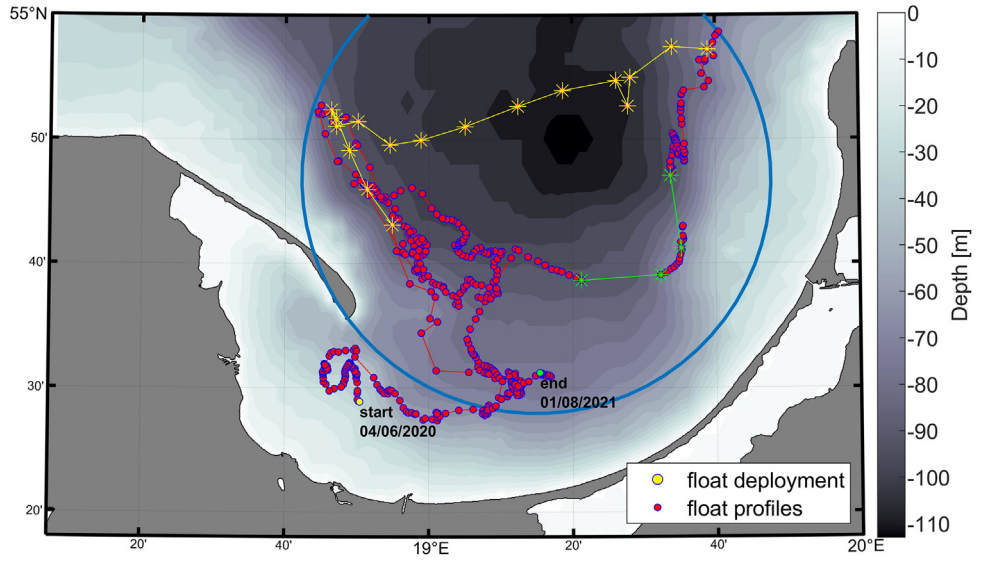

Figure 4 Region of measurements performed by the first Argo 'virtual mooring' in the Baltic Sea.

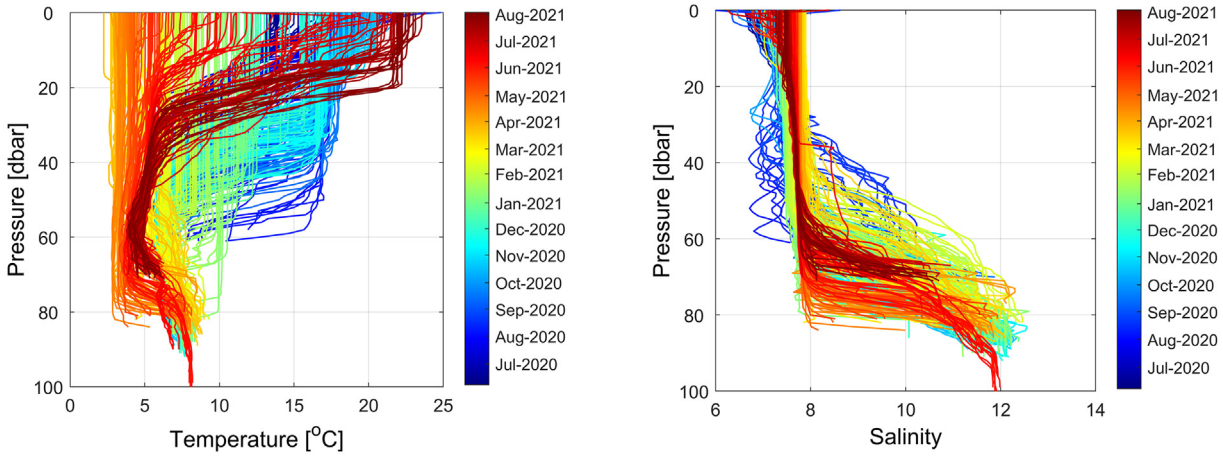

Figure 5 Temperature (left) and salinity (right) profiles performed by the WMO 3902109 float. The colour bar indicates the time of measurements.

deployment of the float in an area influenced by the waters of the Vistula River. Therefore, data obtained in the shallowest part of the Gulf of Gdańsk were excluded from further analysis. Not all the observed changes were due to seasonal variability. Measurements were not made at one point, which is important in an environment with such strong gradients, both horizontal and vertical. However, the collected data may characterise the average properties of a given body of water.

The success of virtual mooring in the Gdańsk Basin meant that the next Argo float launched as part of the Argo-Poland project in the Bornholm Basin, the parking depth was also set below the depth of the reservoir. Float 3902115 was launched on June 15, 2021 in the Bornholm Basin (Figure 6). Such settings were primarily implemented to prevent the float from passing over the Slupsk Sill and subsequently drifting to the Gdańsk Basin. The float was deployed on 15 June 2021 and recovered in February 2023, so even longer semi-homogeneous time series were obtained. All analysed measurements are contained within a circle with a radius of 40 km (Figure 6). The CTD data were processed and presented in the same way as for the 3902109 float (Figure 7). Due to the float's presence in shallower waters, there is a gap in the time series for the analysed 60—70 meter layer between February and August 2022.

To obtain more representative results, the temperature and salinity were averaged in layers every 10 m. Based on these data, time series of temperature and salinity for various layers were constructed for both study areas. Both time series cover more than two and a half years, from July 2020 to January 2023 and overlap in summer 2021. Although these are results from different regions, it was decided to present them in one figure (Figure 8). This makes it possible to track seasonal changes in temperature and salinity in the South Baltic Sea over a longer period. For simplicity, we present only the results for the temperature of the three layers. While the surface layer of 0 to 10 m represents changes occurring in the upper layer of the studied

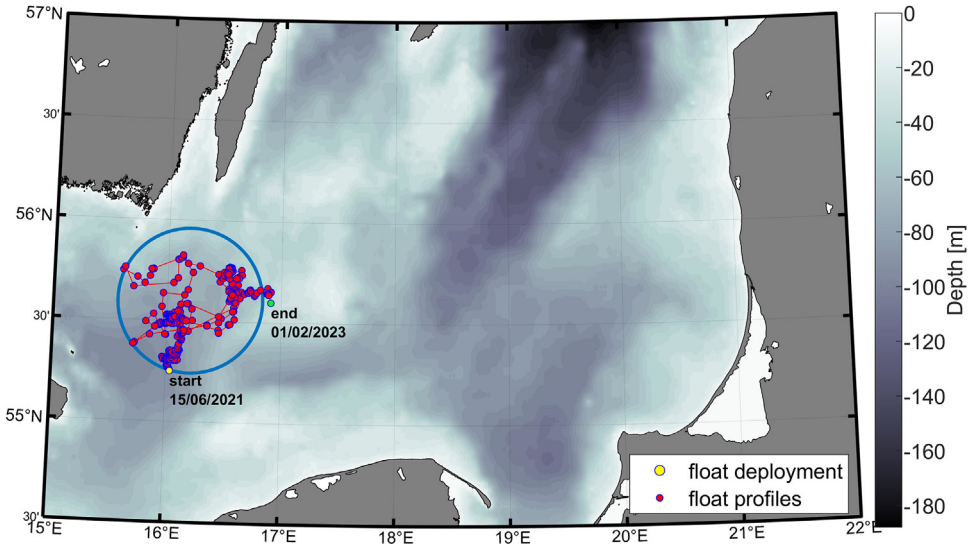

Figure 6 Region of measurements performed by the second Argo 'virtual mooring' in the Baltic Sea.

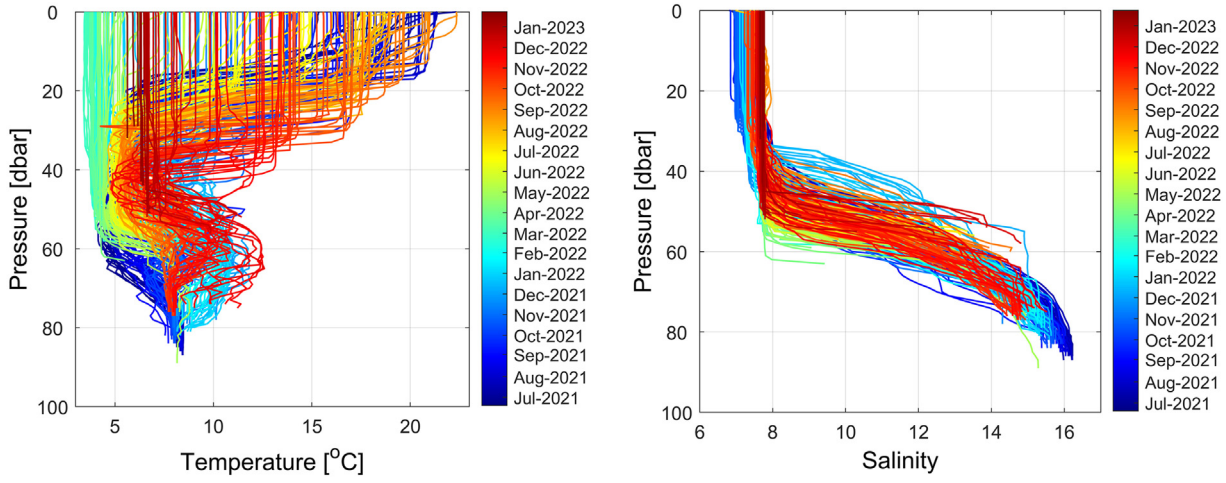

Figure 7 Temperature (left) and salinity (right) profiles performed by the WMO 3902115 float. The colour bar indicates the time of measurements.

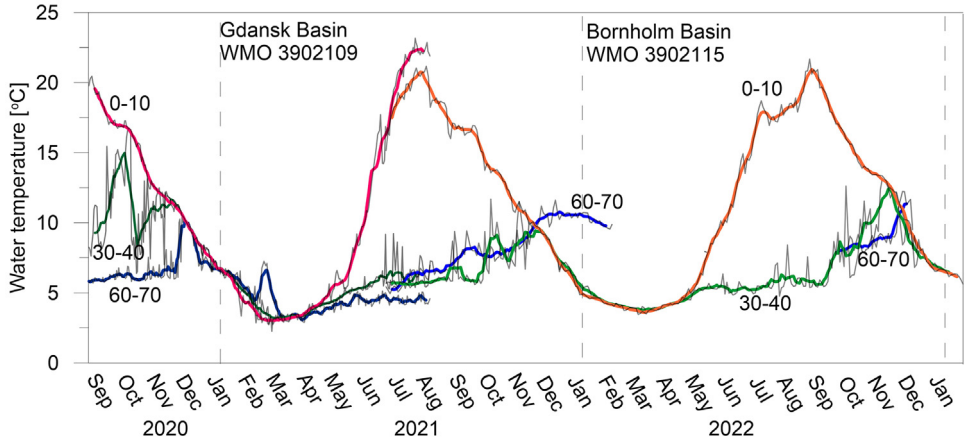

Figure 8 Time series of raw (black, thin lines) and smoothed by 13 days of moving average filter (colour lines) temperatures at various levels in the Gdańsk Basin (2020—2021, float WMO 3902109) and Bornholm Basin (2021—2022, float WMO 3902115).

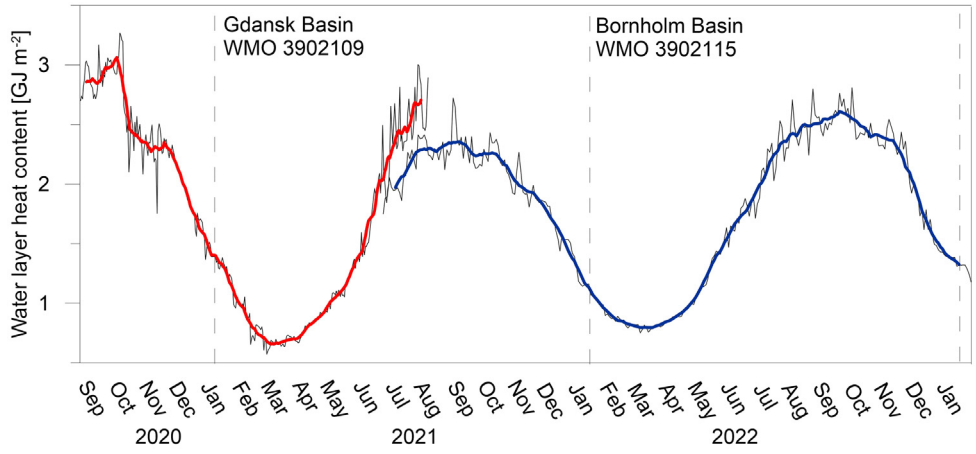

Figure 9 Time series of the 0—50 m water column raw (grey lines) and smoothed by 13 days moving average filter (colour lines) of heat content [GJ m^{-2}] for the Gdańsk Basin (2020—2021, float WMO 3902109, red line) and Bornholm Basin (2021—2022, float WMO 3902115, blue line).

water bodies, the 60—70 m layer shows changes in deep waters, below the halocline. A 30—40 m was chosen between them. Here, we call it the 'transitional layer' although the transitional layer boundaries are variable, between 30 and 60 m (Rak and Wieczorek, 2012). The time series thus obtained were smoothed with a moving average filter with a time step of 13 days. It allows for filtering out short-term temperature changes induced by dynamic processes occurring in the sea. Based on these comprehensive temperature data, the water column heat content (HC) was also calculated: $HC = A \int \rho_w \, c_p^w T_w dz$, where HC is a heat content in a water column of area A and depth z, ρ_w the water density, c_p^w the specific heat of water and T_w water temperature. HC were calculated in reference to temperature 0°C. The determination of HC changes enables the calculation of heat fluxes between the water and the atmosphere for the investigated region: $Q = \frac{dHC}{dt}$, where t is time. To avoid the effect of advection from the North Sea on the lower layers, and to compute seasonal changes, HC was calculated for the mixed layer 0—50 m (Janecki et al., 2022; Rak and Wieczorek, 2012). As in the case of temperature, the results from both basins are presented in one figure (Figure 9). These time series have also been smoothed with a moving average filter with a time step of 13 days, which allows for a better exposure of seasonal changes.

4. Results

In both the Gdańsk Basin and the Bornholm Basin the most significant seasonal temperature variability occurs in the upper layer (Figure 8). In the Gdańsk Basin, during the study period, the temperature in the upper 0—10 metre layer ranged from 2.25°C on February 19, 2021, to 23.17°C on July 17, 2021. The greatest short-time difference in average temperature for profiles taken within a 24-hour interval was 1.85°C, with a profile distance of 0.3 km. In the Bornholm Basin, the mean temperature on the 10-meter thick surface layer varied from 3.55°C on February 27, 2022 to 21.67°C on August 20, 2022. The course of the surface temperature averaged in the 0—10 m layer has a sinusoidal shape in both cases. The mean salinity in the 0—10 metre layer of the Gdańsk Basin was 7.44, with variations between 6.80 and 7.90. In the Bornholm Basin, the mean salinity for the same layer was 7.50 and ranged from 6.84 to 7.77. In both basins, no distinct seasonal cycle of surface salinity was observed.

On the other hand, the temperature courses for the 30—40 m are much more complicated, especially in the case of the transitional layer in 2020 for the Gdańsk Basin. The temperature varies from 2.74°C to 17.62°C, with temperature differences between consecutive measurements reaching up to 8°C. For example, from measurements taken with a 24-hour interval on October 2 and October 3, 2020, the average temperatures of the transitional layer were 16.51°C and 8.83°C, respectively. The distance between the profiles was only 1.2 km. These abrupt temperature changes are likely caused by vertical movements of the thermocline. For the same layer in the Bornholm Basin, the temperature ranges from 3.59°C to 13.17°C. The largest recorded difference in average temperature amounts to 6.3°C, observed in measurements taken 1.3 kilometres apart and with a 48-hour interval (September 29—October 1, 2021). In both basins, in December, there is a homogenisation of the water column between the surface and transitional layers, and the temperature in both layers becomes equal. Similarly to the surface layer, the salinity in the transitional layers of both basins does not exhibit seasonal variability. In the Gdańsk Basin, the mean salinity was 7.65, ranging from 6.95 to 8.36, while in the Bornholm Basin, the average salinity was 7.72 and varied between 7.30 and 8.74.

Changes in the temperature of the deep waters in both basins are not seasonally dependent. At these depths, the primary mechanism influencing the physical properties is the advection of saltwater from the North Sea. The temperature is primarily influenced by the season in which the inflow occurs (Rak and Wieczorek, 2012). In the Gdańsk Basin, the average temperature of the 60—70 metre layer ranges from 2.83°C to 10.18°C. In this layer as well, strong spatiotemporal temperature gradients can occur. For example, the difference between the measurements taken on

November 22 and November 25, 2022, which were 1.7 kilometres apart, amounted to 4.04°C. In the Bornholm Basin temperature at 60—70 metre layer ranges from 4.95°C to 12.24°C. The average salinity for this 60—70 metre layer in the Gdańsk Basin is 8.76 and varies from 7.68 to 11.51. The average salinity for the same layer in the Bornholm Basin is considerably higher, 13.52, with variations ranging from 11.49 to 15.01.

During winter, the upper and transitional layers cool down to the extent that a temperature inversion occurs between these layers and the deep layer; the bottom layer is warmer than the surface and transitional layers. In the Bornholm Basin, the temperature inversion is much stronger than in the Gdańsk Basin. This is the effect of the advection of warm salty waters from the North Sea. While the temperature in the surface and transitional layers varies with the seasons, it remains season independent in the deep layer and decreases during the advection of salty water to the east (Rak and Wieczorek, 2012).

HC for a layer of 0—50 m also exhibits a sinusoidal waveform. In the Bornholm Basin, both summer HC and seasonal HC changes are smaller than in the Gdańsk Basin (Figure 9).

By utilising changes in the heat capacity of the water column over time, it becomes feasible to estimate the heat balance at the water's surface with some approximation. In the initial approximation, we assume that alterations in heat capacity primarily stem from the balance of solar radiation, long-wave radiation, latent and sensible heat, while disregarding the influences of advection and vertical exchanges with deeper layers. We also assume that the obtained time series is representative of a given area. To change the smoothed HC for the layer of 0—50 m in the Gdańsk Basin during 156 days, from a maximum of 3.063 GJ m^{-2} that occurred on 2 October 2020 to a minimum of 0.568 GJ m^{-2} (6 March 2021), mean fluxes between water and the atmosphere are −178.0 W m^{-2}. In the Bornholm Basin, during 166 days between 15 October 2021 (2.261 GJ m^{-2}) and 9 March 2022 (0.801 GJ m^{-2}) mean fluxes are lower, on the order of −117.3 W m^{-2}. Unfortunately, the measurements do not overlap during this period, and it is still difficult to determine whether this is due to the specificity of the basins or the exceptionally warm summer of 2020.

The results of the sea surface energy balance obtained from the SatBaltyk model for these periods are not significantly different from the results obtained from Argo measurements. According to the model for the period from 2 October 2020 to 6 March 2021 in one model grid in the Gdańsk Basin, the average daily energy balance (solar and long-wave radiation plus latent and sensible heat) is −176.3 W m^{-2}, the median is −158.3 W m^{-2}. For the Bornholm Basin, the average daily surface energy balance for the period from 15 October 2021 to 9 March 2022 is −136.7 W m^{-2}, and the median is −119.0 W m^{-2}.

5. Discussion and conclusions

In the southern Baltic Sea region, two experiments were conducted using Argo floats that function as 'virtual moorings'. The mission settings aimed to significantly reduce the drift of the float and enable the float to remain within the confines of a single Baltic Sea basin. We believe that such a limitation is highly beneficial. Previous analyses have shown that for monitoring the Baltic Sea using Argo floats, it is necessary to place at least one float in each basin (Euro-Argo ERIC, 2017; Siiriä et al., 2020). It is much easier to meet this criterion when the floats do not move between basins. Additionally, maintaining the float within a single basin simplifies DMQC of its data. This is because substantial horizontal salinity gradients and the resulting variations in water properties in different basins require the use of distinct DMQC criteria for each basin. Finally, confining the float to a specific area enables the acquisition of extensive time series data from the studied region.

Experiments conducted by Finnish oceanographers (Siiria et al., 2018) have already shown the possibility of confining the profiling area of an Argo float to a single basin. However, the free-drifting Argo float's speed was significantly higher. For the calculations, the average daily drift of the Finnish float was estimated to be 3 km. In our case, the average daily drift of the float is 1.19 km in the Gdańsk Basin and 1.43 km in the Bornholm Basin. These averages encompass periods of abrupt float displacement, likely caused by fishermen's activities. The median daily displacement for the Gdańsk Basin and the Bornholm Basin is 0.73 km and 0.50 km respectively. Thus, experiments conducted in the Gdańsk and Bornholm basins have demonstrated the possibility of constraining the drift of Argo floats and maintaining them within one basin for an extended period. A comparison of the 'virtual mooring' (WMO 3902115) and free-floating (WMO 3902110) velocities illustrates this effectively (Figure 10).

The data obtained from virtual moorings can significantly enrich our knowledge of the studied environment. Although there are numerous studies on the temporal and spatial variability of sea surface temperature (SST), far fewer describe changes throughout the entire water column, primarily due to the limited availability of data. However, climate changes affect the entire water column (Stockmayer and Lehmann, 2023). The temperature trends show a three-layer (surface, intermediate, and bottom) pattern with fast warming at the surface (Dutheil et al., 2022). However, individual studies differ in terms of the value of the warming trend, especially in the bottom layer.

The spatiotemporal variability of the physical fields of the Baltic Sea is substantial. Therefore, the need for measurements with high spatial and temporal resolution has been emphasised before (Karlson et al., 2009). Measurements taken by vessels at the same location, even every month, can provide a distorted representation, given that the temperature in the measured water column can change by several degrees within a single day.

In shallow and shelf waters, Eulerian methods, such as buoys or measurement platforms anchored to the seabed, are good solutions. Time-series data from such systems are also collected in the Baltic Sea. A prime example is the monitoring network of three autonomous measurement stations, known as the Marine Environment Observation Network (MARNET), established and operated by the Leibniz Institute for Baltic Sea Research Warnemünde (IOW) (https://www.io-warnemuende.de/marnet-en.html). Providing near-real-time data on meteorological conditions, water temperature

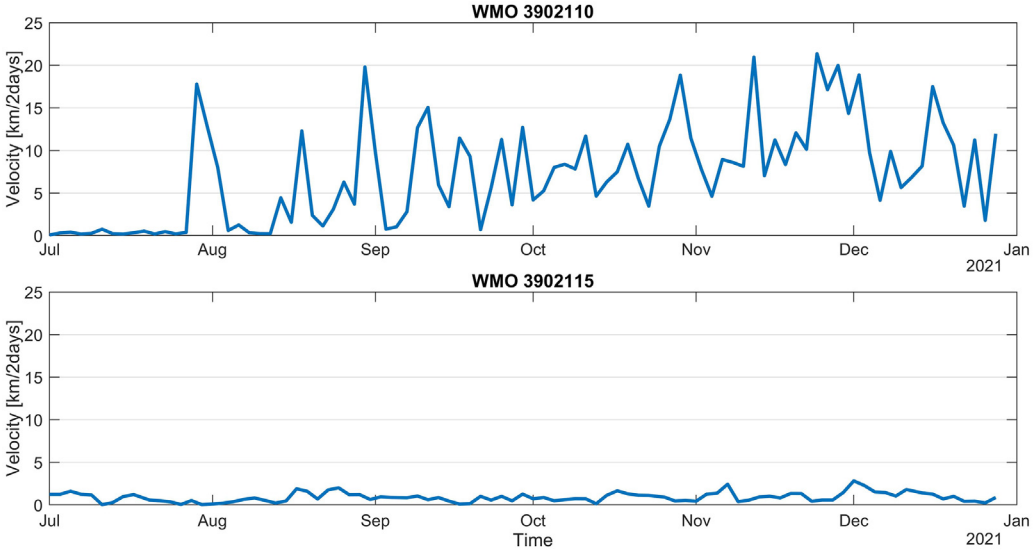

Figure 10 The velocity of the free drifting float WMO 3902110 and 'virtual mooring' WMO 3202115 at the same time.

and salinity at various levels, and other information (dissolved oxygen concentration in water, ocean currents), it offers invaluable insights into processes occurring in the western part of the Baltic Sea. However, these technologies are costly, the measuring devices are heavy and require secure anchoring to the seabed.

For some time, profiling devices have also been used. These are installed on seabed winches, deploying a set of sensors on a platform or profiling instruments moving along a tight line. The Gotland Deep Environmental Sampling Station (GODESS) was launched by IOW oceanographers in the Eastern Gotland Basin for the first time in 2010 (Prien and Shultz-Bull, 2016). Profiles are taken between depths of 180 m and 30 m. Estonian oceanographers also employ profiling instruments. In the summers of 2009—2012, an autonomous profiler in the central part of the Gulf of Finland recorded vertical profiles of CTD, Chl *a* and fluorescence in the water column from 2 to 50 m with a temporal resolution of 3 hours (Lips et al., 2016). A bottom-mounted profiler was also intermittently used in the vicinity of Keri Island in the Gulf of Finland in 2016—2017 (Stoicescu et al., 2019). It collected environmental data between 4 and 100 m, and pre-processed data were stored in the device memory. Similarly, in the southern Baltic Sea, profiling devices have been successfully applied (Rak et al., 2020). A profiler deployed by the Institute of Oceanology, Polish Academy of Sciences in collaboration with the Institute of Oceanology, P.P. Shirshov Russian Academy of Sciences at the eastern slope of the Slupsk Sill operated for a year, from May 2016 to May 2017. The Moored Aqualog System (Ostrovskii et al., 2013) collected data from a depth of 15 m to 68 m (3 m above the seabed) with a frequency of 3 hours. Unlike previous devices, Aqualog is powered by an electric motor and moves along a taut line held by a subsurface float.

Vertical profilers provide high-resolution data but in most cases do not reach the surface. The main drawback of profilers is that they typically do not provide real-time data. Data are stored in the device's memory and retrieved after recovery.

Gliders are also used in the Baltic Sea. Gliders operating in virtual mooring mode have been used as well (e.g., Karstensen et al., 2014). These measurements are available in real-time but typically do not have a monitoring character; glider missions are typically oriented toward studying processes and involve the collection of short time series data. Furthermore, the operation of gliders requires the supervision of highly qualified pilots.

Argo floats do not possess these features. They are relatively inexpensive, perform profiles to the surface, transmit data in near-real-time, and do not require continuous monitoring. Furthermore, the range of properties measured by Argo floats increases (Argo Biogeochemical). Hence, the use of floats for monitoring the Baltic Sea is of great significance. The time series obtained from both floats that worked as virtual moorings provided valuable material for the analysis of the hydrography of the basins. There are no such long, high temporal resolution time series of measurements from the entire water column of the investigated basins.

The data obtained from Argo used as a 'virtual mooring' can be a valuable dataset for the analysis of various aspects of the hydrology of the basin. The work focused mainly on the analysis of the temperature and heat content. Oceans are an essential element of the Earth's climate system, which generally mitigates climate. In the current Anthropocene period, it also mitigates the effects of anthropogenic warming. The Baltic Sea is a shallow body of water and, as such, it is even more vulnerable to changes resulting from human activities. However, it may constitute a certain buffer that mitigates these changes. For these reasons, systematic observation of changes in the thermals of the Baltic Sea basins is extremely important. Monitoring cruises providing data 4—5 times a year are not enough; observations with a much greater temporal resolution are needed. Argo measurements show that the temporal and spatial variabil-

ity of the observed fields of temperature, salinity, or other properties of seawater is very high (especially in the Baltic Sea), and to correctly determine the average properties of the basin and their temporal variability, we need much more data. Such data are provided by satellite observations, but they do not extend deep into the water column. Therefore, the use of Argo floats with the possibility of 'parking at the bottom' may be of great importance in future observations of the shallow seas.

Declaration of competing interest

The authors declare that they have no known competing financial interests or personal relationships that could have appeared to influence the work reported in this paper.

Acknowledgements

This publication was supported by the following projects: The Argo-Poland project funded by the Polish Minister of Education and Science [grant number 2022/WK/04]; The Euro-Argo Research Infrastructure Sustainability and Enhancement (EA-RISE) project funded by the European Union's Horizon 2020 research and innovation programme [grant agreement No 824131]; CSI-POM, financed from the state budget under the Polish Minister of Education and Science programme entitled "Science for Society" No. NdS/546027/2022/2022; SufMix, financed by the National Science Center, the OPUS 17 programme, contract no. UMO-2019/33/B/ST10/02189. We would also like to thank the crew of the r/v *Oceania* for their support and help at sea.

References

Asakawa, K., Nakamura, M., Maeda, Y., Hyakudome, T., Ishihara, Y., 2016. Development of underwater glider for long-term virtual mooring: Aiming 6,000 m depth with ceramic housing. Techno-Ocean, Kobe, Japan, 419—424. https://doi.org/10.1109/Techno-Ocean.2016.7890690

Christensen, O.B., Kjellström, E., Dieterich, C., Gröger, M., Meier, H.E.M., 2022. Atmospheric regional climate projections for the Baltic Sea region until 2100. Earth Syst. Dynam. 13 (1), 133—157. https://doi.org/10.5194/esd-13-133-2022

Davis, R.E., Webb, D.C., Regier, L.A., Dufour, J., 1992. The Autonomous Lagrangian Circulation Explorer (ALACE). J. Atmos. Oceanic Technol. 9, 264—285. https://doi.org/10.1175/1520-0426(1992)009⟨0264:TALCE⟩2.0.CO;2

Desbruyères, D., McDonagh, E.L., King, B.A., Thierry, V., 2017. Global and full-depth ocean temperature trends during the early twenty-first century from Argo and repeat hydrography. J. Clim. 30 (6), 1985—1997. https://doi.org/10.1175/JCLI-D-16-0396.1

Dutheil, C., Meier, H.E.M., Gröger, M., Börgel, F., 2022. Warming of Baltic Sea water masses since 1850. Clim. Dynam. 61, 1311—1331. https://doi.org/10.1007/s00382-022-06628-z

Döscher, R., Meier, H.M., 2004. Simulated sea surface temperature and heat fluxes in different climates of the Baltic Sea. AMBIO 33 (4), 242—248. https://doi.org/10.1579/0044-7447-33.4.242

Euro-Argo ERIC, 2017. Strategy for the evolution of Argo in Europe, v3.2., EA-2016-ERIC-STRAT. https://dx.doi.org/10.13155/48526

Haavisto, N., Tuomi, L., Roiha, P., Siiriä, S.M., Alenius, P., Purokoski, T., 2018. Argo floats as a novel part of the monitoring of the hydrography of the Bothnian Sea. Front. Mar. Sci. 5, 324. https://doi.org/10.3389/fmars.2018.00324

HELCOM, 2013. Climate change in the Baltic Sea Area: HELCOM thematic assessment in 2013. Balt. Sea Environ. Proc. (137).

Janecki, M., Dybowski, D., Rak, D., Dzierzbicka-Glowacka, L., 2022. A New Method for Thermocline and Halocline Depth Determination at Shallow Seas. J. Phys. Oceanogr. 52 (9), 2205—2218. https://doi.org/10.1175/JPO-D-22-0008.1

Karlson, B., Axe, P., Funkquist, L., Kaitala, S., Sørensen, K., 2009. Infrastructure for marine monitoring and operational oceanography. Swedish Meteorological and Hydrological Institute.

Karstensen, J., Liblik, T., Fischer, J., Bumke, K., Krahmann, G., 2014. Summer upwelling at the Boknis Eck time-series station (1982 to 2012) — a combined glider and wind data analysis. Biogeosciences 11, 3603—3617. https://doi.org/10.5194/bg-11-3603-2014

Klein, B., Angel-Benavides, I., Siiriä, S.-M., Merchel, M., Notarstefano, G., Gallo, A., Allen, J., Marasco, M., Díaz, L., Nilsen, J.E.Ø., 2022. D2.7: A report on the adaptation of existing DMQC methods to marginal seas. Zenodo. https://doi.org/10.5281/zenodo.8366257

Laakso, L., Mikkonen, S., Drebs, A., Karjalainen, A., Pirinen, P., Alenius, P., 2018. 100 years of atmospheric and marine observations at the Finnish Utö Island in the Baltic Sea. Ocean Sci. 14 (4), 617—632. https://doi.org/10.5194/os-14-617-2018

Levitus, S., Antonov, J.I., Boyer, T.P., Baranova, O.K., Garcia, H.E., Locarnini, R.A., Mishonov, A.V., Reagan, J.R., Seidov, D., Yarosh, E.S., Zweng, M.M., 2012. World ocean heat content and thermosteric sea level change (0—2000 m), 1955—2010. Geophys. Res. Lett. 39 (10). https://doi.org/10.1029/2012GL051106

Lips, U., Kikas, V., Liblik, T., Lips, I., 2016. Multi-sensor in situ observations to resolve the sub-mesoscalefeatures in the stratified Gulf of Finland, Baltic Sea. Ocean Sci. 12 (3), 715—732. https://doi.org/10.5194/os-12-715-2016

Meier, H.M., Dieterich, C., Gröger, M., Dutheil, C., Börgel, F., Safonova, K., Kjellström, E., 2022. Oceanographic regional climate projections for the Baltic Sea until 2100. Earth Syst. Dyn. 13 (1), 159—199. https://doi.org/10.5194/esd-13-159-2022

Merchel, M., Walczowski, W., 2020. Increases in the temperature and salinity of deep and intermediate waters in the West Spitsbergen Current region in 1997—2016. Oceanologia 62 (4), 501—510. https://doi.org/10.1016/j.oceano.2020.08.001

Nakamura, M., Hyodo, T., Koterayama, W., 2007. "LUNA" testbed vehicle for virtual mooring. ISOPE International Ocean and Polar Engineering Conference (pp. ISOPE-I) https://doi.org/10.1109/Oceans-Spain.2011.6003667

Notarstefano, G., Pacciaroni, M., Kassis, D., Palazov, A., Slabakova, V., Tuomi, L., Siiriä, S., Walczowski, W., Merchel, M., Allen, J., Ruiz, I., Diaz, L., Taillandier, V., Arduini Plaisant, L., Cancouët, R., 2021. D6.1: Tailoring of the controlling and monitoring tools for operations in shallow coastal waters. Zenodo. https://doi.org/10.5281/zenodo.7101583

Omstedt, A., Hansson, D., 2006. The Baltic Sea ocean climate system memory and response to changes in the water and heat balance components. Cont. Shelf Res. 26, 236—251. https://doi.org/10.1016/j.csr.2005.11.003

Ostrovskii, A.G., Zatsepin, A.G., Soloviev, V.A., Tsibulsky, A.L., Shvoev, D.A., 2013. Autonomous system for vertical profiling of the marine environment at a moored station. Oceanology 53, 233—242. https://doi.org/10.1134/S0001437013020124

Pouliquen, S., 2018. Euro-Argo Research Infrastructure Sustainability and Enhancement. Project proposal.

Prien, R.D., Schulz-Bull, D.E., 2016. Technical note: GODESS - a profiling mooring in the Gotland Basin. Ocean Sci. 12 (4), 899—907. https://doi.org/10.5194/os-12-899-2016

Purkey, S.G., Johnson, G.C., 2010. Warming of global abyssal and deep Southern Ocean waters between the 1990s and 2000s: Contributions to global heat and sea level rise budgets. J. Clim. 23 (23), 6336—6351. https://doi.org/10.1175/2010JCLI3682.1

Rak, D., Wieczorek, P., 2012. Variability of temperature and salinity over the last decade in selected regions of the southern Baltic Sea. Oceanologia 54 (3), 339—354. https://doi.org/10.5697/oc.54-3.339

Rak, D., Walczowski, W., Dzierzbicka-Głowacka, L., Shchuka, S., 2020. Dissolved oxygen variability in the southern Baltic Sea in 2013—2018. Oceanologia 62 (4), 525—537. https://doi.org/10.1016/j.oceano.2020.08.005

Rhein, M., Rintoul, S.R., Aoki, S., Campos, E., Chambers, D., Feely, R.A., Gulev, S., Johnson, G.C., Josey, S.A., Kostianoy, A., Mauritzen, C., Roemmich, D., Talley, L.D., Wang, F., 2013. Observations: Ocean. In: Stocker, T.F., Qin, D., Plattner, G.-K., Tignor, M., Allen, S.K., Boschung, J., Nauels, A., Xia, Y., Bex, V., Midgley, P.M. (Eds.), Climate Change 2013: The Physical Science Basis. Contribution of Working Group I to the Fifth Assessment Report of the Intergovernmental Panel on Climate Change. Cambridge University Press, Cambridge, United Kingdom and New York, NY, USA.

Roemmich, D., Church, J., Gilson, J., Monselesan, D., Sutton, P., Wijffels, S., 2015. Unabated planetary warming and its ocean structure since 2006. Nat. Clim. Change 5 (3), 240. https://doi.org/10.1038/nclimate2513

Roiha, P., Siiriä, S.M., Haavisto, N., Alenius, P., Westerlund, A., Purokoski, T., 2018. Estimating currents from argo trajectories in the Bothnian Sea, Baltic Sea. Front. Mar. Sci. 5, 308. https://doi.org/10.3389/fmars.2018.00308

Rudnick, D.L., Davis, R.E., Eriksen, C.C., Fratantoni, D.M., Perry, M.J., 2004. Underwater gliders for ocean research. Marine Technol. Soc. J. 38 (2), 73—84. https://doi.org/10.4031/002533204787522703

Siiriä, S., Merchel, M., Walczowski, W., Tuomi, L., Arduini Plaisant, L., 2020. D6.4: Preliminary results of shallow coastal float operations in the Baltic Sea. Zenodo. https://doi.org/10.5281/zenodo.7104069

Siiriä, S., Roiha, P., Tuomi, L., Purokoski, T., Haavisto, N., Alenius, P., 2018. Applying area-locked, shallow water Argo floats in BalticSea monitoring. J. Oper. Oceanogr. 12 (1), 58—72. https://doi.org/10.1080/1755876X.2018.1544783

Stoicescu, S.T., Lips, U., Liblik, T., 2019. Assessment of eutrophication status based on sub-surface oxygen conditions in the Gulf of Finland (Baltic Sea). Front. Mar. Sci. 6, 54. https://doi.org/10.3389/fmars.2019.00054

Stramska, M., Białogrodzka, J., 2015. Spatial and temporal variability of sea surface temperature in the Baltic Sea based on 32-years (1982—2013) of satellite data. Oceanologia 57 (3), 223—235. https://doi.org/10.1016/j.oceano.2015.04.004

Stockmayer, V., Lehmann, A., 2023. Variations of temperature, salinity and oxygen of the Baltic Sea for the period 1950 to 2020. Oceanologia 65 (3), 466—483. https://doi.org/10.1016/j.oceano.2023.02.002

Swallow, J.C., 1955. A neutral-buoyancy float for measuring deep currents. Deep-Sea Res. 3 (1), 74—81. https://doi.org/10.1016/0146-6313(55)90037-X

Walczowski, W., Merchel, M., Rak, D., Wieczorek, P., Goszczko, I., 2020. Argo floats in the southern Baltic Sea. Oceanologia 62 (4), 478—488. https://doi.org/10.1016/j.oceano.2020.07.001

Wong, A., Keeley, R., Carval, T., Argo Data Management Team, 2022. Argo Quality Control Manual for CTD and Trajectory Data. https://doi.org/10.13155/33951

Oceanologia 66 (2024) 111—138

Available online at www.sciencedirect.com

ScienceDirect

journal homepage: www.journals.elsevier.com/oceanologia

ORIGINAL RESEARCH ARTICLE

Submarine groundwater discharge into a semi-enclosed coastal bay of the southern Baltic Sea: A multi-method approach

Cátia Milene Ehlert von Ahn[a,*], Olaf Dellwig[a], Beata Szymczycha[b], Lech Kotwicki[b], Jurjen Rooze[a,j], Rudolf Endler[c], Peter Escher[a,d], Iris Schmiedinger[a], Jürgen Sültenfuß[e], Magdalena Diak[b], Matthias Gehre[f], Ulrich Struck[g], Susan Vogler[a], Michael Ernst Böttcher[a,h,i,*]

[a] *Geochemistry & Isotope Biogeochemistry, Leibniz Institute for Baltic Sea Research (IOW), Warnemünde, Germany*
[b] *Institute of Oceanology, Polish Academy of Sciences (IOPAN), Sopot, Poland*
[c] *Marine Geophysics, Leibniz Institute for Baltic Sea Research (IOW), Warnemünde, Germany*
[d] *current address: Ecoandmore Freiburg, Germany*
[e] *Institute of Environmental Physics, University of Bremen, Bremen, Germany*
[f] *Department of Isotope Biogeochemistry, Helmholtz Centre for Environmental Research (UFZ), Leipzig-Halle, Germany*
[g] *Free University Museum for Natural History, Berlin, Germany*
[h] *Marine Geochemistry, University of Greifswald, Greifswald, Germany*
[i] *Interdisciplinary Faculty, University of Rostock, Rostock, Germany*
[j] *Department of Physical Oceanography and Instrumentation, Leibniz Institute for Baltic Sea Research (IOW), Warnemünde, Germany*

Received 28 February 2023; accepted 10 January 2024
Available online 2 February 2024

KEYWORDS
Stable isotopes;
Radium isotopes;
Acoustic survey;
Diagenesis;
Gulf of Gdańsk;
Puck Bay

Abstract The present study aims to understand the impact of submarine groundwater discharge (SGD) on a coastal area with different lithology and degrees of SGD. Sampling campaigns took place in Puck Bay and the Gulf of Gdańsk, southern Baltic Sea encompassing years between 2009 and 2021. The methodological approach combined geophysical characterization of the surface sediments with detailed spatial and temporal (isotope) biogeochemical investigations of pore and surface waters, and was supported by nearshore groundwater and river surveys. Acoustic investigations identified areas of disturbance that may indicate zones of pref-

* Corresponding authors at: Geochemistry & Isotope Biogeochemistry, Leibniz Institute for Baltic Sea Research (IOW), Warnemünde, Germany.
E-mail addresses: catia.vonahn@io-warnemuende.de (C.M. Ehlert von Ahn), michael.boettcher@io-warnemuende.de (M.E. Böttcher).
Peer review under the responsibility of the Institute of Oceanology of the Polish Academy of Sciences.

Production and hosting by Elsevier

https://doi.org/10.1016/j.oceano.2024.01.001

erential SGD release. The composition of porewater and the differences in the bay's surface waters disclosed SGD as common phenomenon in the study area. Regional SGD was estimated through a radium mass balance. Local estimation of SGD, based on porewater profiles, revealed highest SGD fluxes at the sandy shoreline, but relatively low elemental fluxes. Though SGD was low at the muddy sites corresponding elemental fluxes of nutrients and dissolved carbon exceeded those determined at the sandy sites due to intense diagenesis in the top sediments. SGD appears to be sourced from different freshwater endmembers; however, diagenesis in surface sediments substantially modified the composition of the mixed solutions that are finally discharged to coastal waters. Overall, this study provides a better understanding of the SGD dynamics in the region by a multi-approach and emphasizes the need to understand the processes occurring at the sediment-water interface when estimating SGD.

1. Introduction

Coastal regions are ecosystems subject to intense and dynamic water and elemental fluxes. In addition to surface water discharge, the role of submarine groundwater discharge (SGD) acting as a potential source and carrier of dissolved substances in the coastal ocean has attracted increasing interest from the scientific community over the last decades (Böttcher et al., 2024; Mayfield et al., 2021; Moore, 1996, 2010; Santos et al., 2021; Taniguchi et al., 2002; Zektzer et al., 1973). The term SGD covers a wide range of processes, compositions and origins, including not only the direct discharge of fresh groundwater but also a mixture with recirculated saline porewater through permeable surface sediments (Burnett et al., 2003; Church, 1996; Taniguchi et al., 2002), the quantitative contribution to the water flux across the land-sea interface belonging to the still open questions in hydrology (Blöschl et al., 2019).

The mixing between fresh groundwater and saline water promotes physicochemical and biogeochemical processes, which depend on the lithological and sedimentological boundary conditions. In addition, the composition of the solution may be further superimposed by diagenetic processes, thereby modifying associated benthic-pelagic element fluxes.

While surface estuaries provide essentially oxygenated waters to the ocean, SGD may also add anoxic waters to the coastal environment (Church, 1996; Moosdorf et al., 2021; Paytan et al., 2006; Santos et al., 2021; Slomp and Van Cappelen, 2004).

Most studies on water and elemental fluxes associated with SGD are derived from the characterization of endmembers (e.g., groundwater, rivers, and surface seawater), with less attention paid to the processes in the mixing zone. However, processes within the subterranean estuary, and particularly in the sediments overlying the aquifers can be impacted by biotic and abiotic transformations, resulting in sources and/or sinks of reactive elements (Böttcher et al., 2024; Charette et al., 2005; Froelich et al., 1979; Goyetche et al., 2022; Huettel et al., 1998; Moore, 1999; Moosdorf et al., 2021; Szymczycha et al., 2023) modifying the composition of the SGD. Ion sorption, mineral dissolution, precipitation, and remineralization of organic matter are among the processes occurring in the aquifers and along the flow path of SGD (Moore, 1999; Moosdorf et al., 2021). In addition, substrate availability, aquifer rock composition, and groundwater residence time are also of great importance. Therefore, the controls on non-conservative behavior must be understood and taken into account when estimating SGD element fluxes to coastal waters (Beck et al., 2007b; Cerdà-Domènech et al., 2017; Donis et al., 2017; von Ahn et al., 2021).

The fresh and saline components of SGD are usually well mixed, making the quantification and its impact on coastal waters complex (e.g. Sadat-Noori et al., 2016). Detection and estimation of SGD have been carried out through various approaches (Böttcher et al., 2024; Burnett et al., 2006; Taniguchi et al., 2019). For example, geophysical techniques identified fluid/gas fluxes across surface sediments (e.g., Hoffmann et al., 2020; Idczak et al., 2020); direct measurements based on piezometers and seepage meters assessed porewater gradients, and quantified SGD and the associated chemical fluxes (e.g., Donis et al., 2017; Oberdorfer et al., 2008; Tamborski et al., 2018).

Among the geochemical tracers, radium, methane, and stable isotopes have been applied in the majority of SGD studies, and the results are promising for detecting, evaluating, and quantifying SGD. For example, water isotopes allowed quantification of mixing processes, as groundwater is depleted in heavier isotopes compared to seawater (Gat, 1996; Povinec et al., 2008). The concentrations and stable carbon isotope composition of DIC, DOC, and CH_4 are powerful tracers to access the biogeochemical processes within the subterranean estuary (Böttcher et al., 2014; Donis et al., 2017; Sadat-Nouri et al., 2016; Winde et al., 2014). Radium is generally more abundant in groundwater than surface water and, therefore, can provide quantitative and qualitative information on the regional occurrence of SGD (Beck et al., 2007a; Moore, 1996, 2006; Moore et al., 2011; Rodellas et al., 2017; Taniguchi et al., 2019; Top et al., 2001; von Ahn et al., 2021).

Studies on SGD have been carried out in the Baltic Sea (e.g., Krall et al., 2017; Peltonen 2002; Purkamo et al., 2022; Purkl and Eisenhauer, 2004; Schlüter et al., 2004; Virtasalo et al., 2019; Viventsowa and Voronow, 2003; von Ahn et al., 2021), particularly in the Gulf of Gdańsk and the Puck Bay, already since the 90s (e.g., Falkowska and Piekarek-Jankowska, 1999; Piekarek-Jankowska, 1996). Dif-

ferent sites of SGD occurrence have been identified throughout the Gulf of Gdańsk and Puck Bay. They act as hot spots for SGD to the surface waters impacting to different degrees the coastal water balance and the biogeochemical cycles within the coastal waters. For example, based on seepage meters, measurement fluxes of SGD and their associated chemical fluxes were estimated for different areas in Puck Bay (Donis et al., 2017; Szymczycha et al., 2012, 2016, 2023). Furthermore, the impact of SGD on the meiofaunal community was investigated by Kotwicki et al. (2014). Donis et al. (2017) evaluated the impact of SGD on the sandy sediments of Hel Bight, Puck Bay. The impact of pharmaceuticals and caffeine via SGD on the Puck Bay surface waters was also evaluated (Szymczycha et al., 2020). A pockmark associated with SGD in the Gulf of Gdańsk was assessed by Idczak et al. (2020). Moreover, a lowered bottom water salinity was observed almost across Puck Bay, indicating an extended impact by SGD (Matciak et al., 2015).

Due to the high number of identified SGD sites along the Polish coast, this area represents a key SGD site in the Baltic Sea. Taking this opportunity, our study in the Gulf of Gdańsk and the Puck Bay evaluated the dynamics of SGD in different lithologies and the importance of the subterranean estuary on the element fluxes associated with SGD. Therefore, the objectives of the present study are 1) to evaluate the impact of SGD on the chemical gradients in surface sediments taking into account the lithology, 2) to estimate the (isotopic) hydrochemical composition of the fresh water component of SGD entering the Puck Bay compared to the possible endmembers (e.g. groundwater and river waters) around Puck Bay, and 3) to estimate the contribution of SGD to the Puck Bay based on local porewater gradients, seepage meters, and for the first time, regionally, using a Ra isotope balance.

The potential physical pathways and indicators of SGD in the central Puck Bay were characterized using acoustic methods. The investigation was further supplemented by a sedimentological and geochemical characterization of sediments under different degrees of SGD impact. Water column and porewater samples were analyzed for major and trace elements, nutrients, sulfide, total alkalinity, dissolved inorganic carbon (DIC), $\delta^{13}C_{DIC}$, methane (CH_4), $\delta^{13}C_{CH4}$, $\delta^{2}H_{CH4}$, $\delta^{2}H_{H2O}$, $\delta^{18}O_{H2O,}$ radium isotopes (^{223}Ra and $^{224}Ra_{ex}$), tritium (^{3}H) and helium (He) isotopes. This multi-method approach highlights the role of SGD in the local and regional water and elemental budgets of the coastal waters of the Baltic Sea. Finally, it provides a basis for future assessments of the hydrological and ecosystem consequences of coastal areas affected by climate change.

2. Methods

2.1. Study area

The Gulf of Gdańsk is located in the southern Baltic Sea (Figure 1). The maximum water depth is about 118 m, and the surface and bottom layer salinity are about 8 and 12, respectively. As the tidal influence is minimal in the southern Baltic Sea, small hydrodynamic of the bay is mainly due to wind and the river plume front of the Vistula River (Dippner et al., 2019). The shallower sediments of the central gulf are covered by clays that, in some places, contain fine-grained sand and silt, whereas the deepest part is dominated by clayey silt (Idczak et al., 2020; Majewski, 1990, Figure 1).

In the eastern part of the Gulf of Gdańsk, the Hel Peninsula forms a semi-enclosed basin called Puck Bay. The bay has a total area of 359.2 km^2 and is divided into two parts: the outer bay, with an average depth of 20.5 m, and the inner bay, a markedly shallower part, called the Puck Lagoon, with an average depth of 3.1 m (Matciak et al., 2011), covering an area of 104 km^2 (Kramarska et al., 1995).

The outer Puck Bay comprises diverse sediments with coarse-grained sands dominating to a depth of about 20 m. Fine sands, silts, silt-clay, and sand-silt-clay are the composition in the deepest parts, and in addition, some sandy beaches, gravel beds, stony outcrops, clay cliffs, and vegetated river mouths are found (see Kłostowska et al. (2019) and references therein, Figure 1). Sediments in the inner part of Puck Bay have a relatively constant grain distribution dominated by fine and medium sands (Figure 1).

Puck Bay is the main drainage area of Cretaceous, Tertiary, and Quaternary aquifers. It affects the direction of the groundwater flow, thereby modeling the groundwater regime of the piezometric groundwater surface. Groundwater flows into the bay occur mainly via seepage through the seabed. The Hel Peninsula also receives groundwater from Holocene aquifers, but these flow directly into the Baltic Sea (see Piekarek-Jankowska (1996) and references therein).

Different areas along the Puck Bay coastline show impact by SGD (e.g., Donis et al., 2017; Kotwicki et al., 2014; Kłostowska et al., 2019; Szymczycha et al., 2012, 2020, 2023), and the present study is both, an initiation and continuation of these studies by applying new approaches. The investigated SGD sites are Hel, Chałupy, Swarzewo, and Osłonino (Figure 1).

2.2. Material and methods

2.2.1. Sampling and sample preparation

The sampling campaigns were carried out in 2009—2011, 2019, and 2021. Fresh groundwater from wells and piezometers, river water, porewater, sediments, and surface water from the Puck Bay, the Gulf of Gdańsk, and the coastal Baltic Sea were sampled (Figure 1). Additional information on the sampling sites is given in Supplementary Table 1.

The outer Puck Bay water column was sampled at 16 sites in June 2009 onboard r/v *Professor Albrecht Penck* (07PE0919) using a conventional CTD and a pump CTD system (Strady et al., 2008) both equipped with a free-flow bottle rosette. In October 2019 surface waters were sampled onboard the r/v *Oceania* at 40 sites (0.5 m), including the central Gulf of Gdańsk and the coastal Baltic Sea, using a pump attached to the vessel. In addition, bottom water was sampled at four sites using Niskin bottles.

Surface water sampling in the inner Puck Bay was done in October 2019 using a rubber boat and in June 2021 using a sailing boat. Water samples were taken via PE syringes and filtered with 0.45 μm cellulose acetate disposable filters (Carl Roth, Karlsruhe, Germany). For Ra isotopes, 100—150 liters of surface water were pumped through a 1 μm

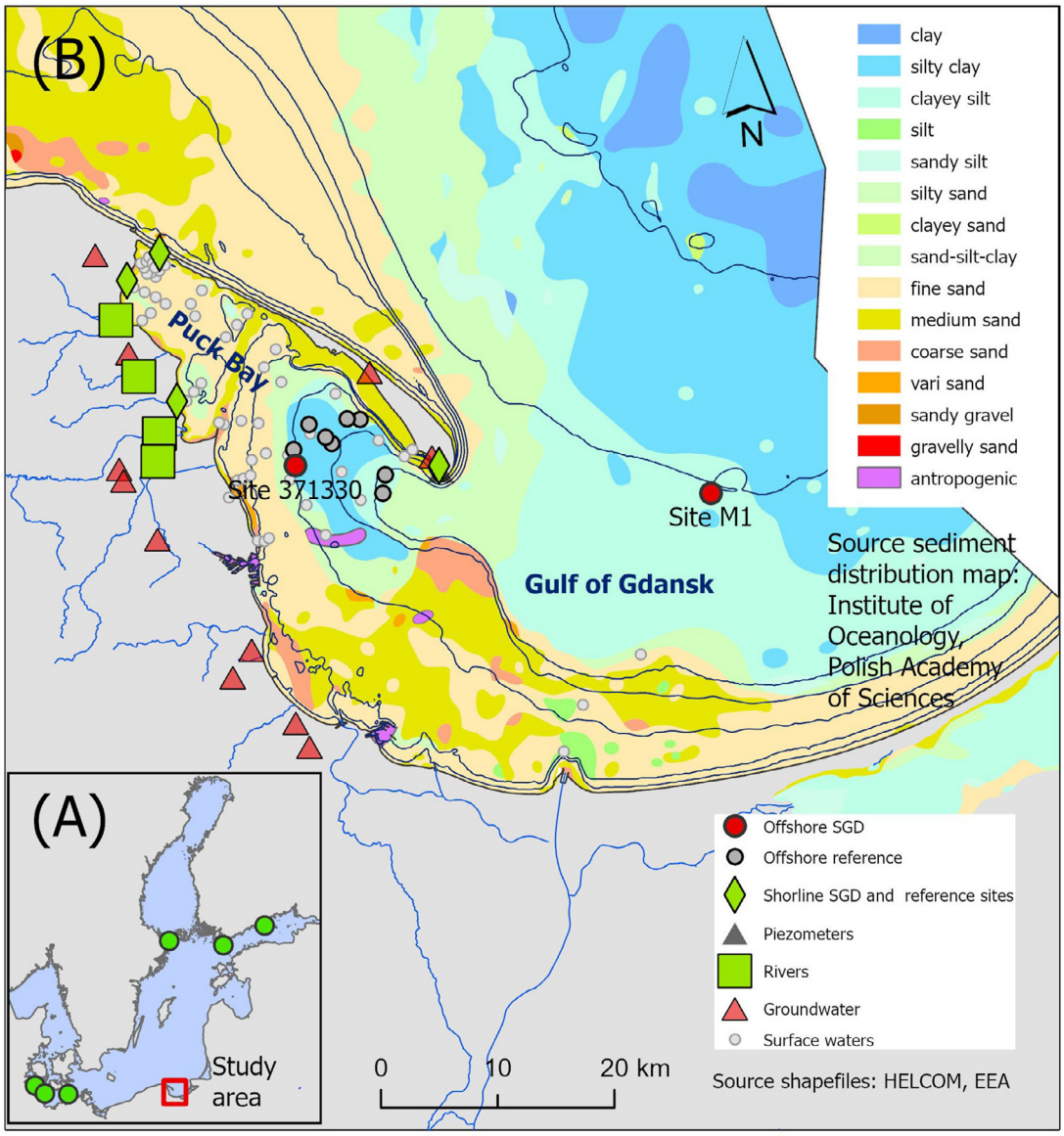

Figure 1 (A) Map showing the location of the study area (red dot) and some of the SGD investigated sites along the Baltic Sea (green dots — Jurasinski et al., 2018; Krall et al., 2017; Purkamo et al., 2022; Racasa et al., 2021; Schlüter et al., 2004; Virtasalo et al., 2019; Viventsova and Voronov, 2003; von Ahn et al., 2021). (B) Map of the study area in the Gulf of Gdańsk/Puck Bay showing the different sampling sites (surface waters, porewater, groundwaters, and rivers). Source of the shapefiles: *European Environmental Agency* (EEA, 2024) *and HELCOM* (HELCOM, 2024) *database*, Atlas of Polish marine area bottom habitats (2009), Environmental valorization of marine habitats (2009) Institute of Oceanology PAS. (The sediment distribution map (modified) was added as a background for a rough overview of the sediment composition of the study area. The map is not georeferenced to the sampled sites.)

filter into barrels. By using a submersible pump, the filtered water from the barrels was pumped through manganese-coated acrylic fibers (Mn-fiber) at a flow rate of around 1 L min^{-1} to quantitatively extract the Ra isotopes. The fibers were washed to remove salt and partially dried for measurements (Garcia-Solsona et al., 2008).

During the cruise in June 2009, sediment cores were retrieved from five sites by a multi-corer device (sites: 371370, 371290, 371330, 37160, 371270), and in October 2019, four sediment cores were retrieved using a GEMAX corer (sites M2, 12M, 15M, 13M) in the outer Puck Bay (Figure 1). In addition, one sediment core was taken in the central Gulf of Gdańsk in 2019 (Site M1). These sites are referred to as offshore sites in this study.

Sediment cores were sliced and frozen for further geochemical analysis. Porewater was extracted from a parallel core via 0.1—0.2 μm rhizons (Rhizosphere Research — Wageningen, The Netherlands; Seeberg-Elverfeldt et al., 2005) and stored in cold or frozen for geochemical analyses. Salinity and pH were measured in situ using a refractometer and handheld pH meter.

Sampling campaigns along the coastline at Hel took place in September and November 2009, March, May, and October 2010, and June 2021. Chałupy, Swarzewo, and Osłonino

were only sampled in June 2021. These sites are referred to as shoreline sites in this study.

Along the shoreline of Puck Bay, porewater was extracted during the campaigns between 2009 and 2011 via pre-established porewater samplers (Donis et al., 2017). During the 2019 and 2021 campaigns, porewater was extracted via push point lances (MHE products) using PE syringes and filtered with 0.45 μm cellulose acetate disposable filters (Carl Roth, Karlsruhe, Germany). For Ra isotopes, 5—10 liters of porewater were transferred into canisters without filtration by a peristaltic pump. From the canister, the sample was filtered through a Mn-fiber as described for the surface water samples from the Puck Bay cruises. Additionally, sediment cores were taken and sliced for further analysis.

Seepage meters were used to measure seepage water fluxes and collect samples for further chemical analysis from sites at Hel, Chałupy, and Swarzewo during the campaign in 2021. The seepage meter consists of a PE chamber with a surface area of 0.7 m^2 connected to a PE bag at the end. The seepage flux rate was calculated from the change in water volume in the bag as a function of time.

Groundwater was sampled in April 2009 and June 2021 from 17 wells and two piezometers at depths varying between 2 and 180 m. Six groundwater wells and two piezometers were located on the peninsula and 11 groundwater wells were located on the mainland. River water samples were collected in April 2011 and June 2021 from the Reda (0.6 km inland from the mouth) the Zagórska Struga (0.1 km inland from the mouth), the Płutnica (0.2 km inland from the mouth), and Gizdepka (0.2 km inland from the mouth). Samples were taken via PE syringe and filtered using 0.45 μm SFCA disposable filters (Carl Roth, Karlsruhe, Germany). For Ra isotopes, 60 L of river water was pumped through a 1 μm filter into barrels, and 20 L of groundwater was transferred without filtration into canisters. The sampled water was filtered from the barrels/canisters through a Mn-fiber as described above.

For the determination of total carbon (TC), total nitrogen (TN), total sulfur (TS), total inorganic carbon (TIC), and total mercury (Hg), sediment aliquots were stored in centrifuge tubes (Sarstedt) and kept frozen until freeze-drying and homogenization using an agate ball mill.

Filtrated water samples for major and trace element analysis were filled into acid-cleaned PE bottles and acidified to 2 vol.% with concentrated HNO_3. Nutrient water samples were filled into pre-cleaned PE bottles. Dissolved sulfide (H_2S) water samples were filled into PE bottles prefilled with ZnAc 5%. Porewater samples for total alkalinity (TA) were collected in PE vials prefilled with 0.1M HCl. Water samples for dissolved inorganic carbon (DIC) and $\delta^{13}C_{DIC}$ were filled without headspace into Exetainer® tubes prefilled with saturated $HgCl_2$ solution. Samples for $\delta^{13}C_{CH4}$ and $\delta^{2}H_{CH4}$ were kept closed in glass containers sealed with a butyl septum (black) and preserved with NaOH solution (Jørgensen et al., 2004). Samples for $\delta^{18}O_{H2O}$ and $\delta^{2}H_{H2O}$ analyses were collected in 1.5 mL glass vials (Zinser) sealed with PTFE-coated septum caps. Samples for ^{3}H were stored in PE bottles. For helium isotopes, samples were allowed to flow through and finally stored in head-space-free copper tubes. All samples were stored in the dark cool, or frozen until further analyses.

The diffuse Ra flux from the bottom sediments of Puck Bay was quantified following the approach outlined by Rodellas et al. (2012), using sediments from the Site Osłonino (Figure 1). The sediments were mainly composed of sand. The sediments were placed in a 3L beaker, and the overlying water was extracted and replaced with Ra-free surface water from Puck Bay (2 L). A closed loop system was assembled, and the water was continuously circulated through the tubing and the Mn-fiber. The Mn-fibers were replaced after 12, 24, 36 and 48 h. The overlying water was constantly aerated to prevent changes in redox conditions. The diffusion rate was calculated from the slope of the accumulated $^{224}Ra_{ex}$ activity (in Bq) per incubation time (h) (Supplementary Figure 2).

2.2.2. Geophysical investigations

High-resolution sub-bottom profiling using an INNOMAR SES96 Standard parametric sediment echo sounder was performed during a cruise with r/v *Professor Albrecht Penck* in 2009. A motion reference unit was used to steer/keep the acoustic beam in the vertical direction to correct the ship's vertical movements. The track plots of the acoustic profiles are shown in Supplementary Figure 1. Detailed descriptions of the SES96 echo sounder system are available at www.innomar.com. During the acoustic survey, the parametric echo sounder transmitted acoustic pulses in a very narrow sound beam with virtually no side lobes and a narrow opening angle of 4 degrees. This resulted in a sonified seafloor area of about 4 m^2 at a water depth of 30 m. The acoustic pulses were built up by a primary frequency component of 100 kHz and a selectable secondary frequency component ranging from 5—15 kHz. Only the secondary low-frequency components penetrated the sub-bottom because the seafloor sediments strongly attenuated the primary high-frequency parts of the acoustic pulses. Depending on the selected secondary frequency, a vertical resolution of sediment layers in the range of 0.2—0.5 m was obtained.

2.2.3. Geochemical analyses

Freeze-dried and homogenized sediments were analyzed for their TC, TN, and TS contents with a CHNS Elemental Analyzer (Eurovector 3000). Combustion was catalyzed by V_2O_5, and the resulting gaseous products were chromatographically separated and quantified via infrared spectrophotometry. Total inorganic carbon (TIC) was determined with an Elemental Analyzer multi-EA (Analytik Jena) after treatment with 40% phosphoric acid followed by infrared spectrophotometric quantification of CO_2. The precision of both methods for the samples from 2019—2021 was about 13, 6, 14, and 6%, and the accuracy was about 2, 12, 8, and 1% for TC, TN, TS, and TIC, respectively, using MBSS- (CNS) and OBSS (TIC) in-house reference materials. The content of TOC was calculated from the difference between TC and TIC. Total mercury (Hg) was analyzed using a DMA-80 (Milestone Microwave Laboratory Systems) analyzer by external calibration with 142R and MBSS reference materials. The detection limit was 0.15 μg kg^{-1} (Leipe et al., 2013) and the precision and accuracy of the measurement for 2019-21 was better than ± 4.5 and ±0.6%, respectively.

In the water samples, the major ions (Na, Mg, Ca, K, S) and trace elements (Ba, Fe, Mn) were analyzed by inductively coupled plasma optical emission spectrometry (ICP-

OES; iCAP 6400 Duo (before 2016), iCAP 7400 Duo, Thermo Fischer Scientific) using matrix-matched external calibration and Sc as internal standard. Precision and accuracy were checked with spiked CASS-4 and SLEW-3 (NRCC) and were better than 4 and 5% for CASS-4, and 7 and 7% for SLEW-3, respectively. In all water samples, the measured total dissolved S is considered to consist mainly of SO_4.

Concentrations of H_2S were determined by the methylene blue method (Cline, 1969) using a Spekord 40 spectrophotometer (Analytik Jena). Nutrients were analyzed using QuAAtro autoanalyzer system (Seal Analytical, Southampton, UK) following Grasshoff et al. (2009).

Total alkalinity (TA) was measured by potentiometric titration (Van den Berg and Rogers, 1987). Dissolved inorganic carbon (DIC) and $\delta^{13}C_{DIC}$ values were determined by means of continuous-flow isotope-ratio mass spectrometry (CF-IRMS) using a Thermo Finnigan MAT253 gas mass spectrometer attached to a Thermo Electron Gas Bench II via a Thermo Electron Conflo IV split interface, as described by Winde et al. (2014). Solutions were allowed to react for at least 18 h at room temperature before introduction into the mass spectrometer. The international NBS19 standard, a carbonate from Solnhofer Platternkalk, and in-house $NaHCO_3$ were used to calibrate measured isotope ratios towards the V-PDB scale. Concentrations of DIC from 2009–2011 were determined based on pH and TA values.

Values of $\delta^{18}O_{H2O}$ and $\delta^{2}H_{H2O}$ were analyzed by a laser cavity-ring-down-spectroscopy (LCRDS) system Picarro L1102-I (2009–2011 data) and Picarro L2140-I (2019–2021 data) (Böttcher and Schmiedinger, 2021; Gupta et al., 2009). Six replicate injections were performed for each sample, and arithmetic averages and standard deviations (1 sigma) were calculated. The reproducibility of the replicate measurements was generally better than 0.7‰ and 0.6‰ (2009–2011 data) and better than 0.06‰ and 0.3‰ (2019–2021 data) for oxygen and hydrogen, respectively. The reference materials SLAP and VSMOW were used to calibrate measured isotope ratios towards the V-SMOW scale. The stable isotope composition of dissolved methane in porewater was carried out at the Centre of Environmental Research (UFZ) (Tamisier et al., 2022). The given '‰' values are equivalent to mUr (Milli Urey; Brand and Coplen, 2012).

^{3}H and He isotopes (^{3}He and ^{4}He) were measured as described by Sültenfuß et al. (2009). Short-lived Ra isotopes (^{223}Ra, $t_{1/2} = 11.4$ d, and ^{224}Ra $t_{1/2} = 3.7$ d) were measured within 3 and 7 days after sampling with a radium-delayed coincidence counter (RaDeCC) (Moore and Arnold, 1996). After about a month, a further measurement was conducted to determine ^{224}Ra supported by ^{228}Th ($t_{1/2} = 1.9$ years). This measurement is then subtracted from the initial ^{224}Ra to obtain the excess of ^{224}Ra activities ($^{224}Ra_{ex}$). The activities of ^{223}Ra, ^{224}Ra, and $^{224}Ra_{ex}$ have been calculated and the expected error of the measurement is 12 and 7% for ^{223}Ra and ^{224}Ra, respectively (Garcia-Solsona et al., 2008). The detectors are calibrated once a month using ^{232}Th with certificate activities.

2.2.4. Flux calculations

Exchange fluxes between sediment and the overlying water were estimated based on measured porewater profiles. To constrain the upward porewater velocity, the salinity gradient formed by mixing fresh groundwater with seawater near the sediment-water interface was fitted. The partial differential equation

$$0 = \frac{d}{dx}\left[\left(\frac{D_m}{\tau^2} + D_e\right)\frac{dC}{dx} - uC\right] \quad (1)$$

describes the concentration profile of sodium, where u is the upward flow velocity, C is the concentration, D_m is the ionic diffusion coefficient, which was corrected for temperature and salinity, $\tau^2 = 1 - 2log\varphi$ is the tortuosity, and φ is the porosity (Boudreau, 1997). The equation does not account for the gradient in porosity, as this would require additional fitting of the porosity while it had almost no impact on the fitted advective velocities. Here, we used D_e to account for additional mixing near the sediment-water interface, which may result from currents and groundwater recirculation (Donis et al., 2017; Qian et al., 2009). This mixing coefficient was the highest value at the sediment-water interface and could be constant in a surficial layer varying between 0 and 7 cm thickness before decaying exponentially over depth.

Our approach was to set D_e to zero when mixing in the top was not apparent and generally used low values, leading to conservative estimates of the upward porewater velocities and submarine groundwater discharge. The bottom-water sodium concentration was used as the upper boundary condition. A zero concentration was imposed as a lower boundary condition. Except in cases where there was no clear gradient at depth signaling the occurrence of SGD, a non-zero concentration was imposed. The equation was solved both numerically with the ReacTran package in R (R Core Team, 2022; Soetaert and Meysman, 2012) and analytically. For the latter, the concentration was assumed to be constant in the upper mixing zone if present, and D_e was set to 0 below. The analytical solution was used to check if the domain depth was sufficiently long so that it did not affect the outcome. The numerical and analytical solutions only differed significantly in cases with weak mixing in the top layer, and then the numerical solution was preferred.

The fluxes of chemicals were estimated by

$$F = -\varphi\frac{D_m}{\tau^2}\frac{dC}{dx} - \varphi D_e\frac{dC}{dx} + \varphi uC \quad (2)$$

where the first, second, and third terms on the right-hand side represent the diffusive, additional mixing, and advective fluxes. Linear regression was used to fit the concentration gradient $\frac{dC}{dx}$ either through points near the sediment-water interface or, in cases with strong mixing at the top, the depth from where a clear gradient was visible. For the porosity, measurements were directly used. The porosity was assumed to be 0.4 for sandy sites, where the porosity had not been measured.

3. Results

An overview of the (isotopic) hydrochemical composition of the surface waters from the open Baltic Sea, surface and porewaters of the Gulf of Gdańsk and Puck Bay, fresh groundwater, and rivers is provided in Table 1.

Table 1 Chemical average, minimum, maximum and, number of samples of the Baltic Sea, Gulf of Gdańsk, outer Puck Bay, inner Puck Bay, rivers, groundwater from wells, groundwater from piezometers, offshore porewaters, shoreline porewaters, the estimated fresh component of SGD, and the seepage meter sample. River results also contain data from Ehlert von Ahn et al. (2023)

Variables	Baltic Sea	Gdańsk Bay	PB outer	PB inner	Rivers	GW_Well Deep	GW piazometer shallow	Offshore SGD impacted PW	Offshore reference PW	Shoreline SGD impacted PW	Shoreline reference PW	Fresh SGD component	Seepage meters
Years	2019	2019	2009 and 2019	2019 and 2021	2011 and 2021	2009 and 2021	2009 to 2021	2009 and 2019	2009 and 2019	2009 to 2021	2009 to 2021	2009 to 2021	2021
Salinity		6.8	6.9	6.8	0.2	0.1	0.3	8	8	3.3	6.4		6.5
		(1)	6.1/7.6 (26)	5.8/7.3 (68)	0.2/0.3 (4)	0.1/0.3 (17)	0.0/0.8 (6)	6/10 (26)	6/9 (83)	0.4/7.2 (103)	5.1-7.3 (27)		5.8/6.9 (4)
pH	8.0	7.8	7.9	8.1	7.7	7.5	7.1	7.3	7.4	7.2	7.3	6.9	7.9
	(1)	7.8 (4)	7.7/8.2 (31)	6.6/8.8 (66)	7.3/8.4 (8)	7.2/8.4 (25)	6.3/7.5 (5)	7.0/7.5 (13)	6.9/7.7 (51)	6.2/8.3 (80)	6.4-8.0 (27)	5.8/8.2 (6)	7.2/8.9 (4)
TA [mM]			1.7						4.9	3.8	2.2	5.1	
			(2)						0.4-15.0 (54)	0.8/7.2 (80)	0.4/7.8 (27)	2.5/7.1 (6)	
DIC [mM]	1.6	1.7	1.6	1.8	4.0		4.6	11	4.7	3.6	2.5	5.7	1.9
	(1)	1.6/1.8 (4)	0.7/1.7 (41)	1.6/2.3 (49)	3.6/4.4 (2)	3.1/9.6 (19)	2.9/6.2 (3)	1.3/24.1 (20)	1.4/13.1 (38)	0.5/8.4 (31)	0.5-7.6 (21)	3.2/8.8 (4)	1.5/2.6 (4)
$\delta^{13}C_{DIC}$ [‰ VPDB]	0	-0.8	-0.5	-0.8	-12.3	-11.8	-20.1	-3.6	-10.4	-9.7	-8.0	-13.6	-8.4
	(1)	-2.5/0.0 (4)	-1.7/-0.1 (32)	-7/0.8 (59)	-13/-11 (2)	-19/-8 (20)	-24/-13 (3)	-14/14 (26)	-18/-1.6 (55)	-26/2.9 (47)	-12/-3.5 (9)	-32.8/-0.6 (5)	-15.5/-5.1 (4)
$\delta^{13}C_{CH4}$ [‰VPDB]										-60			
										-63-(-48) (7)			
$\delta^{2}H_{CH4}$ [‰ VSMOW]										-222			
										-248-(-132) (6)			
$\delta^{18}O_{H2O}$ [‰VSMOW]	-6.4	-6.5	-6.4	-6.3	-9.7	-10.6	-9.6	-6.1	-6.4	-8.7	-6.2	-9.7	-6.7
	(1)	-6.5/-6.4 (4)	-6.7/-6.2 (42)	-7/-5 (53)	-10.2/-9.2 (6)	-13.7/-9.8 (20)	-11.0/-9.1 (6)	-6.6/-5.7 (11)	-6.6/-6.0 (28)	-10.4-(-6.1) (32)	-7.0-5.4 (9)	-10.9/-7.8 (5)	-7.3/-5.8 (4)
$\delta^{2}H_{H2O}$ [‰ VSMOW]	-48.8	-48.7	-48.3	-48.0	-67.2	-74.1	-67.8	-45.8	-48.3	-64.0	-48.3	-69.4	-51.2
	(1)	-49.2/-48.5 (4)	-47.1/-52.6 (42)	-56/-42 (41)	-69.8/-65.3 (6)	-102.2/-66.9 (20)	-80.0/-62.0) (6)	-49.5/-43.1 (11)	-49.2/-47.6 (28)	-76.2-(-47.5) (32)	-51.7-44.0 (9)	-78.4/-56.7 (5)	-54.7/-46.1 (4)
Na [mM]			101	92	0.6	2.3	3.2	107	103	47.2	87.1	3.2	84.4
			84/126 (9)	76/104 (39)	0.2/1.2 (6)	0.2/7.2 (25)	2.8/3.6 (4)	89/135 (26)	87/112 (93)	4-102 (93)	70/103 (24)	0/14 (6)	74/90 (4)
Mg [mM]			11.6	10.7	0.3	0.4	0.3	12.3	11.4	5.2	9.9	0.5	9.9

(*continued on next page*)

Table 1 (*continued*)

Variables	Baltic Sea	Gdańsk Bay	PB outer	PB inner	Rivers	GW_Well Deep	GW piazometer shallow	Offshore SGD impacted PW	Offshore reference PW	Shoreline SGD impacted PW	Shoreline reference PW	Fresh SGD component	Seepage meters
			10.1/13.6 (9)	8.3/11.8 (39)	0.3/0.4 (6)	0.0/0.7 (25)	0.2/0.4 (4)	9.6/16.0 (26)	9.6/13.7 (93)	0.5-11.5 (93)	8.1/11.7 (24)	0/0.9 (6)	8.7/10.3 (4)
Ca [mM]			2.8	2.7	2.0	1.8	2.3	3.1	2.8	2.6	2.9	1.9	2.8
			2.7/3.2 (9)	2.3/3.0 (39)	1.8/2.4 (6)	1.1/3.4 (25)	2.0/2.6 (4)	2.5-3.7 (26)	2.4-3.1 (93)	1.0-8.4 (93)	2.3/4.1(24)	0.7/3.0 (6)	2.7/2.9 (4)
K [mM]			2.1	2.1	0.1	0.1	0.5	2.6	2.4	1.1	1.9	0.4	2.0
			1.8/2.6 (9)	1.6/2.8 (39)	0.0/0.1 (6)	0.0/0.5 (25)	0.4/0.5 (4)	2.1/3.3 (26)	2.0/2.7 (93)	0.2-2.2 (93)	1.3/2.2 (24)	0.1/1.4 (6)	1.8/2.0 (4)
SO_4 [mM]				6.0	0.4	0.7	0.3	3.6	4.2	2.7	4.9	0.1	5.4
				5.1/6.6 (39)	0.3/0.6 (6)	0.0/2.4 (25)	0.2/0.4 (4)	0.2/6.3 (26)	0.3/7.1 (92)	0.0-6.0 (86)	2.6-6.1 (24)	0/0.6 (6)	4.6/5.8 (4)
H_2S [μM]								345	327	87	185		0.5
								0/2041 (26)	0/1683	0-1585 (87)	0-1248 (24)		0/1.0 (4)
Si [mM]			0	0.1	1.1	0.4	0.4	0.5	0.5	0.2	0.1	3.1	0
			(7)	0-0.7 (39)	0.1/1.9 (6)	0.2/0.6 (14)	0.3/0.4 (2)	0.0-0.9 (26)	0.0-0.8 (82)	0/0.6 (44)	0/0.3 (12)	0.2/6.3 (6)	0/0.1 (4)
P [μM]			0.4	1.4	1.6	2.2	43.5	266	112	40	18.0	49.2	3.9
			0.2/1.3 (9)	0.3/9.9 (39)	0.4/3,5 (6)	0.1/5.9 (20)	41.0/46.2 (4)	1.0-668.2 (26)	1.4-310 (93)	0.5/113 (93)	0.6/54.4 (24)	1.8/64.6 (6)	1.5/10.1 (4)
Ba [μM]			0.1	0.1	0.6	0.1	0.2	0.7	0.3	0.1	0.2	0.4	0.2
			0.1/0.2 (9)	0.1-0.2 (39)	0.1/1.3 (6)	0.1/0.7 (25)	0.0/0.5 (4)	0.1-1.7 (26)	0.1-0.5 (93)	0/1.4 (91)	0.1/0.3 (24)	0/2.3 (6)	0.1/0.2 (4)
Fe [μM]			0	0.2	2.2	15	1.5	69	24	48	116	54.8	2.4
			(9)	0/1.3 (39)	1.0/3.9 (6)	0.2/52 (25)	0.1/2.5(4)	0.1-317 (26)	0.0-193 (93)	0/1032(92)	0/795 (24)	0.7/324 (6)	0.4/5.8 (4)
Mn [μM]			0	0.1	1.4	1.8	0.7	8.2	2.6	1.9	1.3	4.2	0.8
			0/0.1 (9)	0.0/0.1 (39)	0.3/3.2 (6)	0.0/4.1 (25)	0.2/1.1 (4)	0.5-21.1 (26)	0-13.5 (93)	0/9.9 (91)	0/6.6 (24)	0.2/15.3 (6)	0.1/2.1 (4)
NH_4 [μM]				0.0	3.7	35	25	1134	200	244	131		7.1
				0.0/0.7 (18)	1.5/5.5 (4)	1.1/170 (15)	15.0/43 (4)	0-4103.0 (25)	53/635 (17)	0/1068 (91)	0.8/974 (27)		1.3/16.2 (4)
^{224}Ra [Bq m^{-3}]	0.3	0.6	0.5	2	0.8	5	21			50			36
	(1)	0.2/1.3 (8)	0.1/0.9 (32)	0.9/10 (28)	0.6/1.2 (4)	0.4/13 (14)	6/49 (3)			10/86 (4)			12/64 (3)
^{223}Ra [Bq m^{-3}]	0	0	0	0	0.1	0.1	1			1.2			1
	(1)	(8)	(30)	0.0/1 (28)	0/0.2 (4)	0/0.4 (13)	0/1 32)			0.5-2.4 (3)			0/2 (2)
$^{224}Ra_{ex}$ [Bq m^{-3}]	0.3	0.5	0.4	2	1	5	20			45			30
	(1)	0.1/1.2 (8)	0.1/0.8 (32)	0.8/10 (24)	0.5/1.0 (4)	0.4/13 (14)	6/48 (3)			10/79 (4)			6/54 (3)

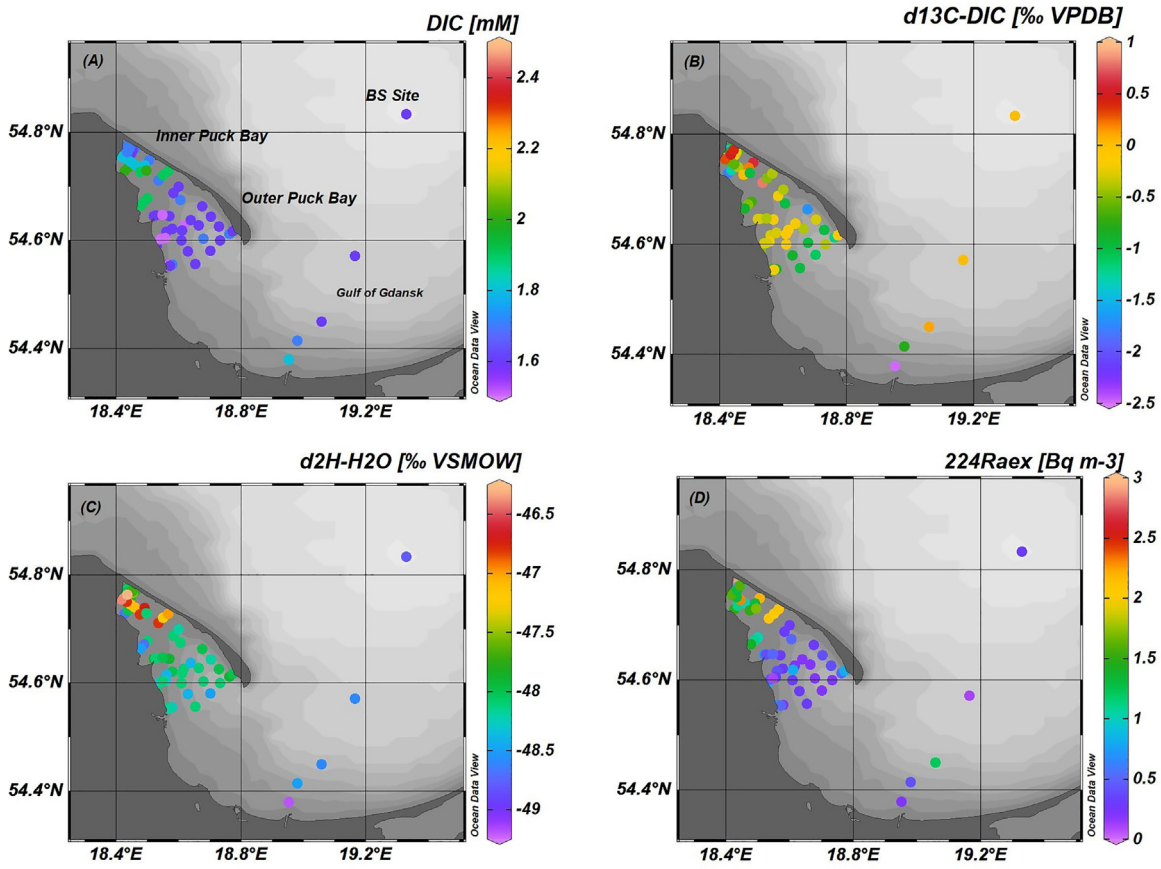

Figure 2 Variation of (A) dissolved inorganic carbon (DIC), (B) δ^{13}C-DIC, (C) δ^{2}H-H_2O, (D) ^{224}Radium-excess. Data of the outer Puck Bay corresponds to the campaign in 2019. Data of the inner Puck Bay correspond to the campaigns in 2019 and 2021. The concentration maps were plotted using Ocean Data View (Schlitzer, 2001). The results from shoreline sites are not presented in the figures.

3.1. Surface water composition

The Puck Bay water isotopic composition varied from −7 to −5‰ and −56 to −42‰ for δ^{18}O and δ^{2}H, respectively (Table 1), with the inner part of the Puck Bay showing heavier values (Figure 2). The samples from the Gulf of Gdańsk and the Baltic Sea revealed a composition in the same range (Table 1).

The DIC concentrations in the Puck Bay surface waters ranged between 0.7 and 2.3 mM, with slightly higher concentrations in the inner part of the bay (Figure 2). The Gulf of Gdańsk and the Baltic Sea showed similar DIC concentrations of about 1.7 mM. The $\delta^{13}C_{DIC}$ signatures ranged from −1.7 to 0.8‰. At sites near the shoreline where SGD has been observed, the signatures reached −6‰. The Gulf of Gdańsk showed $\delta^{13}C_{DIC}$ values between −2.4 and 0.1‰, with the isotopically lightest value being close to the coastline and probably affected by the Vistula River discharge (Figure 2). The Baltic Sea Site had a carbon isotopic signature of DIC of about 0‰ during sampling.

The $^{224}Ra_{ex}$ activities in the surface waters varied between 0.1 and 3 Bq m^{-3} (Table 1, Figure 2). The average activities in the Baltic Sea, Gulf of Gdańsk, and outer Puck Bay were 0.2, 0.5, and 0.4 Bq m^{-3}, respectively, while the inner part showed a much higher level up to 3 Bq m^{-3}. Activities of ^{223}Ra showed similar behavior to $^{224}Ra_{ex,}$ with values ranging between near 0 and 0.2 Bq m^{-3} (Table 1).

Bottom water $^{224}Ra_{ex}$ activities measured at three sites in the outer Puck Bay showed slightly higher values of 0.3, 0.3, and 0.6 Bq m^{-3} than the surface water activities of 0.2, 0.2, and 0.4 Bq m$^{-3,}$ respectively. In contrast, a more distinct difference appeared in the Gulf of Gdańsk, where bottom and surface water $^{224}Ra_{ex}$ activities were 4 and 0.1 Bq m$^{-3,}$ respectively.

The investigated shoreline sites Hel, Chałupy, Swarzewo, and Osłonino (Figures 1 and 2) revealed particularly high Ra activities in surface waters with activities of $^{224}Ra_{ex}$ of 2, 9, 9, and 3 Bq m^{-3}, and ^{223}Ra activities were 0.1, 0.3, 0.5, and 0 Bq m^{-3}, respectively.

3.2. Geophysical characterization of sediments of the outer Puck Bay

Acoustic sub-bottom images from the muddy central part of the outer Puck Bay are displayed in Figure 3. In both images, the sea bottom echo is weak, indicating a low contrast in acoustic impedance between the water and bottom sediments, a typical feature for soft mud sediments. The thickness of this nearly acoustic transparent mud layer is about 1 m in the central part of the bay and thins out towards the SE slope of the basin. Moreover, it is possible to observe that

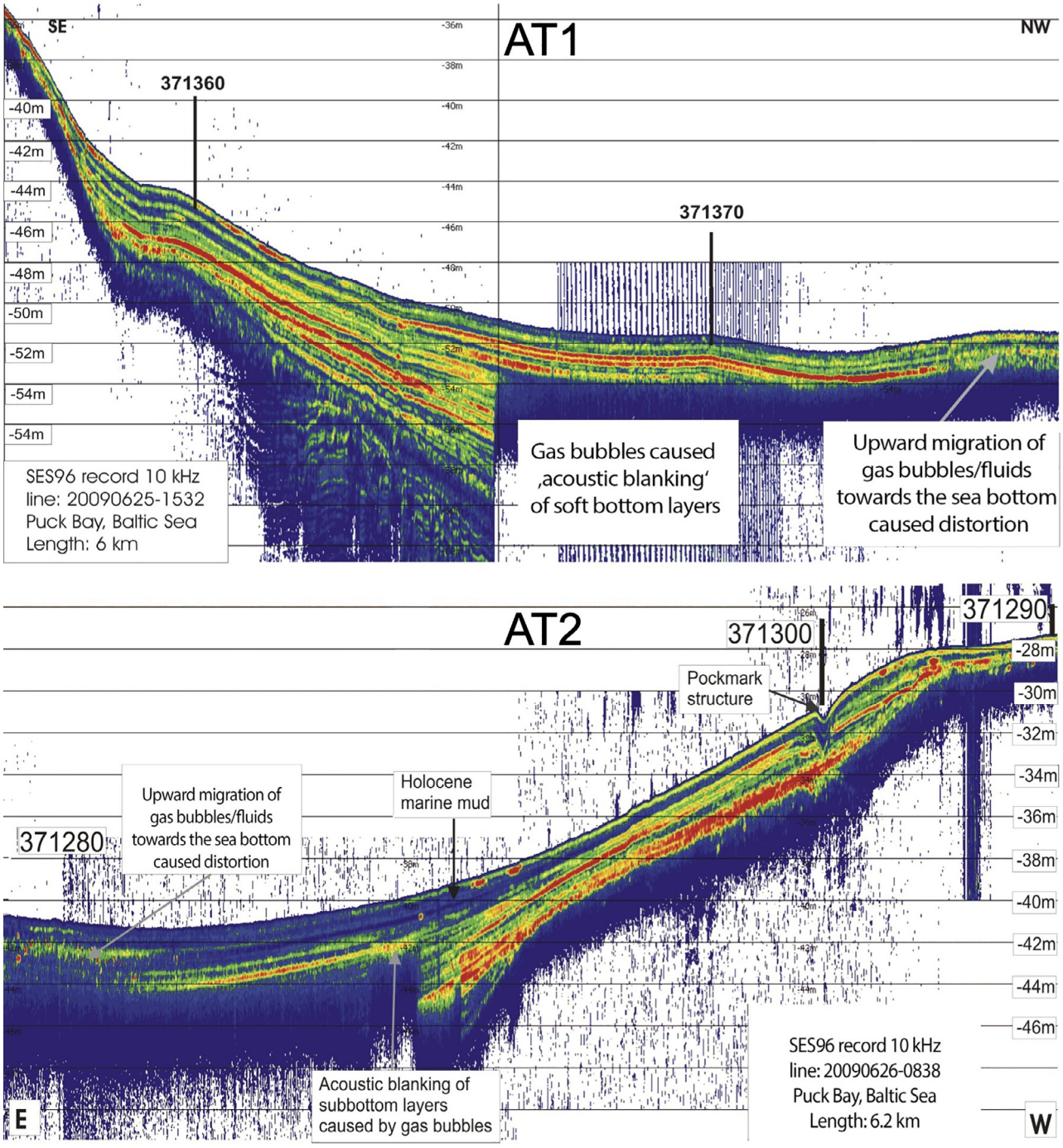

Figure 3 Acoustic transects AT1 and AT2 modified from Böttcher et al. (2024) from the Outer Puck Bay from the campaign in 2009.

the deposits below are well-stratified and reflect the different stages of the Holocene's marine, brackish, and limnic periods. Some of the deepest reflections may originate from late Pleistocene deposits.

The well-stratified sub-bottom images of both transects are suddenly interrupted in the center of the bay at a depth of about 2.5 m below the seafloor. This is caused by tiny gas bubbles present in the pore space of the sediments. Depending on the frequency-gas bubble size ratio, these bubbly layers can act as an acoustic shield, thereby, absorbing, scattering acoustic energy, and hiding deeper structures. Gas bubbles (mainly CH_4) may originate from the decomposition of organic matter in the underlying sediments. The absence of gas bubbles in the uppermost sediments is likely caused by anaerobic CH_4 oxidation (Iversen and Jørgensen, 1985; Whiticar and Faber, 1986).

Towards the NW end of the transect (Figure 3B), the acoustic image of the uppermost mud layer changes to a

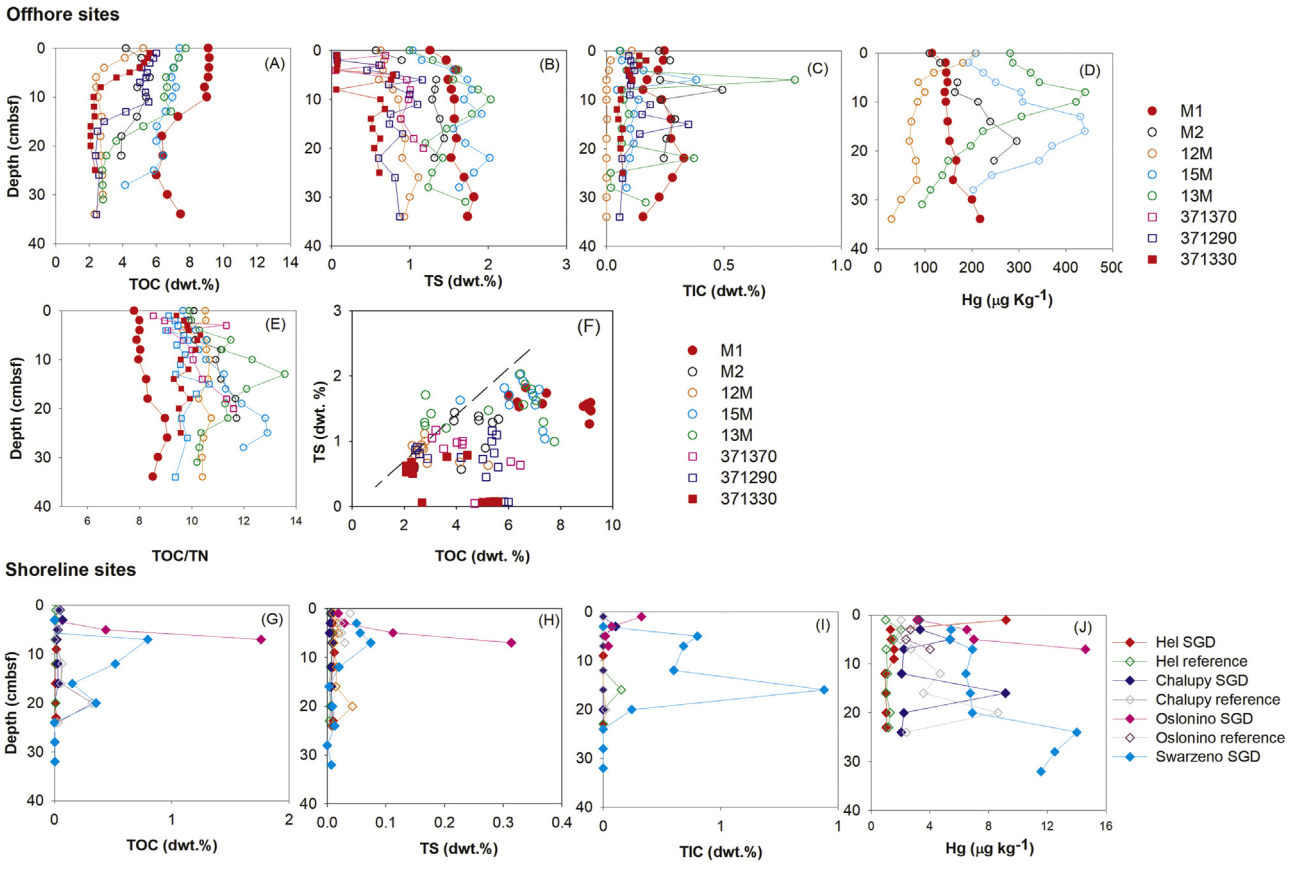

Figure 4 Vertical profiles of bulk geochemical parameters in the sediments from muddy sites (A—F), data from 2009—2019, and sandy sites (G—J) from 2021. Sediment profiles of TOC/TN at the muddy sites (A). Dashed line marks in panel F mean the relationship suggested for Holocene siliciclastic sediments (Berner, 1982). Note: The original definition of (B), (F), and (H) are based on the reducible sulfur (TRIS) content.

more diffuse appearance. This might indicate additional diffusive fluid flow from deeper sources toward the sea bottom, transporting small amounts of gas bubbles. These gas bubbles act as acoustic scatters, masking the sedimentary structure. Moreover, related diagenetic changes of the solid phase, e.g., by precipitation, may produce dispersive distributed acoustic scatters.

Although pockmarks were found, there were no indications of gas bubbles in the sediment or in the water column. Fluid flow along permeable, fractured zones in the sub-bottom may cause these pockmark structures.

3.3. Sediment geochemistry

The site in the Gulf of Gdańsk (Site M1) had the highest TOC content reaching 9% dwt in the top sediments. The content of TOC at the sites of the outer Puck Bay ranged from 2 to 8% dwt, with values decreasing with depth (Figure 4A). In contrast, the surface sediments from the sandy sites at the shoreline were characterized by distinctly lower TOC contents (< 1% dwt., Figure 4G), except for one site located in the inner part of the bay (Osłonino), which showed a maximum of 2% dwt. at 7 cmbsf.

Along with the TOC content, the molar TOC/TN ratio ranged between 8 and 10 at Site M1 (Figure 4E), indicating a dominant proportion of marine organic matter. The sites at the outer Puck Bay showed values between 8 and 13.

Contents of TS at the site in the Gulf of Gdańsk and the outer bay sites varied between near zero and 2% dwt. without apparent differences between the sites (Figure 4B). The accumulation of sedimentary TS indicates the activity of dissimilatory sulfate reduction and deposition of authigenic sulfides. TS further displayed a positive correlation with the TOC content, typical of brackish marine sediments that are limited by the availability of organic matter (Berner and Raiswell, 1983) (Figure 4F). Most of the surface sediments contained calcium carbonate, likely biogenic shell remains, as indicated by the vertical TIC profiles (Figure 4C) that could interact with pore fluids to build up alkalinity.

Vertical profiles of Hg content (Figure 4D) partially indicate the zone of surface sediments deposited during times of high anthropogenic impact (Leipe et al., 2013). However, some profiles are superimposed by physical disturbance such as sediment resuspension, ripple movement, and bioturbation (e.g., Huettel et al., 1998). Pronounced differences in the shape of Hg gradients and absolute contents at several sites suggest different exposures and sediment reworking. While Site M1 showed constant Hg values at depth and some sites even intense mixing down to the observation depth, three sites in the more protected outer Puck Bay displayed

Hg maxima in the top 10 to 20 cmbsf, other sites showed intense mixing down to the observation depth. Different from the offshore sites, the shoreline sandy sites did not exceed Hg contents of 15 $\mu g\ kg^{-1}$ due to the low abundance of substrate for Hg fixation (organic matter and metal sulfides) and strong dilution by quartz.

3.4. Porewater geochemistry

The porewater profile from Site M1, in the Gulf of Gdańsk, showed a decrease in salinity from 10 at the top to 8 at the bottom. The region where Site M1 is situated is already known for gas, and freshwater upflow (Idczak et al., 2020). The porewater salinity of the majority of the sites in the outer Puck Bay displayed values between 6 and 9 and an increase with depth (Figure 5A). In contrast, the salinity at Site 371330 also located in the outer Puck Bay decreased from 7.3 to 6.4.

At the sandy shoreline sites, all sampled porewater profiles showed some freshening at depth, indicating a substantial influence of fresh groundwater at the shoreline of Puck Bay (Figure 6A). Therefore, porewater profiles with at least a 70% decrease in salinity at depth are considered, in this study, as SGD-impacted sites, whereas all others are used as reference sites. The salinity in the reference profiles ranged from 7.3 to 5.1, and at the SGD-impacted sites, salinity even dropped to 0 at depth. Conservative ions such as Na, K, and Mg followed the salinity trends in all profiles.

The $\delta^{18}O_{H2O}$ and $\delta^{2}H_{H2O}$ isotope compositions at the outer Puck Bay sites ranged from −6.6 to −6.0‰ and −49.2 to −47.6‰ respectively. At Site M1 values decreased from −5.7‰ at the sediment-water interface to −6.6‰ at depth and from −43.1 to −49.5‰, respectively. At the reference sites from the shoreline, $\delta^{18}O_{H2O}$ and $\delta^{2}H_{H2O}$ signatures varied from −7.0 to −5.4 and −51.7 to −44.0‰ respectively, whereas at the SGD-impacted sites, the values showed a substantial difference throughout the profile. There, the signatures ranged between −10.4 and −6.1‰ and −76.2 and −47.5‰ for $\delta^{18}O_{H2O}$ and $\delta^{2}H_{H2O,}$ respectively. In addition, analyses of ^{3}H showed higher values in the porewaters of the SGD-impacted sites compared to the bottom waters of Puck Bay (Supplementary Table 2).

Values of pH increased with depth at the offshore sites. Conversely, the pH values at the sandy sites showed a typical decrease with depth from 8.3 to 6.2 (Figure 6E). Concentrations of DIC at the Puck Bay sites, including Site 371330, ranged between 2.0 and 13 mM, whereas Site M1 showed higher concentrations of up to 25 mM in the deeper sediments (Figure 5E). The $\delta^{13}C_{DIC}$ signatures decreased with depth at most sites. However, there were two sites where the $\delta^{13}C_{DIC}$ signatures became heavier with depth, especially at Site M1 showing values up to +13‰ (Figure 5F). Concentrations of DIC at the shoreline sites ranged between 0.5 and 8.4 mM, with the SGD-impacted sites showing higher concentrations (Figure 6F). Signatures of $\delta^{13}C_{DIC}$ were between −11.9 and −3.5‰ at the reference sites on the shoreline. The SGD-impacted sites displayed considerable variability with values ranging between −25.9 and +2.9‰.

At the sandy site on the Hel Peninsula, SGD was associated with CH_4 contributed from the fresh water component (Donis et al., 2017). The stable C and H isotopic composition of CH_4 was measured in 2010 and was found to be isotopically light with stable isotope values varying from −63 to −60‰ and −248 to 240‰ for $\delta^{13}C_{CH4}$ and $\delta^{2}H_{CH4}$ respectively (Table 1). However, a sample close to the sediment-water interface showed a heavier isotopic composition of −48‰ for $\delta^{13}C_{CH4}$ and −132‰ for $\delta^{2}H_{CH4}$ than those taken from deeper sediment sections (Supplementary Figure 4).

Concentrations of SO_4 at the offshore sites ranged between 0.1 and 6.4 mM, decreasing with depth. Some of the sites already had values close to 0 at 20 cmbsf. At Site 371330, a less pronounced decrease in the SO_4 concentrations was found, dropping from 6.1 to 2.6 mM at depth. Site M1 showed lower SO_4 values already at the sediment-water interface compared to the bottom waters, and SO_4 was consumed at a depth of about 15 cmbsf. Most sites showed the typical decrease in SO_4 and an increase in H_2S with depth, with concentrations of the latter ranging between 0 and 1683 μM. In contrast, Site 371330 showed no accumulation of H_2S along the entire profile. Site M1 showed a decrease in H_2S concentrations with depth, with values higher than 2000 μM in the top sediments. At all sandy sites, rapid depletion of SO_4 from bottom water concentrations of around 6 mM down to values below the detection limit was observed. Mixing with fresh groundwater seems to be the dominant factor for very low SO_4 concentrations already at 10 cmbsf at the SGD-impacted sites. In contrast, the SO_4 ranged from 6.1 to 2.6 mM at the reference sites. The sandy shoreline sites did not show any accumulation of H_2S, except for Site Chałupy, which showed values up to 1500 μM at depth.

Without showing clear vertical gradients, concentrations of dissolved Ba ranged between 0.1 and 0.5 μM at all sites in Puck Bay. Site M1 reached values up to 1.7 μM (Figure 5J). The sandy sites displayed spatial variation with higher concentrations found in Osłonino and Swarzewo, where values reached up to 1.4 μM. In contrast, all values were below 0.5 μM at the Hel site. In agreement with an assumption that the solubility of BaSO4 may lead to a reversed concentration behavior, the trends in dissolved trace Ba tend to show the opposite trend and increase with depth. A comparison between Site M1 and the other ones from the central Puck Bay make clear that also the processes or reservoir sizes for metal sources in the fluids differ.

With maximum values in the top sediment, dissolved Fe concentrations varied between near zero levels and 192 μM for most offshore sites. Site 371330 showed the same trend, but the values in the top sediments reached up to 317 μM (Figure 5J). Site M1 showed concentrations close to the detection limit over the entire core depth. Similar to Fe, concentrations of Mn were higher in the top sediments reaching a maximum of 14 μM, with the Site 371330 showing the highest values (Figure 5L). Dissolved Fe revealed very heterogeneous profiles among the shoreline sites, ranging between near zero and 1032 μM. There was no difference between SGD-impacted and reference sites; however, the concentrations showed a high temporal variability at the Hel site. For example, samples collected in 2009 showed maximum Fe concentrations of only 27 μM, whereas the values exceeded 1000 μM in 2010. At the sandy sites, the concentrations of Mn showed a pronounced variability, as observed for Fe. There, the Mn concentrations ranged between near zero and 10 μM. The highest Mn levels were observed at Swarzewo

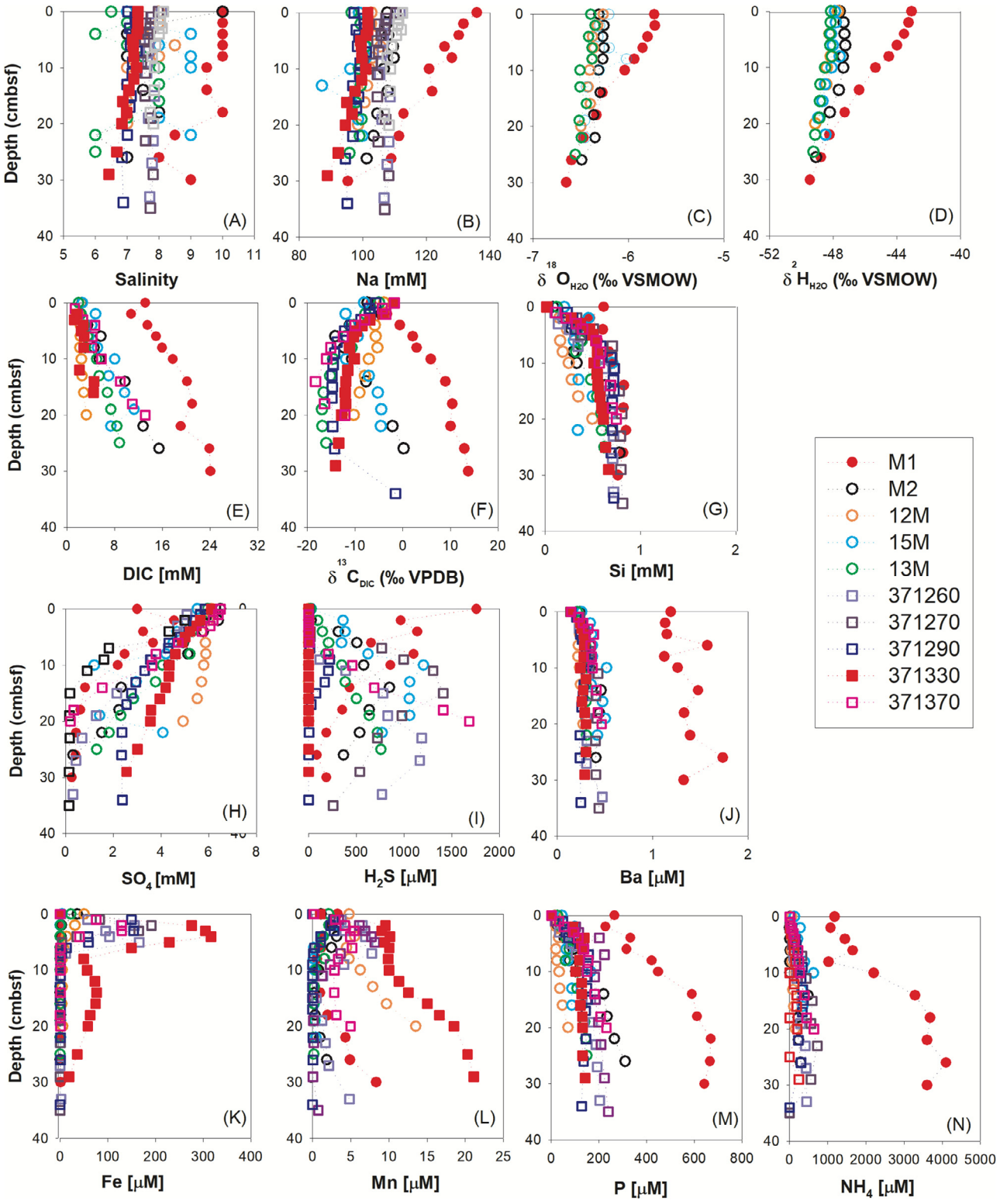

Figure 5 Porewater gradients of geochemical parameters in sediment cores from the muddy sites in Puck Bay and one in the Gdańsk Bay (Gdańsk SGD). Samples from 2009 are represented by circles and from 2019 by squares. Filled symbols refer to SGD-impacted sites.

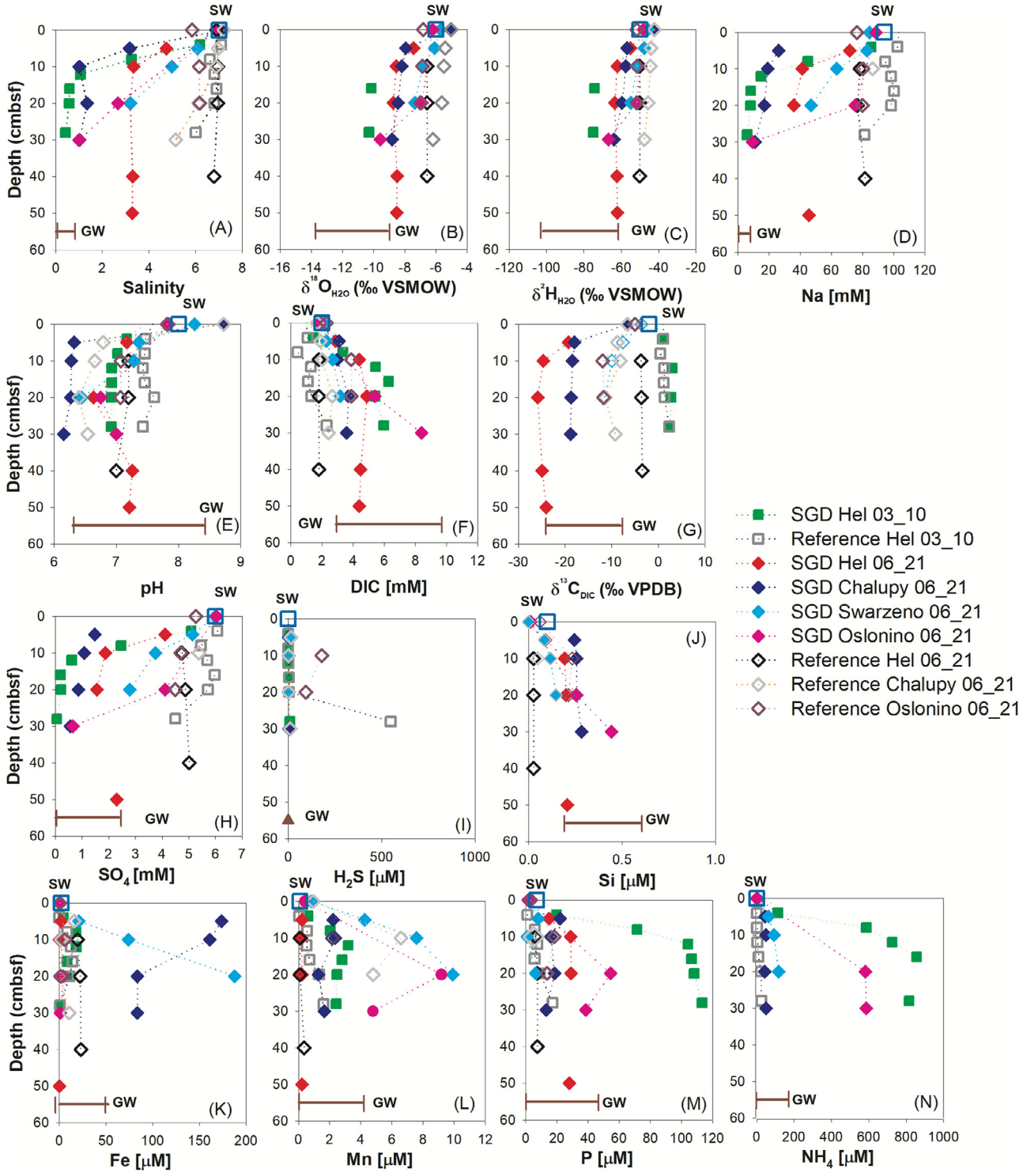

Figure 6 Porewater profiles from the selected sandy site from Hel, Chałupy, Swarzewo, and Osłonino in Puck Bay. Filled symbols represent SGD-impacted sites. All porewater profiles collected from 2009 to 2021 are presented in Supplementary Figure 3.

and Osłonino, and the Hel site again showed higher concentrations in 2010.

Regarding the nutrients, Si concentrations were between near zero and 0.8 mM, with only minor differences between the offshore muddy sites. In contrast, the shoreline sites revealed a difference between the reference and SGD-impacted sites (Figure 6J). While Si increased up to 0.3 mM at the reference sites, twice as high a concentration of 0.6 mM was reached at the SGD sites. Concentrations of P ranged between 0.1 and 240 µM and increased with depth at all offshore sites. Site M1 showed the highest concentration up to 668 µM at depth. Concentrations of P also increased with depth at the sandy sites. The SGD-impacted sites showed a maximum value of 113 µM, whereas the con-

centrations at the reference site remained below 60 μM. Concentrations of NH_4 ranged between 1.4 and 724 μM at the offshore sites in Puck Bay, with Site M1 again showing the highest value (4103 μM) with depth. At the shoreline sites, concentrations of NH_4 were higher at the SGD-impacted sites showing values increasing from near zero at the sediment-water interface to 1068 μM at depth. The reference sites reached a maximum value of 146 μM at a depth of 30 cmbsf.

Activities of $^{224}Ra_{ex}$ were measured in the porewaters at the shoreline sites at a depth of around 50 cmbsf, and the values were 37, 54, 79 and 10 Bq m^{-3} for Hel, Chałupy, Swarzewo, and Osłonino, respectively.

3.5. Direct measurement of seepage rate

Seepage meters were applied in Hel, Chałupy, and Swarzewo (Figure 1) to measure the volumetric seepage rates during the campaign in 2021. These measurements determined the total water flux, but not necessarily the freshwater discharge. However, lowered salinity and water isotopic values demonstrate at least the presence of a freshwater compound.

At the Hel site, the water volume change in the seepage meter bags over time intervals of 85 and 120 minutes equaled a seepage rate of 45 and 30 L m^{-2} d^{-1} respectively. The amount of water collected at the Chałupy Site over 143 minutes yielded a seepage rate of 3 L m^{-2} d^{-1}. At the Swarzewo Site, a flux of 1.6 L m^{-2} d^{-1} was obtained over 170 minutes.

The salinity of the samples collected at Hel was 5.7 and 6.6, and the corresponding surface water salinity was 6.9. The isotopic composition of the water was lighter than the surface water of Puck Bay (Table 1, Figure 6), reaching values for $\delta^{18}O_{H2O}$ of −7.1 and −6.6‰ and $\delta^{2}H_{H2O}$ of −53.4 and 50.8‰. At Chałupy Site, the salinity of the seepage water (6.9) was only marginally lower than that of surface water (7.2). The water isotopic signature revealed $\delta^{18}O_{H2O}$ values of −7.3‰ and $\delta^{2}H_{H2O}$ of −54.7‰. At Site Swarzewo, the salinity was 6.6 in the seepage water and 6.9 in the surface water. The water isotopic signature was relatively light in the seepage water compared to the surface water (Table 1), with values of −5.8 and −46.1‰ for $\delta^{18}O_{H2O}$ and $\delta^{2}H_{H2O}$ respectively.

The fresh groundwater fraction for each site was calculated by assuming that the sample collected in the seepage bag is a mixture of groundwater and recirculated seawater and by applying an end-member model as:

$$V_s \times S_S = V_{gw} \times S_{gw} + V_{sw} \times S_{sw} \quad (3)$$

where *S* and *V* are salinity and volume, the subscripts *S*, *G*, and *SW* represent the sample, groundwater, and seawater fractions, respectively.

The fresh groundwater fractions at the Site Hel were 4 and 17%, corresponding to fresh groundwater fluxes of 0.05 and 0.5 L m^{-2} d^{-1}. For site Chałupy, a fraction of 4% freshwater was estimated, which corresponds to a flux of 0.01 L m^{-2} d^{-1}. At Site Swarzeno, the fresh fraction was 3%, and a fresh groundwater flux of 0.004 L m^{-2} d^{-1} was obtained.

3.6. Coastal groundwater and surface water entering the Puck Bay

3.6.1. Groundwaters

The groundwater comprises the water sampled from wells (deep groundwater) and piezometers (shallow groundwater) around the coastal zone of Puck Bay. A summary of the measured parameters is presented in Table 1.

The groundwater isotopic composition of the deep groundwaters varied from −13.7 to −9.8‰ and −102.2 to −66.9‰, whereas the groundwater at the piezometers ranged from −11.0 to −9.1‰ and −80.0 to −62.0‰ for $\delta^{18}O_{H2O}$ and $\delta^{2}H_{H2O,}$ respectively (Table 1, Figure 7). The measured isotopic signatures from the groundwater wells represent groundwater coming from the Cretaceous, Tertiary, and Quaternary deposit based on Piekarek—Jankowska (1996). In contrast, the heavier signatures of the shallow groundwaters were influenced by meteoric water.

^{3}H values were highest in the shallow groundwater flowing within the Quaternary strata. Very low activity was found in the groundwaters from the Tertiary and Cretaceous aquifers (Supplementary Table 2). A combined evaluation of ^{3}H and He isotope analyses indicates ages of about 30, 50—100, 28, > 60, and >>>60 years for wells Wladyslawowo 2, Reda IV (low ^{3}H, but no ^{4}He), Reda 12c, Rumia (low ^{3}H, but low ^{4}He), and the deep production well on Hel Island (low ^{3}H, but high ^{4}He), respectively (Supplementary Table 2). ^{3}H free older water appears to be further mixed into the Wladyslawowo 2 groundwater.

The hydrogeochemical groundwater composition for most deep and shallow groundwaters is classified as Ca-Mg-HCO_3 type (Figure 7B). Some groundwaters contain higher Na contents, indicating a mixed type. According to Löffler et al. (2010), this water can be further classified as “old groundwater”. Groundwater coming from Cretaceous aquifers was classified as HCO_3-Na according to Piekarek-Jankowska (1996).

Concentrations of DIC were between 3.1 and 6.2 mM, except in Chałupy, where the piezometer sample revealed a value of 2.9 and 9.0 mM in the groundwater well. The $\delta^{13}C_{DIC}$ signatures were spatially heterogeneous. The shallow groundwater showed $\delta^{13}C_{DIC}$ values ranging between -23.8 and −12.1 ‰, with lighter signatures at Hel Site. Signatures in the deeper groundwaters ranged between −12.5 and −8.1‰. Heavier values in deeper groundwaters might be associated with the interaction with carbonates, and less contact with organic matter is expected in confined aquifers. Calcium concentrations were higher in the shallow groundwater, with an average concentration of 2.3 mM, whereas the deep groundwater had an average concentration of 1.8 mM.

Activities of $^{224}Ra_{ex}$ in the deep groundwater ranged between 0.3 and 13 Bq m^{-3}, and the ^{223}Ra activities ranged between 0 and 0.4 Bq m^{-3}. The $^{224}Ra_{ex}$ activities in the groundwater from the piezometers at the Hel site were 7 and 4 Bq m^{-3} for the campaigns in 2019 and 2021, respectively. The piezometer in Chałupy showed higher $^{224}Ra_{ex}$ activities of 48 Bq m^{-3} in 2019. Activities of ^{223}Ra were 0.2 and 1 Bq m^{-3} for Hel and Chałupy during the campaign in 2019.

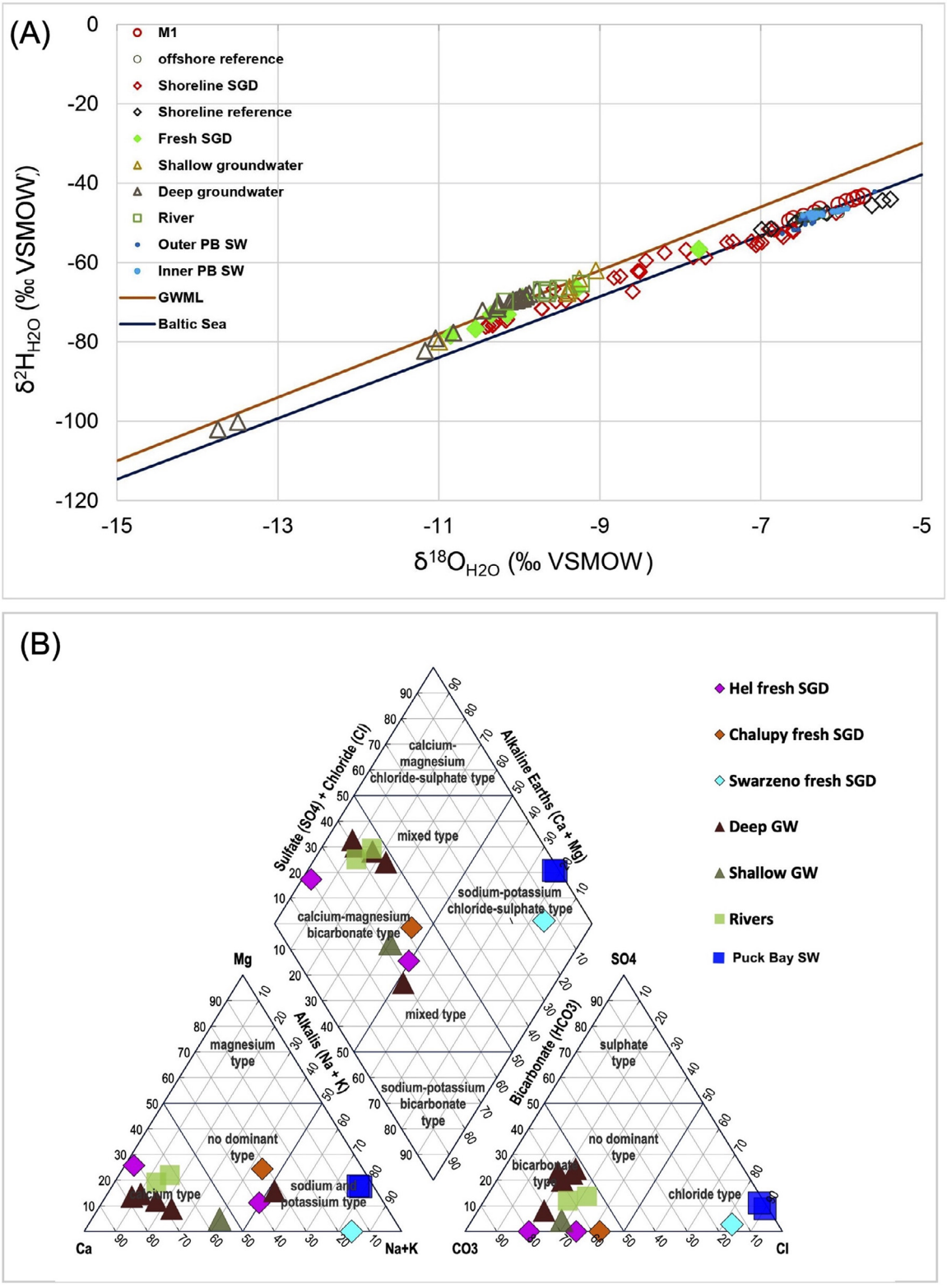

Figure 7 (A) The covariation of $\delta^{18}O_{H2O}$ and $\delta^{2}H_{H2O}$ of sandy sites impacted and non-impacted by SGD, muddy sites impacted and non-impacted by SGD, groundwaters, rivers, and Puck Bay surface water. The global meteoric water line (GMWL), and the Baltic Sea line (Böttcher et al., unpublished data.) are given for comparison. (B) Piper diagram of the major ions of the rivers (green square), deep groundwater (brown triangle), shallow groundwater (dark green triangle), extrapolated porewater from the SGD impacted sites (pink and orange diamond), and porewater. (Graph created from Stosch, 2022).

3.6.2. Rivers

The sampled rivers draining into Puck Bay were Reda, Płutnica, Zagórska Struga, and Gizdepka. A summary of the results is presented in Table 1.

The rivers showed water isotope signatures ranging from −10.2 to −9.7‰ and −69.8 to −67.0‰ for $\delta^{18}O_{H2O}$ and $\delta^{2}H_{H2O}$ respectively. The hydrogeochemical composition of the rivers is classified as Ca-Mg-HCO_3, similar to most groundwaters (Figure 7B).

Average DIC and $\delta^{13}C_{DIC}$ values were 4.0 mM and −12.3‰, respectively. Concentrations of Ca ranged between 1.8 and 2.4 mM.

The Ra activities in the river samples exhibited a small variability with average $^{224}Ra_{ex}$ and ^{223}Ra activities of 1.1 Bq m^{-3} and 0.1 Bq m^{-3}, respectively.

4. Discussion

4.1. Submarine groundwater discharge in the Gulf of Gdańsk and Puck Bay

The bottom waters of Site M1 located in the Gulf of Gdańsk were characterized by high $^{224}Ra_{ex}$ activities compared to the surface waters, indicating the occurrence of SGD, as Ra is mainly derived from groundwater (Beck et al., 2007b; Moore, 2000a; Rodellas et al., 2012). Furthermore, at this site, the sediment porewater showed a decrease in salinity and water isotope signatures at depth (Figure 5A), which could be caused by an upward flux of fresh groundwater. This finding is in line with previous investigations conducted in the region of Site M1, where upward flows of freshwater and gas coming from a pockmark structure were reported (Brodecka-Goluch et al., 2022; Idczak et al., 2020).

The outer part of Puck Bay revealed also higher $^{224}Ra_{ex}$ activities in the bottom water when compared to the surface water at some sites. In addition, acoustic images revealed sediment layers with a pronounced diffuse appearance (Figure 3) than what would be expected only from CH_4 bubble formations, indicating an additional flow. In these images, pockmark structures are also visible. Pockmarks are craters on the seabed that are considered to result from fluid flow (Hovland et al., 1987), including groundwater discharge. It is worth mentioning that pockmarks associated with SGD have been found in many places around the Baltic Sea, for example, in Eckernförde Bay (Germany), Hanko Bay (Finland) and the Gulf of Gdańsk (Hoffman et al., 2020; Idczak et al., 2020; Purkamo et al., 2022; Virtasalo et al., 2019; Whiticar and Werner, 1981). Therefore, it can be inferred that SGD is not just limited to specific spots, but can also occur in multiple areas throughout the bay.

In the outer Puck Bay, the Site 371330 showed a decrease in the porewater salinity with depth, thus considered to be an SGD spot in the central outer Puck Bay.

When comparing the two parts of Puck Bay, submarine groundwater discharge was more evident in the surface water of the inner part of the bay than in the outer part, particularly when pointing out the Ra activities, which showed a more than 4-fold enrichment compared to the activities determined in the more open coastal Baltic Sea. This is partly due to the lower water depths, which allow a stronger signal from mixing with freshwaters and less volume for dilution. In addition to Ra activities, the stable isotope tracers revealed a contribution from different water masses to this area. For example, $\delta^{2}H_{H2O}$ and $\delta^{13}C_{DIC}$ showed high spatial variability, with some areas presenting lighter isotopic signatures (Figure 2) potentially contributed by porewater and/or groundwaters. Concentrations of DIC were slightly higher in the inner bay (Figure 2), indicating impact by porewater fluxes.

Besides the offshore SGD sites (sites M1 and 371330), the shoreline of Puck Bay is also known for several SGD spots (e.g., Donis et al., 2017; Kotwicki et al., 2014; Kłostowska et al., 2018, 2019; Szymczycha et al., 2012, 2020). At four shoreline sites sampled in this study (Figure 1), higher Ra activities were found in combination with lighter $\delta^{2}H_{H2O}$ and $\delta^{13}C_{DIC}$ signatures. At these locations, the sediment porewater salinity of several sites generally showed a concave shape indicating an upward advective groundwater flow of fresh groundwater (Figure 6).

4.2. Early diagenesis and the impact of submarine groundwater discharge on the surface sediments of the Gulf of Gdańsk and Puck Bay

4.2.1. Offshore sites

Site M1 in the Gulf of Gdańsk displayed a decrease in both porewater salinity and the water isotope signatures at depth (Figure 5A), which suggests an upward flow of fresh groundwater. This site is located in an area dominated by clayish silt (Figure 1) with sediments that are characterized by high TOC contents and low C:N ratios (Figure 3A,E) mainly due to the influence of the Vistula River (Szymczak- Żyła and Lubecki 2022). The Hg values in the sediments were constant with depth, possibly due to the high sediment mixing caused by gas flow, as observed at a nearby site by Brodecka-Goluch et al. (2022) and Idczak et al. (2020), and the groundwater discharge.

Also, at this site, intensive organic matter mineralization was observed. Sediment porewater DIC and NH_4 reached concentrations four times higher than the porewaters at the outer Puck Bay sites. Concentrations of SO_4 were already lower in the top sediments due to intense organic matter mineralization combined with the impact of groundwater low in SO_4. Following or overlapping the zone of sulfate reduction, methanogenesis became a pathway for organic matter mineralization already in the surface sediments, confirmed by the heavier values of $\delta^{13}C_{DIC}$ (+14‰). This is commonly observed in coastal settings with high rates of organic matter deposition (Thang et al., 2013). As a result of the low availability of SO_4 and the absence of Fe at the sediment-water interface for possible CH_4 oxidation, CH_4 may easily migrate and impact the bottom waters, as observed by Idczak et al. (2020) at a nearby pockmark. Concentrations of Ba are enriched in the porewaters as has been described by Aloisi et al. (2004) for cold seep sites.

Most of the outer Puck Bay sites, except Site 371330, revealed porewater gradients with constant salinity and uniform concentrations of conservative elements with depth. The surface sediments at these sites are composed of silty clay, clayey silt, and sandy silt (Figure 1). Sediment composition was different between the sites, but the TOC/TS

contents remained below the predicted Holocene saturation line (Figure 5F), indicating sulfate mineralization processes (Berner, 1982; Jørgensen and Kasten, 2006). Most sites showed Hg profiles with enhanced contents at 10 and 20 cmbsf, and thus a relatively continuous sedimentation with little disturbance. In contrast, Site M2 showed constant Hg values with depth, indicating some disturbance probably related to gas outflow. Site M2 is located over an extensive regular shallow gas accumulation (Brodecka-Goluch et al., 2022 and references therein).

The porewater profiles from the outer Puck Bay are shaped by organic matter mineralization and a continuous increase in metabolite concentrations by using, in particular, SO_4 (Figure 5H,I). The $\delta^{13}C_{DIC}$ composition was typical of marine sediments where high rates of mineralization of organic matter are found (Meister et al., 2019). Lighter isotopic signatures in the uppermost sediments at most sites may be indicative of CH_4 oxidation. In addition, no disturbance from bubbles was observed in the acoustic images of the top sediment layer. Porewater displayed high concentrations of the main metabolites originating from organic matter mineralization. Site M2 was impacted by methanogenesis already in the top sediments, as indicated by SO_4 rapidly decreasing to 0, and corresponding $\delta^{13}C_{DIC}$ values that became heavier. Similar to Site M1, this site could also act as a source of CH_4 to the bottom waters.

The low Fe concentrations are probably due to the precipitation of Fe sulfides in the anoxic zone (Balzer, 1982; de Beer et al., 2005). However, in some sites dissolved Fe and Mn were mobilized in the top sediment due to the development of a suboxic zone.

Porewater salinity at Site 371330 displayed a slight decrease in porewater salinity together with the other conservative elements (Figure 5A), suggesting an impact of fresh groundwater in the deeper sediments. This site is located in an area composed mainly of silty clay (Figure 1). The content of TS was lower compared to the other sites in the bay, especially in the top sediments, due to some reoxidation of sedimentary sulfur species such as Fe monosulfides. No substantial bacterial sulfate reduction is observed and therefore H_2S did not accumulate. The lack of H_2S in the porewater may allow higher concentrations of dissolved Fe as no precipitation of Fe phases occurred. Dissolved Fe and Mn were mobilized in the top sediments (Figure 5K,L).

Although Site 371330 showed some freshening with depth, the chemical gradients were similar to the other sites in the outer Puck Bay originating from a strong diagenetic processes.

4.2.2. Shoreline sites

The sediments along the shoreline sites are mainly comprised of medium sandy sediments (Figure 1) and are characterized by low TOC and TS contents (Figure 4G,H) due to their continuous physical reworking, causing clay losses (Morse and Berner, 1995) and intense mineralization of standing stock of organic matter (de Beer et al., 2005). In agreement with these sedimentological features, the porewater gradients (Figure 6) suggest that diffusion is strongly superimposed by porewater advection. Driving forces for this process taking place in the top sediments are bottom currents (Cook et al., 2007; de Beer et al., 2005), and, at SGD-impacted sites, also the upward fluid movements (Billerbeck et al., 2006). These physical processes may be seasonally superimposed to a certain degree by in situ biogeochemical transformations of variable spatial and temporal intensity (Cook et al., 2007).

Porewater salinity displayed a large variability between the study sites. While only some sites showed no or only a slight vertical decrease in salinity (Figure 6, Supplementary Figure 3), most of the sites showed a downward decrease in salinity and reaching freshwater conditions with depth. These sites were chosen to represent the impact of SGD.

The sites with slightly decreasing salinity showed porewater isotopic compositions (δ^2H and $\delta^{18}O$) close to the Baltic Sea signature and were, therefore, not significantly impacted by fresh groundwater. A decrease in pH between 5 and 30 cmbsf accompanied by a slight increase in DIC, indicates active organic matter mineralization probably by sulfate reduction. In addition, some sites were impacted by methanogenesis as the $\delta^{13}C_{DIC}$ reached positive values. Dissolved P, NH_4, and Mn concentrations increased with depth, most likely due to organic matter mineralization. However, the concentration of the metabolites was very low at these sites as the upward advective flow limited the accumulation of these elements in the surface sediments.

Sites with a steeply downward decrease of salinity and porewater isotopic composition indicated clear mixing between the Baltic Sea and the groundwater (Figure 6A–C), indicating the impact of fresh groundwater.

The concentrations of SO_4 dropped down in the top 10 cmbsf due to the influence of fresh groundwater depleted in SO_4. The application of a binary mixing shows a slight SO_4 deficit found in most SGD-impacted porewaters (Supplementary Figure 5), which indicates minor net bacterial sulfate reduction rates (e.g. Donis et al., 2017). Previous investigations further demonstrated the importance of aerobic processes in surface sediments (Cook et al., 2007; Donis et al., 2017).

The concentrations of DIC and the $\delta^{13}C_{DIC}$ signatures indicated different biogeochemical processes (Figure 6F,G). Mixing between fresh groundwater characterized by higher DIC concentrations and lighter and variable $\delta^{13}C_{DIC,}$ and brackish water characterized by lower DIC concentrations and heavier $\delta^{13}C_{DIC}$ composition (Table 1). The mixing is further superimposed by the mineralization of organic matter resulting in lighter $\delta^{13}C_{DIC}$ values (Supplementary Figure 6). In addition, methanogenesis was observed at depth for the Hel Site (Donis et al., 2017; Kotwicki et al., 2014), and possible re-oxidation effects led to shifts towards isotopically lighter stable isotope signatures. In the top sediments, signatures were lighter than those found in the non-SGD-impacted sites, likely indicating possible oxidation of CH_4.

The stable H and C isotope composition of dissolved CH_4 in porewater at the SGD-impacted profiles showed a biogenic origin. They fall within the intermediate region predicted for methanogenesis following the methyl-type fermentation and carbonate reduction pathways (Table 1; Supplementary Figure 4) (e.g., Egger et al., 2017; Whiticar, 1999). Following the classification of Whiticar (1999), the isotope signatures of porewater CH_4 are dominated by the impact of hydrogenotrophic carbonate reduction. A sample close to the sediment-water interface was heavier in both $\delta^{13}C_{CH4}$ and δ^2H_{CH4} than other samples.

This difference is most likely due to the aerobic oxidation of methane in the surface sediment, which has been shown to yield a similar relative isotopic enrichment (Drake et al., 2015).

Concentrations of dissolved nutrients (P, NH_4, and Si) were higher in the SGD-impacted sites compared to the non-impacted sites (Figure 6 J,M,N, Supplementary Figure 6), demonstrating that the fresh SGD component acts as a nutrient source, which is further enhanced by organic matter mineralization. It should also be noted that most elements are expected to flow toward the bottom waters due to the strong upward flow of groundwater, which suppresses the reaction of the elements within the sediments. The higher concentrations of nutrients at SGD sites agree with previous observations (Donis et al., 2017; Szymczycha et al., 2012).

Fe and Mn exceed the concentrations expected based on binary mixing between the bottom and groundwater (Supplementary Figure 5) due to reductive release within the mixing zone of the surface sediments (Balzer, 1982; de Beer et al., 2005). Higher dissolved Fe concentrations were found at two sites impacted by SGD in the inner Puck Bay (Chałupy and Swarzewo, Figure 1), indicating different processes or sedimentary Fe sources for the different sites.

The profiles captured during different seasons of the years 2009 and 2010 did not show a clear seasonal variation between them (Supplementary Figure 3) except for $\delta^{13}C_{DIC}$, which showed some variability associated with different mineralization rates.

4.2.3. Element fluxes

Dissolved constituents in porewater from the 15 selected sites with and without impact by SGD were modeled to estimate the water and element fluxes across the sediment-water interface to learn about the relative importance of diagenesis versus SGD-induced advection (Figure 8, Supplementary Table 3).

Concentrations of Na of the porewaters were used to estimate the groundwater discharge across the sediment-water interface. Using the model approach (section 2.2.3), it was found that the fluxes at the offshore sites (M1, 371330, 371370, M2) are mainly driven by molecular diffusion. The calculated flux of fresh groundwater at Site M1 was 0.005 cm d^{-1} and 0.003 cm d^{-1} for Site 371330. The groundwater flow of the sites where SGD had not been noticed was smaller, about 0.001 cm d^{-1}.

At the sandy shoreline sites, where advective processes shaped the profiles, high groundwater flow was estimated compared to the offshore sites (Figure 8). The modeled groundwater flow at the SGD-impacted sites varied between 0.01 and 0.03 cm d^{-1}. Advection at the non-SGD-impacted sites was found to be much lower and varied in a range of 0 and 0.002 cm d^{-1}.

The associated elemental fluxes were found to vary between the sites as well as they are presented in Supplementary Table 3. The offshore sites were characterized by higher fluxes of DIC, TA, NH_4, and P (Figure 8) out of the sediment, particularly at Site M1, resulting from pronounced organic matter mineralization. These results further highlight the importance of microbial-catalyzed biogeochemical processes for the development of the chemical gradients in the surface sediments.

The elemental fluxes at the sandy shoreline sites were comparatively low despite high advection rates. The calculated fluxes are based on net fluxes, and the advective fluxes might inhibit the accumulation of elements and result in lower element fluxes. However, enhanced fluxes of elements were observed in the profiles impacted by SGD (theoretically, the sites with higher advective flux), suggesting that the groundwater can be a source of these elements and therefore contribute to the addition of elements to surface waters. Moreover, the physical pressure of the upward groundwater flow may facilitate the benthic fluxes at the sediment-water interface.

Despite the lower fluxes obtained, the sandy permeable sediments must be considered when addressing the global cycles of matter as they also represent a source of new or recycled elements to the surface waters (Santos et al., 2012).

4.3. The composition of the submarine groundwater discharge freshwater component: Shoreline sites

The porewater isotopic signatures at the shoreline sites impacted by SGD (Figure 1) were lying on a mixing line between the surface waters of Puck Bay and the groundwaters (Figure 7). The lighter signatures were found at the bottom profile and plotted close to the groundwater signatures (Figure 7).

The SGD-impacted porewater profiles indicate spatial and temporal variability (Supplementary Figure 3). The groundwater-seawater mixing zone moves according to external factors such as wind direction, precipitation, and sea level (Kłostowska et al., 2019; Massel et al., 2004). However, from the salinity gradients, it is possible to roughly estimate that the freshwater composition could be found between 20 and 100 cmbsf at the sandy shoreline sites.

The fresh component of SGD was characterized by extrapolating the profiles to freshwater conditions (the calculation was based on the Mg concentrations in groundwater of 0.4 mM, Table 1). Porewater profiles from Hel, Chałupy, Swarzewo, and Osłonino (Figure 1) were evaluated and compared with values from the groundwater and river water around Puck Bay.

The hydrogeochemical composition of the fresh component of SGD at Hel and Chałupy was Ca-Mg-HCO_3 type, similar to the groundwater and the rivers in this region, and the site in Swarzewo showed some impact by saline water. The fresh component of the SGD on Hel showed a mixed-type composition (Figure 7B).

The Hel site further showed the lightest water isotopic signatures reaching −10.9 and −78.4‰ for $\delta^{18}O_{H2O}$ and $\delta^{2}H_{H2O}$, respectively, which is probably influenced by groundwater from deep aquifers related to the Cretaceous deposits (Piekarek—Jankowska, 1996). The ^{3}H activities found in the porewaters of Hel (Supplementary Table 2) indicate the presence of low/free ^{3}H groundwater. In addition to Hel, a land-based site (Osłonino) appears to be influenced by groundwater from Cretaceous aquifers as implied by the lighter water isotope values (Figure 7).

Although the $\delta^{13}C_{DIC}$ signatures vary over a wide range (Figure 6G, Supplementary Figure 3, L, Supplementary Fig-

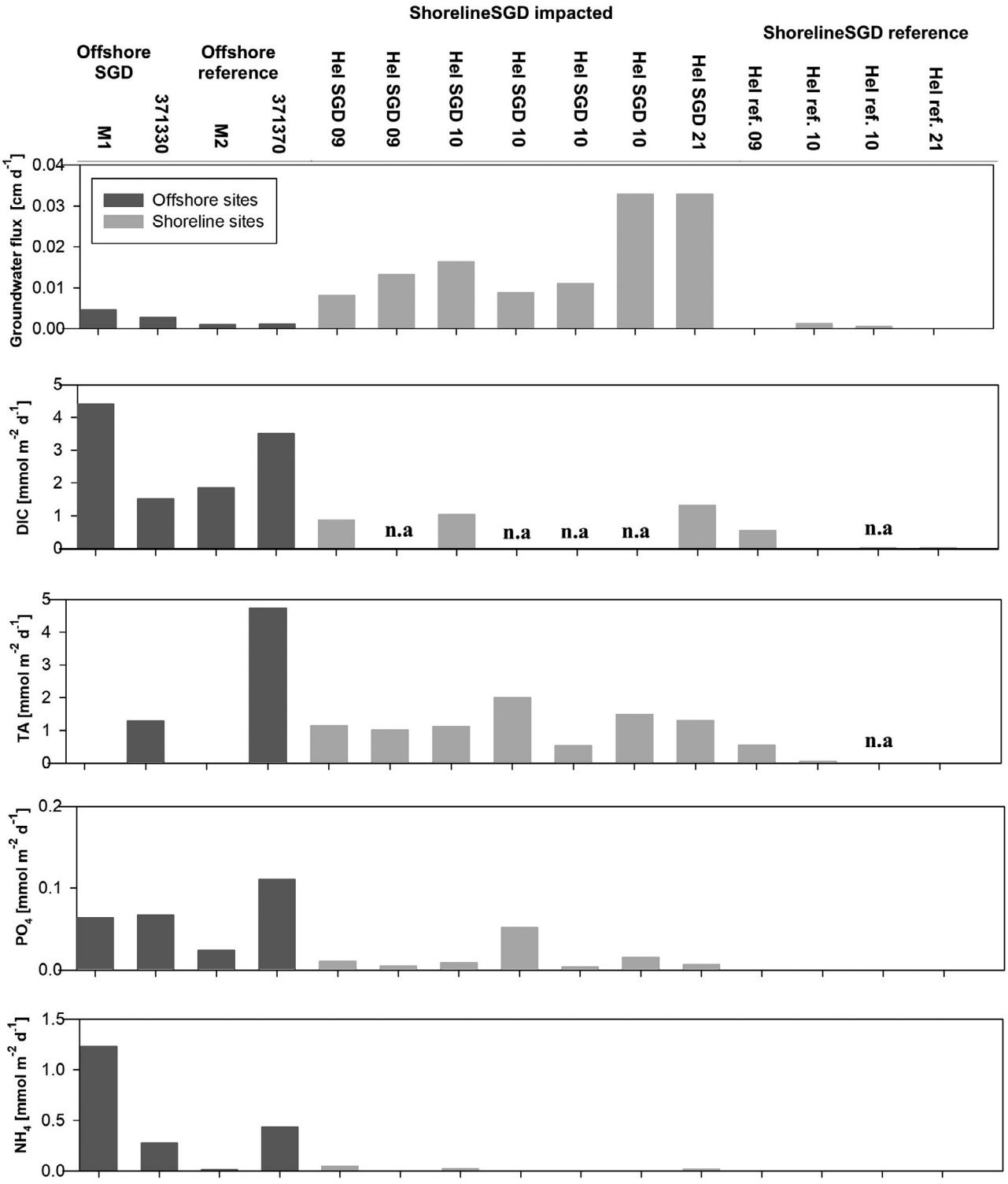

Figure 8 Total fluxes (diffuse + mixing + advective) of water and chemical elements for the offshore muddy SGD and reference sites and selected shoreline sandy SGD and reference sites. The fluxes are presented in Supplementary Table 3.

ure 6, D), the freshwater composition could be calculated to be −19, −16, and −16‰ for Chałupy, Swarzewo and Osłonino, respectively. These values were similar to the signatures found in the deep groundwaters (Table 1), and are probably the result of the mixing of soil CO_2 and C3 Plants, which contribute to the lighter isotopes, and Ca dissolution with the heavier isotopes (e.g. Deines et al., 1974).

4.4. Local and regional estimates of submarine groundwater discharge contribution for the Puck Bay

4.4.1. Local scale of fresh SGD

The modeled groundwater discharge, estimated from the Na gradient, of Site 371330 in the central part of the outer Puck Bay was 0.03 L m^{-2} d^{-1}. Higher groundwater flow estimates were obtained for the shoreline site in Hel, varying between 0.1 and 0.3 L m^{-2} d^{-1}. These estimates refer to the fresh upward groundwater flow.

The SGD fluxes obtained by the seepage meter also include the recirculated component. The fluxes at the Hel shoreline site were between 30 and 45 L m^{-2} d^{-1}. The fluxes obtained for the sites located in the inner part of the Puck Bay, Chałupy, and Swarzewo, were 1.6 and 3.0 L m^{-2} d^{-1}, respectively.

In this study, the seepage fluxes measured with seepage meters are characteristic of the active SGD sites at the shoreline. Estimates from the present study agree with those previously estimated by applying seepage meters ranging from 3 to 187 L m^{-2} d^{-1} (e.g., Donis et al., 2017; Kotwicki et al., 2014; Szymczycha et al., 2012). The fluxes are very heterogeneous because the outflow from the seepage meters is controlled by the geological properties of the selected seafloor (Burnett et al., 2006).

4.4.2. Regional scale SGD

Submarine groundwater discharge is generally a potential source of Ra (Beck et al., 2007b; Charette et al., 2001; Rodellas et al., 2012). In the present study, a Ra isotope mass balance was applied to estimate the total SGD in Puck Bay, following Rodellas et al. (2017). Separate balances for the outer and the inner part of Puck Bay were calculated.

As sources, SGD, rivers, and diffusion from sediments are considered. The sinks are radioactive decay and net export from the study area. Assuming a steady state, the mass balance can be expressed as:

$$Q_{SGD} * Ra_{SGD} + R + F_D - D - O = 0 \quad (4)$$

Where Q_{SGD} is the volumetric SGD (m^3 d^{-1}), Ra_{SGD} is the $^{224}Ra_{ex}$ activity of porewater samples in the study area (Bq m^{-3}). The porewater activities were used as an endmember, since they represent the final solution delivered to the bay. R is the input from rivers (Bq d^{-1}), F_D is the contribution from diffuse fluxes from the sediment (Bq d^{-1}), D is the radioactive decay (Bq d^{-1}) and O is the outflow from the inner and outer Puck Bay (Bq d^{-1}).

The river input is estimated as the product of the discharge and the corresponding $^{224}Ra_{ex}$ activities. The Reda River contributes about 76% of the volume of all rivers discharging into the inner bay (Szymczak and Piekarek-Jankowska, 2007). Therefore, it is considered that the discharge of Zagórska Struga, Gizdepka, and Płutnica together represents 24% of the Reda River discharge.

The diffusive flux determined from the Ra diffusion experiment was multiplied by the area of the bay to obtain F_D.

The radioactive decay is the product of the measured $^{224}Ra_{ex}$ activity of the bay, the volume of the considered part of the bay, and the decay constant.

The outflow was calculated as:

$$O: \frac{(224Ra_{ex}(inner\ or\ outer\ bay) - 224Ra_{ex}(outer\ bay\ or\ Baltic\ Sea)) * V(inner\ or\ outer\ bay)}{WA} \quad (5)$$

Where the WA is the apparent water age, which was estimated by using the short-lived Ra isotopes as described by Moore (2000b):

$$WA: \frac{ln(\frac{224Ra}{223Ra})inner\ or\ outer\ PB - ln(\frac{224Ra}{223Ra})RaSGD}{\lambda 223 - \lambda 224} \quad (6)$$

The Ra-derived estimate of the water age is 4 ± 2 and 15 ± 8 days for the outer and inner parts of Puck Bay, respectively. It should be noted that the water age represents the time elapsed since the water sample became enriched in Ra and was isolated from the source (Moore, 2000b). This application is more appropriate for ages in the range of the half-life of the isotope used.

Considering all the inputs and outputs of the Ra mass balance in the outer Puck Bay, the Q_{SGD} was estimated to be 77 ± 35 10^6 m^3 d^{-1} (301 L m^{-2} d^{-1}) (Table 2). In order to obtain a discharge in the range of the values already estimated for Puck Bay, we estimated that SGD is taking place in the whole bay (255 km^2). This assumption could be realistic to some extent as acoustic imagery showed anomalies in the surface sediments (Figure 3) and salinity in the water column decreased with depth at some sites (Matciak et al., 2015). However, the SGD fluxes estimated here are the sum of the fresh and saline components of SGD, and a balance using long-lived Ra isotopes is required to differentiate between porewater exchange and SGD (Rodellas et al., 2017).

Considering the $^{224}Ra_{ex}$ sources to the outer bay, the SGD represents 94%, whereas the outflow from the inner Puck Bay represents and the diffusion each account for only 3%. In this balance, the Vistula River is not considered as a source of Ra to Puck Bay, which could have an impact depending on the wind direction. Moreover, the contribution from the sediments could also be higher if the diffusion experiment was done for the different sediments found across the bay.

Regarding the inner Puck Bay, Q_{SGD} was estimated to be 6 ±6 10^6 m^3 d^{-1} (55 L m^{-2} d^{-1}) (Table 2). As assumed in the outer Puck Bay, we assume that SGD occurs in the entire inner bay (104 km^2) as well. Here, SGD dominates again with 91%, rivers 0.5%, and diffusion represents 9%.

It is worth noting that the present balances have high levels of uncertainties. Among the factors, the Ra activities found in the end members were very heterogeneous showing a wide range of activities between them. Salinity has been recognized as the main factor controlling the activities in the endmembers since Ra desorption increases with salinity (e.g. Cho and Kim, 2016). In addition, high variability was observed in the $^{224}Ra_{ex}$ activities of the groundwaters around Puck Bay, which ranged between 0 and 14 Bq m^{-3} (Table 1), which suggests that the groundwater discharging into Puck Bay may be formed and flow through a different lithology.

The SGD in the inner part of Puck Bay was found to be about 24 times higher than the discharge of the Reda River on the day of sampling (3 m^3 s^{-1}, IMGW, 2022).

Table 2 Summary of the terms and values used in the Ra mass balance.

Term	Definition	Outer Puck Bay	Inner Puck Bay	Source
A	Area of the bay [m^2]	255200000	104000000	Kramarska et al. (1995)
V	Volume of the bay [m^3]	5231600000	322400000	Szymczak and Szmytkiewicz (2014)
h	average depht of the bay [m]	20.5	3	Matciak et al. (2011)
Q_{rivers}	Total discharge of Gizdepka, Plutnica and Zagorska Struga rivers [m^3 d^{-1}]		73667.37	24% of Reda discharge Szymczak and Piekarek-Jankowska (2007), IMGW (2022)
Q_{Reda}	Discharge of Reda River [m^3 d^{-1}]		233280	IMGW (2022)
λ224	$^{224}Ra_{ex}$ decay constant [d^{-1}]	0.19	0.19	
λ223	$^{223}Ra_{ex}$ decay constant [d^{-1}]	0.06	0.06	
WA	Water age [d]	4	15	Eq. (6)
Ra_{Reda}	$^{224}Ra_{ex}$ concentration in Reda River [Bq m^{-3}]		2.2	this study
Ra_{rivers}	$^{224}Ra_{ex}$ activties in the Gizdepka River [Bq m^{-3}]		0.5	this study
Ra_{rivers}	$^{224}Ra_{ex}$ concentration in the Płutnica River [Bq m^{-3}]		0.9	this study
Ra_{rivers}	$^{224}Ra_{ex}$ concentration in the Zagórska Struga River [Bq m^{-3}]		1	this study
$Ra_{Baltic\ Sea}$	$^{224}Ra_{ex}$ concentration in the Baltic Sea site [Bq m^{-3}]	0.3		this study
$Ra_{outer\ PB}$	Average $^{224}Ra_{ex}$ concentration in the Outer Puck Bay [Bq m^{-3}]	0.5	0.5	this study
$Ra_{inner\ PB}$	Average of $^{224}Ra_{ex}$ in the inner Puck Bay [Bq m^{-3}]	1.6	1.6	this study
F_{dif}	Ra flux out from bottom sediments [Bq m^{-2} d^{-1}]	0.1	0	this study
Ra_{SGD}	$^{224}Ra_{ex}$ of porewater Sopot (SGD) [Bq m^{-3}]	13.6		this study
Ra_{SGD}	$^{224}Ra_{ex}$ of porewater Hel (SGD) [Bq m^{-3}]	7		this study
Ra_{SGD}	$^{224}Ra_{ex}$ of porewater Chalupy (SGD) [Bq m^{-3}]		31	this study
Ra_{SGD}	$^{224}Ra_{ex}$ of porewater Swarzeno (SGD) [Bq m^{-3}]		9	this study
Ra_{SGD}	$^{224}Ra_{ex}$ of porewater Oslonino (SGD) [Bq m^{-3}]		79	this study

Term	Calculations	Outer Puck Bay	Inner Puck Bay	Source
O	Ra output fluxes [Bq d^{-1}]	261580000	23642667	Eq. (5)
D	Radioactive decay [Bq d^{-1}]	497002000	98009600	$^{224}Ra_{ex}PB*V*λ224$, Rodellas et al. (2017)
R	contribution from the inner Puck Bay [Bq d^{-1}]	23642667		Eq. (5)
R	contribution from rivers [Bq d^{-1}]		572150	(Q_{rivers} * average of Ra_{rivers}) + (Q_{Reda}* Ra_{Reda})
F_D	contribution from diffuse fluxes out of bottom sediments [Bq d^{-1}]	25520000	10400000	F_{dif} * A
Q_{SGD}*Ra_{SGD}	contribution from SGD [Bq d^{-1}]	640362213	106424437	$(D + O) - (R + F_D)$
Q_{SGD}	Flux of SGD [10^6 m^3 d^{-1}]	77	6	Balance/Ra_{SGD}
Q_{SGD}	Flux of SGD per area [L m^{-2} d^{-1}]	301	55	Q_{SGD}/A

Table 3 Information of SGD fluxes estimated in different studies for Puck Bay, and, for some sites along the Baltic Sea.

Location	Year sampling	Approach	Discharge [L m^{-2} d^{-1}]	Reference
Puck Bay	1994	only Fresh SGD	0.4	Piekarek—Jankowska (1994, 1996)
Hel — outer Puck Bay	2009—2010	Seepage meter	3—22	Szymczycha et al. (2012)
Hel — outer Puck Bay	2009/2010	Benthic seepage meters	10 —150	Kotwicki et al. (2014)
Hel — outer Puck Bay	2009	Benthic chamber	86 ±16	Donis et al. (2017)
outer Puck Bay (Hel, Jurata, Swarzewo, and Puck)	2017/2018	Chloride tracer	156—242	Kłostowska et al. (2019)
inner Puck Bay (Chałupy and Osłonino)	2017/2018	Chloride tracer	156—242	Kłostowska et al. (2019)
Hel — outer Puck Bay	2021	Seepage meter	30—45	This study
Chalupy — inner Puck Bay	2021	Seepage meter	2	This study
Swarzewo — inner Puck Bay	2021	Seepage meter	3	This study
Site 371330 — outer Puck Bay	2009	Na profile - only fresh SGD	0.003	This study
Hel — outer Puck Bay	2009—2021	Na profile	0.01—0.03	This study
outer Puck Bay	2019	Ra isotopes	301	This study
inner Puck Bay	2021	Ra isotopes	55	This study
Gulf of Finland		geological and hydrogeological methods	0.1	Viventsova and Voronov (2003)
Eckernforde Bay, Germany	1998/2001	Chloride tracer	<9	Schlüter et al. (2004)
Forsmark, Gulf of Bothnia	2013	Ra isotopes	0.3—59	Krall et al. (2017)

The estimates from the Ra mass balance are overall in agreement with those measured by seepage meters or porewater profiles (this study, Donis et al., 2017; Kłostowska et al., 2019; Kotwicki et al., 2014; Szymczycha et al., 2012, Supplementary Table 2). This regional approach based on Ra isotopes further provides for the first time an integrated estimate of the SGD over the whole Puck Bay area.

The different methods used in this study proved that SGD is taking place with high spatial heterogeneity and a wider range in the volumetric and elemental fluxes. The variability is due to the fact that SGD is a local phenomenon, and the calculations are subject to assumptions and uncertainties depending on the number of active SGD sites, which is still unknown. In addition, our values exceed those reported for other regions of the Baltic Sea due to the favorable geological, sedimentological and/or hydrological conditions for SGD in the Puck Bay (Table 3).

5. Conclusions

Puck Bay can be considered a hotspot for submarine groundwater discharge compared to other coastal areas of the Baltic Sea. The current multi-method approach applied to the water column, porewater, and sediment samples identified SGD mainly along the sandy shoreline, but also in the deeper central part of Puck Bay.

Local and regional SGD fluxes derived from seepage meters measurements and a Ra isotope mass balance yielded values between 3 and 300 L m^{-2} d^{-1}. Fluxes of SGD at sandy sites clearly exceed the values determined at muddy sites. Elemental fluxes across the sediment-water interface of organic-rich muds (impacted and non-impacted sites) were found to be driven by early diagenesis and were higher at the muddy sites. The SGD-impacted sandy sites showed intense mixing between upward-moving freshwater and seawater, and early diagenetic processes were less pronounced in shaping the porewater gradients. SGD leads to the release of DIC and TA into the bottom waters. The carbon isotopic composition of DIC shows temporal changes, likely driven by changes in the availability and re-oxidation of biogenic CH_4. This indicates that CH_4 is probably not derived from the original aquifer, but rather from a zone between the deeper aquifer and the overlying sands. Our approach enabled the detection of different freshwater endmembers originating from different aquifers. It also indicates that the SGD-derived chemical fluxes strongly depend on the composition and processes occurring in the surface sediments.

Therefore, future studies need to take into account the non-conservative behavior of constituents in subterranean estuaries in order to better resolve the potentially important quantitative role of SGD in coastal areas. Moreover, climate and land-use changes should be considered, for instance sea level rise, land uplift, wind pattern and the amount of precipitation which can modify the hydraulic gradient between the land and the ocean, and thus the direction, velocity and composition of the SGD flows.

Declaration of competing interest

The authors declare that they have no known competing financial interests or personal relationships that could have appeared to influence the work reported in this paper.

Acknowledgments

The authors wish to thank the staff at the Hel Marine Station (Institute of Oceanography, University of Gdańsk) for their continuous support during the field campaigns and the stimulating working atmosphere. We also thank the crew and captain of r/vs *Professor Albrecht Penck* and *Oceania* for technical support. Karol Kuliński, Jacek Bełdowski, Maciej Chełchowski, Marta Borecka, Monika Lengier, Piotr Balazy, and Seyed Reza Saghravani are thanked for the support during the fieldwork. Anne Köhler, Ines Scherff, and Dagmar Benesch from IOW and Marta Borecka from IOPAN are thanked for their expert support in the laboratory. Jacek Urbański for the help with the study area map. Jan Scholten and Patricia Roeser are thanked for the insightfull discussions, that helped to improve this manuscript. The water utility companies: "Saur Neptun Gdańsk", "Pucka Gospodarka Komunalna", MPWiK "EKOWIK", "PEWIK GDYNIA", "EKO-HEL BIS", especially Radosław Walczak, Konrad Krampichowski, Julia Nowak, Jarosław Myślisz, Michał Twardowski, Zbigniew Rydz, and all staff members are thanked for their support during groundwater sampling.

Funding

Financial support for this work was provided by a DAAD stipend to CMEvA (Doctoral program in Germany 2018/2019, project no. 57381412), to MEB by the BONUS+ project AMBER (BMBF project No.03F0485A), the European Union's Horizon 2020 research and innovation programme under grant agreement no. 730984 (Assemble Plus project), and the Leibniz Institute for Baltic Sea Research. It was furthermore supported to BS by the Institute of Oceanology Polish Academy of Sciences (IOPAN) and project nr.2019/34/E/ST10/00217 funded by the Polish National Science Centre. This work was conducted within the framework of the Research Training Group "Baltic TRANSCOAST" funded by the DFG (Deutsche Forschungsgemeinschaft) under the grant GRK 2000 (www.baltic-transcoast.uni-rostock.de) . This is Baltic TRANSCOAST publication no. GRK2000/0068.

Data availability

The raw data supporting the conclusions of this article will be made available by the authors via the PANGEA database. Further information will be made available by the authors upon request.

Supplementary materials

Supplementary material associated with this article can be found, in the online version, at https://doi.org/10.1016/j.oceano.2024.01.001.

References

Aloisi, G., Wallmann, K., Bollwerk, S., Derkachev, A., Bohrman, G., Suess, E., 2004. The effect of dissolved barium on biogeochemical processes at cold seeps. Geochim. Cosmochim. Ac. 68, 1735—1748.

Atlas of Polish marine area bottom habitats, 2009. Atlas of Polish marine area bottom habitats. Environmental valorization of marine habitats. Institute of Oceanology PAN, Available at:. https://www.iopan.gda.pl/hm/atlas/Atlas_all.pdf.

Balzer, W., 1982. On the distribution of iron and manganese at the sediment/water interface: thermodynamic versus kinetic control. Geochim. Cosmochim. Ac. 46, 1153—1161. https://doi.org/10.1016/0016-7037(82)90001-1

Beck, A.J., Rapaglia, J.P., Cochran, K., Bokuniewicz, H.J., 2007a. Radium mass-balance in Jamaica Bay, NY: Evidence for a substantial flux of submarine groundwater. Mar. Chem. 106, 419—441. https://doi.org/10.1016/j.marchem.2007.03.008

Beck, A.J., Tsukamoto, Y., Tovar-Sanchez, T., Huerta-Diaz, M., Bokuniewicz, H.J., Sanudo-Wilhelmy, S.A., 2007b. Importance of geochemical transformations in determining submarine groundwater discharge-derived trace metal and nutrient fluxes. Appl. Geochem. 22, 477—490. https://doi.org/10.1016/j.apgeochem.2006.10.005

Berner, R.A., 1982. Burial of organic carbon and Pyrite sulfur in the modern ocean: its geochemical and environmental significance. Am. J. Sci. 282 (4), 451—473. https://doi.org/10.2475/ajs.282.4.451

Berner, R.A., Raiswell, R., 1983. Burial of organic carbon and pyrite sulfur in sediments over Phanerozoic Time: a new theory. Geochim. Cosmochim. Ac. 47 (5), 855—862. https://doi.org/10.1016/0016-7037(83)90151-5

Billerbeck, M., Werner, U., Bosselmann, K., Walpersdorf, E., Huettel, M., 2006. Nutrient release from an exposed intertidal sand flat. Mar. Ecol. Prog. Ser. 316, 35—51.

Boudreau, B.P., 1997. Diagenetic models and their implementation: Modelling transport and reactions in aquatic sediments. Springer-Verlag, Berlin, Heidelberg, New York, 414 pp.

Blöschl, G., Bierkens, M.F.P., Chambel, A., Cudennec, C., Destouni, G., Fiori, A., et al., 2019. Twenty-three Unsolved Problems in Hydrology (UPH) — a Community Perspective. Hydrolog. Sci. J. 64, 1141—1158. https://doi.org/10.1080/02626667.2019.1620507

Böttcher, M.E., Lipka, M., Winde, V., Dellwig, O., Böttcher, E.O., Böttcher, T.M.C., Schmiedinger, I., 2014. Multi-isotope composition of freshwater sources for the southern North and Baltic Sea. In: Proc. 23rd SWIM conference, Husum, 46—49.

Böttcher, M.E., Schmiedinger, I., 2021. The Impact of Temperature on the Water Isotope ($^{2}H/^{1}H$, $^{17}O/^{16}O$, $^{18}O/^{16}O$) Fractionation upon Transport through a Low-Density Polyethylene Membrane. Isot. Environ. Healt. S. 57, 183—192. https://doi.org/10.1080/10256016.2020.1845668

Böttcher, M.E., Mallast, U., Massmann, G., Moosdorf, N., Mueller-Petke, M., Waska, H., 2024. Coastal-Groundwater Interfaces (Submarine Groundwater Discharge). In: Krause, S., Hannah, D.M., Grimm, N. (Eds.), Ecohydrological Interfaces. Wiley & Sons, New York, 123—148.

Brand, W.A., Coplen, T.B., 2012. Stable isotope deltas: tiny, yet robust signatures in nature. Isotopes Environ. Health Stud. 48, 393—409. https://doi.org/10.1080/10256016.2012.666977

Brodecka-Goluch, A., Lukawska-Matuszewska, L., Kotarba, M.J., Borkowski, A., Idczak, J., Bolalek, J., 2022. Biogeochemistry of three different shallow gas systems in continental shelf sediments of the South-Eastern Baltic Sea (Gulf of Gdańsk): Carbon cycling, origin of methane and microbial community composition. Chem. Geol. 597, 120799. https://doi.org/10.1016/j.chemgeo.2022.120799

Burnett, W.C., Bokuniewicz, H., Huettel, M., Moore, W.S., Tamiguchi, M., 2003. Groundwater and porewater inputs to the coastal zone. Biogeochemistry 66, 3—33.

Burnett, W.C., Aggarwal, P.K., Aureli, A., Bokuniewicz, H., Cable, J.E., Charette, M.A., Kontar, E., Krupa, S., Kulkarni, K.M., Loveless, A., Moore, W.S., Oberdorfer, J.A., Oliveira, J., Ozyurt, N., Povinec, P., Privitera, A.M.G., Rajar, R., Ramessur, R.T., Turner, J.V., 2006. Quantifying Submarine Groundwater Discharge in the Coastal Zone via Multiple Methods. Sci. Total. Environ. 367, 498—543. https://doi.org/10.1016/j.scitotenv.2006.05.009

Cerdà-Domènech, M., Rodellas, V., Folch, A., Garcia-Orellana, J., 2017. Constraining the temporal variations of Ra isotopes and Rn in the groundwater end-member: Implications for derived SGD estimates. Sci. Total. Environ. 595, 849—857. https://doi.org/10.1016/j.scitotenv.2017.03.005

Charette, M.A, Buesseler, K., Andrews, J., 2001. Utility of radium isotopes for evaluating the input and transport of groundwater-derived nitrogen to a Cape Cod estuary. Limnol. Oceanogr. 46 (2), 465—470. https://doi.org/10.4319/lo.2001.46.2.0465

Charette, M.A., Sholkovitz, E.R., Hansel, C.M., 2005. Trace element cycling in a subterranean estuary Part 1. Geochemistry of the permeable sediments. Geochim. Cosmochim. Ac. 69 (8), 2095—2109. https://doi.org/10.1016/j.gca.2004.10.024

Cho, H-M., Kim, G., 2016. Determining groundwater Ra end-member values for the estimation of the magnitude of submarine groundwater discharge using Ra isotope tracers. Geophys. Res. Let. 43 (8), 3865—3871. https://doi.org/10.1002/2016GL068805

Church, T., 1996. An underground route for the water cycle. Nature 380, 579 pp.

Cline, J.D., 1969. Spectrophotometric Determination of Hydrogen Sulfide in Natural Waters. Limnol. Oceanogr. 14, 454—458.

Cook, P.L.M., Wenzhöfer, F., Glud, R.N., Janssen, F., Huettel, M., 2007. Benthic solute exchange and carbon mineralization in two shallow subtidal sandy sediments: Effect of advective porewater exchange. Limnol. Oceanogr. 52, 1943—1963. https://doi.org/10.4319/lo.2007.52.5.1943

de Beer, D., Wenzhöfer, F., Ferdelman, T.G., Boehme, S.E., Huettel, M., van Beusekom, J.E.E., Böttcher, M.E., Musat, N., Dubilier, N., 2005. Transport and mineralization rates in North Sea sandy intertidal sediments, Sylt-Rømø basin, Wadden Sea. Limnol. Oceanogr. 50 (1), 113—127. https://doi.org/10.4319/lo.2005.50.1.0113

Deines, P., Langmuir, D., Harmon, R.S., 1974. Stable carbon isotope ratios and the existence of a gas phase in the evolution of carbonate ground waters. Geochim. Cosmochim. Ac. 38, 1147—1164. https://doi.org/10.1016/0016-7037(74)90010-6

Dippner, J.W., Bartl, I., Chrysagi, E., Holtermann, P., Kremp, A., Thoms, F., Voss, M., 2019. Lagrangian Residence Time in the Bay of Gdańsk, Baltic Sea. Front. Mar. Sci. 6, 725. https://doi.org/10.3389/fmars.2019.00725

Drake, H., Åström, M., Heim, C., Broman, C., Åström, J., Whitehouse, M., Ivarsson, M., Siljeström, S., Sjövall, 2015. Extreme 13C depletion of carbonates formed during oxidation of biogenic methane in fractured granite. Nat. Commun. 6, 7020. https://doi.org/10.1038/ncomms8020

Donis, D., Janssen, F., Liu, B., Wenzhöfer, F., Dellwig, O., Escher, P., Spitzy, A., Böttcher, M.E., 2017. Biogeochemical impact of submarine groundwater discharge on coastal surface sands of the southern Baltic Sea. Estuar. Coast. Shelf Sci. 189, 131—142. https://doi.org/10.1016/j.ecss.2017.03.003

Egger, M., Hagens, M., Sapart, C.J., Dijkstra, N., van Helmond, N.A.G.M., Mogollón, J., Risgaard-Petersen, N., van der Veen, C., Kasten, S., Riedinger, N., Böttcher, M.E., Röckmann, T., Jørgensen, B.B., Slomp, C.P., 2017. Iron oxide reduction in methane-rich deep Baltic Sea sediments. Geochim. Cosmochim. Ac. 207, 256—276. https://doi.org/10.1016/j.gca.2017.03.019

Ehlert von Ahn, C.M., Böttcher, M.E., Malik, C., Westphal, J., Rach, B., Nantke, C.K., Jenner, A., Saban, R., Winde, V., Schmiedinger, I., 2023. Spatial and temporal variations in the isotope hydrobiogeochemistry of a managed river draining towards the southern Baltic Sea. Geochemistry 83 (3), 125979. https://doi.org/10.1016/j.chemer.2023.125979

EEA. European Environment Agency. Data and Maps. EEA coastline. available at: http://www.eea.europa.eu/data-and-maps/data/eea-coastline-for-analysis-2/gis-data/eea-coastline-polygon/@@rdf (accessed at 22.10.2022).

Falkowska, L., Piekarek-Jankowska, H., 1999. Submarine seepage of fresh groundwater: disturbance in hydrological and chemical structure of the water column in the Gdańsk Basin. ICES J Mar. Sci. 56, 153—160. https://doi.org/10.1016/j.jmarsys.2013.06.009

Froelich, P.N., Klinkhammer, G.P., Bender, M.L., Luedtke, N.A., Heath, G.R., Cullen, D., Dauphin, P., Hammond, D., Hartman, B., Maynard, V., 1979. Early oxidation of organic matter in pelagic sediments of the eastern equatorial Atlantic: Suboxic diagenesis. Geochim. Cosmochim. Ac. 43, 1075e1090. https://doi.org/10.1016/0016-7037(79)90095-4

Garcia-Solsona, E., Garcia-Orellana, J., Masqué, P., Dulaiova, H., 2008. Uncertainties Associated with ^{223}Ra and ^{224}Ra Measurements in Water via a Delayed Coincidence Counter (RaDeCC). Mar. Chem. 109, 198—219. https://doi.org/10.1016/j.marchem.2007.11.006

Gat, J.R., 1996. Oxygen and hydrogen isotopes in the hydrologic cycle. Annu. Rev. Earth Planet. Sci. 24, 225—262. https://doi.org/10.1146/annurev.earth.24.1.225

Goyetche, T., Luquot, L., Carrera, J., Martínez-Pérez, L., Folch, A., 2022. Indentification and quantification of chemical reactions in a coastal aquifer to assess submarine groundwater discharge composition. Sci. Total. Environ. 838 (1), 155978. https://doi.org/10.1016/j.scitotenv.2022.155978

Grasshoff, K., Kremling, K., Ehrhardt, M., 2009. Methods of Seawater Analysis. Wiley & Sons, Weinheim, 600 pp.

Gupta, P., Noone, D., Galewsky, J., Sweeney, C., Vaughn, B.H., 2009. Demonstration of high-precision continuous measurements of water vapor isotopologues in laboratory and remote field deployments using wavelength-scanned cavity ring-down spectroscopy (WS-CRDS) technology. Rapid Commun. Mass Sp. 23, 2534—2542. https://doi.org/10.1002/rcm.4100

HELCOM. River and lake outlines around the Baltic Sea based on 1:1,000,000 scale source maps. available at: https://metadata.helcom.fi/geonetwork/srv/eng/catalog.search#/metadata/f0edff62-d9fa-4fda-9b42-da3947ee248a. (accessed at 22.05.2022).

Hoffmann, J.J.L., von Deimling, J.S., Schröder, J.F., Schmidt, M., Held, P., Crutchley, G.J., Scholten, J., Gorman, A.R., 2020. Complex Eyed pockmarks and submarine groundwater discharge revealed by acoustic data and sediment cores in Eckernförde Bay. SW Baltic Sea. Geochem. Geophy. Geosy. 21, e2019GC008825. https://doi.org/10.1029/2019GC008825

Hovland, M., Talbot, M., Olaussen, S., Aasberg, L., 1987. Methane-related carbonate cements in pockmarks of the North Sea. J. Sediment. Res. 57 (5), 881—892. https://doi.org/10.1306/212f8c92-2b24-11d7-8648000102c1865d

Huettel, M., Ziebis, W., Forster, S., Luther, W., 1998. Advective transport affecting metal and nutrient distributions and interfacial fluxes in permeable sediments. Geochim. Cosmochim. Ac. 62 (4), 613—631. https://doi.org/10.1016/S0016-7037(97)00371-2

IMGW, 2022. The data have been processed at the Institute of Meteorology and water management — National Research Institute Poland.

Idczak, J., Brodeck-Goluch, A., Lukawska-Matuszewska, K.,

Graca, B., Gorska, N., Klusek, Z., Pezacki, P.D., Bolalek, J., 2020. A geophysical, geochemical and microbiological study of a newly discovered pockmark with active gas seepage and submarine groundwater discharge (MET1-BH, central Gulf of Gdańsk, southern Baltic Sea). Sci. Total. Environ. 742, 140306. https://doi.org/10.1016/j.scitotenv.2020.140306

Iversen, N., Jørgensen, B.B., 1985. Anaerobic methane oxidation rates at the sulfate-methane transition in marine sediments from Kattegat and Skagerrak (Denmark). Limnol. Oceanogr. 30 (5), 944—955. https://doi.org/10.4319/lo.1985.30.5.0944

Jørgensen, B.B., Böttcher, M.E., Lüschen, H., Neretin, L.N., Volkov, I.I., 2004. Anaerobic methane oxidation and a deep H_2S sink generate isotopically heavy sulfides in Black Sea sediments. Geochim. Cosmochim. Ac. 68 (9), 2095—2118. https://doi.org/10.1016/j.gca.2003.07.017

Jørgensen, B.B., Kasten, S., 2006. Sulfur cycling and methane oxidation. In: Schulz, H.D., Zabel, M. (Eds.), Marine Geochemistry. Springer-Verlag, Berlin, Heidelberg, 271—309.

Jurasinski, G., Janssen, M., Voss, M., Böttcher, M.E., Brede, M., Burchard, H., Forster, S., Gosch, L., Gräwe, U., Gründling-Pfaff, S., Haider, F., Ibenthal, M., Karow, N., Karsten, U., Kreuzburg, M., Lange, X., Langer, S., Leinweber, P., Rezanezhad, F., Rehder, G., Romoth, K., Schade, H., Schubert, H., Schulz-Vogt, H., Sokolova, I., Strehse, R., Unger, V., Westphal, J., Lennartz, B., 2018. Understanding the Coastal ecocline: Assessing sea-land-interactions at non-tidal, low-lying coasts through interdisciplinary research. Front. Mar. Sci. 5, 1—22. https://doi.org/10.3389/fmars.2018.00342

Kłostowska, Z., Szymczycha, B., Kuliński, K., Lengier, M., Łęczyński, L., 2018. Hydrochemical characterization of various groundwater and seepage water resources located in the Bay of Puck, Southern Baltic Sea. E3S Web of Conferences 54, 00013. https://doi.org/10.1051/e3sconf/20185400013

Kłostowska, Z., Szymczycha, B., Lengier, M., Zarzeczanska, D., Dzierzbicka-Glowacka, L., 2019. Hydrogeochemistry and magnitude of SGD in the Bay of Puck, southern Baltic. Oceanologia 62 (1), 1—11. https://doi.org/10.1016/j.oceano.2019.09.001

Krall, L., Garcia-Orellana, J., Trezzi, G., Rodellas, V., 2017. Submarine Groundwater Discharge at Forsmark, Gulf of Bothnia, provided by Ra Isotopes. Mar. Chem. 162, 162—172.

Kramarska, R., Uscinowicz, S., Zachowicz, J., Kawinska, M., 1995. Origin and Evolution of the Puck Lagoon. J. Coast. Res. 22, 187—191. https://doi.org/10.1016/j.marchem.2017.09.003

Kotwicki, L., Grzelak, K., Czub, M., Dellwig, O., Gentz, T., Szymczycha, B., Böttcher, M.E., 2014. Submarine groundwater discharge to the Baltic coastal zone: Impacts on the meiofaunal community. J. Marine Syst. 129, 118—126. https://doi.org/10.1016/j.jmarsys.2013.06.009

Leipe, T., Moros, M., Kotilainen, A., Vallius, H., Kabel, K., Endler, M., Kowalski, N., 2013. Mercury in Baltic Sea Sediments — Natural Background and Anthropogenic Impact. Geochemistry 73, 249—259. https://doi.org/10.1016/j.chemer.2013.06.005

Löffler, H., Adam, C., Brinschwitz, D., Gieseler, W., Ginzel, G., Grunske, K.-A., Heeger, D., Meinert, N., Nillert, P., Richter, C., Victor, N., 2010. Hydrochemische Typisierung für Grundwasser im Lockergestein Bereich des norddeutschen Flachlandes. Schriftenreihe für Geowissenschaften 18, 369—399.

Majewski, A., 1990. The Gulf of Gdańsk. Wydawnictwo Geologiczne, Warsaw, (in Polish).

Massel, S.R., Przyborska, A., Przyborski, M., 2004. Attenuation of wave-induced groundwater pressure in shallow water. Part 1. Oceanologia 46 (3), 383—404.

Matciak, M., Nowacki, J., Krzyminski, W., 2011. Upwelling intrusion into shallow Puck Lagoon, a part of Puck Bay (the Baltic Sea). Oceanol. Hydrobiol. St. 40, 2. https://doi.org/10.2478/s13545-011-0021-8

Matciak, M., Bieleninik, S., Botur, A., Podgórski, M., Trzcinska, K., Draganska, K., Jasniewicz, D., Kurszewska, A., Wenta, M., 2015. Observations of presumable groundwater seepage occurrence in Puck Bay (the Baltic Sea). Oceanol. Hydrobiol. St. 44 (2), 267—272. https://doi.org/10.1515/ohs-2015-0025

Mayfield, K.K., Eisenhauer, A., Ramos, D.P.S., Higgins, J.A., Horner, T.J., Auro, M., Magna, T., Moosdorf, N., Charette, M.A., Gonneea, M.E., Brady, C.E., Komar, N., Peucker-Ehrenbrink, B., Paytan, A., 2021. Groundwater discharge impacts marine isotope budgets of Li, Mg, Ca, Sr, and Ba. Nat. Commun. 12, 148. https://doi.org/10.1038/s41467-020-20248-3

Meister, P., Liu, B., Khalili, A., Böttcher, M.E., Jørgensen, B.B., 2019. Factors controlling the carbon isotope composition of dissolved inorganic carbon and methane in marine porewater: An evaluation by reaction transport modelling. J. Marine Syst. 200, 103227. https://doi.org/10.1016/j.jmarsys.2019.103227

Moore, W.S., 1996. Large groundwater inputs to coastal waters revealed by ^{226}Ra enrichments. Nature 380, 612—614. https://doi.org/10.1038/380612a0

Moore, W.S., Arnold, R., 1996. Measurement of ^{223}Ra and ^{224}Ra in Coastal Waters Using a Delayed Coincidence Counter. J. Geophys. Res. 101, 1321—1329. https://doi.org/10.1029/95JC03139

Moore, W.S., 1999. The subterranean estuary: a reaction zone of ground water and sea water. Mar. Chem. 65, 111—125. https://doi.org/10.1016/S0304-4203(99)00014-6

Moore, W.S., 2000a. Determining coastal mixing rates using radium isotopes. Cont. Shelf Res. 20, 1993—2007. https://doi.org/10.1016/S0278-4343(00)00054-6

Moore, W.S., 2000b. Ages of continental shelf waters determined from ^{223}Ra and ^{224}Ra. J. Geophys. Res. 105, 22117—22122. https://doi.org/10.1029/1999JC000289

Moore, W.S., 2006. Radium isotopes as tracers of submarine groundwater discharge in Sicily. Cont. Shelf. Res. 26, 852—861. https://doi.org/10.1016/j.csr.2005.12.004

Moore, W.S., 2010. The effect of submarine groundwater discharge on the Ocean. Annu. Rev. Mar. Sci. 2, 59—88. https://doi.org/10.1146/annurev-marine-120308-081019

Moore, W.S., Beck, M., Riedel, T., Rutgers van der Loeff, M., Dellwig, O., Shaw, T.J., Schnetger, B., Brumsack, H.-J., 2011. Radium-based pore water fluxes of silica, alkalinity, manganese, DOC, and uranium: A decade of studies in the German Wadden Sea. Geochim. Cosmochim. Ac. 75, 6535—6555. https://doi.org/10.1016/j.gca.2011.08.037

Moosdorf, N., Böttcher, M.E., Adyasari, D., Erkul, E., Gilfedder, B.S., Greskowiak, J., Jenner, A-K., Kotwicki, L., Massmann, G., Müller-Petke, M., Oehler, T., Post, V., Prien, R., Scholten, J., Siemon, B., Ehlert von Ahn, C.M., Walther, M., Waska, H., Wunderlich, T., Mallast, U., 2021. A State-Of-The-Art Perspective on the Characterization of Subterranean Estuaries at the Regional Scale. Front. Earth Sci. 9, 601293, 1—26. https://doi.org/10.3389/feart.2021.601293

Morse, J.W., Berner, R.A., 1995. What determines sedimentary C/S ratios? Geochim. Cosmochim. Ac. 59 (6), 1073—1077. https://doi.org/10.1016/0016-7037(95)00024-T

Oberdorfer, J.A., Charette, M., Allen, M., Martin, J.B., Cable, J.E., 2008. Hydrogeology and geochemistry of near-shore submarine groundwater discharge at Flamendo Bay, Ubatuba, Brazil. Estuar. Coast. Shelf Sci. 76, 457—465. https://doi.org/10.1016/j.ecss.2007.07.020

Paytan, A., Shellenbarger, G.G., Street, J.J., Davis, K., Young, M.B., Moore, W.S., 2006. Submarine groundwater discharge: An important source of new inorganic nitrogen to coral reef ecosystems. Limnol. Oceanogr. 51 (1), 343—348. https://doi.org/10.4319/lo.2006.51.1.0343

Peltonen, K., 2002. Direct Groundwater Inflow to the Baltic Sea. TemaNord, Nordic Councils of Ministers, Copenhagen, the Netherlands, 79 pp.

Piekarek-Jankowska, H., 1994. Zatoka Pucka jako Obszar Drenażu Wód Podziemnych. Rozp. Monogr., Wyd. UG, Gdańsk 31—32, 204.
Piekarek-Jankowska, H., 1996. Hydrochemical effects of submarine groundwater discharge to the Puck Bay (Southern Baltic Sea, Poland). Geographia Polonica 67.
Povinec, P.P., Bokuniewicz, H., Burnett, W.C., Cable, J., Charette, M., Comanducci, J-F., Kontar, E.A., Moore, W.S., Oberdorfer, J.A., de Oliveira, J., Peterson, R., Stieglitz, T., Taniguchi, M., 2008. Isotope tracing of submarine groundwater discharge offshore Ubatuba, Brazil: results of the IAEA-Unesco SGD project. J. Environ. Radioactiv. 99, 1596—1610. https://doi.org/10.1016/j.jenvrad.2008.06.010
Purkamo, L., von Ahn, C.M.E., Jilbert, T., Muniruzzaman, M., Bange, H.W., Jenner, A-K., Böttcher, M.E., Virtasalo, J.J., 2022. Impact of submarine groundwater discharge on biogeochemistry and microbial communities in pockmarks. Geochim. Cosmochim. Ac. 334, 14—44. https://doi.org/10.1016/j.gca.2022.06.040
Purkl, S., Eisenhauer, A., 2004. Determination of radium isotopes and ^{222}Rn in a groundwater affected coastal area of the Baltic Sea and the underlying sub-sea floor aquifer. Mar. Chem. 87, 137—149. https://doi.org/10.1016/j.marchem.2004.02.005
Qian, Q., Clark, J.J., Voller, V.R., Stefan, H.G., 2009. Depth-dependent dispersion coefficient for modeling of vertical solute exchange in a lake bed under surface waves. J. Hydraul. Eng. 135 (3), 187—197. https://doi.org/10.1061/(ASCE)0733-9429(2009)135:3(187)
R Core Team. R: a language and environment for statistical computing. In: R Foundation for Statistical Computing. Austria, Vienna.
Racasa, E.D., Lennartz, B., Toro, M., Janssen, M., 2021. Submarine Groundwater Discharge From Non- Tidal Coastal Peatlands Along the Baltic Sea. Front. Earth. Sci. 9, 665802. https://doi.org/10.3389/feart.2021.665802
Rodellas, V., Garcia-Orellana, J., Garcia-Solsona, E., Masque, P., Dominguez, J.A., Ballesteros, B.J., Mejias, M., Zarroca, M., 2012. Quantifying groundwater discharge from different sources into a Mediterranean wetland by using ^{222}Rn and Ra isotopes. J. Hydrol. 466-467, 11—22. https://doi.org/10.1016/j.jhydrol.2012.07.005
Rodellas, V., Garcia-Orellana, J., Trezzi, G., Masque, P., Stieglitz, T.C., Bokuniewicz, H., Cochran, J.K., Berdalet, E., 2017. Using the radium quartet to quantify submarine groundwater discharge and porewater exchange. Geochim. Cosmochim. Ac. 196, 58—73. https://doi.org/10.1016/j.gca.2016.09.016
Sadat-Noori, M., Maher, D.T., Santos, I.R., 2016. Groundwater Discharge as a Source of Dissolved Carbon and Greenhouse Gases in a Subtropical Estuary. Estuar. Coast. 36, 639—656. https://doi.org/10.1007/s12237-015-0042-4
Santos, I.R., Eyr, B.D., Huette, M., 2012. The driving forces of porewater and groundwater flow in permeable coastal sediments: A review. Estuar. Coast. Shelf Sci. 98, 1—15. https://doi.org/10.1016/j.ecss.2011.10.024
Santos, I.R., Chen, X., Lecher, A.L., Sawyer, A.H., Moosdorf, N., Rodellas, V., Tamborski, J., Cho, H-M., Dimova, N., Sugimoto, R., Bonaglia, S., Li, H., Hajati, M-C., Li, L., 2021. Submarine groundwater discharge impacts on coastal nutrient biogeochemistry. Nat. Rev. Earth Environ. 2, 307—323. https://doi.org/10.1038/s43017-021-00152-0
Schlitzer, R., 2001. Ocean Data View available at:. http://www.awi-bremerhaven.de/GEO/ODV.
Schlüter, M., Sauter, E., Andersen, C.E., Dahlgaard, H., Dando, P.R., 2004. Spatial Distribution and Budget for Submarine Groundwater Discharge in Eckernförde Bay (Western Baltic Sea). Limnol. Oceanogr. 49, 157—167. https://doi.org/10.4319/lo.2004.49.1.0157
Seeberg-Elverfeldt, J., Schlüter, M., Feseker, T., Kölling, M., 2005. Rhizon sampling of porewaters near the sediment-water interface of aquatic systems. Limnol. Oceanogr.-Meth. 3, 361—371. https://doi.org/10.4319/lom.2005.3.361
Slomp, C., Van Cappellen, P., 2004. Nutrients inputs to the coastal ocean through submarine groundwater discharge: controls and potential impact. J. Hydrol. 295, 64—86. https://doi.org/10.1016/j.jhydrol.2004.02.018
Soetaert, K., Meysman, F., 2012. Reactive transport in aquatic ecosystems: Rapid model prototyping in the open source software R. Environ. Modell. Softw. 32, 49—60. https://doi.org/10.1016/j.envsoft.2011.08.011
Strady, E., Pohl, C., Yakushev, E.V., Krüger, S., Hennings, U., 2008. Pump-CTD-System for trace metal sampling with a high vertical resolution. A test in the Gotland Basin, Baltic Sea. Chemosphere 70, 1309—1319. https://doi.org/10.1016/j.chemosphere.2007.07.051
Sültenfuß, J., Rhein, M., Roether, W., 2009. The Bremen mass spectrometric facility for the measurement of helium isotopes, neon and tritium in water. Isot. Environ. Health. S. 45 (2), 1—13. https://doi.org/10.1080/10256010902871929
Szymczak, E., Piekarek-Jankowska, H., 2007. The transport and distribution of the river load from the Reda River into the Puck Lagoon (southern Baltic Sea, Poland). Oceanol. Hydrobiol. St. XXXVI, 103—124. https://doi.org/10.2478/v10009-007-0012-7
Szymczak, E., Szmytkiewicz, A., 2014. Sediment deposition in the Puck Lagoon (Southern Baltic Sea, Poland). BALTICA 27, 105—118. https://doi.org/10.5200/baltica.2014.27.20
Szymczycha, B., Böttcher, M.E., Diak, M., Koziorowska-Makuch, K., Kuliński, K., Makuch, P., von Ahn, C.M.E., Winogradow, A., 2023. The benthic-pelagic coupling affects the surface water carbonate system above groundwater-charged coastal sediments. Front. Mar. Sci. 10, 1218245. https://doi.org/10.3389/fmars.2023.1218245
Szymczycha, B., Klostowska, Z., Lengier, M., Dzierzbicka-Glowacka, L., 2020. Significance of nutrients fluxes via submarine groundwater discharge in the Bay of Puck, southern Baltic Sea. Oceanologia 62 (2), 117—125. https://doi.org/10.1016/j.oceano.2019.12.004
Szymczycha, B., Vogler, S., Pempkowiak, J., 2012. Nutrient fluxes via submarine groundwater discharge to the Bay of Puck, southern Baltic Sea. Sci. Total. Environ. 438, 86—93. https://doi.org/10.1016/j.scitotenv.2012.08.058
Szymczycha, B., Kroeger, K.D., Pempkowiak, J., 2016. Significance of groundwater discharge along the coast of Poland as a source of dissolved metals to the southern Baltic Sea. Mar. Pollut. Bull. 109, 151—162. https://doi.org/10.1016/j.marpolbul.2016.06.008
Szymczak-Zyla, M., Lubecki, L., 2022. Biogenic and anthropogenic sources of sedimentary organic matter in marine coastal areas. A multi-proxy approach based on bulk and molecular markers. Mar. Chem. 239, 104069. https://doi.org/10.1016/j.marchem.2021.104069
Stosch, H.-G., 2022. Excel template to plot hydrochemical data into a Piper diagram (1.0). Zenodo. doi:10.5281/zenodo.5994293.
Tamborski, J., Bejannin, S., Garcia-Orellana, J., Souhaut, M., Charbonnier, C., Anschutz, P., Pujo-Pay, M., Conan, P., Crispi, O., Monnin, C., Stieglitz, T., Rodellas, V., Andriosa, A., Claude, C., van Beek, P., 2018. A comparison between water circulation and terrestrially-driven dissolved silica fluxes to the Mediterranean Sea traced using radium isotopes. Geochim. Cosmochim. Ac. 238, 496—515. https://doi.org/10.1016/j.gca.2018.07.022
Tamisier, M., Schmidt, M., Vogt, C., Kümmel, S., Stryhanyuk, H., Musat, N., Richnow, H.-H., Musat, F., 2022. Iron corrosion by methanogenic archaea characterized by stable isotope effects and crust mineralogy. Environ. Microbiol. 24 (2), 583—595. https://doi.org/10.1111/1462-2920.15658
Taniguchi, M., Burnett, W.C., Cable, J.E., Turner, J.V., 2002. Inves-

tigation of submarine groundwater discharge. Hydrol. Proc. 16, 2115—2129. https://doi.org/10.1002/hyp.1145

Taniguchi, M., Dulaim, H., Burnett, K.M., Santos, I.R., Sugimoto, R., Stieglitz, T., Kim, G., Moosdorf, N., Burnett, W., 2019. Submarine Groundwater Discharge Updates on its Measurement Techniques, Geophysical Drivers, Magnitudes, and Effects. Front. Environ. Sci. 7, 141. https://doi.org/10.3389/fenvs.2019.00141

Top, Z., Brand, L.E., Corbett, R.D., Burnett, W., Chanton, J., 2001. Helium and radon as tracers of groundwater input into Florida Bay. J. Coast. Res. 17 (4), 859—868. http://www.jstor.org/stable/4300245.

Thang, N.M., Brüchert, V., Formolo, M., Wegener, G., Ginters, L., Jørgensen, B.B., Ferdelman, T.G., 2013. The Impact of Sediment and Carbon Fluxes on the Biogeochemistry of Methane and Sulfur in Littoral Baltic Sea Sediments (Himmerfjärden, Sweden). Estuar. Coast. 36, 98—115. https://doi.org/10.1007/s12237-012-9557-0

Van den Berg, C.M.G., Rogers, H., 1987. Determination of alkalinities of estuarine waters by a two-point potentiometric titration. Mar. Chem. 20, 219—226. https://doi.org/10.1016/0304-4203(87)90073-9

Virtasalo, J.J., Schroeder, J.F., Luoma, S., Majaniemi, J., Mursu, J., Scholten, J., 2019. Submarine Groundwater Discharge Site in the First Salpausselkä Ice-Marginal Formation, South Finland. Solid Earth-EGU 10, 405—432. https://doi.org/10.5194/se-10-405-2019

Viventsowa, E.E., Voronov, A.N., 2003. Groundwater discharge to the Gulf of Finland (Baltic Sea): ecological aspects. Environ. Geol. 45, 221—225. https://doi.org/10.1007/s00254-003-0869-z

von Ahn, C.M.E., Scholten, J.C., Malik, C., Feldens, P., Liu, B., Dellwig, O., Jenner, A-K., Papenmeier, S., Schmiedinger, I., Zeller, M.A., Böttcher, M.E., 2021. A multi-tracer study of freshwater sources for a temperate urbanized coastal bay (Southern Baltic Sea). Front. Environ. Sci. 9, 642346. https://doi.org/10.3389/fenvs.2021.642346

Winde, V., Böttcher, M.E., Escher, P., Böning, P., Beck, M., Liebezeit, G., Schneider, B., 2014. Tidal and spatial variations of $DI^{13}C$ and aquatic chemistry in a temperate tidal basin during winter time. J. Marine Syst. 129, 394—402. https://doi.org/10.1016/j.jmarsys.2013.08.005

Whiticar, M.J., Werner, F., 1981. Pockmarks: Submarine Vents of Natural Gas or Freshwater Seeps? Geo-Mar. Lett. 1, 193—199. https://doi.org/10.1007/BF02462433

Whiticar, M.J., Faber, E., 1986. Methane oxidation in sediment and water column environments — Isotope evidence. Adv. Org. Geochem. 10, 759—768. https://doi.org/10.1016/S0146-6380(86)80013-4

Whiticar, M.J., 1999. Carbon and hydrogen isotope systematics of bacterial formation and oxidation of methane. Chem. Geol. 161, 291—314. https://doi.org/10.1016/S0009-2541(99)00092-3

Zektzer, I.S., Ivanov, V.A., Meskheteli, A.V., 1973. The problem of direct groundwater discharge to the seas. J. Hydrol. 20, 1—36. https://doi.org/10.1016/0022-1694(73)90042-5

Oceanologia 66 (2024) 139—152

Available online at www.sciencedirect.com

ScienceDirect

journal homepage: www.journals.elsevier.com/oceanologia

ORIGINAL RESEARCH ARTICLE

Continuing long-term expansion of low-oxygen conditions in the Eastern Gulf of Finland

Stella-Theresa Stoicescu [1,*], Laura Hoikkala [2], Vivi Fleming [2], Urmas Lips [1]

[1] *Tallinn University of Technology, Tallinn, Estonia*
[2] *Finnish Environment Institute (SYKE), Helsinki, Finland*

Received 31 March 2023; accepted 19 February 2024
Available online 2 March 2024

KEYWORDS
Dissolved oxygen;
Baltic Sea;
Eastern Gulf of Finland;
Eutrophication;
Climate change effects

Abstract To develop an oxygen indicator for the eastern part of the Gulf of Finland (EGOF), a dataset covering 1900—2021 was compiled. The analysis revealed a long-term declining trend in dissolved oxygen concentrations in the EGOF deep layer of 0.022 mg L^{-1} a^{-1} and multi-decadal variations associated with the observed changes in hydrographic conditions. About 27% of the decline in oxygen concentrations for 1900—2021 and 40% for 1990—2021 can be explained by the decrease in solubility due to the temperature increase and changes in hydrographic conditions. The water volume and bottom area under low oxygen conditions in 2016—2021, characterized by dissolved oxygen concentrations <= 6 mg L^{-1}, have increased, compared to the selected reference period with almost no human impact in the 1920s—1950s, from 9.8 km^3 to 78.0 km^3 (from 2.6% to 20.9% of the EGOF total volume) and from 1190 km^2 to 4950 km^2 (from 13.4% to 56.0% of the EGOF total area), respectively. The environmental status of the EGOF was assessed as not good based on the introduced oxygen indicator. We conclude that, in the long-term, low oxygen conditions have expanded mostly due to the excess load and accumulation of nutrients in the system and temperature-related changes in biogeochemical processes and fluxes. However, on a decadal scale, changes in hydrographic conditions, i.e. stratification and mixing, can significantly impact the sub-surface oxygen conditions in the EGOF and similar estuarine basins.

* Corresponding author at: Department of Marine Systems, Tallinn University of Technology, Tallinn, 19086, Estonia
E-mail address: stella.stoicescu@taltech.ee (S.-T. Stoicescu).
Peer review under the responsibility of the Institute of Oceanology of the Polish Academy of Sciences.

Production and hosting by Elsevier

https://doi.org/10.1016/j.oceano.2024.02.002

1. Introduction

The Baltic Sea is influenced by eutrophication (Kabel et al., 2012) and the changing climate (Conley et al., 2009; Gustafsson et al., 2012). The driving force behind eutrophication is the excess amount of nutrients reaching the marine environment via rivers and the atmosphere (e.g., Reusch et al., 2018). Climate change has affected the seas and will continue to do so in the future, mainly through increased temperature, which decreases oxygen solubility and may accelerate respiration and strengthen stratification (e.g., Bindoff et al., 2019; Oschlies et al., 2018). Stronger stratification hinders vertical mixing, which, together with a prolonged stratified period, could lead to more frequent seasonal oxygen depletion in the near-bottom layer of coastal basins (Stoicescu et al., 2022).

To describe and manage the eutrophication-related negative anthropogenic effects on the marine environment, Baltic Sea countries have agreed to assess the status of open sea areas, focusing on nutrients, chlorophyll-a levels, cyanobacterial blooms, water transparency, and near-bottom oxygen conditions and/or bottom fauna, according to the MSFD (European Parliament and Council, 2008). The environmental status of coastal waters is assessed under the WFD (European Parliament and Council, 2000), and the outcome relies mainly on the biological quality elements (phytoplankton, bottom flora and fauna). The physical and chemical parameters, e.g., nutrient concentrations, provide supplementary information. In the frames of the Baltic Marine Environment Protection Commission (HELCOM), open sea and coastal areas are assessed similarly, grouping different indicators into nutrient levels and direct and indirect effects of eutrophication and compiling an aggregated eutrophication status assessment (HELCOM, 2014, 2018d).

In the previous HELCOM assessment of the state of the Baltic Sea, HOLAS II, covering 2011—2016, oxygen conditions were assessed using an oxygen debt indicator applicable in deeper areas where a permanent halocline exists (HELCOM, 2018d). However, this indicator cannot be applied in the shallower eastern Gulf of Finland (EGOF; Figure 1) due to the absence of the halocline in most of this sub-basin. Subsequently, a new oxygen indicator is needed since the criterion “oxygen conditions” is one of the primary criteria of MSFD descriptor 5 on eutrophication. Recently, different approaches have been suggested and tested (Piehl et al., 2022; Stoicescu et al., 2019), and “shallow-water oxygen indicators” are currently being developed in the frames of HELCOM (HELCOM, 2023d).

One of the challenges in using oxygen as a status assessment indicator in the EGOF and similar estuarine regions (Codiga et al., 2022; Liblik et al., 2020) is the difficulty of pinpointing the reasons behind the changes in oxygen concentrations. Although the excess amount of nutrient inputs (past and present) is considered to be the main culprit causing oxygen decline in the Baltic Sea, climate change, more specifically, the increase in water temperature, and water exchange are important factors influencing oxygen conditions (Carstensen et al., 2014). The River Neva carries the largest waterborne nutrient load to the Baltic Sea (Alenius et al., 1998), and with the nutrient input levels exceeding the set maximum allowable inputs (HELCOM, 2023c), the river load has strong implications on the health of the EGOF (HELCOM, 2014, 2018d). However, the near-bottom oxygen concentrations in the EGOF are also strongly influenced by changes in hydrographic conditions (Alenius et al., 1998).

Due to the lack of major sills on the western border of the Gulf of Finland (GOF), its deep layer is influenced by the deep water from the Northern Baltic Proper (NBP), which, among other factors, is affected by the Major Baltic Inflows (e.g., Liblik et al., 2018). The Major Baltic Inflows bring ‘new’ oxygenated water to the deeper central areas of the Baltic Sea, while the ‘old’ oxygen-depleted water gets pushed to more northerly positions, e.g., the NBP (Liblik et al., 2018). East-west spread of the more saline, low-oxygen deep water from the NBP towards the GOF also depends on the prevailing wind pattern (e.g., Alenius et al., 2016; Lehtoranta et al., 2017).

In the EGOF, the deep layer is influenced by the spread of saline water from the west, and the surface layer is affected by freshwater input from the river Neva in the east (Alenius et al., 1998). High river discharge, occurrence of Major Baltic Inflows and calm weather conditions (or prevailing north-easterly winds) strengthen vertical stratification. In contrast, low river discharge, low inflow activity and prevailing strong westerlies alter the hydrographic conditions towards a partially stratified estuary (Lips et al., 2017) according to the estuarine parameter space introduced by Geyer and MacCready (2014). Since corresponding changes in estuarine circulation alter the salinity distribution (Elken et al., 2003; Liblik and Lips, 2011; Lips et al., 2008), we suggest using deep-layer salinity as a proxy of prevailing hydrographic conditions.

The aim of the present study was to analyze the long-term changes in the sub-surface oxygen conditions and the reasons behind these changes in the Eastern Gulf of Finland and to suggest a potential indicator for the eutrophication status assessment. The data series are examined to reveal the long-term trends, interannual variations and relationships between the changes in oxygen concentrations and hydrographic variables (temperature and salinity) and nutrient load. To address primarily the anthropogenic factors causing the decline in oxygen concentrations, we introduce a method to reduce the hydrography (advection and mixing) effects on oxygen conditions. We also estimate the probable decrease in oxygen concentrations caused by the temperature increase and assess the extent of its influence.

2. Material and methods

2.1. Core data set

All available data on oxygen concentrations, temperature and salinity in the eastern part of the Gulf of Finland (the area is shown in Figure 1) were pooled from ICES, Finnish Environment Institute’s national database Hertta (http://www.syke.fi/en-US/Open_information, in Finnish), Gulf of Finland Year database (GOF2014 dataset) CTD oxygen data from stations in the national monitoring program from Finnish Meteorological Institute, and Estonian environmental database (KESE). After removing duplicates, a core dataset was compiled for further analysis. The data are available from 1900, resulting in almost 1500 unique

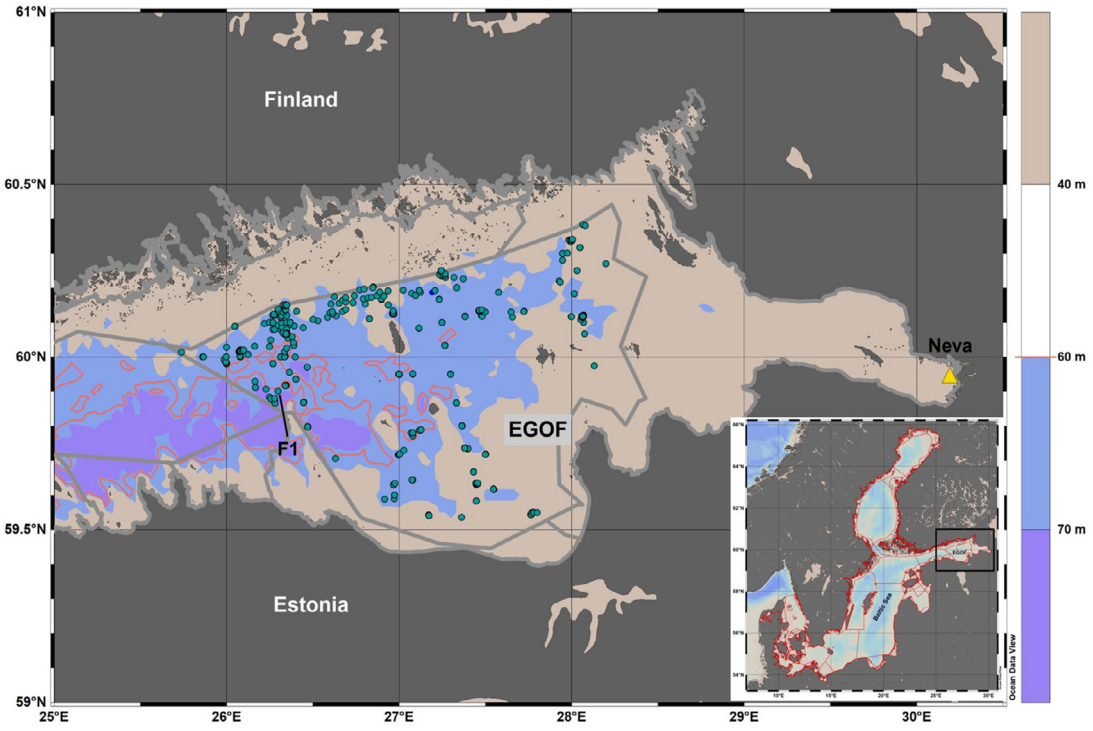

Figure 1 Study area — Eastern Gulf of Finland (EGOF). Blue dots indicate the locations of monitoring stations used in the analysis, Neva river mouth by the yellow triangle, and HELCOM sub-basin division lines by the grey lines, including open sea and coastal area division. The light blue area defines the 40—70 m bottom depth range. The orange line defines the 60 m depth contour.

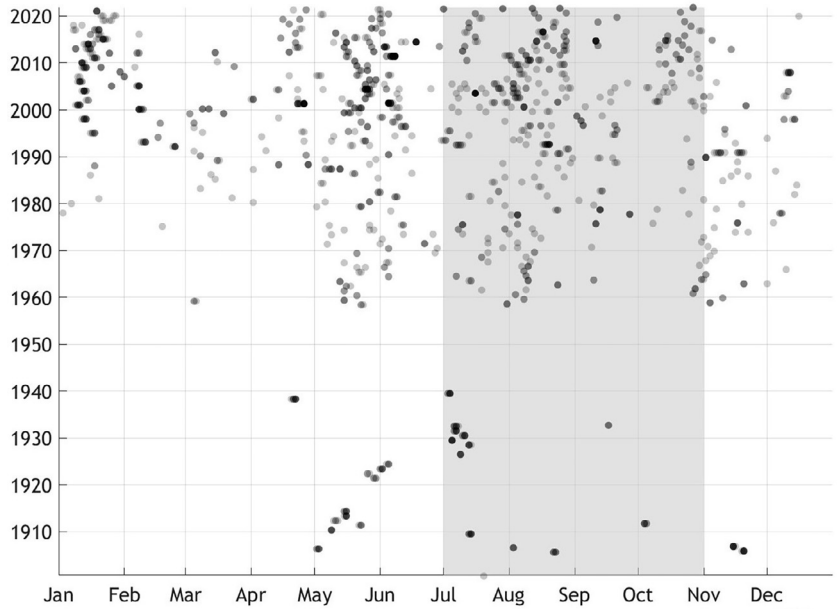

Figure 2 Availability of data used in the analysis in the EGOF area (x-axis: month, y-axis: year). Each dot represents one unique measurement (either a profile or a single measurement). The grey area indicates July—October, from where the data are used for the analysis and indicator calculation.

measurements (station locations are shown in Figure 1 and data availability in Figure 2). However, more consistent data with multiple measurements per season and at least three depths per profile have been available since the late 1950s.

We used all available data regardless of the analysis method. Most of the earlier oxygen concentrations were determined by the Winkler method. Recent data are partly obtained using electrochemical sensors or analyzers, but the relevant HELCOM guidelines (HELCOM, 2018c) are followed. We did not incorporate data on hydrogen sulfide concentration since these were not available for the first half of the 20th century.

2.2. Long-term trends and relationships

Long-term trends in oxygen concentrations, temperature and salinity are estimated for the entire period with available data since the early 1900s and for selected shorter periods with certain visible tendencies. As the minimum near-bottom dissolved oxygen (DO) concentrations in the Baltic Sea basins without the permanent halocline are observed in late summer—early autumn (Piehl et al., 2022; Stoicescu et al., 2022), we focused our analysis on July—October data (Figure 2). The trends are analyzed for three layers, representing the surface layer (0—20 m), the layer just below the summer thermocline (20—40 m) and the deep layer (40—70 m) where seasonal low-oxygen conditions occur.

Earlier studies (Lehtoranta et al., 2016, 2017; Lips et al., 2017; Stoicescu et al., 2019) have shown that deep—layer oxygen concentration and salinity are negatively correlated in the Gulf of Finland. This negative relationship holds because the vertical gradients of salinity and oxygen are opposite, and oxygen concentrations in the saltier inflowing deep water are lower than those in the less saline inflowing water. We found linear regressions between the annual average July—October oxygen concentration and salinity for the defined layers to estimate the effects of changing hydrography on oxygen conditions. The long-term linear trend in oxygen concentrations was removed from the 1900—2021 time series before regression analysis. Uncertainties of using a linear relationship are evaluated.

To estimate the effect of climate change on dissolved oxygen concentrations, we analyzed the changes in oxygen solubility and will discuss other temperature-related processes influencing oxygen conditions. Oxygen saturation concentrations were estimated according to TEOS-10 (IOC, SCOR and IAPSO, 2010). To describe the long-term air temperature trends, data from ERA5 reanalysis were used from a grid point located in the EGOF (59.9N, 26.5E; Hersbach et al., 2023). To find long-term trends in nutrient inputs, supplementary data from the HELCOM indicator 'Inputs of nutrients' (HELCOM, 2023c) and river Neva inputs from the HELCOM/PLC database (https://nest.su.se/helcom_plc/) were used. To estimate the changes in river discharge, river Neva flow data from Väli et al. (2019) were analyzed.

2.3. Defining the extent of low-oxygen waters

To estimate the basin bottom area and volume affected by low-oxygen conditions, we chose a dissolved oxygen concentration of 6.0 mg L^{-1} as a limit. This concentration is considered to be a threshold value where approximately 75% of fish will experience stress caused by low oxygen conditions (Vaquer-Sunyer and Duarte, 2008). Baltic bottom fauna is sensitive to oxygen concentrations below 4.6 mg L^{-1} (Norkko et al., 2015). It has been suggested as a precautionary limit, which would maintain all but the most sensitive species (Vaquer-Sunyer and Duarte, 2008). However, since such low concentrations do not occur at all open sea stations in the EGOF area yearly, the former (6 mg L^{-1}) was selected as the threshold for the volume estimation.

A challenge for finding a characteristic depth of DO isoline 6 mg L^{-1} in the entire assessment area and period is the temporally and spatially sparse data. Station data from July to October were used to compile the yearly characteristic/average oxygen profile from the sea surface to the maximum depth of 106 m. The third-order polynomial fit was chosen for this since it best followed a common oxygen profile in the study area in summer — the season with the thermocline. If DO concentrations estimated by this method remained above 6 mg L^{-1} in the entire water column, as it was found for the period of weak stratification from the mid-1980s to the mid-1990s, the maximum depth in the area and the volume and bottom area equal to zero were used as the respective estimates.

To calculate the area and volume of the low-oxygen bottom water, the hypsographic curve constructed for the EGOF based on EMODnet bathymetry data (https://portal.emodnet-bathymetry.eu/) and an assumption that isosurface 6 mg L^{-1} is a horizontal plane were applied. Although an east-west inclination of the isosurface was identified, it was not applied in the indicator calculation. The reasoning for this choice and the differences in indicator results are elaborated in the discussion.

The earliest available data, before 1926, were obtained at very few stations — 11 stations/sampling sites/events altogether. Because of the low number of available profiles at the beginning of the 1900s, we proposed a later period — 1926 to 1960, as a period with no or low human-induced impact (the reference period).

2.4. Adjusting indicator results to the changes in hydrographic conditions

The changes in hydrographic conditions affecting oxygen conditions, as the movement of saltier and less oxygenated waters along the GOF axis and vertical stratification strength, are assessed based on salinity in the 40—70 m water layer. The suggested oxygen correction is applied to the average salinity in the reference period. Considering the large gap in data from 1940—1957 and the increase in salinity measured at 200 m in the Gotland basin from the 1930s to 1950s (Mohrholz, 2018), the reference period salinity was found as a mean of the average salinity values measured in the 1920s—1930s and the late 1950s. Salinity-adjusted oxygen ($O_{2\ adjusted}$) profiles were calculated by adding a correction to the measured oxygen ($O_{2\ measured}$; Eq. (1)). The correction was equal to the difference between the 40—70 m average salinity within the assessment period (S) and the reference period (S_{ref}) multiplied by the slope of the linear regression line ($slope_g$) between the yearly average salinity and oxygen, as

$$O_{2\ adjusted} = O_{2\ measured} + slope_g * (S_{ref} - S) \quad (1)$$

The ordinary least squares method was used, and the long-term linear trend was removed from the oxygen concentration time series from 1900—2021 before regression analysis. All salinity values in the present paper are given according to the Practical Salinity Scale 1978 as stored in the databases. Although dimensionless, we present salinity in the graphs and text in units [psu].

Equation (1) gives higher adjusted DO values (compared to measured DO) when the average measured salinity is

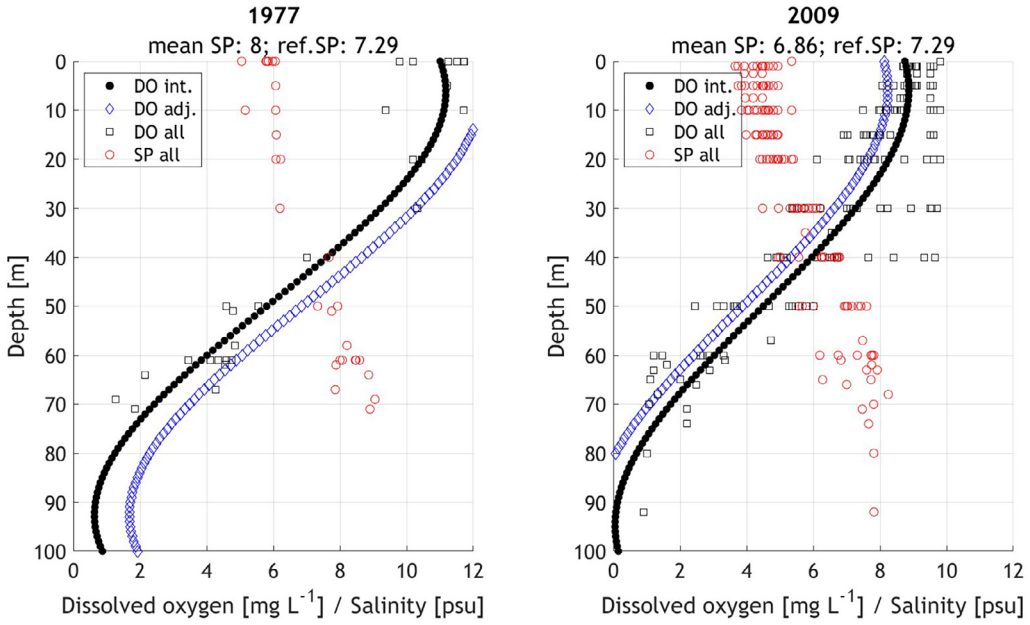

Figure 3 Examples of correcting oxygen values to salinity during a selected assessment period. Available salinity measurements are denoted with hollow red circles (SP all) and oxygen with hollow black squares (DO all). The oxygen profiles derived using third-order polynomial fit are shown with filled black circles (DO int), and the adjusted oxygen profiles are denoted with hollow blue diamonds (DO adj). The left panel represents a period with higher and the right panel with lower mean salinity than the reference period mean salinity in the 40–70 m layer.

Table 1 Long-term linear trends of July–October (yearly average) dissolved oxygen (DO) concentration, salinity (SP), temperature (TEM) and oxygen solubility (OSOL) in three selected depth groups in the eastern Gulf of Finland. Bold numbers indicate a p-value less than the significance level (0.05).

Depth range (m)	1900–2021				1990–2021			
	DO mg L^{-1} a^{-1}	SP psu a^{-1}	TEM°C a^{-1}	OSOL mg L^{-1} a^{-1}	DO mg L^{-1} a^{-1}	SP psu a^{-1}	TEM°C a^{-1}	OSOL mg L^{-1} a^{-1}
0–20	−0.003	0.000	**0.024**	**−0.006**	0.009	0.004	0.027	−0.007
20–40	**−0.021**	0.002	0.012	−0.003	**−0.049**	**−0.012**	**0.120**	**−0.033**
40–70	**−0.022**	−0.002	**0.018**	**−0.006**	**−0.147**	**0.022**	**0.077**	**−0.027**

higher than the average salinity in the reference period (see examples in Figure 3). Higher adjusted DO values, compared to measured DO, move the isoline DO = 6 mg L^{-1} deeper in the water column, resulting in a smaller estimated area and volume of low-oxygen waters. Thus, the applied method allows us to reduce the hydrographic (natural) impacts in the indicator results.

3. Results

3.1. Long-term trends in near-bottom oxygen, salinity and temperature

The deep-layer (40–70 m) oxygen concentrations in the EGOF in July–October show a declining long-term trend of −0.22 mg L^{-1} per decade ($n = 71$, $R^2 = 0.13$, $p < 0.05$; Figure 4 and Table 1), and a total decrease in oxygen concentrations of −2.52 mg L^{-1} for 1905–2021. A steeper decline of −1.47 mg L^{-1} per decade is revealed from 1990–2021 ($n = 31$, $R^2 = 0.42$, $p < 0.05$). The analysis did not include the hydrogen sulfide data due to the lack of earlier measurements. However, H_2S can rarely occur at depths of 40–70 m. According to the monitoring data from recent years, the average H_2S concentration at 77–80 m depth at station F1 in July–October 2014–2021 was 0.1 mg L^{-1}, and the maximum concentration observed was 1.1 mg L^{-1}.

A significant positive trend in temperature of 0.18°C per decade is detected based on July–October data from 40–70 m layer for 1905–2021 ($n = 70$, $R^2 = 0.32$, $p < 0.05$), which is especially steep in the last three decades (0.77°C per decade, $n = 30$, $R^2 = 0.46$, $p < 0.05$; see Figure 4). The long-term increase in temperature in the surface layer was larger (0.24°C per decade) than in the deep layer. Note that the effect of the temperature increase on density (decrease) is much larger in the surface layer than in the deep layer. For instance, if the surface layer temperature increased from 13 to 16°C at salinities of about 5 psu, the density decrease would be 0.43 kg m^{-3}. If a similar increase in temperature (3°C) occurred in the deep layer, e.g., from

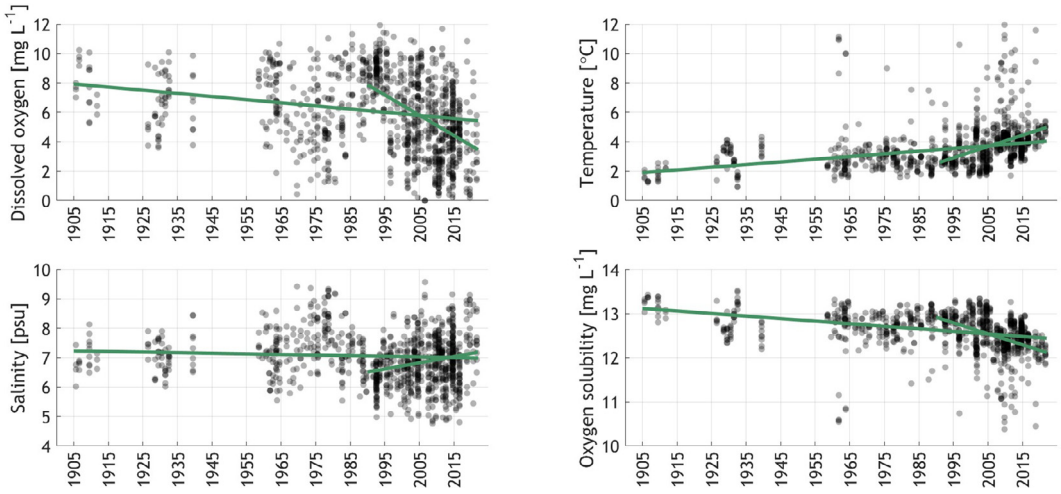

Figure 4 Oxygen (top left), salinity (bottom left), temperature (top right), and oxygen solubility (bottom right) values from 40—70 m layer in the Eastern Gulf of Finland in July—October of 1905—2021. The trendlines (1905—2021 and 1990—2021) are based on annual means.

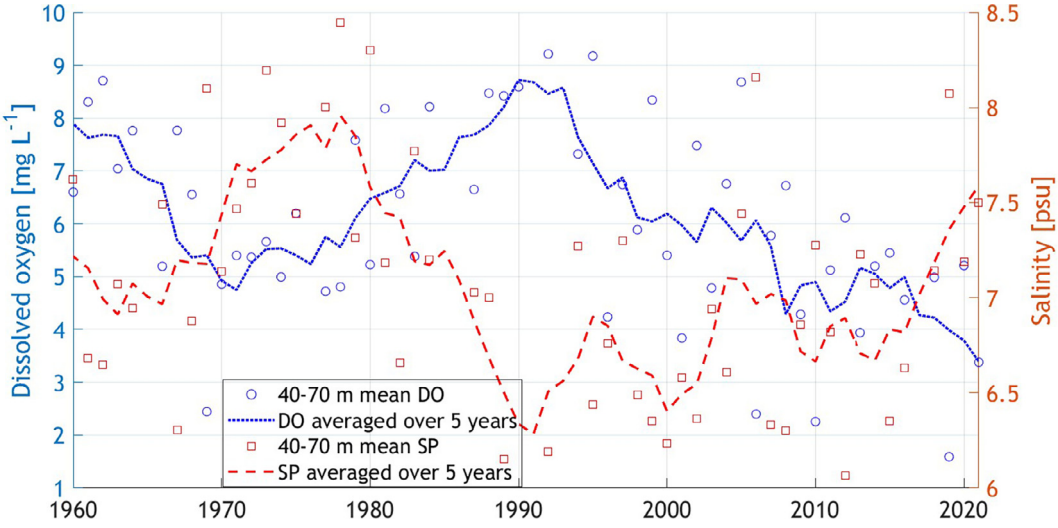

Figure 5 The yearly average July—October oxygen concentrations and salinity in 40—70 m layer in the Eastern Gulf of Finland in 1960—2021. The 5-year moving averages are shown as dashed/dotted curves.

2 to 5°C (at characteristic salinities of 7 psu), the density decrease would be as low as 0.04 kg m^{-3}. Thus, a simultaneous increase in temperature in the surface and sub-surface layers causes the strengthening of vertical stratification.

The near-bottom salinity does not have a significant long-term trend; however, periods with decreasing (from the late 1970s until the early 1990s) and increasing (from the mid-1990s to nowadays) salinities can be observed (Figure 4). These periods are associated with distinct changes in oxygen conditions — a decrease in salinity corresponds to an increase in oxygen values, and *vice versa* (Figures 4—5). Since the observed lower salinities in the deep layer coincided with the slightly higher sea surface salinities in the 1980s — the early 1990s compared to the periods before and after, vertical stratification of the water column was significantly weaker during this period.

The long-term trends of DO and oxygen solubility indicate that oxygen concentrations have decreased in the surface layer primarily due to reduced solubility — the statistically insignificant decrease in DO concentrations is less than the identified decrease in oxygen solubility (Table 1). The decrease in oxygen saturation concentrations was similar in the deep layer and slightly less (and insignificant) in the middle layer than in the surface. However, more importantly, the negative trend in DO was significantly larger in both analyzed sub-surface layers than near the sea surface. During the last 30 years, DO concentrations have declined in the deep layer much faster than the 100-year average trend. Although the trend in oxygen solubility in the deep layer was also larger during the last 30 years than the 100-year average trend, the proportion of its impact in the negative DO trend was lower (oxygen solubility made up 1/6 of the DO trend) than in the centennial trend (oxygen solubility made up 1/4 of the DO trend, Table 1).

To demonstrate the concurrent decadal-scale changes in the deep-layer DO concentrations and salinity, the yearly

Table 2 Parameters of linear regression between yearly average salinity (SP) and dissolved oxygen (DO), and temperature (TEM) and dissolved oxygen (DO) in three selected depth groups in the eastern Gulf of Finland in July—October 1905—2021. All correlations are significant — p-values were below 0.001.

Depth range (m)	SP vs DO			TEM vs DO		
	R^2	n	Slope estimate mg L^{-1} psu^{-1}	R^2	n	Slope estimate mg L^{-1}°C^{-1}
0—20	0.09	71	0.40	0.17	71	—0.13
20—40	0.01	71	—0.17	0.02	71	—0.07
40—70	0.18	70	—1.34	0.33	70	—1.06

average July—October values of both parameters are shown from the last 70 years (Figure 5). A maximum in salinity coincides with a minimum in DO concentrations in the 1970s and a minimum in salinity with a maximum in DO concentrations around 1990. The latter is related to the prolonged stagnation period without Major Baltic Inflows from 1976 until 1993. The effects of the latest MBIs in 1993, 2003 and 2014—2016 are visible in temporal salinity increases in the mid-1990s, mid-2000s and late 2010s. Slightly faster decreases in DO concentrations can be associated with these inflow events. However, DO concentrations have, on the background of high interannual variability, in general, continuously decreased since the early 1990s (Figure 5).

The correlations between the yearly average July—October salinity/temperature and oxygen were all significant (p-value less than 0.001), and the strongest linear relationships were found in the 40—70 m layer (Table 2). The significant correlation of oxygen with salinity in the 40—70 m layer supports our choice of using salinity as a proxy for the effect of changing hydrographic conditions on oxygen conditions. After removing the linear trend from the oxygen time series (to account for the long-term change in the oxygen-salinity relationship), the slope of the regression line between salinity and detrended oxygen of −1.47 mg L^{-1} psu^{-1} ($n = 70$, $R^2 = 0.25$, $p < 0.05$) was found. The limits of its 95% confidence interval were −2.09 mg L^{-1} psu^{-1} and −0.85 mg L^{-1} psu^{-1} (Figure 6). A division of the time series into two periods of 1900—1980 and 1981—2021 resulted in the slope estimates within the ranges of the confidence interval (Figure 6) — it is additional evidence that the relationship is applicable over the entire study period.

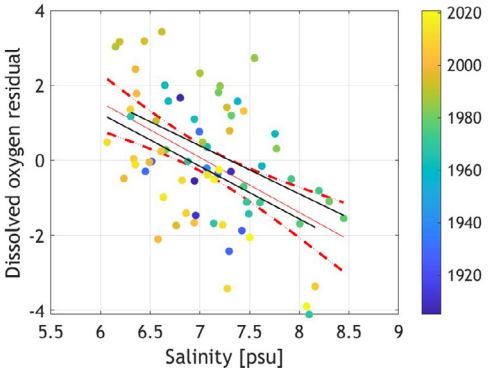

Figure 6 Scatter plot and linear regression line between yearly average (July—October) salinity and residuals of oxygen concentrations from the long-term linear trend line in 40—70 m layer in the Eastern Gulf of Finland in 1905—2021. The regression line is the red solid line; red dashed lines indicate the 95% confidence level limits. The coloring of the dots represents years. Black lines correspond to the regression lines for 1900—1980 (upper line) and 1981—2021 (lower line).

3.2. Defining the extent of low-oxygen waters

To define the bottom area and volume of low-oxygen waters, we looked for the yearly average DO = 6 mg L^{-1} isoline depth in July—October. To assess the status, we compared the estimated area and volume with the threshold values, indicating good environmental status (GES) derived from the conditions in the reference period from 1926 to 1960, exemplifying a time with no/low human influence. The reference period DO = 6 mg L^{-1} isoline depth was 61.4 meters, and the corresponding area and volume estimates were 1190 km^2 or 13.4% and 9.8 km^3 or 2.6% of the total area and volume, respectively.

A threshold value corresponding to good environmental status (GES) can be set by defining the allowable deviation from the reference state. Usually, the acceptable deviation from the reference value of 50% is used to define the threshold (HELCOM, 2013). Thus, we can define the GES as a 50% increase in the low-oxygen bottom area compared to the reference period, i.e. 1780 km^2 or 20.1% of the total EGOF area. The corresponding 6 mg L^{-1} isoline depth would be 56.8 meters (it yields 16.5 km^3 or 4.4% of the total volume). Another option is to use the volume of water with oxygen concentrations below 6 mg L^{-1}. Since the initial (reference) volume was quite small, we propose that the GES conditions correspond to at least the two-fold reference volume. The applied acceptable deviation of 100% yields the GES volume of waters with DO <= 6 mg L^{-1} of 19.7 km^3 or 5.3% of the total EGOF volume. This GES volume corresponds to the 6 mg L^{-1} isoline depth at 55.2 meters (an area estimate would be 2150 km^2 or 24.2% of the total area). These different GES options and the hypsographic curve of the EGOF area are presented in Figure 7.

To reduce the hydrography effects on the status assessment, we adjusted the average oxygen profiles considering the 40—70 m layer differences between the yearly average salinities in the assessment period and the reference period (see examples in Figure 3). This tuning resulted in higher adjusted DO values and deeper location of the 6.0 mg L^{-1} isoline than the observed concentrations and actual isoline depth in periods when the 40—70 m mean salinity was higher than during the reference period, e.g., in the 1970s (Figure 7). During the period of lower deep-layer salinities

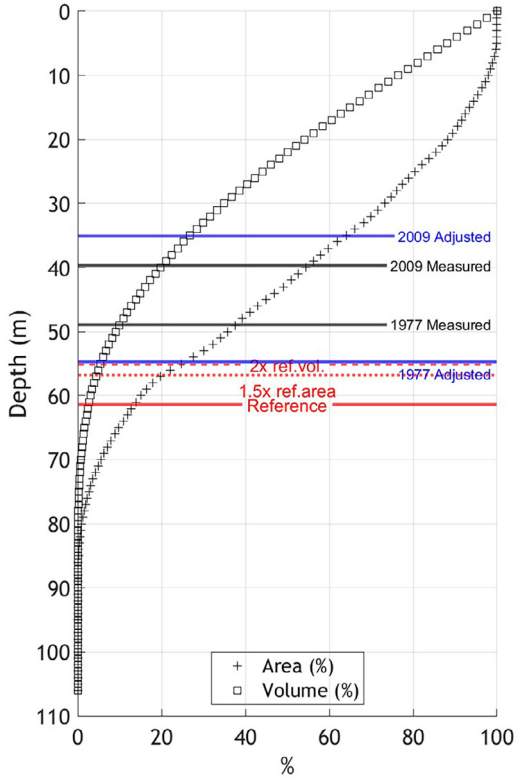

Figure 7 Hypsographic curves — area and volume — of the Eastern Gulf of Finland. The extent of low oxygen (DO <= 6 mg L^{-1}) waters during the reference period (red solid line), with possible GES options, based on reference period area and volume estimates and introduced maximum allowable deviations (a 50% increase of the area, red dashed line and a 100% increase of the volume, red dotted line). Assessment period estimates for 1977 and 2009 are shown based on monitoring data (black lines) and adjusted oxygen profiles (blue lines).

than in the reference period, the adjusted DO values were decreased and the 6.0 mg L^{-1} isoline depth moved upward (e.g., 2009 shown in Figure 7).

Figure 8 demonstrates how the introduced indicator has changed during the last 60 years. An overall increase in the low-oxygen area and volume from the 1960s is evident. Two periods with deviations from this trend can be identified — a rapid increase in the extent of low-oxygen water in the late 1960s and its absence in the late 1980s and early 1990s. The assessed status corresponded to GES for the latter period when low deep-layer salinities and weak stratification were also observed. This outcome and the noticed changes in salinity and oxygen conditions a few years after every known Major Baltic Inflow (after 1993, 2003, and 2014—2016; see also Figure 5) will be discussed later in the paper.

The volume of waters with DO < 6.0 mg L^{-1} in 2016—2021 (matching the latest HELCOM assessment period) was 78.0 km^3 or 20.9% of the EGOF total volume and the bottom area 4950 km^2 or 56.0% of the EGOF total area. When adjusting DO values to salinity using the suggested method, the 6.0 mg L^{-1} isoline depth at 39.1 m was moved to the depth at 38.1 m since the average salinity in the majority of the years in the latest assessment period was slightly lower than the reference period salinity of 7.29 psu. Accordingly, the estimates of the extent of low oxygen waters increased to 83.1 km^3 or 22.3% of the volume and to 5110 km^2 or 57.8% of the bottom area. The increase in the extent of the low-oxygen waters in the EGOF compared to the period with no or low human impact before 1960 is demonstrated in Figure 9. The area and volume of water with DO <= 6 mg L^{-1} have increased from 1190 km^2 to 4950 km^2 (from 13.4% to 56.0% of the total area) and from 9.8 km^3 to 78.0 km^3 (from 2.6% to 20.9% of the total volume). As a result, the status of the EGOF based on sub-surface oxygen conditions in 2016—2021 is assessed as non-GES.

3.3. Impacts of different factors on long-term changes in oxygen conditions

We suggest that the oxygen solubility change induced by the temperature increase dominated the DO decrease in the surface layer of the EGOF in 1900—2021 (Table 1). In the deep layer (40—70 m), oxygen concentrations decreased almost four times faster than oxygen solubility. The respective trends were —0.022 mg L^{-1} a^{-1} and —0.006 mg L^{-1} a^{-1}, indicating that the decrease in saturation concentrations due to the temperature increase could have caused about 27% of the deep-layer DO decrease from 1900—2021. The oxygen solubility trend in the deep layer for the last 30 years was more than four times larger (—0.027 mg L^{-1} a^{-1}) than the long-term trend, but the share of the oxygen solubility influence on the declining DO conditions has been smaller (~18% of the DO trend of —0.147 mg L^{-1} a^{-1} in 1990—2021).

Since the long-term trend in the deep layer salinity was practically absent (the trend was insignificant for 1900—2021; Table 1), we concluded that the long-term changes in hydrographic conditions revealed by the salinity changes could not be responsible for the long-term decline in DO concentrations. For the last 30 years, with a clear deep-layer salinity trend, the change in hydrographic conditions could have caused a 22% (13—32%) decline in DO concentrations. This estimate is obtained by multiplying the detected salinity trend (0.022 psu a^{-1}; see Table 1) with the respective linear regression slope estimate (and its 95% confidence limits) between oxygen concentrations from where the long-term trend was subtracted and salinity (—1.47 mg L^{-1} psu^{-1}). Thus, we can explain 27% of the decline in oxygen concentrations for 1900—2021 and 40% (31—50%) for 1990—2021 by the decrease in solubility and changes in hydrographic conditions. This estimate suggests that most of the long-term changes in deep-layer oxygen conditions have to be caused by other factors, such as the increase in external nutrient loads compared to the early 1900s and changes in internal biogeochemical processes, e.g., due to the temperature increase and accumulated excess nutrients and organic matter (Kuliński et al., 2022).

We analyzed whether the changes in river discharge and meteorological conditions could impact the changes in EGOF deep-layer oxygen conditions since the early 1960s, i.e., the chosen reference period. The July—October DO concentrations in the EGOF deep layer were not significantly correlated with the Neva River discharge in 1962—2018 (corresponding to the entire period with available discharge data from Väli et al., 2019). However, if we divided the data

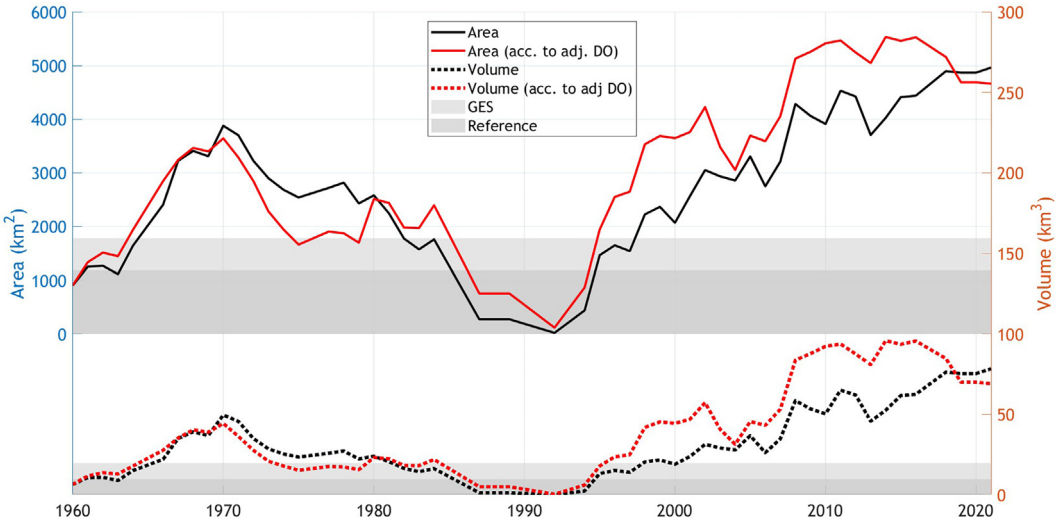

Figure 8 The estimated bottom area (solid lines) and volume of water (dotted lines) with DO <= 6 mg L^{-1} in the EGOF based on the 5-year moving average DO = 6 mg L^{-1} isoline depths. The dark grey area denotes the reference period conditions, and the entire grey area denotes the conditions corresponding to good environmental status (either with a 50% deviation from the reference period area or a 100% deviation from the reference period volume, respectively). The results based on monitoring data are shown in black, and those based on adjusted oxygen profiles are shown in red.

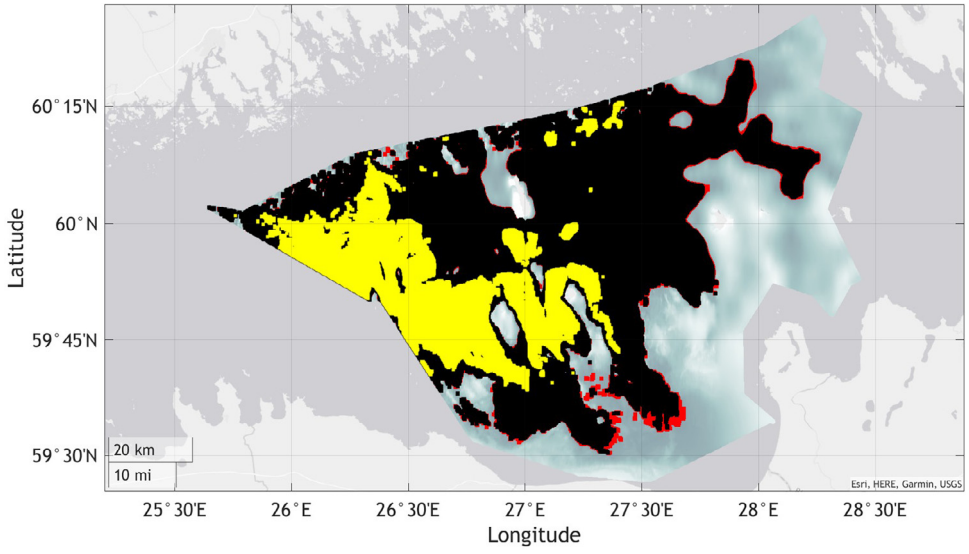

Figure 9 The extent of low oxygen (DO <= 6 mg L^{-1}) water during the reference period (yellow) and the latest assessment period 2016—2021 (yellow and black areas based on non-adjusted oxygen profiles and yellow, black and red areas based on adjusted profiles).

series into two periods — before and after 1993, a significant correlation is detected for the former period but not for the latter. Since this correlation is positive, with cooccurring higher discharges and DO concentrations, the direct causal link is not obvious. Increasing air temperatures are well known for the study area, and statistically significant trends can be derived from the ERA5 data in 1958—2021 and 1993—2021 when the increase was as high as 0.064°C a^{-1}. Significant correlations between the average deep-layer DO concentrations and air temperatures in July—October are detected for the entire period with available data (1958—2021) and the last 30 years (1993—2021) — $R^2 = 0.13$ (n = 59, $p < 0.05$) and $R^2 = 0.23$ (n = 28, $p < 0.05$), respectively. Thus, the warming reflected in air temperatures and water temperatures (Tables 1 and 2) could be a major factor causing the observed decrease in DO concentrations, especially during the last 30 years with a steep temperature increase.

To assess how much the changes in hydrographic conditions can explain the observed improvement in oxygen conditions during the stagnation period, we calculated the trends in 1978—1993 when a fast decrease in salinity was observed (see Figure 5). The estimated trend in DO concentrations was 0.200 mg L^{-1} a^{-1}, and the trend in salinity was −0.110 psu a^{-1}. Using the same slope estimate of 1.47 mg

L^{-1} psu^{-1} suggests that the changes in hydrographic conditions (described as a salinity decrease) can explain most of the increase in DO concentrations — estimated as 0.162 mg L^{-1} a^{-1} (0.094—0.230 mg L^{-1} a^{-1}) and 0.200 mg L^{-1} a^{-1}, respectively. However, DO concentrations started to increase earlier than in 1978, and as seen in Figure 8, the introduced adjustment of DO profiles for changes in salinity did not completely remove the decadal oscillations in the indicator results.

HELCOM Pollution Load Compilation (PLC) data on nutrient loads have been available since 1995 (HELCOM, 2023c; supplementary material). According to the HELCOM load estimates, the total inputs of nitrogen and phosphorus into the GOF have decreased in 1995—2020 by 10% and 58%, respectively, while the riverine flow has increased by 21%. The Neva River load, which is the largest nutrient source for the EGOF, has also decreased at similar rates. However, the trend was statistically significant only for the phosphorus input. Although the trends in loads suggest a potential improvement in environmental conditions, the trends in near-bottom oxygen concentrations are opposite. A similar tendency of worsening eutrophication conditions is revealed by the increasing phosphate concentrations in the surface layer of the GOF in winter (HELCOM, 2023b). Furthermore, no significant correlation was found between July—October DO concentrations in the deep layer of the EGOF and annual loads or river discharge into the entire GOF or via the Neva River in 1995—2020. The exceptions were significant correlations between the total annual phosphorus load and DO concentrations, as well as between the phosphorus load from the Neva River and DO concentrations. Since these correlations were positive, they reflect the observed trends, and no causal link can be attributed to them, knowing also that no significant correlation between the DO concentrations and river discharge was found.

Among all the possible effects of the temperature increase on oxygen conditions, we accounted only for the decrease in oxygen solubility when the temperature rises. However, it has been suggested that the change in saturation concentration could cause only 25% of the deterioration in near-bottom oxygen conditions due to temperature increase (Bendtsen and Hansen, 2013), and other effects, e.g. increased respiration rates, are more important than the solubility decrease impact. Since we do not have direct experimental data, and the effects depend on the water temperatures (effects differ at low and higher temperatures, e.g., Tian et al., 2022), we can make only very rough estimates. We will discuss this issue in the next section.

4. Discussion

Eutrophic conditions with the accompanying decline in oxygen concentrations have been observed and are under concern in many coastal systems around the world, including the Baltic Sea (e.g. Carstensen et al., 2014; Conley et al., 2009). Long-term monitoring data since the beginning of the 1900s revealed a statistically significant decreasing trend in deep-layer oxygen values in the eastern Gulf of Finland (0.22 mg L^{-1} per decade). This trend could be related to the anthropogenic impact either via the increase in nutrient loads (Carstensen et al., 2014) or climate change (Caballero-Alfonso et al., 2015).

The significant trend in deep layer temperature of 0.18°C per decade from July—October 1905 to 2021 and a steeper trend of 0.77°C per decade in the last 30 years agree with the earlier analyses of deep-water temperature changes in the Baltic Sea (e.g. Dutheil et al., 2022; Liblik and Lips, 2019). Dutheil et al. (2022) reported a temperature increase in 1850—2008 in the bottom and intermediate layer of the Baltic Sea of >0.04°C per decade and <0.04°C per decade, respectively, while Liblik and Lips (2019) estimated the trends in the ranges of 0.35—0.6°C per decade in the central Gulf of Finland (layer below 50 m) in 1982—2016. In a more recent analysis, Kankaanpää et al. (2023) reported that the near-bottom temperature increased in the deeper areas of the EGOF by 0.60°C per decade in 1960—2021 and 0.70°C per decade in 1994—2021. Thus, the trend estimates depend on the period under investigation, but a steeper increase in water temperature in the last 30—35 years is a common conclusion. Similar fast warming of waters in recent decades has been observed in other estuarine regions, such as the Chesapeake Bay (Du et al., 2018).

Our results show that in the long term, the warming of the surface layer was larger than the deep layer. However, even if the magnitude of the temperature increase throughout the water column was the same, the effect on the density decrease would be much larger in the warm surface layer than in the cold deep layer because a temperature increase at low temperatures (close to the temperature of maximum density) causes a very modest density decrease. Thus, in brackish sea areas, an increase in water temperature in the entire water column strengthens vertical density stratification in summer.

The near-bottom salinity revealed no significant long-term trend, but an oscillatory nature of the changes was observed. Such decadal-scale fluctuations in hydrographic conditions (Meier et al., 2019; Schimanke and Meier, 2016) would play an important role in changes in oxygen conditions. In the Gulf of Finland, this variability could be interpreted as an influence of the lateral (longitudinal) movements of the deep layer, as described by, e.g., Alenius et al. (2016) and Lehtoranta et al. (2017). The decline in deep-layer salinities in the Baltic Sea from the 1960s/70s to the 1990s has been related to the positive trend in the NAO index in the same period (Meier et al., 2022). The positive NAO trend means that the Baltic Sea region is influenced by stronger westerlies, which in the GOF/EGOF force the saltier/low-oxygen deep layer to more westerly positions. From the mid-1990s to the early 2010s, the NAO index has shown a negative tendency (Meier et al., 2022), coinciding with the observed salinity increase during the last 30—35 years in the Baltic Sea deep basins (Liblik and Lips, 2019) and the EGOF deep layer shown in this study.

We developed a method to reduce the impact of changes in hydrography on the oxygen indicator assessment. The proposed adjustment of oxygen concentrations to changes in salinity decreases the interannual variability of the low-oxygen area/volume in the EGOF (as seen in Figure 8). This result and previous studies (e.g. Liblik et al., 2013; Lips et al., 2017; Stoicescu et al., 2019) demonstrate that low oxygen conditions in the GOF area are strongly influenced by lateral deep-water advection. Deep-layer salin-

ity also correlates strongly with stratification strength that controls vertical oxygen ventilation, thus contributing to the extent of oxygen deficiency (Lehtoranta et al., 2017; Liblik and Lips, 2019). We suggest that in the case of weak stratification, the vertical mixing is intense enough to mask the eutrophication effects in the near-bottom layer — vertical oxygen fluxes prevail over near-bottom oxygen consumption even in the presence of relatively high consumption rates. Since the weakening of stratification also occurred in the western and central Gulf of Finland (Liblik and Lips, 2011), likely more intense vertical mixing resulted in more oxygen in the deep-layer water reaching the EGOF. These conditions occurred in the case of the long-term absence of Major Baltic Inflows and prevailing stronger westerlies (positive NAO index). Thus, the Gulf of Finland was forced towards a partially stratified estuary (Geyer and MacCready, 2014; Lips et al., 2017) with lower salinity difference between the outflowing surface water and inflowing deep-layer water and more intense mixing in the gulf (Burchard et al., 2018).

A statistically significant increase in the surface-layer and deep-layer temperature in the last 100+ years affected the oxygen conditions in the deep layer, as the increasing water temperature decreases oxygen solubility (e.g. Carstensen et al., 2014). We estimated that the decrease in DO solubility explains 27% of the oxygen decline in long-term (100+ years) and 18% from 1990 to 2021. Besides the change in oxygen solubility, temperature increase also affects the consumption and degradation processes by increasing metabolism rates and enhancing respiration rates, which in turn reduce oxygen in water (Boesch et al., 2007; Rabalais et al., 2009). For the Bothnian Sea, it was estimated that the observed 0.78°C increase in deep water temperature from 1992 to 2012 could have led to a 29% increase in respiration rate (Ahlgren et al., 2017). Meier et al. (2018) have suggested that deep-water oxygen depletion has been aggravated in the Gulf of Finland in recent years due to an increase in zooplankton biomass, which enhances the oxygen respiration of zooplankton and higher trophic levels, decreasing the effectiveness of natural deep-water ventilation.

A modeling experiment by Bendtsen and Hansen (2013) suggested that in the case of an increase of deep-water temperature by 3°C about 25% of the predicted decrease in bottom water oxygen concentration in the North Sea-Baltic Sea transition zone could be assigned to the decreased solubility. Tian et al. (2022) simulated the near-bottom oxygen conditions in the Chesapeake Bay for 1995—2025 and reported that the change in DO solubility consisted of 55% of the total climate warming effect, 33% of biological rates, and 11% of strengthening of stratification. If we make a very rough assumption that about 50% of the temperature increase effects could be assigned to the solubility decrease, the total warming-related effect could be about 54% in 1900—2021 and 36% in 1990—2021. Accounting for the hydrography-related effects of 22% in the latter period leads to the estimates that 46% of the oxygen decline in 1900—2021 and 42 (31—50)% in 1990—2021 occurred due to factors other than changes in hydrography and warming. We can conclude that the relative scale of other factors (mostly eutrophication) influencing oxygen conditions has remained roughly the same. It agrees with a suggestion that the decrease in nutrient inputs to an earlier level does not necessarily bring the environment to an earlier state because the effects of eutrophication (internal loading of nutrients, changes in food webs) and climate change can affect the recovery of the system — the trajectories of the ecosystem are not directly reversible (Duarte et al., 2008).

For managing the human influence on marine ecosystems, in regards to eutrophication, an oxygen indicator, characterizing the indirect effects of excess nutrient inputs, has been missing in the relatively shallow open sea areas of the Baltic Sea (HELCOM, 2018d). We have developed an indicator and, using data from the reference period (1926—1960), proposed reference and GES values for the area and volume of low-oxygen waters in the EGOF. If applying a DO = 6.0 mg L^{-1} isoline as the boundary of low-oxygen waters, the suggested reference and GES threshold values correspond to 2.6% and 5.3% of the total EGOF volume, respectively. The assumptions made involve some uncertainties due to the limited data availability from the reference period and subjective decisions regarding an allowable deviation from the reference state. We based our estimate of reference conditions on data from 1926—1960, as also for a developed shallow water oxygen indicator in the southern Baltic Sea, the desirable reference period before the 1960s was indicated (Piehl et al., 2022).

Our method for estimating the area and volume of low-oxygen waters assumes that the DO = 6 mg L^{-1} iso-surface is a horizontal plane. To evaluate the probable error of this approximation, we estimated relationships between the station-based DO = 6.0 mg L^{-1} isoline depths and monitoring station longitudes and latitudes. A significant linear correlation was detected between the DO isoline depth and longitude, while a decrease in DO isoline depths towards the coasts was revealed in the south-north direction. The estimated differences between the area and volume of the horizontal and inclined plane for the latest assessment period 2016—2021 were 14% and 4%, respectively, depending on the depth ranges of the DO = 6.0 mg L^{-1} isoline. Applying also the second-order polynomial fit in the south-north direction resulted in area and volume estimates differing by 6% and 21%, respectively, from the estimates with a horizontal plane. Thus, we conclude that the indicator results include some uncertainties due to the applied approach. However, more significantly, the main uncertainty is related to the availability and temporal and spatial distribution of data. While we could detect statistically significant average shapes of the DO = 6.0 mg L^{-1} isoline depth, the inclination and shape of the isoline could vary remarkably between the years and months. Thus, the above evaluation can be used as a characteristic error estimate of the indicator results, and we decided not to introduce a more precise approximation of the iso-surface to keep the indicator as simple as possible.

Applying the proposed indicator and threshold for the 2016—2021 assessment period shows that good environmental status regarding oxygen conditions has not been achieved in the eastern Gulf of Finland. This result agrees with the higher-than-maximum allowable inputs of nitrogen and phosphorus to the GOF (HELCOM, 2023c). However, the estimated expansion of the low-oxygen waters in the EGOF despite the observed significant decrease in nutrient loads in the recent 20—30 years (HELCOM, 2023c) has to be

analyzed in more detail. First, the nutrient loads at present are still significantly higher than they were at the beginning of the 20th century (Savchuk et al., 2008; Kuliński et al., 2022). The expansion of the low-oxygen waters is also influenced by the internal loading of phosphorus, the so-called vicious cycle, which influences the decline in oxygen conditions by providing additional nutrients to the productive zone (Vahtera et al., 2007). The retention of phosphorus in the sediments and import of phosphorus from the Baltic Proper vary with changes in winter wind forcing (Liblik et al., 2013; Lips et al., 2017), masking the notable reductions in phosphorus loading to the gulf (Lehtoranta et al., 2017). We conclude that even when the nutrient inputs would achieve the HELCOM Baltic Sea Action Plan targets (nutrient input ceilings; see HELCOM, 2021), no improvement in the water quality would be expected anytime soon due to the exceptionally long time scale of eutrophication in the stratified and enclosed Baltic Sea (Gustafsson et al., 2012; Lønborg and Markager, 2021).

The developed indicator targets the anthropogenic effects on oxygen conditions by considering the overall eutrophication status assessment, and it is not directly related to the oxygen levels critical to the benthic communities. Therefore, the indicator should be applied along with an indicator of the status of the benthic macrofauna (HELCOM, 2018d), to take into account the ecological effects of the oxygen conditions. The prerequisite for this is that eutrophication is the main pressure affecting the benthic community in the area. The 2011—2016 assessment of the state of the soft-bottom macrofauna community indicator showed the achievement of GES (HELCOM, 2018d), whereas the nutrient-related indicators revealed all a sub-GES status (HELCOM, 2018a, 2018b). For the HOLAS3 period (2016—2021), the macrofauna indicator displayed a non-GES status (HELCOM, 2023e) with the nutrient-related indicators being also sub-GES (HELCOM, 2023a, 2023b). Ideally, at least the GES/sub-GES level assessment results would coincide, meaning that harmonization could be needed between the indicators.

5. Conclusions

The analysis of long-term monitoring data from the eastern Gulf of Finland revealed a statistically significant decline in near-bottom oxygen concentrations since the early 1900s. Also, the long-term near-bottom temperature increase and decadal-scale fluctuations of salinity have been detected. The changes in the deep-layer oxygen concentrations are significantly correlated with salinity, indicating a strong impact of the along-gulf movement of saltier near-bottom waters and changes in vertical stratification on oxygen conditions. The availability of long-term monitoring data enabled us to determine the reference conditions for the deep-layer oxygen in the eastern Gulf of Finland. For the period 1926—1960, assumed to be with no or low human-induced impact, the average area and volume with oxygen concentrations below 6 mg L^{-1} were 1190 km^2 or 13.4% of the total area and 9.8 km^3 or 2.6% of the total volume of the EGOF. The seabed and waters with low-oxygen have expanded since then to 4950 km^2 or 56.0% of the EGOF total area and 78.0 km^3 or 20.9% of the EGOF total volume. In the long term, since the early 1900s, the worsening of oxygen conditions can be mainly attributed to eutrophication, i.e. excess load of nutrients, and temperature increase. Increasing temperature affects the oxygen concentrations by reducing DO solubility, strengthening vertical stratification and intensifying biogeochemical processes, including respiration and oxygen consumption for the degradation of organic matter. The observed fast widening of low-oxygen areas in the EGOF since the 1990s is related to the changes in hydrographic conditions and together with the climate change effect, they make up about half of the factors influencing the oxygen decline. This means that the relative proportion of other influencing factors, including eutrophication, has remained the same in influencing the expansion of low-oxygen bottoms.

Declaration of competing interest

The authors declare that they have no known competing financial interests or personal relationships that could have appeared to influence the work reported in this paper.

Acknowledgements

We thank the agencies and institutes for funding and implementing the marine environmental monitoring programs in countries bordering the Gulf of Finland, data providers and databases collecting and handling environmental data. The work of Stella-Theresa Stoicescu and Urmas Lips has been supported by the Estonian Research Council grant (PRG602). The indicator development was also partly supported by the JERICO-3 project (funded by the European Commission's Horizon 2020 Research and Innovation program under grant agreements No 871153 and 951799).

References

Ahlgren, J., Grimvall, A., Omstedt, A., Rolff, C., Wikner, J., 2017. Temperature, DOC level and basin interactions explain the declining oxygen concentrations in the Bothnian Sea. J. Marine Syst. 170, 22—30. https://doi.org/10.1016/j.jmarsys.2016.12.010

Alenius, P., Myrberg, K., Nekrasov, A., 1998. The physical oceanography of the Gulf of Finland: a review. Boreal Environ. Res. 3, 97—125.

Alenius, P., Myrberg, K., Roiha, P., Lips, U., Tuomi, L., Pettersson, H., Raateoja, M., 2016. Gulf of Finland physics. In: Raateoja, M., Setälä, O. (Eds.), The Gulf of Finland assessment. Rep. Finnish Environ. Inst., 27 pp.

Bendtsen, J., Hansen, J.L.S., 2013. Effects of global warming on hypoxia in the Baltic Sea—North Sea transition zone. Ecol. Model. 264, 17—26. https://doi.org/10.1016/j.ecolmodel.2012.06.018

Bindoff, N.L., Cheung, W.W.L., Kairo, J.G., Arístegui, J., Guinder, V.A., Hallberg, R., Hilmi, N., Jiao, N., Karim, M.S., Levin, L., O'Donoghue, S., Cuicapusa, S.R.P., Rinkevich, B., Suga, T., Tagliabue, A., Williamson, P., et al., 2019. Changing Ocean, Marine Ecosystems, and Dependent Communities. In: Pörtner, H.-O., et al. (Eds.), IPCC Special Report on the Ocean and Cryosphere in a Changing Climate, in press.

Boesch, D.F., Coles, V.J., Kimmel, D.G., Miller, W.D., et al., 2007. Ramifications of climate change for Chesapeake Bay

hypoxia. In: Ebi, K., et al. (Eds.), Regional Impacts of Climate Change: Four Case Studies in the United States, Pew Center on Global Climate Change, Arlington, VA., 57—70. Available from: https://www.c2es.org/site/assets/uploads/2007/12/regional-impacts-climate-change-four-case-studies-united-states.pdf

Burchard, H., Bolding, K., Feistel, R., Gräwe, U., Klingbeil, K., MacCready, P., Mohrholz, V., Umlauf, L., van der Lee, E.M., 2018. The Knudsen theorem and the Total Exchange Flow analysis framework applied to the Baltic Sea. Prog. Oceanogr. 165, 268—286. https://doi.org/10.1016/j.pocean.2018.04.004

Caballero-Alfonso, A.M., Carstensen, J., Conley, D.J., 2015. Biogeochemical and environmental drivers of coastal hypoxia. J. Marine Syst. 141, 190—199.

Carstensen, J., Andersen, J.H., Gustafsson, B.G., Conley, D.J., 2014. Deoxygenation of the Baltic Sea during the last century. P. Natl. Acad. Sci. USA 111 (15), 5628—5633. Available from: http://www.pubmedcentral.nih.gov/articlerender.fcgi?artid=3992700&tool=pmcentrez&rendertype=abstract

Codiga, D.L., Stoffel, H.E., Oviatt, C.A., Schmidt, C.E., 2022. Managed Nitrogen Load Decrease Reduces Chlorophyll and Hypoxia in Warming Temperate Urban Estuary. Front. Mar. Sci. 9. https://doi.org/10.3389/fmars.2022.930347

Conley, D.J., Björck, S., Bonsdorff, E., Carstensen, J., Destouni, G., Gustafsson, B.G., Hietanen, S., Kortekaas, M., Kuosa, H., Meier, H.E.M., Müller-Karulis, B., Nordberg, K., Norkko, A., Nürnberg, G., Pitkänen, H., Rabalais, N.N., Rosenberg, R., Savchuk, O.P., Slomp, C.P., Voss, M., Wulff, F., Zillén, L., 2009. Hypoxia-Related Processes in the Baltic Sea. Environ. Sci. Technol. 43 (10), 3412—3420. Available from: http://pubs.acs.org/doi/abs/10.1021/es802762a

Du, J., Shen, J., Park, K., Wang, Y.P., Yu, X., 2018. Worsened physical condition due to climate change contributes to the increasing hypoxia in Chesapeake Bay. Sci. Total Environ. 630, 707—717. https://doi.org/10.1016/j.scitotenv.2018.02.265

Duarte, C.M., Conley, D.J., Carstensen, J., Sánchez-Camacho, M., 2008. Return to Neverland: Shifting Baselines Affect Eutrophication Restoration Targets. Estuar. Coast. 32, 29—36. https://doi.org/10.1007/s12237-008-9111-2

Dutheil, C., Meier, H.E.M., Gröger, M., Börgel, F., 2022. Warming of Baltic Sea water masses since 1850. Clim. Dynam. 61, 1311—1331. https://doi.org/10.1007/s00382-022-06628-z

Elken, J., Raudsepp, U., Lips, U., 2003. On the estuarine transport reversal in deep layers of the Gulf of Finland. J. Sea Res. 49, 267—274.

European Parliament and Council, 2000. Directive 2000/60/EC of the European Parliament and of the Council of 23 October 2000 establishing a framework for Community action in the field of water policy. Available from: http://data.europa.eu/eli/dir/2000/60/2014-11-20

European Parliament and Council, 2008. Directive 2008/56/EC of the European Parliament and of the Council of 17 June 2008 establishing a framework for community action in the field of marine environmental policy (Marine Strategy Framework Directive). Off. J. Eur. Union L164, 19—40. Available from: http://data.europa.eu/eli/dir/2008/56/2017-06-07

Geyer, W.R., MacCready, P., 2014. The Estuarine Circulation. Annu. Rev. Fluid Mech. 46 (1), 175—197. https://doi.org/10.1146/annurev-fluid-010313-141302

Gustafsson, B.G., Schenk, F., Blenckner, T., Eilola, K., Meier, H.E.M., Müller-Karulis, B., Neumann, T., Ruoho-Airola, T., Savchuk, O.P., Zorita, E., 2012. Reconstructing the Development of Baltic Sea Eutrophication 1850—2006. Ambio 41, 534—548.

HELCOM, 2013. Approaches and methods for eutrophication target setting in the Baltic Sea region Baltic Sea Environ. Proc. No. 133.

HELCOM, 2014. Eutrophication status of the Baltic Sea 2007-2011. A concise thematic assessment Baltic Sea Environ. Proc. No. 143.

HELCOM, 2018a. Dissolved inorganic nitrogen (DIN). HELCOM core indicator report. Available from: https://helcom.fi/wp-content/uploads/2019/08/Dissolved-inorganic-nitrogen-DIN-HELCOM-core-indicator-2018.pdf

HELCOM, 2018b. Dissolved inorganic phosphorus (DIP). HELCOM core indicator report. Available from: https://helcom.fi/wp-content/uploads/2019/08/Dissolved-inorganic-phosphorus-DIP-HELCOM-core-indicator-2018.pdf

HELCOM, 2018c. Guidelines for sampling and determination of dissolved oxygen in seawater. Available from: https://helcom.fi/wp-content/uploads/2019/08/Guidelines-for-sampling-and-determination-of-dissolved-oxygen.pdf

HELCOM, 2018d. HELCOM thematic assessment of eutrophication 2011—2016 Baltic Sea Environ. Proc. No. 156.

HELCOM, 2021. Baltic Sea Action Plan 2021 update. Available from: https://helcom.fi/wp-content/uploads/2021/10/Baltic-Sea-Action-Plan-2021-update.pdf

HELCOM, 2023a. Dissolved inorganic nitrogen (DIN) HELCOM core indicator report. Available from: https://indicators.helcom.fi/indicator/dissolved-inorganic-nitrogen/

HELCOM, 2023b. Dissolved inorganic phosphorus (DIP) HELCOM core indicator report. Available from: https://indicators.helcom.fi/indicator/dissolved-inorganic-phosphorus/

HELCOM, 2023c. Inputs of nutrients to the sub-basins (2020) HELCOM core indicator report. Available from: https://indicators.helcom.fi/indicator/inputs-of-nutrients/

HELCOM, 2023d. State of the Baltic Sea. Third HELCOM holistic assessment 2016—2021. Baltic. Sea Environ. Proc 194.

HELCOM, 2023e. State of the soft-bottom macrofauna community HELCOM core indicator report. Available from: https://indicators.helcom.fi/indicator/soft-bottom-macrofauna

Hersbach, H., Bell, B., Berrisford, P., Biavati, G., Horányi, A., Muñoz Sabater, J., Nicolas, J., Peubey, C., Radu, R., Rozum, I., Schepers, D., Simmons, A., Soci, C., Dee, D., Thépaut, J-N., 2023. ERA5 monthly averaged data on single levels from 1940 to the present. Copernicus Climate Change Service (C3S) Climate Data Store (CDS). https://doi.org/10.24381/cds.f17050d7

IOC, SCOR and IAPSO, 2010. The International thermodynamic equation of seawater, 2010: calculation and use of thermodynamic properties. In: Intergovernmental Oceanographic Commission. Manuals and Guides No. 56, 196 UNESCO (English).

Kabel, K., Moros, M., Porsche, C., Neumann, T., Adolphi, F., Andersen, T.J., Siegel, H., Gerth, M., Leipe, T., Jansen, E., Damsté, J.S.S., 2012. Impact of climate change on the Baltic Sea ecosystem over the past 1,000 years. Nat. Clim. Change 2, 871—874.

Kankaanpää, H.T., Alenius, P., Kotilainen, P., Roiha, P., 2023. Decreased surface and bottom salinity and elevated bottom temperature in the Northern Baltic Sea over the past six decades. Sci. Total Environ. 859, 160241. https://doi.org/10.1016/j.scitotenv.2022.160241

Kuliński, K., Rehder, G., Asmala, E., Bartosova, A., Carstensen, J., Gustafsson, B., Hall, P.O.J., Humborg, C., Jilbert, T., Jürgens, K., Meier, H.E.M., Müller-Karulis, B., Naumann, M., Olesen, J.E., Savchuk, O., Schramm, A., Slomp, C.P., Sofiev, M., Sobek, A., Szymczycha, B., Undeman, E., 2022. Biogeochemical functioning of the Baltic Sea. Earth Syst. Dynam. 13, 633—685. https://doi.org/10.5194/esd-13-633-2022

Lehtoranta, J., Dahlbo, K., Raateoja, M., Kauppila, P., Savchuk, O., Kuosa, H., Räike, A., Pitkänen, H., 2016. Processes controlling P storages. In: Raateoja, M., Setälä, O. (Eds.), The Gulf of Finland assessment, 27 Rep. Finnish Environ. Inst.

Lehtoranta, J., Savchuk, O.P., Elken, J., Kim, D., Kuosa, H., Raateoja, M., Kauppila, P., Räike, A., Pitkänen, H., 2017. Atmospheric forcing controlling inter-annual nutrient dynamics in the open Gulf of Finland. J. Marine Syst. 171, 4—20.

Liblik, T., Lips, U., 2011. Characteristics and variability of the vertical thermohaline structure in the Gulf of Finland in summer. Boreal. Environ. Res. 16A, 73—83.

Liblik, T., Lips, U., 2019. Stratification Has Strengthened in the Baltic Sea — An Analysis of 35 Years of Observational Data. Front. Earth. Sci. 7, 174. https://doi.org/10.3389/feart.2019.00174

Liblik, T., Laanemets, J., Raudsepp, U., Elken, J., Suhhova, I., 2013. Estuarine circulation reversals and related rapid changes in winter near-bottom oxygen conditions in the Gulf of Finland. Baltic Sea. Ocean Sci. 9, 917—930.

Liblik, T., Naumann, M., Alenius, P., Hansson, M., Lips, U., Nausch, G., Tuomi, L., Wesslander, K., Laanemets, J., Viktorsson, L., 2018. Propagation of impact of the recent Major Baltic Inflows from the Eastern Gotland Basin to the Gulf of Finland. Front. mar. sci. 5 (222), 1—23. https://doi.org/10.3389/fmars.2018.00222

Liblik, T., Wu, Y., Fan, D., Shang, D., 2020. Wind-driven stratification patterns and dissolved oxygen depletion off the Changjiang (Yangtze) Estuary. Biogeosciences 17, 2875—2895. https://doi.org/10.5194/bg-17-2875-2020

Lips, U., Laanemets, J., Lips, I., Liblik, T., Suhhova, I., Suursaar, Ü., 2017. Wind-driven residual circulation and related oxygen and nutrient dynamics in the Gulf of Finland (Baltic Sea) in winter. Estuar. Coast. Shelf S. 195, 4—15. https://doi.org/10.1016/j.ecss.2016.10.006

Lips, U., Lips, I., Liblik, T., Elken, J., 2008. Estuarine transport versus vertical movement and mixing of water masses in the Gulf of Finland (Baltic Sea). US/EU-Baltic Symposium Ocean Observations. In: Ecosystem-Based Management & Forecasting, 27—29. IEEE Conference Proceedings, Tallinn, 1—8. https://doi.org/10.1109/BALTIC.2008.4625535

Lønborg, C., Markager, S., 2021. Nitrogen in the Baltic Sea: Long-term trends, a budget and decadal time lags in responses to declining inputs. Estuar. Coast Shelf S. 261. https://doi.org/10.1016/j.ecss.2021.107529

Meier, H.E.M., Väli, G., Naumann, M., Eilola, K., Frauen, C., 2018. Recently Accelerated Oxygen Consumption Rates Amplify Deoxygenation in the Baltic Sea. J. Geophys. Res. Oceans 123 (5), 3227—3240. https://doi.org/10.1029/2017JC013686

Meier, H.E.M., Eilola, K., Almroth-Rosell, E., Schimanke, S., Kniebusch, M., Höglund, A., Pemberton, P., Liu, Y., Väli, G., Saraiva, S., 2019. Disentangling the impact of nutrient load and climate changes on Baltic Sea hypoxia and eutrophication since 1850. Clim. Dynam. 53 (1), 1145—1166. https://doi.org/10.1007/s00382-018-4296-y

Meier, H.E.M., Kniebusch, M., Dieterich, C., Gröger, M., Zorita, E., Elmgren, R., Myrberg, K., Ahola, M.P., Bartosova, A., Bonsdorff, E., Börgel, F., Capell, R., Carlén, I., Carlund, T., Carstensen, J., Christensen, O.B., Dierschke, V., Frauen, C., Frederiksen, M., Gaget, E., Galatius, A., Haapala, J.J., Halkka, A., Hugelius, G., Hünicke, B., Jaagus, J., Jüssi, M., Käyhkö, J., Kirchner, N., Kjellström, E., Kulinski, K., Lehmann, A., Lindström, G., May, W., Miller, P.A., Mohrholz, V., Müller-Karulis, B., Pavón-Jordán, D., Quante, M., Reckermann, M., Rutgersson, A., Savchuk, O.P., Stendel, M., Tuomi, L., Viitasalo, M., Weisse, R., Zhang, W., 2022. Climate change in the Baltic Sea region: a summary. Earth Syst. Dynam. 13 (1), 457—593. https://doi.org/10.5194/esd-13-457-2022

Mohrholz, V., 2018. Major Baltic Inflow Statistics — Revised. Front. Mar. Sci. 5, 384. https://doi.org/10.3389/fmars.2018.00384

Norkko, J., Gammal, J., Hewitt, J.E., Josefson, A.B., Carstensen, J., Norkko, A., 2015. Seafloor Ecosystem Function Relationships: In Situ Patterns of Change Across Gradients of Increasing Hypoxic Stress. Ecosystems 18 (8), 1424—1439.

Oschlies, A., Brandt, P., Stramma, L., Schmidtko, S., 2018. Drivers and mechanisms of ocean deoxygenation. Nat. Geosci. 11 (7), 467—473. https://doi.org/10.1038/s41561-018-0152-2

Piehl, S., Friedland, R., Heyden, B., Leujak, W., Neumann, T., Schernewski, G., 2022. Modeling of Water Quality Indicators in the Western Baltic Sea: Seasonal Oxygen Deficiency. Environ. Model. Assess. https://doi.org/10.1007/s10666-022-09866-x

Rabalais, N.N., Turner, R.E., Diaz, R.J., Justić, D., 2009. Global change and eutrophication of coastal waters. ICES J. Mar. Sci. 66 (7).

Reusch, T.B.H., Dierking, J., Andersson, H.C., Bonsdorff, E., Carstensen, J., Casini, M., Czajkowski, M., Hasler, B., Hinsby, K., Hyytiäinen, K., Johannesson, K., Jomaa, S., Jormalainen, V., Kuosa, H., Kurland, S., Laikre, L., MacKenzie, B.R., Margonski, P., Melzner, F., Oesterwind, D., Ojaveer, H., Refsgaard, J.C., Sandström, A., Schwarz, G., Tonderski, K., Winder, M., Zandersen, M., 2018. The Baltic Sea as a time machine for the future coastal ocean. Sci. Adv. 4 (5) eaar8195. https://doi.org/10.1126/sciadv.aar8195

Savchuk, O.P., Wulff, F., Hille, S., Humborg, C., Pollehne, F., 2008. The Baltic Sea a century ago — a reconstruction from model simulations, verified by observations. J. Marine Syst. 74 (1), 485—494. https://doi.org/10.1016/j.jmarsys.2008.03.008

Schimanke, S., Meier, H.E.M., 2016. Decadal to centennial variability of salinity in the Baltic Sea. J. Climate. 29 (20), 7173—7188. https://doi.org/10.1175/JCLI-D-15-0443.1

Stoicescu, S.-T., Lips, U., Liblik, T., 2019. Assessment of Eutrophication Status Based on Sub-Surface Oxygen Conditions in the Gulf of Finland (Baltic Sea). Front. Mar. Sci. 6, 54. https://doi.org/10.3389/fmars.2019.00054

Stoicescu, S.-T., Laanemets, J., Liblik, T., Skudra, M., Samlas, O., Lips, I., Lips, U., 2022. Causes of the extensive hypoxia in the Gulf of Riga in 2018. Biogeosciences 19 (11), 2903—2920. https://doi.org/10.5194/bg-19-29032022

Tian, R., Cerco, C.F., Bhatt, G., Linker, L.C., Shenk, G.W., 2022. Mechanisms Controlling Climate Warming Impact on the Occurrence of Hypoxia in Chesapeake Bay. J. Am. Water. Resour. As. 58 (6), 855—875. https://doi.org/10.1111/1752-1688.12907

Vahtera, E., Conley, D.J., Gustafsson, B.G., Kuosa, H., Pitkänen, H., Savchuk, O.P., Tamminen, T., Viitasalo, M., Voss, M., Wasmund, N., Wulff, F., 2007. Internal Ecosystem Feedbacks Enhance Nitrogen-fixing Cyanobacteria Blooms and Complicate Management in the Baltic Sea. Ambio 36, 186—194.

Väli, G., Meier, H.E.M., Placke, M., Dieterich, C., 2019. River runoff forcing for ocean modeling within the Baltic Sea Model Intercomparison Project. Meereswiss. Ber. No. 113 1—25. https://doi.org/10.12754/msr-2019-0113

Vaquer-Sunyer, R., Duarte, C.M., 2008. Thresholds of hypoxia for marine biodiversity. P. Natl. Acad. Sci. USA 105 (40), 15452—15457. https://doi.org/10.1073/pnas.0803833105